Effects of pharmacological inhibition and knockdown of TRAF6 on prostate cancer-induced bone cell activity and osteolysis

A thesis submitted in fulfilment of the requirements

for the degree of Doctor of Philosophy by

Denise Giovana Carrasco Gonzalez

June 2020

Department of Oncology and Metabolism

Faculty of Medicine, Dentistry and Health

The University of Sheffield

A mi familia

Declaration

I confirm that I shall abide by the University of Sheffield's regulations on plagiarism and that all written work shall be my own and will not have been plagiarised from other paper-based or electronic sources. Where used, material gathered from other sources will be clearly cited in the text.

Acknowledgements

I would like to thank my supervisor Dr. Aymen Idris for his constant guidance and support, for letting me be a part of his lab group throughout my MSc and PhD and for giving me his full trust. Also, I would like to express my gratitude for the opportunities you offered me in getting involved in science and disseminating my research. I have learned very much from this experience.

Additionally, I would like to thank my second supervisor Dr. Ning Wang for his disposition and guidance on crucial inputs and suggestions on the project and career development. I would like to express my gratitude for your patience, encouragement and for allowing me to take part in many activities in your lab group.

I would like to thank my former and current lab group colleagues, Dr. Ryan Bishop, Dr. Daniëlle De Ridder, Dr. Abdullah Al Jeffery and soon to be Dr. Boya Li for their support and encouragement throughout the project and also to my colleague Hector Arredondo for his help, understanding and support, having a shared interest in the field.

Importantly, I would like to thank Dr. Michelle Lawson for her support and assistance in her role as a PGR lead. Additionally, I would like to express my gratitude to Dr. Claudia Tulotta, Dr. Karan Shah, Dr. Paris Avgoustou, Dr. Ameera Ahmad Jailani, Orla Gallagher and the staff from the Medical School flow cytometry core facility for their technical support.

I would like to thank the National Council of Science and Technology (CONACYT) and the State Council of Science and Technology from Querétaro (CONCyTEQ) for their economic support to develop my studies in the MSc in Molecular Medicine (Cancer) and the PhD in Medicine.

Lastly and very importantly, I would like to express my appreciation to my family and friends from México and the UK for their support and encouragement, particularly, Aryan Kaveh for

his constant motivation and help in my academic development and my parents and sister, whose support and care I could not be without and who greatly contributed, supported and motivated me to pursue my academic endeavours, everything I am is because of you. Finally, to María de las Mercedes, who is and always will be a constant inspiration.

Publications

Accepted publications

- Bishop, R.T., Marino, S., **Carrasco, G.,** Li, B., Allen, R.J., Sparatore, A., Ottewell, P.D., Mollat, P., Sims, A. H., Capulli, M., Wang, N. and Idris, A. I. (2020) Combined administration of a small-molecule inhibitor of TRAF6 and Docetaxel reduces breast cancer skeletal metastasis and osteolysis. *Cancer Letters,* DOI: 10.1016/j.canlet.2020.05.021.

- Marino, S., **Carrasco, G.,** Li, B., Shah, K. M., Lath, D. L., Sophocleous, A., Lawson, M. A. and Idris, A.I. (2020) JZL184, a monoacylglycerol lipase inhibitor, induces bone loss in a multiple myeloma model of immunocompetent mice. *Calcified Tissue International,* DOI: https://doi.org/10.1007/s00223-020-00689-0.

- Marino, S., Bishop, R. T., **Carrasco, G.**, Logan, J. G. Li, B. and Idris, A. I. (2019) Pharmacological Inhibition of NFκB Reduces Prostate Cancer Related Osteoclastogenesis In Vitro and Osteolysis Ex Vivo. *Calcified Tissue International*, DOI: https://doi.org/10.1007/s00223-019-00538-9, p.p. 193-204.

- Marino, S., De Ridder, D., Bishop, R.T., Renema, N., Ponzetti, M., Sophocleous, A., Capulli, M., Aljeffery, A., **Carrasco, G.**, Gens, M. D., Khogeer, A., Ralston, S. H., Gertsch, J., Lamoureux, F., Heymann, D., Rucci, N. and Idris, A. I. (2019) Paradoxical effects of JZL184, an inhibitor of monoacylglycerol lipase, on bone remodelling in healthy and cancer-bearing mice. *EBio Medicine*, DOI: https://doi.org/10.1016/j.ebiom.2019.05.048, p.p. 452-466.

Manuscripts in preparation

- **Carrasco, G.**, Willis, R., Li, B., Sophocleous, A. and Idris, A. I. TRAF proteins in prostate cancer bone metastasis: a systematic review and meta-analysis. In preparation.
- **Carrasco, G.**, Bishop, R.T., Li, B., Maurizi, A., Capulli, M., Basanini, I., Sparatore, A., Arredondo, H., Wang, N. and Idris, A. I. The effects of knockdown and pharmacological inhibition of TRAF6 on bone remodelling in cancer-bearing mice. In preparation.

Abstracts for presentations

- Poster presentation for CONACyT delegation visit (2017), University of Sheffield, United Kingdom. Project: "The role of TRAF6/NFκB in Prostate Cancer Progression and Metastasis". **Carrasco, G.**, Aljeffery, A., Bishop, R.T. and Idris, A.I.

- Oral presentation at the "XVI Symposium of Mexican Students and Studies in the UK" (2018), University of Southampton, United Kingdom. Project: "Regulation of prostate cancer cell – macrophage – osteoclast interactions by TRAF6". **Carrasco, G.**, Bishop, R.T., Marino, S., Wang, N. and Idris, A.I.

- Poster presentation at the "46th ECTS Congress" (2019), Budapest, Hungary. Project: "Disruption of prostate cancer cell – macrophage – osteoclast crosstalk by a novel

TRAF6 inhibitor". **Carrasco, G.**, Bishop, R.T., Maurizi, A., Capulli, M., Sparatore, A., Marino, S. and Idris, A.I.

- Poster presentation at the "15th Annual University of Sheffield Medical School Research Meeting" (2019), University of Sheffield, United Kingdom. Project: "Disruption of prostate cancer cell – macrophage – osteoclast crosstalk by a novel TRAF6 inhibitor". **Carrasco, G.**, Bishop, R.T., Maurizi, A., Capulli, M., Sparatore, A., Marino, S. and Idris, A.I.

- Poster and oral presentation at the "2019 NCRI Cancer Conference", Glasgow, United Kingdom. Project: "Inhibition of prostate cancer cell growth, motility and ability to alter monocyte/macrophage lineage commitment by a novel TRAF6 inhibitor". **Carrasco, G.**, Bishop, R.T., Maurizi, A., Marino, S., Sparatore, A., Capulli, M. and Idris, A.I.

Other publications

- HubLE Doodle. "Reduction of prostate cancer growth, migration, invasion and ability to influence macrophage lineage commitment by TRAF6 inhibition". **Carrasco, G.**

Awards

- Funding for travelling support from the Learned Society Fund of the University of Sheffield (2018).

- Funding for travelling support for the "XVI Symposium of Mexican Students and Studies in the UK" (2018).

- Funding for travelling support from the Learned Society Fund of the University of Sheffield (2019).

- Grant for "Think Ahead Sheffield Undergraduate Research Experience (SURE) scheme" at the University of Sheffield involving the supervision of an undergraduate student to develop a short term project (2019).

List of contents

List of figures

List of supplementary figures

List of tables

List of abbreviations

A	Ampere.
ADT	Androgen deprivation therapy.
Akt	Protein kinase B.
ALP	Alkaline phosphatase.
ALZ	Alizarin Red S.
Amp	Amplification.
ANOVA	Analysis of variance.
APCs	Antigen-presenting cells.
AR	Androgen receptor.
ATP	Adenosine triphosphate.
BCA	Bicinchoninic Acid Assay.
BMPs	Bone-morphogenetic proteins.
BRCA1	Breast cancer 1.
BSA	Bovine Serum Albumin.
BV421	Brilliant Violet 421.
BV/TV%	Percentage of bone volume/tissue volume.
CAPE	Caffeic acid phenethyl ester.
CCL2	Chemokine ligand 2.
CD4+	Cluster of differentiation 4.
CD8+	Cluster of differentiation 8.
CD40	Cluster of differentiation 40.
CD40L	CD40 ligand.
CD68	Cluster of differentiation 68.
CD80	Cluster of differentiation 80.
CD163	Cluster of differentiation 163.
cm^2	Square centimetre.
CNAs	Copy number alterations.
CO_2	Carbon dioxide.
CTAn	CT-Analyser.
CTLA-4	Cytotoxic T lymphocyte-associated protein 4.

CTVol	CT volume software.
CYP17A1	Cytochrome P450 Family 17 Subfamily A Member 1.
DC	Dendritic cells.
Del	Deletion.
DMEM	Dulbecco's Modified Eagle Medium.
DMSO	Dimethyl sulfoxide.
DNA	Deoxyribonucleic acid.
DTT	DL-Dithiothreitol.
ECL	Enhanced Chemiluminescence.
EDTA	Ethylenediaminetetracetic acid.
EMT	Epithelial-mesenchymal transition.
ETH	Eidgenössische Technische Hochschule.
EZH2	Enhancer of zeste homolog 2.
FACS	Fluorescence-activated cell sorting.
FBS	Foetal Bovine Serum.
FDA	US Food and Drug Administration.
FITC	Fluorescein isothiocyanate.
FSC-A	Forward scatter area.
FSC-H	Forward scatter height.
g	Gram.
GEPIA	Gene Expression Profiling Interactive Analysis.
GM-CSF	Granulocyte-macrophage colony-stimulating factor.
GO	Gene ontology.
GWAS	Genome-wide association studies.
HCl	Hydrochloric acid.
HR	Hazard ratio.
HEK293ET	Human embryonic kidney EBNA T cells.
hrs.	Hours.
ICAM-1	Intracellular adhesion molecule 1.
IC$_{50}$	Half maximal inhibitory concentration.
IFN-γ	Interferon gamma.
IGF-1	Insulin-like growth factor 1.
IGF-1R	IGF-1 receptor.

IgG (H+L)	Immunoglobulin G (heavy+light chains).
IκB-α	NFκB inhibitor alpha.
IKK	IκB kinase.
IL-1β	Interleukin 1 betha.
IL-4	Interleukin 4.
IL-6	Interleukin 6.
IL-10	Interleukin 10.
IL-13	Interleukin 13.
IP	Intraperitoneal.
IR	Infrared.
JNK	c-Jun N-terminal kinases.
KD	Knockdown.
kDa	Kilodalton.
KEGG	Kyoto Encyclopedia of Genes and Genomes.
kg	Kilogram.
kV	Kilovolt.
kVp	Kilovoltage peak.
LFA3	Lymphocyte function-associated antigen 3.
LHRH	Luteinizing hormone-releasing hormone.
LNCaP	Lymph node Carcinoma of the Prostate.
Log2	Binary logarithm.
LPS	Lipopolysaccharides.
M-CSF	Macrophage colony-stimulating factor.
mAb	Monoclonal antibody.
MAPK	Mitogen-activated protein kinases.
mCRPC	Metastatic castration-resistant prostate cancer.
MDSCs	Myeloid-derived suppressor cells.
MET	Mesenchymal-epithelial transition.
mg	Miligram.
MgCl$_2$	Magnesium chloride.
micro-CT	Microcomputed tomography.
min.	Minute.
miR	MicroRNA.

ml	Millilitre.
mm	Milimetre.
mM	Milimolar.
MMPs	Matrix metalloproteinases.
MRI	Magnetic resonance imaging.
mRNA	Messenger RNA.
Mut	Mutation.
M1	Anti-tumorigenic macrophages.
M2	Pro-tumorigenic macrophages.
Mø	Uncommitted macrophages.
NaCl	Sodium chloride.
NEMO	NFκB essential modulator.
NFκB	Nuclear factor κ-light-chain-enhancer of activated B cells.
ng	Nanogram.
No.	Number.
OPG	Osteoprotegerin.
PAP	Prostatic acid phosphatase.
PARP	Poly (ADP-ribose) polymerase.
PBS	Phosphate buffered saline.
PCa	Prostate cancer.
PE	Phycoerythrin.
PEI	Polyethylenimine.
pg	Picogram.
pH	Power of hydrogen.
PI3K	Phosphoinositide 3-kinase.
PKC	Protein kinase C.
PMA	Phorbol 12-myristate 13-acetate.
PNAS	Proceedings of the National Academy of Sciences.
Po.tot%	Percentage of total porosity.
PRAD	Prostate adenocarcinoma.
Prostvac-VF	Rilimogene galvacirepvec/rilimogene glafolivec.
PSA	Prostate-specific antigen.
PTEN	Phosphatase and tensin homolog.

PTH	Parathyroid hormone.
PTHrP	Parathyroid hormone-related protein.
PVDF	Polyvinylidene.
R	Correlation coefficient.
RANK	Receptor activator for NFκB.
RANKL	RANK ligand.
RB1	Retinoblastoma protein.
RELA (p65)	REL-associated protein.
RIPA	Radioimmunoprecipitation assay buffer.
RM1-BM	Ras+Myc transformed cells-Bone metastatic.
RNA	Ribonucleic acid.
RNA-seq	RNA sequencing.
RPMI	Roswell Park Memorial Institute.
Runx2	Runt-related transcription factor 2.
R^2	Square of the correlation.
SD	Standard deviation.
shRNA	Short hairpin RNA.
shT6KD	shRNA TRAF6 knockdown.
SKP2	S-phase kinase-associated protein 2.
SMI	Structure Model Index.
SPARTAN	Selective prostate AR targeting with ARN-509.
SRE	Skeletal-related events.
SSC-A	Side scatter area.
STRING	Search tool for retrieval of interacting genes/proteins.
TAK1	TGF-β-activated kinase 1.
TAMs	Tumour-associated macrophages.
TBS	Tris buffered saline.
TBST	TBS with Tween.
Tb.N	Trabecular number.
Tb.Sp	Trabecular separation.
Tb.Th	Trabecular thickness.
TCGA	The Cancer Genome Atlas.
TGF-β	Transforming growth factor betha.

TGF-Rβ	TGF-β receptor.
TGS	Tris-Glycine-SDS.
THP-1	Tamm-Horsfall protein 1.
TIMER	Tumour Immune Estimation Resource.
TLR4	Toll-like receptor 4.
TM	Trademark.
TNF	Tumour necrosis factor.
TNF-α	Tumour necrosis factor alpha.
TNFR	TNF receptor.
TNFRSF1A (TNF-αR)	TNFR superfamily member 1A.
TPM	Transcripts per million.
TP53	Tumour protein 53.
TRAcP	Tartrate resistant acid phosphatase.
TRAFs	TNF receptor-associated factors.
TRICOM	Triad of costimulatory molecules.
U	Units.
UCSC	University of California Santa Cruz.
UK	United Kingdom.
V	Volt.
vs.	Versus
v/v	Volume/volume.
Wnt	Wingless-related integration site.
Wnt3a	Wnt family member 3A.
w/v	Weight/volume.
1X	One time.
3D	Three dimensional.
4T1-Luc2	4T1-firefly luciferase gene.
5X	Five times.
10X	Ten times.
20X	Twenty times.
μA	Microampere.
μg	Microgram.
μl	Microliter.

μm	Micrometre.
μM	Micromolar.
ºC	Degree Celsius.
®	Registered trademark.

Abstract

Prostate cancer (PCa) is the second leading cause of male cancer deaths in the UK and the fifth worldwide. PCa has a 5-year survival rate of approximately 30% and preferentially spreads to the bone. Inflammation majorly contributes to the development and progression of PCa and also plays an important role in bone remodelling. TRAF6, a key component of the pro-inflammatory NFκB pathway, has been implicated in prostate cancer and bone cell activity; however, its role in prostate cancer bone metastasis has not been investigated. Here, *in silico* studies confirmed the involvement of TRAF6 in prostate cancer progression, and specifically TRAF6-DNA amplifications were observed in PCa patients with bone metastasis. Consistently, TRAF6 expression was higher in the osteolytic PC3 cell line when compared to the hormone-sensitive LNCaP cell line. Stable shRNA knockdown and pharmacological inhibition of TRAF6 using the verified 6877002 reduced human PC3 and DU145 cell viability, migration and invasion and their ability to support osteoclast formation and bone nodule formation *in vitro. In vivo*, however, intratibial injection of the TRAF6 knockdown in human PC3 cells failed to prevent osteolysis and, similarly, administration of 6877002 (20mg/kg/daily) failed to reduce PC3-induced bone loss in nude mice. Moreover, the novel FSAS3, congener of 6877002, exerted a significant reduction in the viability of a panel of prostate cancer cells and produced greater sensitivity in PC3 compared to PC3-TRAF6 knockdown cells. Mechanistically, FSAS3 decreased RANKL- and TNF-α-induced phosphorylation of IκB-α in prostate cancer cells and inhibited the pro-tumorigenic effects of M2 macrophages on the viability, migration and invasion of PC3 cells. The novel FSAS3 skewed macrophages to an anti-tumorigenic M1 phenotype and decreased the ability of a panel of PCa cells to promote osteoclast formation. Collectively, these findings suggest that targeting the TRAF/NFκB pathway is a promising treatment for skeletal-related events in advanced prostate cancer.

Graphical abstract
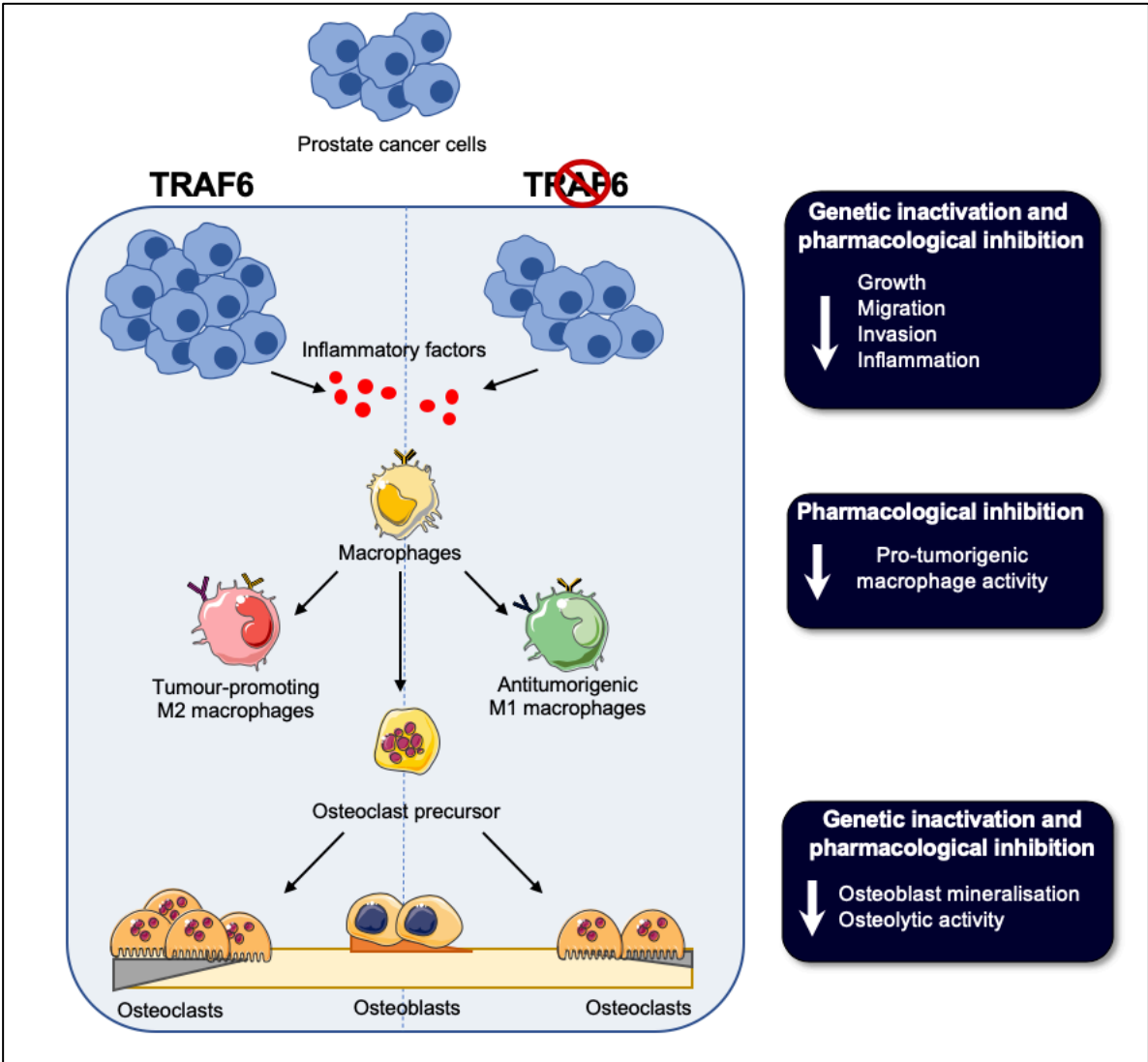
Figure 0.1. Schematic representation of the effects of knockdown and pharmacological inhibition of TRAF6 on prostate cancer cell – macrophage – osteoclast – osteoblast interactions. Knockdown and pharmacological inhibition of TRAF6 using the verified 6877002 and the novel FSAS3 on highly metastatic human prostate cancer cells decreased prostate cancer cell viability, migration, invasion and ability to influence osteoclast formation and osteoblast nodule formation. In addition, the novel FSAS3 altered macrophage commitment and decreased the pro-tumorigenic effects of M2 macrophages on prostate cancer cells *in vitro*.

Chapter 1. Introduction

1.1. Bone microenvironment

The bone is a dynamic environment that provides support and protection to soft tissues and organs in the body. There are two types of bone: cortical and trabecular bone (Shupp *et al.*, 2018). Cortical bone supports weight load and forms the outer layer of the skeleton, whereas trabecular bone encloses the bone marrow and undergoes bone remodelling at a higher rate (Shupp *et al.*, 2018; Zhang, 2019). Bone remodelling is the process by which mature or fractured bone is replaced by new bone and it is regulated by the balanced activity of bone-forming osteoblasts and bone-resorptive osteoclasts (Morrissey and Vessella, 2007; Ziaee *et al.*, 2015; Chen *et al.*, 2018). Osteoblasts derive from mesenchymal stem cells (Ziaee *et al.*, 2015) and account for 4-6% of total bone cells (Shupp *et al.*, 2018). The main function of osteoblasts is synthesizing and mineralising new bone matrix and supporting the formation of osteoclasts (Rucci, 2008). Osteoblasts are the precursors of another bone cell population called osteocytes, which account for 90-95% of cells in bone and support communication between bone-remodelling cells (Shupp *et al.*, 2018). Bone-resorptive osteoclasts are multinucleated cells derived from monocyte-macrophage hematopoietic lineage. Osteoclasts account for 1-4% of bone cells and their main function is to resorb bone organic matrix by secreting various enzymes including tartrate-resistant acid phosphatase (Shupp *et al.*, 2018; Zhang, 2019).

Communication between osteoblasts and osteoclasts during the bone remodelling cycle occurs via indirect or direct cell-cell contact (Chen *et al.*, 2018). The bone remodelling process begins with the recruitment of mature osteoclasts and their precursors to the bone surface, as a result of mechanical loading or via local factors and systemic hormones (Rucci, 2008). Subsequently, osteoclasts resorb bone and pre-osteoblasts proliferate, differentiate and mature to secrete soluble factors such as macrophage colony-stimulating factor (M-CSF) and express member-bound receptor activator for NFκB (RANK) ligand (RANKL) (Ziaee *et al.*, 2015). The activation of osteoblasts also plays an important role in modulating the osteoclastic

resorption phase of bone remodelling, as it leads to the production of the decoy receptor for RANKL, osteoprotegerin (OPG) (Rucci, 2008). The resorptive activity of osteoclasts leads to the release of various matrix-bound factors, peptides and enzymes including phosphatases and matrix metalloproteinases (MMPs), and growth factors like transforming growth factor Betha (TGF-β) and bone-morphogenetic proteins (BMPs). These factors in turn support osteoblast maturation and activity, which promotes bone formation (Rucci, 2008; Shupp *et al.*, 2018) (**Figure 1.1**). Numerous studies have implicated various signalling proteins and transcription factors in the regulation of osteoblast and osteoclast activity during bone remodelling. For example, Runx2, a transcriptional regulator of osteoblast differentiation from mesenchymal stem cells, has been shown to stimulate bone resorption by inducing RANKL expression and inhibiting OPG in osteoblasts. Conversely, enhanced expression of Runx2 by parathyroid hormone (PTH) has been shown to promote bone formation (Chen *et al.*, 2005; Rutkovskiy *et al.*, 2016).

Normal bone remodelling is the main determinant of bone mass and health, thus imbalanced bone remodelling is implicated in various skeletal disorders including osteoporosis, rheumatoid arthritis and Paget's disease (Feng and Mcdonald, 2011; Shupp *et al.*, 2018). In primary bone cancer and bone metastasis, systemic and local growth factors and cytokines produced by tumour cells disrupt the fine balance between bone resorption and bone formation (Jeong, Cho and Park, 2016; Zhang, 2019).
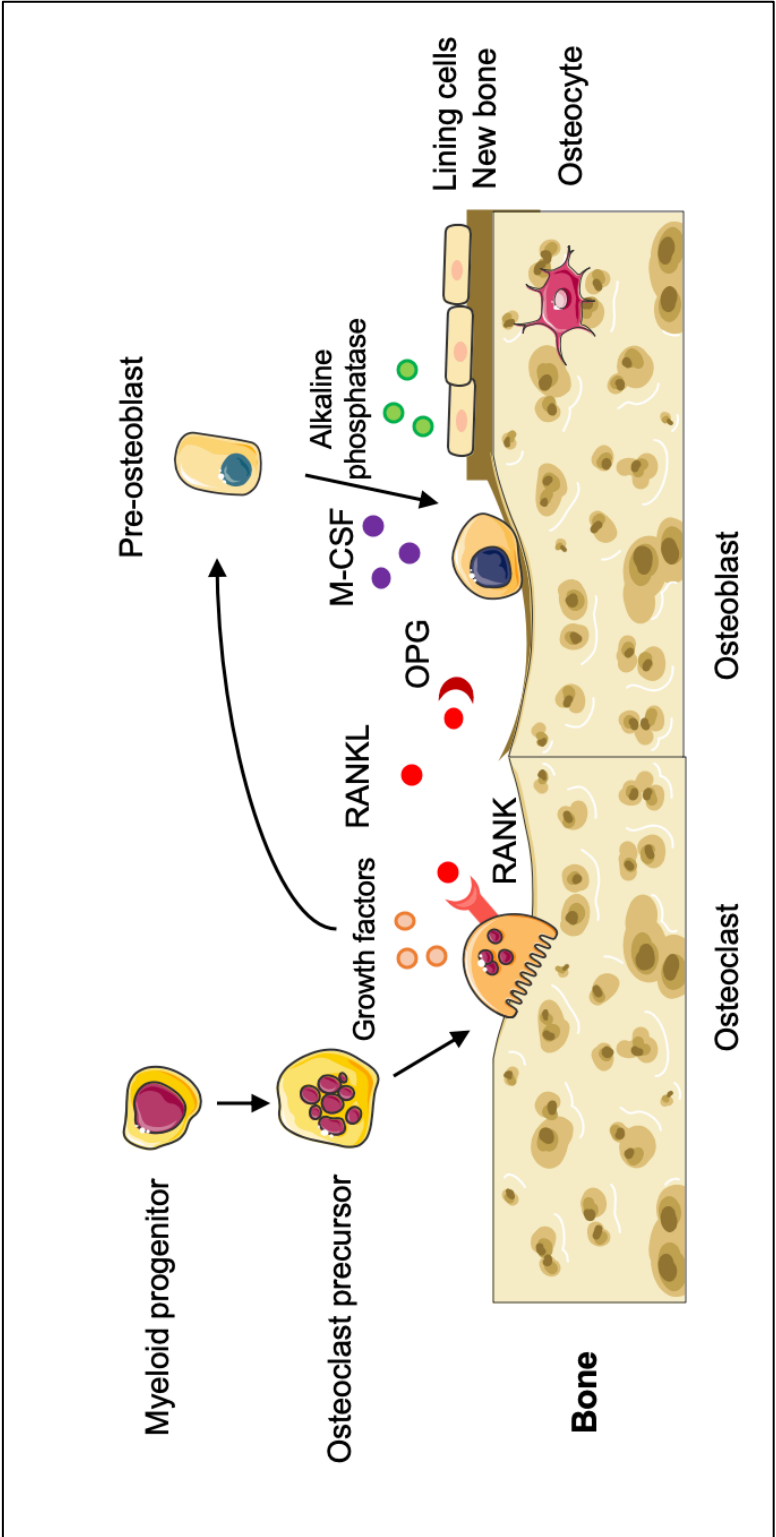
Figure 1.1. Schematic representation of the bone remodelling process. The bone remodelling process is orchestrated by bone-resorptive osteoclasts and bone-forming osteoblasts. Refer to text for details.

1.2.   Prostate cancer

Prostate cancer (PCa) is a slow-growing adenocarcinoma that develops in the prostate gland and is predominantly initiated by mutations in the glandular epithelial cells (Madan *et al.*, 2009; Leslei, Soon-Sutton and Siref, 2018). PCa is the second most commonly diagnosed cancer in men and the fifth leading cause of cancer death in men worldwide (**Figure 1.2**) (Torre *et al.*, 2015), and second in the United Kingdom (Yip *et al.*, 2015). Benign and localised prostate cancer has a 5-year survival rate of around 100%; however, if prostate cancer becomes metastatic, the 5-year survival rate reduces to approximately 30% (Kirby and Patel, 2009; American Cancer Society, 2018).
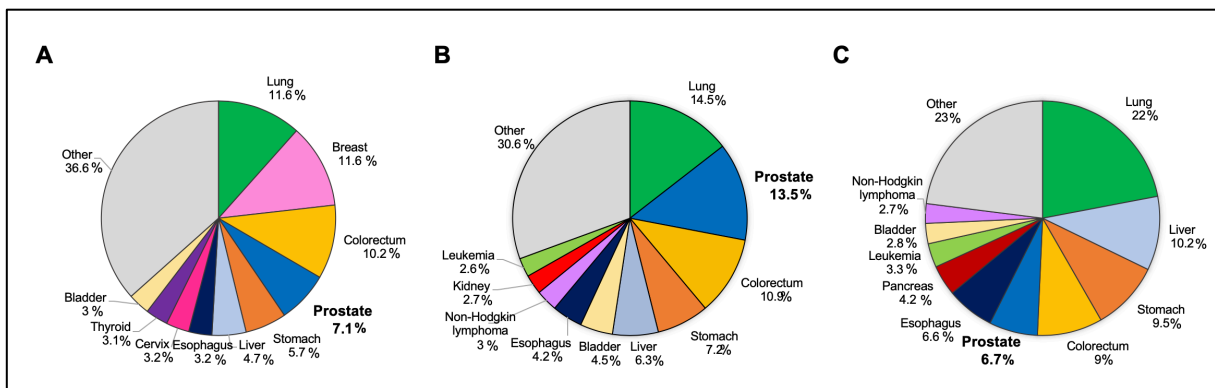
Figure 1.2. Distribution of cancer incidence and mortality worldwide (2018). Pie charts presenting the worldwide distribution of diagnosed cancer cases for (A) both sexes and (B) males and (C) cancer deaths in men (Bray *et al.*, 2018).

1.2.1. Diagnosis and risk factors

Prostate cancer is diagnosed by digital rectal examination in combination with the detection of high levels of the prostate-specific antigen (PSA) in the blood. The PSA test is also used for evaluating PCa at advanced stages and for monitoring treatments (Kirby and Patel, 2009). Even though the PSA test is the most commonly used method for early detection of PCa, it has many limitations (Stephan *et al.*, 2014). For example, 75% of positive tests are deemed to be false positives (Slatkoff *et al.*, 2011). Thus, histological examination of biopsies is used to assess the severity and progression of the disease in patients. The Gleason score is routinely used to categorize the aggressiveness and staging of the disease based on the sum of two prominent grades from 1 to 5, as shown in **Figure 1.3** (Kirby and Patel, 2009).

The D'Amico classification system for prostate cancer patients is based on PSA levels, Gleason score and clinical stage based on the tumour size or T stage (Cotter, Konety and Ordonez, 2016), allowing patients to be categorised as low-, moderate- or high-risk (**Table 1.1**).

The major risk factors of prostate cancer are age (over 65) (Center *et al.*, 2012) and ethnicity, with the highest rates of PCa observed amongst African Americans (Zeigler-Johnson *et al.*, 2008; Attard *et al.*, 2016). Lifestyle factors such as western diet, smoking, non-physical activity, obesity and family history are also considered to play a role in the development and progression of the disease (Kirby and Patel, 2009). In addition, genetic studies have shown that approximately 9% of cases have a genetic basis (Kirby and Patel, 2009). Genome-wide association studies (GWAS) showed that there are 76 single-nucleotide polymorphisms associated with prostate cancer risk (Eeles *et al.*, 2014). Among these genetic variations, alterations in the tumour suppressor genes *TP53, PTEN* and *RB1* are commonly detected at initial stages of the disease and in castration-resistant patient tumours (Hamid *et al.*, 2019). Furthermore, mutations in the tumour suppressor genes *BRCA1* and *BRCA2*, commonly

related with ovarian and breast cancer (Petrucelli, Daly and Feldman, 2010), have also been

identified in prostate cancer patients that have higher Gleason score and worse prognosis than

non-carriers of the mutation (Mitra *et al.*, 2008; Nyberg *et al.*, 2020).
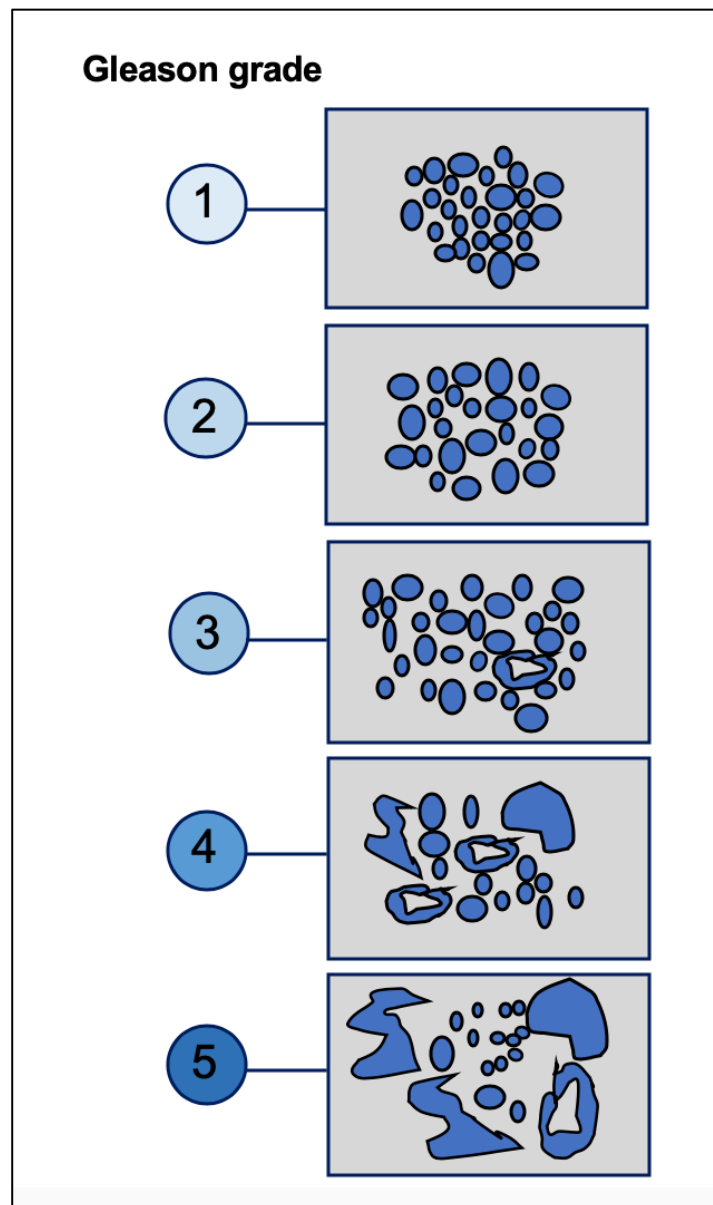
Figure 1.3. Gleason grading system. Progressive deterioration on glands from well-differentiated and healthy glands (grade 1) to larger, separated (grade 2) and disorganised (grade 3), until irregular gland anatomy (grade 4) becomes undifferentiated (grade 5) (Kirby and Patel, 2009).

Table 1.1. Description of D'Amico classification based on PSA levels, Gleason score and tumour size (Jang, Bianco and Scardino, 2007; Kirby and Patel, 2009; Chang *et al.*, 2014)**.**

Risk	Description	Primary tumour stage	
		T0 No evidence of primary tumour.	
		T1 Tumour not palpable or visible by imaging.	T1a
			T1b
Low	PSA ≤10 ng/ml Gleason score ≤6		T1c
		T2 Tumour confined within the prostate.	T2a
Intermediate	PSA 10-20 ng/ml Gleason score 7		T2b
High	PSA ≥20 ng/ml Gleason score ≥8		T2c
		T3 Tumour extends to the prostatic capsule	T3a
Very high	PSA ≥20 ng/ml Gleason score 8-10		T3b
		T4 Tumour invades adjacent organs.	

1.2.2. Pathophysiology

Prostate cancer is a heterogeneous malignancy with phenotypes ranging from non-aggressive to highly aggressive (Peisch *et al.*, 2017). Tumour growth begins in the prostate gland and is supported by several local and systemic factors such as growth factors, cytokines and chemokines, produced by both tumour and host cells in the tumour microenvironment (Jian Zhang, Patel and Pienta, 2010). PCa metastasis begins when a subset of tumour cells migrates to and proliferates at the lymph nodes, subsequently migrating to distant tissues (Wang *et al.*, 2018). Prostate cancer initiation, progression and metastasis is also enhanced by the reduction of anti-tumour immunity (Colotta *et al.*, 2009; Pecorino, 2016).

1.2.2.1. Immune surveillance

At early stages, diverse immune cell populations, including antigen presenting cells (APCs) and lymphocytes, infiltrate the tumour microenvironment (Pitt *et al.*, 2016). During tumour progression, cancer cells acquire the ability to evade immune surveillance (Allen, 2014) or limit immune responses. This is achieved by immunosuppressive factors such as TGF-β and interleukin 10 (IL-10) (Hanahan and Weinberg, 2011; Pecorino, 2016), which are secreted by immunosuppressive cells such as myeloid-derived suppressor cells (MDSCs) and regulatory T cells (Hanahan and Weinberg, 2011; Pitt *et al.*, 2016). Thus, these cells act as tumour-promoters and support cancer cell proliferation, angiogenesis, survival and metastasis (Hanahan and Weinberg, 2011; Weagel *et al.*, 2015; Pecorino, 2016).

Among the APCs, macrophages are one of the most abundant immune cell populations in solid tumours such as prostate cancer (Nielsen and Schmid, 2017; Lo and Lynch, 2018). These cells are derived from myeloid lineage (Weagel *et al.*, 2015), are known to contribute to inflammatory responses by production of cytokines (Pecorino, 2016) and promote the intravasation of cancer cells into the bloodstream (Nielsen and Schmid, 2017). In the tumour microenvironment, there are heterogeneous populations of macrophages that include tumour-

associated macrophages (TAMs), monocytic-like cells or myeloid-derived suppressor cells and tissue-resident macrophages, all of which are implicated in PCa (Dehne *et al.*, 2017).

In response to tumour- or host cell-derived signals, macrophages present in the tumour microenvironment change their phenotypical state from pro-inflammatory M1 to anti-inflammatory M2. The M1 phenotype is known as the classically activated state for macrophages, which exhibits anti-tumour properties that involve recognition and elimination of cancer cells through several mechanisms involving phagocytosis and cytotoxicity (Galli, Borregaard and Wynn, 2011; Weagel *et al.*, 2015). In contrast, M2 macrophages are classically anti-inflammatory, inefficient in antigen presentation and promoters of angiogenesis and tissue repair (Weagel *et al.*, 2015; Dehne *et al.*, 2017). Even though TAMs have markers of both phenotypes, they closely resemble M2 and thus promote tumorigenesis and cancer progression (Dehne *et al.*, 2017; Nielsen and Schmid, 2017).

TAMs recruitment and infiltration into the tumour site is used as a predictor for prostate cancer progression in patients after hormonal therapy (Nonomura *et al.*, 2011). Additionally, TAMs contribute to disease recurrence and resistance to treatments such as androgen deprivation therapy (Escamilla *et al.*, 2015). Lindholm and colleagues (2010) have demonstrated that co-culturing aggressive prostate cancer cell lines with monocyte-lineage cells increases the invasive ability of cancer cells (Lindholm *et al.*, 2010), thus implicating TAMs in the motility and metastatic behaviour of PCa cells (Lo and Lynch, 2018).

1.2.2.2. Chronic inflammation

Inflammation is an innate immune response against bacterial and viral infection, commonly found in the adult prostate (Sfanos and Marzo, 2014). Chronic inflammation is characterised by a continuous inflammatory response based on the production and accumulation of pro-inflammatory cytokines (Lawrence, 2009). A number of pro-inflammatory factors including IL-1β and tumour necrosis factor (TNF, particularly TNF-α) have been implicated in the initiation

and progression of prostate cancer (Zabaleta *et al.*, 2008). These pro-inflammatory mediators and host cells influence all aspects of prostate cancer cell behaviour as well as antitumor immunity. Pro-inflammatory cytokines are known to activate several signalling pathways involved in carcinogenesis (Pecorino, 2016) and induce epithelial-mesenchymal transition (EMT), consequently, enhancing tumour initiation and progression (Allen, 2014). Furthermore, pro-inflammatory factors have also been found to contribute to cellular stress and DNA damage, thereby affecting genetic instability and mutation rates (Xia, L., Shen, S., 2014; Pecorino, 2016). Cancer cells influence the immune system to their advantage by generating a pro-inflammatory tumour microenvironment that triggers tumour-promoting processes such as angiogenesis and infiltration of TAMs (Colotta *et al.*, 2009; Hanahan and Weinberg, 2011; Allen, 2014).

One of the key signalling transduction pathways found to play a role in the promotion of inflammation in the tumour microenvironment is Nuclear factor κ-light-chain-enhancer of activated B cells (NFκB) (Colotta *et al.*, 2009). Increased activation and expression of key components of both the canonical and non-canonical NFκB signalling in tumours have been linked to prostate cancer progression and bone metastasis (Renjie Jin *et al.*, 2013; Xia, L., Shen, S., 2014). Furthermore, NFκB-activating cytokines and chemokines have been reported to produce a pro-inflammatory response that promotes angiogenesis and, subsequently, metastasis (Pecorino, 2016). Furthermore, Mizutani and colleagues (2009) have reported that skeletal CC chemokine ligand 2 (CCL2) recruits monocytes, precursors of TAMs and osteoclasts, to the tumour site, thereby increasing cell growth and leading to bone metastasis in prostate cancer cells (Mizutani *et al.*, 2009). Additionally, TNF-α is another NFκB-activating cytokine that is produced by TAMs and tumour cells and has been found to influence prostate cancer cell motility and metastasis (Chen, 2013; Pecorino, 2016; Maolake *et al.*, 2018). In the skeleton, RANKL is a cytokine known to stimulate NFκB activation and, as a result, promotes osteoclast formation and bone resorption – two key processes implicated in prostate cancer-

associated bone disease (Chen *et al.*, 2006; Lamothe *et al.*, 2007). Cytokines involved in prostate cancer-induced osteoclastogenesis, include RANKL, IL-1β and TNF-α, which activate downstream signalling NFκB (Roato *et al.*, 2008). This is predominantly regulated by adaptor proteins called Tumour necrosis factor receptor-associated factors (TRAFs). TRAFs are a seven member family of intracellular molecules that contain a TRAF domain, except TRAF7, which mediates protein ubiquitination and allows interaction with several receptors and downstream proteins (Shi and Sun, 2018). TRAFs are required for several pathological processes linked to prostate cancer such as the immune response and inflammation (Wu and Arron, 2003).

1.2.2.3. Prostate cancer-related bone disease

Prostate cancer commonly metastasises to nearby and distant tissues. PCa metastasis is a multistep process that involves the escape of tumour cells through the lymphatic system or the bloodstream. This initiates prostate cancer cell growth and invasion to the lymph nodes initially and subsequently to distant organs such as the skeleton, where metastatic cells may remain dormant or proliferate into a solid tumour (Morrissey and Vessella, 2007; Mounier, Bouraoui and Rassart, 2014; Ziaee *et al.*, 2015), as shown in **Figure 1.4.** In order to migrate, prostate cancer cells undergo EMT, a process that plays an important role in both prostate cancer progression and treatment resistance. At metastatic sites such as bone, prostate cancer cells regain epithelial characteristics to anchor in surrounding tissues (Heerboth *et al.*, 2015; Montanari *et al.*, 2017), which promotes their growth and survival by influencing host cells in the tumour microenvironment. TAMs are among the heterogeneous population of inflammatory cells involved in the tumour microenvironment. The differentiation of TAMs, from a common myeloid precursor as bone-resorptive osteoclasts (Reinstein *et al.*, 2017), is triggered by tumour- and host-derived chemokines (Gollapudi *et al.*, 2013; Ziaee *et al.*, 2015; Buenrostro *et al.*, 2016). The pro-tumorigenic M2 phenotype has been implicated in advanced stages of prostate cancer (Erlandsson *et al.*, 2019), including bone metastasis (Mizutani *et al.*, 2009).
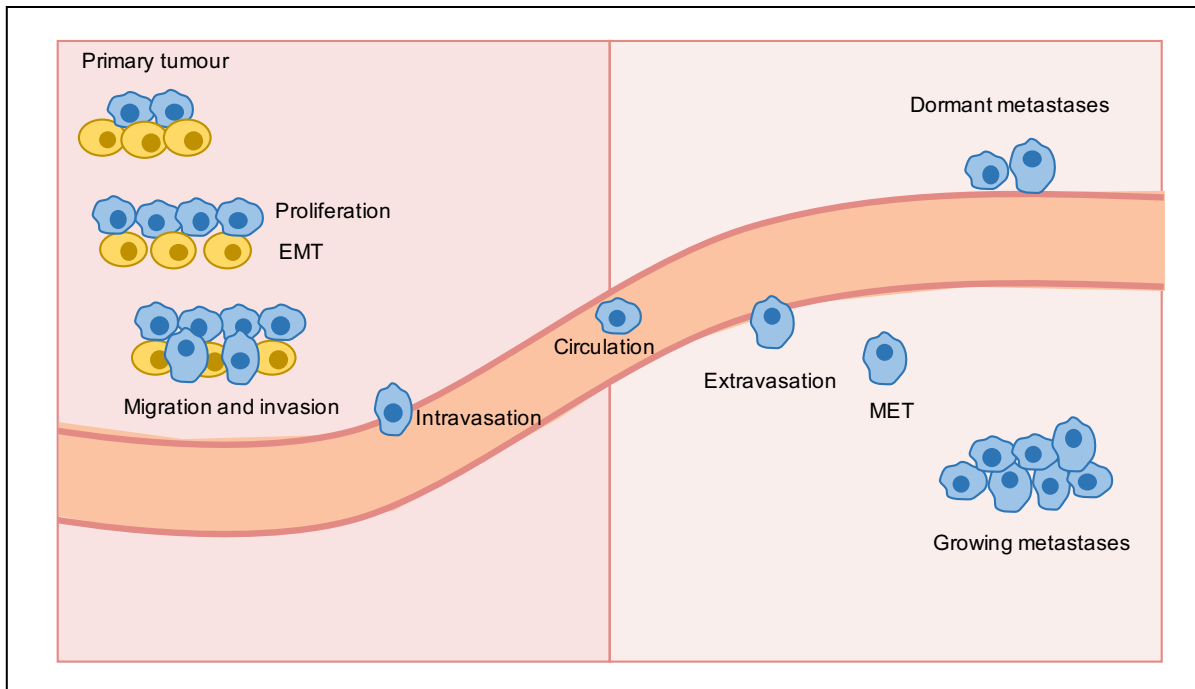
Figure 1.4. Prostate cancer progression and metastasis. Prostate cancer progression initiates with the escape of cancer cells to the bloodstream, travelling to distant sites to proliferate. Refer to text for details.

The most common metastatic sites for prostate cancer are the lymph nodes, liver, lung and bone (Morrissey and Vessella, 2007). Bone metastasis has the least favourable prognosis and an estimated 90% of patients with advanced prostate cancer die due to complications caused by this condition (Buenrostro *et al.*, 2016). Prostate cancer skeletal-related events (SRE) such as hypercalcemia and pathological fractures are known to negatively impact all aspects of patient life (Reinstein *et al.*, 2017).

The skeleton is considered an ideal environment for metastatic cancer cells due to its large surface area, heterogenous cellular compartment and richness in growth factors, cytokines, neovascularization factors, among other elements that support survival (Reinstein *et al.*, 2017; Shupp *et al.*, 2018). Prostate cancer cells in bone (osteotropic) disrupt the balance of bone remodelling process by interacting with a heterogeneous population of cells, particularly osteoclasts and osteoblasts (Morrissey and Vessella, 2007; Buenrostro *et al.*, 2016). In addition, prostate cancer cells secrete and express receptors for various bone and systemic

mediators including pro-inflammatory cytokines such as TNF-α, systemic hormones such as PTH-related protein (PTHrP) and bone-derived factors such as TGF-β (Jones *et al.*, 2006; Ziaee *et al.*, 2015; Buenrostro *et al.*, 2016). This deregulation of normal bone remodelling by cancer cells results in what is known as the "vicious cycle" (**Figure 1.5**), a process with excessive osteolytic bone resorption, enhanced osteoblastic differentiation and osteoclastogenesis, or both (Futakuchi, Fukamachi and Suzui, 2016). In addition to acting directly in osteoclasts and osteoblasts, tumour-derived pro-inflammatory mediators and growth factors have also been shown to stimulate the production of osteolytic factors such as RANKL, IL-1β and TNF-α by immune cells (Vela *et al.*, 2007; Zabaleta *et al.*, 2008; Walsh and Choi, 2014). Factors such as RANKL have shown to directly influence prostate cancer cell growth and EMT by modulating the expression of mesenchymal markers such as N-cadherin and vimentin (Odero-Marah *et al.*, 2008).
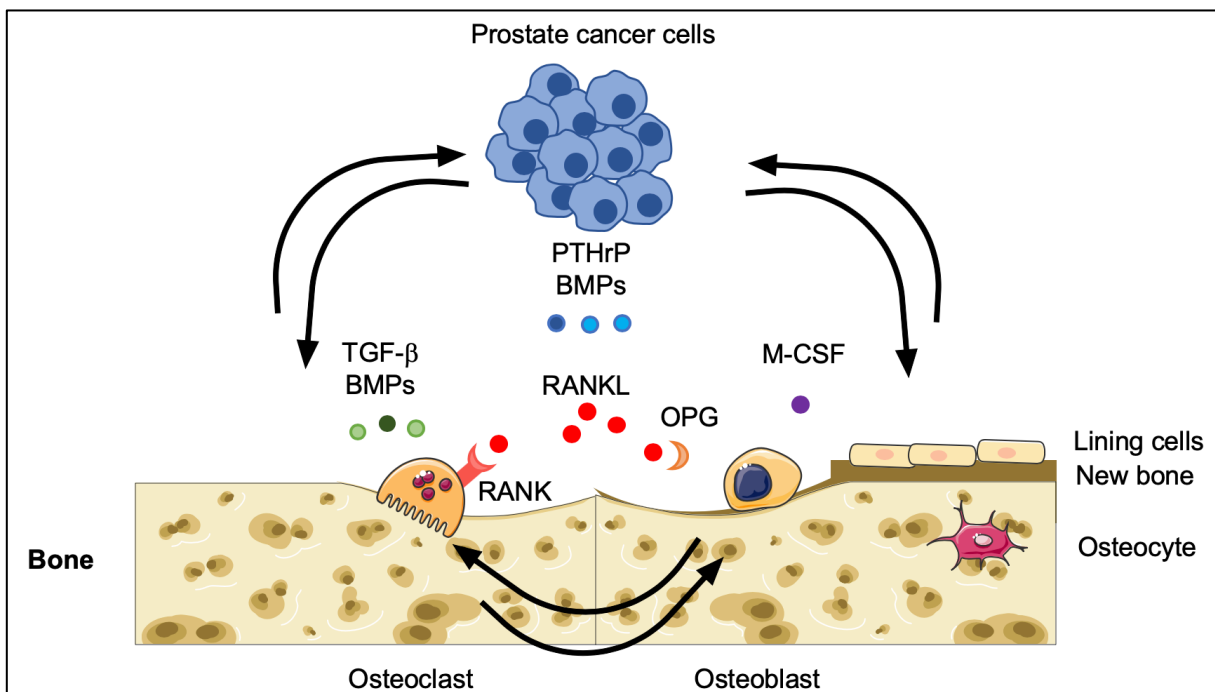
Figure 1.5. Vicious cycle of prostate cancer – bone-cell interactions. Cancer cells produce factors that induce osteoblasts to generate RANKL, which binds to the receptor RANK expressed in pre-osteoclasts, stimulating osteoclast formation and resorption. Additionally, osteoclasts release factors that maintain tumour activity. Refer to text for details.

Prostate cancer cells induce heterogenous bone lesions with a mixed osteoblastic and osteolytic nature; however, osteoblastic bone lesions are predominantly observed in prostate cancer patients with metastatic disease (Rafiei and S. V. Komarova, 2013; Zhang, 2019). Prostate cancer-related bone disease promotes bone resorption by expressing a higher ratio of OPG and RANKL compared to primary prostate cancer tumours or soft-tissue metastasis in prostate cancer patients (Brown *et al.*, 2001). This was confirmed by Chen *et al.* (2006), showing a significantly higher expression of RANKL, RANK and OPG in patients with metastatic prostate cancer and reported the highest OPG/RANKL ratio in bone from metastatic carcinoma tissue (Chen *et al.*, 2006). Furthermore, Jones and colleagues (2006) have shown that high levels of RANKL in the tumour microenvironment increase the migratory behaviour of an aggressive population of prostate cancer cells over-expressing RANK (Jones *et al.*, 2006). Thus, therapeutic agents that attenuate the action of pro-inflammatory mediators such as RANKL and TNF-α could be of value in the treatment of prostate cancer-associated bone disease.

1.2.3. Prostate cancer treatments

Treatments for prostate cancer are guided by risk assessments based on age, Gleason score, PSA levels and clinical stage of the patient (Attard *et al.*, 2016; Nevedomskaya, Baumgart and Haendler, 2018), as summarised in **Table 1.2**. For groups with small volume or low-to-moderate grade prostate cancer, the first therapeutic approach is active surveillance (Kirby and Patel, 2009). Active surveillance relies on monitoring PSA levels (<15 ng/ml), digital rectal examination, Magnetic Resonance Imaging (MRI) and prostate biopsies 6 to 12 months post-diagnosis (Attard *et al.*, 2016). For men of advanced age or with shorter life expectancy, the process of "watchful waiting", involving fewer tests rather than active surveillance, is recommended until signs of prostate cancer progression are observed (Kirby and Patel, 2009).

Table 1.2. Summarised description of prostate cancer treatments according to the stage (Kirby and Patel, 2009; Kantoff *et al.*, 2010; Fizazi *et al.*, 2011a; Kraft *et al.*, 2011; Parker *et al.*, 2013; James *et al.*, 2016; Chong, Oh and Liaw, 2018; Comiskey, Dallos and Drake, 2018; Vitkin *et al.*, 2019).

Treatment	Description	Benefits	Disadvantages
Standard approaches for localised tumours			
Active surveillance/watchful waiting (depending on age)	Assessing progress of disease with PSA levels, examinations and biopsies.	Requires frequent monitoring. Avoid overtreatment.	Risk of undetected prostate cancer progression.
Radical prostatectomy	Removal of prostate, vesicles and adjacent tissue.	Curative therapy for confined tumours.	Erectile dysfunction, urinary incontinence or recurrent disease.
Radiotherapy	DNA damage by high-energy radiation.	Alternative for patients with comorbidities or elderly.	Erectile dysfunction. Healthy cells are affected.
Treatments for advanced prostate cancer			
Androgen deprivation • LHRH agonists and antagonists • Apalutamide • Enzalutamide	Surgical or chemical castration using anti-androgen agents.	Lowers testosterone levels. Lower PSA levels. Improvement in survival when combined with radiotherapy.	Hormonal changes. Potential development of osteoporosis, cardiovascular disease, among others. Development of androgen-independence.
Therapies for metastatic prostate cancer			
Chemotherapy • Mitoxantrone • Taxanes Hormone therapy • Abiraterone	Drugs that induce apoptosis to cancer cells. Approach taken when hormone therapy is not working.	Efficient anti-tumour activities. Generally well-tolerated.	Causes side effects like gastrointestinal problems, skin reactions, among others.
Receptor-signalling inhibitors	Targeting dysregulated signalling pathways involved in cancer progression.	Efficient antiproliferative effects in prostate cancer cells.	Further exploration required.
Immunotherapies • Sipuleucel-T • Prostvac-VF • Ipilimumab	Activation of antigen-presenting cells for T cell recognition and elimination of cancer cells.	Personalised therapies. Prolonged survival. Increased efficiency in combination with other therapies.	Patient-specific. Costly and labour-intensive production. Reduced attraction of immune cells to tumour site.

Treatment	Description	Benefits	Disadvantages
Treatments for prostate cancer bone metastasis			
Radium-223 dichloride	Radioactive isotope binding to newly formed bone to emit high-energy alpha particles, cytotoxic to bone cancer cells.	Improvement in overall survival and pain relief.	Required validation and quantification of administered radiation.
Bisphosphonates • Zoledronic acid	Hydroxyapatite-binding pyrophosphate analogues that inhibit osteoclast differentiation and recruitment.	Prevention of skeletal-related events.	Phase II trials have shown more marked prevention of skeletal-related events with monoclonal antibody Denosumab.
Denosumab	Monoclonal antibody that binds to RANKL and disrupts osteoclast activity.	Better prevention of skeletal-related events compared to zoledronic acid.	FDA approved only for an specific cohort of patients (nonmetastatic and undergoing ADT therapy).

1.2.3.1. Therapies for localised prostate cancer

The recommended procedure for localised tumours is radical prostatectomy, which involves the removal of the prostate with associated vesicles and adjacent tissues (Kirby and Patel, 2009). The procedure has a significant benefit in the overall survival of high-risk patients (Cotter, Konety and Ordonez, 2016). D'Amico classification states that high-risk patients present PSA levels equal or beyond 20 ng/ml, Gleason score of ≥8 or clinical stage ≥T2c (Nazim and Abbas, 2015). Surgery leads to adverse effects such as erectile dysfunction or urinary incontinence (Kirby and Patel, 2009). Data suggests that 10 years after surgery, around 33% of patients develop recurrent disease (Cotter, Konety and Ordonez, 2016).

An alternative for patients unsuitable for surgery at a locally advanced stage is radiation (Attard *et al.*, 2016; Cotter, Konety and Ordonez, 2016). External beam radiotherapy is delivered by aiming high-energy rays to a targeted area as determined by MRI. Although high-energy radiation causes DNA damage in both tumour and healthy tissues, healthy cells can repair DNA damage more efficiently than cancer cells (Baskar *et al.*, 2012). External beam

radiotherapy alone or in combination with brachytherapy (administration of iodine-133 or palladium-103 transperineally emitting radiation) are offered depending on the patient (Attard *et al.*, 2016; Cotter, Konety and Ordonez, 2016). In addition, external beam radiotherapy has shown beneficial effects in sensitising cancer cells and promoting apoptosis when combined with antiandrogen therapy in high-risk prostate cancer patients (Kirby and Patel, 2009; Cotter, Konety and Ordonez, 2016).

Another alternative approach for localised prostate cancer is high-intensity focused ultrasound. This novel approach is based on focused tissue destruction and has shown promising results up to 10 years, with a biochemical survival rate of 61% in patients (Cotter, Konety and Ordonez, 2016).

Patients with limited life expectancy are prescribed hormonal treatment (Cotter, Konety and Ordonez, 2016). Given the major role that androgen receptor (AR) plays in normal prostate function and in the support of supporting prostate cancer progression (Jin *et al.*, 2008), androgen deprivation therapy (ADT) represents an effective approach to decrease androgen levels and, as a result, reduce prostate cancer cell growth. ADT is the standard treatment for locally advanced or metastatic prostate cancer (Sundararajan and Vogelzang, 2014), and is managed with surgical or chemical castration (Kirby and Patel, 2009). Surgical ADT consists of performing surgery to remove one or both testicles (orchidectomy), whereas chemical castration reduces androgen levels by blocking AR function using luteinizing hormone-releasing hormone (LHRH) agonists or antagonists. The mechanism of action of LHRH agonists relies on increasing testosterone levels followed by a desensitization of LHRH receptors. Hence, LHRH antagonists are used with the aim of reducing testosterone secretion (Kirby and Patel, 2009). Side effects of ADT include hot flashes, mood changes, osteoporosis, among others (Kirby and Patel, 2009). Unfortunately, most advanced prostate cancer patients treated with ADT eventually develop a castrate-resistant disease that arises from clonal

selection of androgen-independent surviving cells or ligand-independent activation of AR (Kirby and Patel, 2009; Sundararajan and Vogelzang, 2014).

Treatments approved by the US Food and Drug Administration (FDA) for non-metastatic castration-resistant prostate cancer patients involve the use of the non-steroidal antiandrogen apalutamide (ARN-509). ARN-509 binds with high affinity to the ligand-binding domain of AR and thus prevents its transcriptional activity, reducing PSA levels and improving metastasis-free survival according to the phase III clinical trial SPARTAN (Chong, Oh and Liaw, 2018). Additionally, oral administration of the AR antagonist darolutamide (ODM-201) has shown to increase in metastasis-free survival in phase III clinical trials (Moilanen *et al.*, 2015; Fizazi *et al.*, 2019).

1.2.3.2. Therapies for prostate cancer metastasis

Currently, there is no clinically effective therapy that halts prostate cancer progression to a metastatic stage (Kirby and Patel, 2009). Metastatic castration-resistant prostate cancer (mCRPC) develops during or after ADT (Hotte and Saad, 2010). Treatment with the inhibitor of DNA replication 5-fluorouracil and cyclophosphamide, the alkylating agent that inhibits protein synthesis, have produced palliative benefits in some mCRPC patients. Moreover, mitoxantrone was the first FDA-approved chemotherapeutic agent for the treatment of mCRPC. It was found to be an efficient palliative in combination with glucocorticoid prednisone; however, due to novel drugs with better efficacy, mitoxantrone is currently used as a third- or fourth-line drug (Sundararajan and Vogelzang, 2014).

Currently, the first-line treatment for mCRPC stage is abiraterone acetate (Zytiga®) (Dai, Heemers and Sharifi, 2017; Nevedomskaya, Baumgart and Haendler, 2018). Abiraterone acetate reduces androgen by inhibiting cytochrome P450 Family 17 Subfamily A Member 1 (CYP17A1), a critical enzyme for testosterone synthesis (De Bono *et al.*, 2011). Abiraterone acetate exerts anti-tumour activities alone and in combination with low-doses of glucocorticoids

such as prednisone, in castration-resistant prostate cancer patients previously treated with chemotherapy (Nevedomskaya, Baumgart and Haendler, 2018).

Taxane-based drugs inhibit prostate cancer cell division and transcriptional activation of AR by stabilising cellular microtubules and promoting apoptosis (Kroon *et al.*, 2016). Paclitaxel (Taxol) and its analogues docetaxel and cabazitaxel were approved by the FDA for mCRPC treatment in 2004 and 2010, respectively (Nevedomskaya, Baumgart and Haendler, 2018). Paclitaxel has been clinically used; however, its semisynthetic analogues are more commonly used for the treatment of prostate cancer (Kroon *et al.*, 2016). Treatment with docetaxel has shown promising results in providing a modest improvement in survival (James *et al.*, 2016). Although approximately half of the patients in treatment initially respond to docetaxel, they eventually develop resistance to these agents (Kroon *et al.*, 2016). In addition, cabazitaxel has been used as a second-line treatment for docetaxel-resistant patients, showing an improvement in survival (Sebastian de Bono *et al.*, 2010). Further chemotherapy after docetaxel treatment involves prescribing enzalutamide (MDV3100), a selective AR inhibitor that has shown to improve overall survival of prostate cancer patients (Kirby and Patel, 2009; Cotter, Konety and Ordonez, 2016).

Due to the intratumour heterogeneity and acquired resistance to standard treatments, other approaches, alone or in combination, are required to block multiple downstream proteins related to prostate cancer progression (James *et al.*, 2016). This synergistic approach may lead to the development of more effective treatments. As alterations in the DNA-damage response have been linked to prostate cancer progression, targeting DNA repair represents another approach for treating prostate cancer. Inhibition of Poly (ADP-ribose) polymerase (PARP), a family of proteins involved in DNA repair, with Olaparib in phase II clinical trials in mCRPC patients reduced PSA levels in patients (Mateo *et al.*, 2015; Zhang *et al.*, 2020).

Aberrant histone modifications are also implicated in the development of prostate cancer (Lu *et al.*, 2015). Enhancer of zeste homolog 2 (EZH2) is a catalytic subunit that silences transcription via histone methylation and is a co-activator of androgen receptor (Xu *et al.*, 2012; Nevedomskaya, Baumgart and Haendler, 2018). As overexpression of EZH2 has been correlated with castration-resistant prostate cancer, EZH2 inhibitors have been used as a treatment, and have produced efficient antiproliferative effects in prostate cancer cells (Nevedomskaya, Baumgart and Haendler, 2018).

Deregulation of various signal transduction pathways have also been detected in prostate cancer cells (Narayan Biswal *et al.*, 2017). Negative prostate cancer patient outcomes are associated with hyperactive Phosphoinositide 3-kinase (PI3K) signalling, which is regulated by the tumour suppressor *PTEN* (Rubin and Demichelis, 2018). Loss of *PTEN* is commonly found in prostate cancer and leads to aberrant Akt activation (Hamidi *et al.*, 2017), thus Akt blockade is a promising PCa treatment (Yap *et al.*, 2016; Nevedomskaya, Baumgart and Haendler, 2018). The small-molecule inhibitor Ipatasertib (GDC-0068) is a selective ATP-competitive compound of the three isoforms of Akt. GDC-0068 in combination with abiraterone is in phase II trials and has shown synergistic effects, increasing anti-tumour activity compared to treatment with abiraterone alone in mCRPC patients (De Bono *et al.*, 2019).

Furthermore, compounds targeting the pro-inflammatory NFκB pathway have shown promise in the treatment of prostate cancer. Among these, Bortezomib (Velcade®), an inhibitor of the 26S proteasome and of IκB-α degradation that reduces cell proliferation and induces apoptosis in prostate cancer cells (Zheng, Wang and Wei, 2015). Bortezomib was initially approved by the FDA for the treatment of multiple myeloma (Zheng, Wang and Wei, 2015), and has been tested in prostate cancer patients. As determined by phase II trials performed in early stage prostate cancer patients, weekly doses of Bortezomib for 3 months significantly decreased the

rise of PSA levels (Kraft *et al.*, 2011). However, in patients with mCRPC in phase II trials, bortezomib had no significant anti-tumour effect (Morris *et al.*, 2007).

The anti-malaria drug Quinacrine causes prostate cancer cell apoptosis by inhibiting NFκB activation and inducing p53 function (Gurova *et al.*, 2005). Quinacrine has enhanced the anti-tumour effects of paclitaxel in xenograft models; however, it has not been tested in human clinical trials (Oien *et al.*, 2019). Another agent that inhibits NFκB activation in prostate cancer cells is the statin Simvastatin. Simvastatin inhibits phosphorylation and translocation of p65 by blocking degradation of IκB-α (Tu *et al.*, 2017). Kang and colleagues (2017) showed that Simvastatin decreased castration-resistant prostate cancer cell viability alone and in combination with caffeic acid phenethyl ester (CAPE), a bioactive component that also inhibits NFκB. This combinational therapy reduces the metastatic abilities of prostate cancer and synergistically decreases prostate cancer cell growth (Kang *et al.*, 2017).

From the protein kinase C (PKC) family of kinases, PKCε is overexpressed in prostate cancer and genetic inactivation of PKCε inhibits the development of prostate cancer tumours in transgenic adenocarcinoma mice (Garg *et al.*, 2012; Staal and Beyaert, 2018). However, PKC as a target has not been explored for the clinical treatment of prostate cancer (Jäntti *et al.*, 2018).

1.2.3.3. Immunotherapies for prostate cancer metastasis

As a slow growing disease, prostate cancer is a suitable candidate for a targeted immune response and, as a low-volume tumour, is ideal for vaccine treatments (Madan *et al.*, 2009). Sipuleucel-T (Provenge®) is a therapeutic vaccine that was developed for stimulating a T cell anti-tumour immune response (Cheever and Higano, 2011). As a personalised treatment, APCs are extracted from mononuclear cells taken from the peripheral blood of patients. These mononuclear APCs are activated *ex vivo* with the recombinant protein PA2024, composed of the antigen prostatic acid phosphatase (PAP) fused with the immune cell activator granulocyte-

macrophage colony-stimulating factor (GM-CSF). This generates PAP-specific T cells for the recognition and elimination of PAP-positive prostate cancer cells (Kantoff *et al.*, 2010). The efficacy of Sipuleucel-T varies from dose to dose and each dose progressively increases APC activation and PAP-specificity of T cells (Cheever and Higano, 2011). Sipuleucel-T was the first antigen-specific immunotherapy approved as a cancer treatment by the FDA in 2010, as it prolonged the survival of mCRPC patients in three phase III trials (Small *et al.*, 2006; Higano *et al.*, 2009; Drake, 2010; Kantoff *et al.*, 2010).

The success of Sipuleucel-T led to the development of other novel immunotherapies for prostate cancer treatment (Kittai, Meshikhes and Aragon-Ching, 2014). Prostvac-VF is a vaccine that uses two recombinant viral vectors encoding PSA and 3 molecules named TRICOM (ICAM-1, B7.1, LFA3) to stimulate T cell immune response (Yap *et al.*, 2016; Comiskey, Dallos and Drake, 2018). Prostvac-VF infects and increases the interaction of antigen-presenting cells with T cells, which in turn triggers tumour cell destruction. Phase II clinical trials have shown Prostvac-VF increased overall survival among mCRPC patients and its efficacy can be improved when given in combination with radiation or hormonal manipulation (Madan *et al.*, 2009).

Recently, the inhibitor of cytotoxic T lymphocyte-associated protein 4 (CTLA-4) Ipilimumab has been used for the treatment of mCRPC. Ipilimumab is an immune checkpoint inhibitor that enhances a T cell anti-tumour response and was approved by the FDA for treating metastatic melanoma. In mCRPC patients, Ipilimumab exerts anti-tumour activity and improves progression-free survival; however, it has failed to improve overall survival (Beer *et al.*, 2017; Comiskey, Dallos and Drake, 2018).

1.2.3.1. Treatments for prostate cancer bone metastasis

Current treatments for prostate cancer bone metastasis are purely palliative (Kirby and Patel, 2009). Radium-223 dichloride is a radioactive isotope that mimics calcium and binds to newly

formed bone. Radium-223 emits high-energy alpha particles of short range that induce DNA damage and cell death (Parker *et al.*, 2013; Nevedomskaya, Baumgart and Haendler, 2018). Phase III clinical trials have shown that Radium-223 improves overall survival and reduces bone pain in patients with mCRPC bone metastases (Parker *et al.*, 2013). However, further studies are required to determine the safety of radiation in these patients (Vapiwala and Glatstein, 2013).

Bisphosphonates are hydroxyapatite-binding pyrophosphates that inhibit osteoclast formation and activity (Polascik and Mouraviev, 2008; Reinstein *et al.*, 2017). Nitrogen- and non-nitrogen-containing bisphosphonates bind to bone surfaces with different degrees of efficacy, and are internalised by osteoclasts during bone resorption. Bisphosphonates induce apoptosis and directly inhibit their ability to resorb bone (Polascik and Mouraviev, 2008). Currently, the nitrogen-containing bisphosphonate zoledronic acid (Zometa®) is the only bisphosphonate that efficiently reduces skeletal-related events associated with mCRPC bone metastases in patients (Polascik and Mouraviev, 2008; Cotter, Konety and Ordonez, 2016).

Denosumab is a monoclonal antibody that binds and blocks RANKL expressed on the surface of osteoblasts and prostate cancer cells, thereby inhibiting osteoclast formation (Reinstein *et al.*, 2017). Denosumab is currently being tested in advanced prostate cancer patients (Fizazi *et al.*, 2011b). In a phase III trial, denosumab showed a modest improvement in metastasis-free survival in patients with non-metastatic CRPC (Smith *et al.*, 2012). Interestingly, another phase III study in non-metastatic castration-resistant prostate cancer patients demonstrated that denosumab was more effective in reducing skeletal-related events compared to zoledronic acid (Fizazi *et al.*, 2011b; Cotter, Konety and Ordonez, 2016). However, the FDA stated that treatment with denosumab did not show a significant benefit to be approved for this cohort of patients (Paller, Carducci and Philips, 2012).

1.3. The TRAF6/NFκB signalling pathway

The pro-inflammatory NFκB pathway has been implicated in prostate cancer (Zhang *et al.*, 2009). The constitutive activation and the expression of a number of key components of the canonical and non-canonical NFκB pathway have been correlated with increased AR expression and support its function even in androgen-independent cells (Jin *et al.*, 2008; L. Zhang *et al.*, 2009). Jin and colleagues (2015) have determined the association between NFκB activation and AR by studying the effects of IKKβ knockdown cells and the use of the NFκB inhibitor Bortezomib in prostate cancer models. These studies revealed a decrease in AR expression, tumour growth and restoration of responsiveness to anti-androgen treatments in castration-resistant prostate cancer xenografts (Jin *et al.*, 2015), in agreement with other work reported by Nadiminty and colleagues (Nadiminty *et al.*, 2013). Elevated nuclear accumulation of NFκB p65 has been observed in various prostate cancer metastasis including bone metastasis (R. Jin *et al.*, 2013). Thus, treatment with NFκB inhibitors such as Parthenolide has reduced the growth and progression of castration-resistant tumours, lowered PSA levels and significantly inhibited AR expression in a prostate cancer xenograft model (Jin *et al.*, 2015).

Moreover, elevated expression of TRAFs, key components of NFκB signalling, have also been detected in prostate cancer tissues (S. Huang *et al.*, 2017). TRAFs are adaptor proteins (TRAF1-7) implicated in many physiological and pathophysiological activities, including inflammation, immunity, cancer and bone remodelling (Xie, 2013; Zotti, Scudiero and Vito, 2016). TRAFs function downstream of multiple receptors for pro-inflammatory factors including RANKL, IL-1β and TNF-α (Oeckinghaus, Hayden and Ghosh, 2011) and, particularly TRAF2, TRAF5 and TRAF6 are essential for the regulation of bone remodelling (Darnay *et al.*, 2013). TRAF6/NF-κB signalling is initiated by the interaction of ligands, such as cluster of differentiation 40 (CD40) ligand (CD40L) or RANKL, with their respective receptors. This initiates the recruitment of TRAF6 to the membrane, followed by the binding of various adaptor proteins, such as TAK1 protein from the IKK family, to form a complex. This in turn leads to

the phosphorylation and subsequent ubiquitination and degradation of IκB-α, liberating p50/p65 to translocate to the nucleus where it binds to DNA, and activates the release of various pro-inflammatory mediators (**Figure 1.6**). Unlike other TRAFs, TRAF6 has a unique binding site for RANK and CD40 receptor (Lomaga *et al.*, 1999; Darnay *et al.*, 2013; Jansen *et al.*, 2016) and like TRAF2, it has a E3 ubiquitin ligase activity in immune and non-immune cells (Walsh, Lee and Choi, 2015).
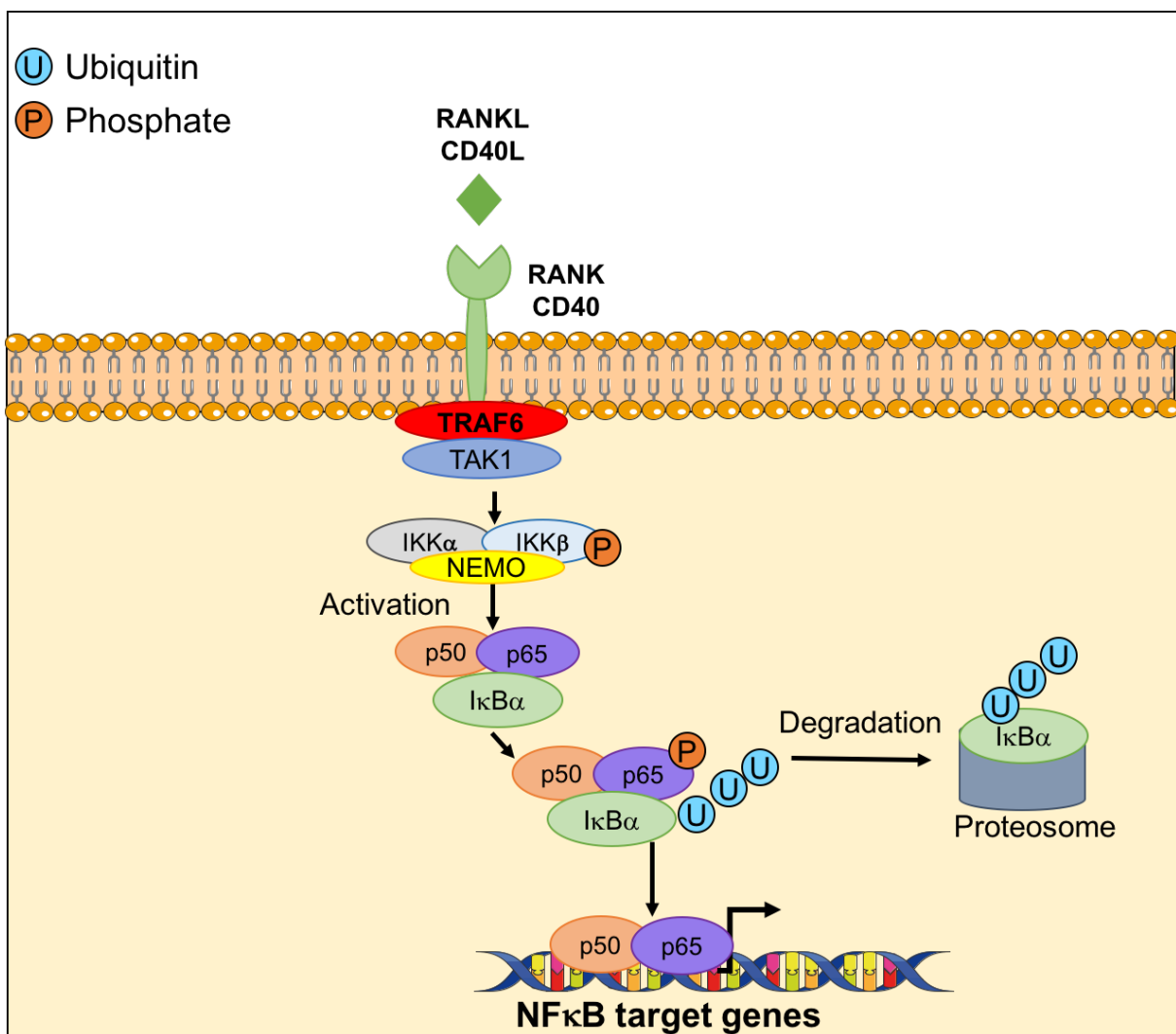
Figure 1.6. The TRAF6/ NF-κB pathway. The TRAF6/NF-κB pathway is initiated by interaction of ligands causing the recruitment of TRAF6 the membrane, followed by the formation of complexes and subsequent release of p50/p65 to bind DNA. Refer to text for details.

1.3.1.   Role of TRAF6 in prostate cancer progression

Current evidence shows that increased expression of several TRAFs leads to the initiation and progression of various cancers (Xie, 2013; Zotti, Scudiero and Vito, 2016). Among the seven known TRAF proteins, TRAF2, TRAF4 and TRAF6 have been linked to prostate cancer (Wei, Ruan, *et al.*, 2017; Singh *et al.*, 2018; Aripaka *et al.*, 2019). Upregulation of TRAF2 is observed in prostate cancer bone metastasis and is associated with a high Gleason scores in patients (Wei, Liang, *et al.*, 2017; Wei, Ruan, *et al.*, 2017). TRAF4 is also highly expressed in prostate cancer and its knockdown in highly metastatic prostate cancer cells reduced cell migration and invasion, and diminished the development of bone metastasis in mice (Singh *et al.*, 2018).

TRAF6 plays a key role in all aspects of prostate cancer. Sundar and colleagues *(*2015) identified that TGF-β-induced activation of TRAF6 promoted the invasion of a highly metastatic clone in an androgen-insensitive human PC3 (PC3U) cell line and androgen-sensitive LNCaP cells (Gudey *et al.,* 2014; Sundar *et al.*, 2015). Consistent with this, Yang and collaborators (2009) showed that TRAF6 knockdown in human PC3 prostate cancer cells decreased their tumorigenic potential in immunocompromised mice compared to control (Yang *et al.*, 2009). Furthermore, a recent study by Aripaka and colleagues (2019) showed that TRAF6 is a key regulator of Wnt3a signalling in the promotion of prostate cancer progression (Aripaka *et al.*, 2019). Overall, these studies indicate that TRAF6 is an attractive therapeutic target for the treatment of prostate cancer.

1.3.2.   Role of TRAF6 in immunity

The NFκB signal transduction pathway is a key orchestrator of innate immunity (Aggarwal, 2004; Staal and Beyaert, 2018). NFκB-activating cytokines such as TNF-α and TNFR receptors such as CD40 are expressed by a variety of immune cells (Jansen *et al.*, 2016), and are known to play crucial roles in regulating immune-cell activation and the inflammatory response (Van Den Berg *et al.*, 2015). Compared to other TRAFs, TRAF6 has a specific

binding site to interact directly with the receptors CD40 and RANK (Antonios Chatzigeorgiou *et al.*, 2014). These receptors are key for regulating bone cell activity, and other cells of the hematopoietic lineage including macrophages, dendritic cells and B cells (Pearson, Castle and Kehry, 2001; Kobayashi *et al.*, 2003; Zhuang *et al.*, 2017). TRAF6-deficiency in T cells reduces their immune and anti-tumour capabilities (Ni *et al.*, 2019). In fact, the novel, small-molecule TRAF6 inhibitor 6877002 and its analogue 6860766 blocked CD40-TRAF6 binding and decreased inflammation and immune cell infiltration in mice (Van Den Berg *et al.*, 2015).

1.3.3.   Role of TRAF6 in bone remodelling

Prostate cancer in bone causes both osteolytic and osteoblastic lesions. Bone-seeking prostate cancer cells produce various cytokines and growth factors that, together with bone-derived factors, successfully colonize the bone, enhance their ability to grow and cause osteolysis (Garraway, 2013). Several studies indicate that the NFκB pathway plays a direct and indirect role in the regulation of this process (R. Jin *et al.*, 2015; Ren *et al.*, 2017; S. Huang *et al.*, 2017).

Among the TRAF protein family, TRAF6 has a specific binding site for RANK (Garraway, 2013), the most important regulator of osteoclast formation and survival (Gohda *et al.*, 2005; Chang *et al.*, 2009). TRAF6-knockout mice present a severe phenotype, with lethality within two weeks of birth. These mice exhibit high osteopetrosis due to the absence of osteoclasts, and having a significantly reduced response to pro-inflammatory cytokines including CD40L, IL-1β, RANKL and LPS (Lomaga *et al.*, 1999). Additionally, Naito and colleagues (1999) found that TRAF6-knockout mice had defective lymph node organogenesis, reduced number of immature B cells and restricted osteoclast differentiation, confirming the crucial roles of TRAF6 in both immunity and bone remodelling (Naito *et al.*, 1999).

1.4. TRAF6 as a potential therapeutic target in prostate cancer-associated bone disease

The involvement of several TRAFs in prostate cancer has been well-studied (Wei, Ruan, *et al.*, 2017; Singh *et al.*, 2018; Aripaka *et al.*, 2019). Despite the important role of TRAF6 in regulating bone remodelling in prostate cancer, very few selective TRAF6 inhibitors have been developed (Jian Zhang, Patel and Pienta, 2010; Zarzycka *et al.*, 2015). Surprisingly, the effects of cancer- and host-specific inhibition of TRAF6 have not been investigated. Previous studies have shown that 6877002 reduced macrophage activation (Seijkens *et al.*, 2018) by a mechanism dependent at least in part via inhibition of TRAF6-mediated increase of CCL2. CCL2 is known to be produced by different cell types in the bone marrow including macrophages, osteoclasts and osteoblasts (Mizutani *et al.*, 2009; J. Zhang, Patel and Pienta, 2010). Working with our collaborators at the Universities of Munich and Amsterdam, we first tested the efficacy of the selective small molecule inhibitor of TRAF6 (6877002) in models of inflammation- and cancer-associated bone disease. 6877002 reduced CD40 signalling via TRAF6 inhibition (A. Chatzigeorgiou *et al.*, 2014) and work performed in our laboratories showed that it inhibited RANKL-induced NFκB activation and osteoclast formation *in vitro* (Bishop *et al.*, 2020). Furthermore, 6877002 reduced the arthritic score and swelling in a mouse model of collagen-induced arthritis (Marino, Bishop and Idris, unpublished work).

Recently, we showed that 6877002 reduced soft tissue and bone metastases in immunocompetent mice following intracardiac injection of mouse 4T1-Luc2 cells. Interestingly, administration of 6877002 in combination with the chemotherapeutic agent Docetaxel, but neither compound alone, reduced osteolytic bone damage in mice bearing 4T1-Luc2 cells (Bishop *et al.*, 2020). Collectively, these data suggest that TRAF6 inhibitors such as 6877002, alone or in combination with conventional chemotherapy, show promise for the treatment of osteolytic bone metastasis. Further studies are required to investigate the effects of pharmacological inhibition and genetic inactivation of TRAF6 during osteoblastic bone

metastasis, such as in prostate cancer. TRAF6, NFκB and overexpression of CCL2 in the highly metastatic human prostate cancer cell line PC3, is known to promote prostate cancer progression (Mizutani *et al.*, 2009; Yazlovitskaya *et al.*, 2015). Despite these findings, the role of TRAF6 in prostate cancer bone metastasis, osteolysis, osteoblastic and osteoclastic changes remains unknown.

1.5. Aims of the study

In this project, we hypothesized that TRAF6 inhibition using molecular biology and pharmacological approaches disrupts prostate cancer–macrophage interactions and reduces prostate cancer-associated bone cell activity and osteolysis. To explore this hypothesis, I investigated the following aims:

1. Assess the expression and biological activity of TRAF1 to 7 in the normal prostate, primary tumour and metastatic prostate cancer and correlate this data with clinical outcomes.

2. Test the effects of genetic knockdown and pharmacological inhibition of TRAF6 using the verified CD40-TRAF6 inhibitor 6877002 on:

- The activation of NFκB signalling in prostate cancer cells and macrophages.

- The viability of a panel of human and mouse prostate cancer cells *in vitro.*

- The motility, namely migration and invasion, of the highly metastatic human PC3 and DU145 prostate cancer cells *in vitro.*

- The ability of the human PC3 prostate cancer cells to influence:

    o Osteoclast formation *in vitro* and osteolysis *in vivo.*

    o Osteoblast differentiation *in vitro.*

3. Test the effects of pharmacological inhibition at the TRAF level using FSAS3, the novel structural congener of 6877002, on:

- The activation of NFκB signalling in prostate cancer cells and macrophages.

- The viability of a panel of human and mouse prostate cancer cells *in vitro.*

- The motility, namely migration and invasion, of the highly metastatic human PC3 and mouse RM1-BM prostate cancer cells *in vitro.*

- The ability of the human PC3 prostate cancer cells to influence

    o Macrophage viability *in vitro.*

- o Osteoclast formation *in vitro.*

- The ability of Mø, M1 and M2 macrophage subtypes to influence the proliferation, migration and invasion of the highly metastatic human PC3 and mouse RM1-BM.

Chapter 2. Materials and Methods

2.1.   Preparation of compounds tested

The verified small-molecule inhibitor of CD40-TRAF6 6877002 was purchased from Abcam (No. ab146829). The novel congeners of 6877002, namely FSAS1-6, were synthesized by the team of Professor Anna Sparatore (University of Milan, Italy). The compounds were dissolved in dimethyl sulfoxide (DMSO; Honeywell, No. D5879) at a concentration of 100 mM, according to the manufacturer's instructions, and stored at 4 ºC.

2.2.   General tissue culture conditions

Cell culture was carried out in a Class II laminar flow cabinet. The cabinet and all items were sterilised with 70% (v/v) Industrial Methylated Spirits before use. All solutions used on cells were warmed at 37ºC prior to use.

Cells were kept in an atmosphere supplied with 5% CO_2 and 95% humidity at 37ºC and cell confluency was assessed by phase-contrast microscopy.

2.2.4.   Cell maintenance

Murine macrophage-like cell line RAW 264.7 were kindly provided by Professor Endre Kiss-Toth (University of Sheffield, UK). RAW 264.7 cells (passage number<15) were cultured in 15-20 ml standard media using Dulbecco's Modified Eagle Medium (DMEM) with GlutaMAX™ (Thermo Fisher Scientific, No. 61965026) supplemented with 10% Fetal Bovine Serum (FBS; Thermo Fisher Scientific, No. 10270106) and 100 U/ml penicillin with 100 µg/ml streptomycin (Thermo Fisher Scientific, No. 15140-122) in 75 cm^2 flasks (Thermo Fisher Scientific, No. 156499) and passaged every 2-3 days by removing 15 ml of media, scrapping cells from the flask and adding 2-4 ml of the cell suspension to a new 75 cm^2 flask with fresh standard DMEM media.

Human THP-1 monocytic cells were kindly provided by Yvonne Stephenson (University of Sheffield, UK). THP-1 cells (passage number<20) were cultured in 75 cm^2 flasks in an upright position with 15-20 ml standard Roswell Park Memorial Institute (RPMI) 1640 medium (Thermo

Fisher Scientific, No. 11875093) supplemented with 10% FBS, 50 μM β-mercaptoethanol (Gibco, No. 31350-010) and 100 U/ml penicillin with 100 μg/ml streptomycin. Cultures were maintained by replacement or addition of fresh standard RPMI media (Tedesco *et al.*, 2018).

Human osteoblast-like Saos-2 cells, DU145, PC3, LNCaP and its derivative C42-B4 prostate cancer cell lines were kindly provided by Dr. Ning Wang, Dr. Colby Eaton, Dr. Allison Gartland and Anne Fowles (University of Sheffield, UK). The murine Ras+Myc transformed cells-Bone metastatic (RM1-BM) cell line, derived from RM1 to generate a metastatic model of prostate cancer (Power *et al.*, 2009), were a kind gift from the laboratory of Dr. Martina Rauner and Professor Lorenz Hofbauer (University of Dresden, Germany). All cells (passage number<30) were cultured in complete DMEM media. Cells were maintained in 75 cm^2 flasks and passaged every 2-3 days with a confluency of 60-80%, by removing the culture medium, washing cells with PBS 1X (Thermo Fisher Scientific, No. 10010023) and treating with 1X Trypsin-ethylenediaminetetracetic acid (EDTA) (Sigma-Aldrich, No. T4174). After a 5-minute incubation at 37ºC in a tissue culture cabinet (supplied with 5% CO_2 and 95% humidity), trypsin was neutralized with twice the volume added by using standard media. The cell suspension was centrifuged at 300g for 5 minutes, the supernatant was discarded and the cell pellet was suspended in 1 ml of complete media. A small volume of cell suspension was added to an equal volume of trypan blue (50% v/v; Sigma-Aldrich, No. T8154) and counted using a Neubauer Haemocytometer (Fisher Scientific, No. 15153675). The desired volume of the cell suspension was then added to a new 75 cm^2 flask in 10 ml of standard media. To freeze cells, the cell pellet obtained from harvesting was stored in a 1:10 solution of DMSO and FBS in a cryogenic vial and kept in -80 ºC.

Frozen cells were harvested by thawing the cryogenic vial in a water bath at 37ºC and the thawed cell suspension was mixed with four times the volume of standard media. Cell suspension was centrifuged at 300g for 5 minutes and the supernatant was discarded. The

cell pellet was suspended in 1 ml of complete media and the desired volume of cell suspension was transferred to a new 25 or 75 cm^2 flask in standard media (5 or 10 ml, respectively). Media was refreshed after 24 hours and then every 48 hours, if necessary.

2.2.5.   Preparation of conditioned media

Murine RM1-BM and human prostate cancer cells DU145 and PC3 transfected with mock or TRAF6 knockdown, LNCaP and C42-B4 (50x10^4 cells/well) were grown in a 6-well plate (Corning, No. 3516) in 2 ml of standard media. After reaching ~70% confluency, the media was replaced with FBS-free media. After 16 hours, conditioned media was collected and filtered with Acrodisc® Syringe filter pore size of 0.45 µm (Pall, No. 4614). Conditioned media from cultures of different macrophage phenotypes derived from human THP-1 monocytic like-cells, namely Mø, M1 and M2, was collected in a similar manner and stored in -20ºC.

2.3.   Macrophage studies

2.3.1.   Macrophage differentiation and stimulation

Human THP-1 monocytic-like cells were used as a model for human macrophages and were polarised to generate M1- and M2-macrophage phenotypes (Genin *et al.*, 2015; Yuan *et al.*, 2015; Ye *et al.*, 2018). Briefly, THP-1 cells (250x10^4 cells) were cultured in 25 cm^2 flasks (Thermo Fisher Scientific, No. 156367) in standard RPMI media supplemented with 5 ng/ml of phorbol 12-myristate 13-acetate (PMA; Sigma-Aldrich, No. P8139) for 48 hours, as previously described (Park *et al.*, 2007). Once adhered, media was replaced with 1% FBS-RPMI media for 24 hours, to remove PMA remnant, and the adhered THP-1 cells were incubated in 1% FBS-RPMI media to maintain uncommitted Mø macrophage lineage. Alternatively, adhered THP-1 cells were stimulated with lipopolysaccharides (LPS; 10 pg/ml; Sigma-Aldrich, No. L4524) and recombinant human interferon-γ (IFN-γ; 20 ng/ml; R&D Systems, No. 285-IF) to generate M1-polarised macrophages, or with recombinant human interleukin 4 (IL-4; 20 ng/ml; R&D Systems, No. 204-IL) and recombinant human interleukin 13 (IL-13; 20 ng/ml; R&D

Systems, No. 213-ILB) to generate M2-macrophages. After 72 hours, all macrophage cultures were washed and incubated in fresh media for 24 hours.

2.3.2. Macrophage phenotype identification by flow cytometry

To identify the different subsets of macrophages generated, the expression of standard macrophage markers were analysed by flow cytometry (Genin *et al.*, 2015; Forrester *et al.*, 2018). Briefly, monocytic THP-1 cells were differentiated and polarised as described in **section 2.3.1**, and were seeded in duplicates in 25 cm^2 flasks to increase cell number. The adhered and polarised cells were then detached by incubation in 5 ml of ice-cold FACS buffer (1X PBS, 5% FBS and 2 mM EDTA; Sigma-Aldrich, No. E7889) for 5 minutes and gentle scraping. The cell suspension was centrifuged at 300g for 5 minutes and the cell pellet was suspended in 1 ml of FACS buffer, diluted in trypan blue (1:2 v/v) and counted using a Neubauer Haemocytometer. Cells were then resuspended in FACS buffer (100x10^4 cells per ml), and centrifuged at 300g for 5 minutes. The cell pellet was resuspended in Human TruStain FcX™ (BioLegend, No. 422301) diluted 20X in PBS to block non-specific staining of Fc receptors (Genin *et al.*, 2015; Forrester *et al.*, 2018), and incubated at room temperature for 10 minutes. Cells were centrifuged at 300g for 5 minutes and resuspended in 0.75 ml of FACS buffer to be separated between a panel of antibodies, as shown in **Table 2.1**. For CD68 intracellular staining (Ramprasad *et al.*, 1996; Yang *et al.*, 2016), THP-1 cells were fixed with 0.5 ml of 10% neutral-buffered formalin for 10 minutes at room temperature (Kunisch *et al.*, 2004). Cells were centrifuged at 300g for 5 minutes and permeabilised with 100 µl of FACS buffer with Triton X-100 (0.5% v/v; Sigma-Aldrich, No. T8787). Cells were then incubated with 5 µl/ml of FITC mouse anti-human CD68 antibody (R&D Systems, No. 562117) for 30 minutes at 4ºC protected from light. For LIVE/DEAD™ fixable near-IR dead viability marker (1 µl/ml; Thermo Fisher Scientific, No. L34975) and cell surface markers PE mouse anti-human CD80 (20 µl/ml; BD Biosciences, No. 557227) and BV421 mouse anti-human CD163 (5 µl/ml; BD Biosciences,

No. 566277), 100 µl of the cell suspension was aliquoted as described in **Table 2.2** and incubated for 30 minutes at 4ºC protected from light. After incubation, 900 µl of FACS buffer was added to each sample and cells were centrifuged at 300g for 5 minutes. All pellets (except for pre-fixed CD68-stained samples), were fixed in neutral buffered formalin (10% v/v in PBS) for 20 minutes at 4ºC as previously described (Genin *et al.*, 2015; Forrester *et al.*, 2018). All cell samples were washed and resuspended in 0.5 ml of FACS buffer for flow cytometry analysis. UltraComp eBeads™ compensation beads (2 drops; Thermo Fisher Scientific, No. 01-2222-41), used as compensation controls, were incubated with each antibody according to the manufacturer's instructions. All samples were analysed using a BD LSR II flow cytometer with 4 lasers and 13 detectors (BD Biosciences) and at least 10,000 events of viable cells were measured per sample. Fluorescence minus one samples were used to assess panel design. Cells of interest (all macrophage subtypes) were identified by gating on morphology by forward scatter area (FSC-A) and side scatter area (SSC-A), on single cells by FSC-A and forward scatter height (FSC-H) and on viability by Red 780/60 and SSC-A. Unstained cells were used as controls in the gating. FlowJo software (BD Biosciences) was used to determine the percentage of expression of the described cell markers. Antibody panel design was selected based on predicted low spillover with the online BD Biosciences Fluorescence Spectrum Viewer tool (BD Biosciences), as shown in **Figure 2.1.**

Table 2.1. Panel of antibodies and settings used for identification of macrophage subtypes by flow cytometry analysis.

Target	Fluorochrome	Laser	Detection filter
LIVE/DEAD™ Fixable near-IR Dead **For viable cells** (Thermo Fisher Scientific, No. L34975)	Near Infrared	Red laser 633 nm	Red 780/60
CD68 (BD Biosciences, No. 562117)	FITC	Blue laser 488 nm	Blue 530/30
CD80 (BD Biosciences, No. 557227)	PE	Blue laser 488 nm	Blue 575/26
CD163 (BD Biosciences, No. 566277)	BV421	Violet laser 405 nm	Violet 450/50

Table 2.2. Master-mixes of antibodies and compensation controls used for identification of macrophage subtypes by flow cytometry analysis.

	Single stains			
	Live/Dead near-IR (1 µl/ml)	**CD68** (5 µl/ml)	**CD80** (20 µl/ml)	**CD163** (5 µl/ml)
1	YES	NO	NO	NO
2	NO	YES	NO	NO
3	NO	NO	YES	NO
4	NO	NO	NO	YES
5	NO	NO	NO	NO
All stains				
6	YES	YES	YES	YES
Compensation beads				
1	-	NO	NO	NO
2	-	YES	NO	NO
3	-	NO	YES	NO
4	-	NO	NO	YES
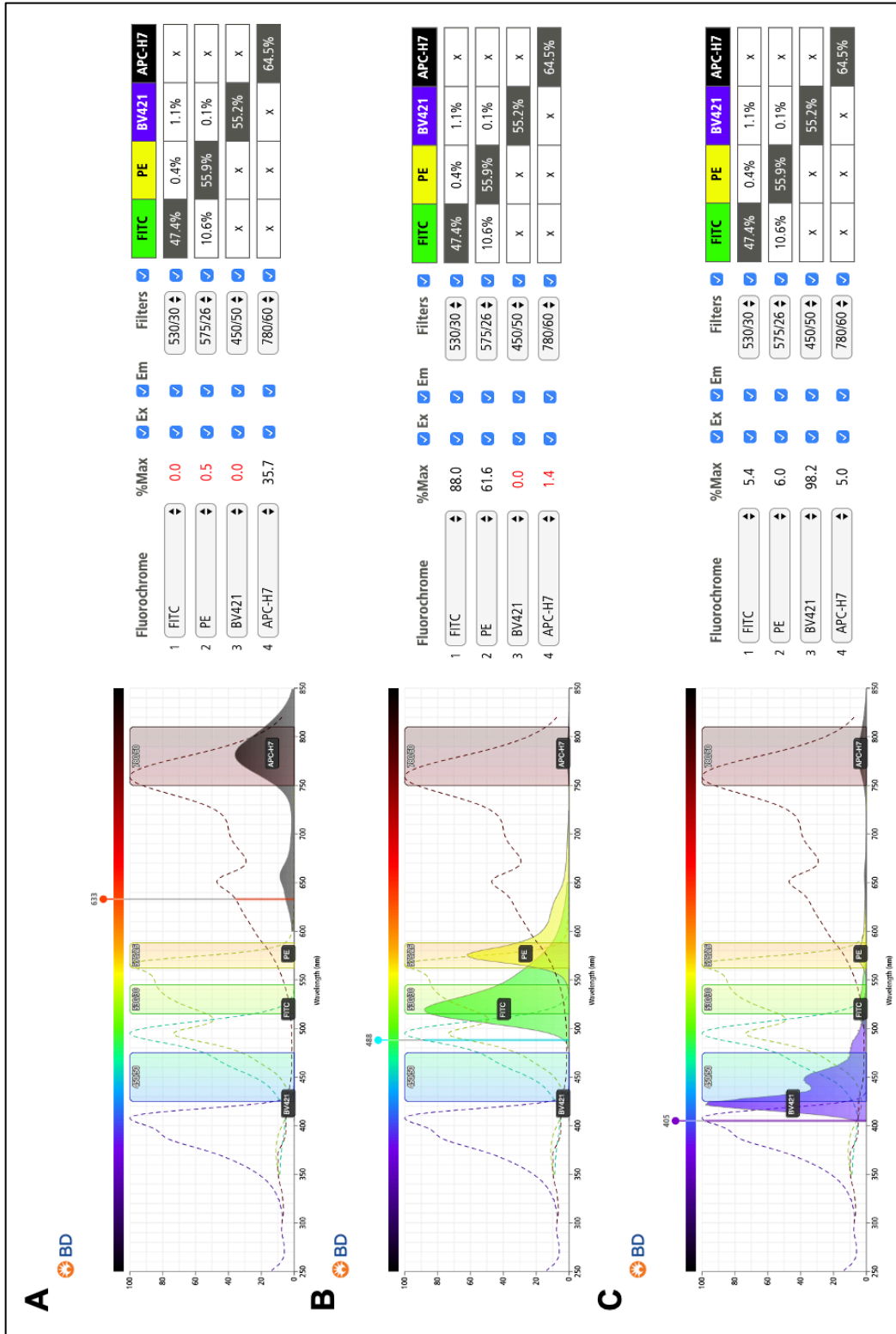
Figure 2.1. Predictions of spillover with BD Biosciences spectrum viewer tool using the BD LSR™ II cytometer. Excitation (dotted lines) and emission (shaded lines) spectral profiles by excitation with (A) red laser 633 nm, (B) blue laser 488 nm and (C) violet laser 405 nm. Fluorochromes used were FITC for CD68+, PE for CD80+, BV421 for CD163+ and APC-H7 for Live/dead™ fixable near-IR stainings. Filled rectangles represent specified detection filters. %Max values represent the percentage of maximum excitation. Values shaded in grey (right panel) represent percentage of spillover.

2.3.3. Macrophage polarisation influenced by treatments

To identify the effects of TRAF6 inhibition in macrophage lineage commitment, cultures of Mø, M1 and M2 macrophage subtypes were determined by flow cytometry. Briefly, THP-1 cells (250×10^4 cells) were cultured in 25 cm^2 flasks with supplemented RPMI and 5 ng/ml of PMA for 48 hours to halt proliferation and generate adherent cells (Park *et al.*, 2007). Once adhered, media was replaced with 1% FBS-RPMI media, to remove PMA remnant, for 24 hours and the adhered THP-1 cells were incubated in 1% FBS-DMEM and treated with 1 µM of FSAS3 or vehicle (DMSO) for 72 hours. Media was refreshed and after 24 hours, cells were processed as described in **2.3.2. Macrophage phenotype identification by flow cytometry.**

2.4. Biomedical studies

2.4.1. Retroviral gene delivery

TRAF6 knockdown in cultures of human DU145 and PC3 prostate cancer cells were obtained by using lentiviral vectors expressing three human short hairpin RNA (shRNA) individual clones (**Table 2.3**), and one non-targeting shRNA construct as control (mock). Use of lentiviral vectors was approved by the University of Sheffield Biosafety Committee under project license GMO2014_11. The described protocol was optimised by Silvia Marino, PhD and Ryan Bishop, PhD at our laboratory (University of Sheffield, UK), from which viral particles were obtained as follows. Briefly, HEK293ET cells (750×10^4 cells/ml) were seeded in a 75 cm^2 flask and when reaching confluency, the media was replaced with a transfection mixture solution (5 µg shRNA of pLKO.1, TRAF6^{KD1}, TRAF6^{KD2} or TRAF6^{KD3} plasmids, 5 µg PPAX2 packaging plasmid, 5 µg pMD2.G envelope plasmid, 40 µl of Polyethylenimine (PEI) transfection reagent and 450 µl of serum-free DMEM in 4.5 ml of standard DMEM media). After 24 hours, the media was refreshed and the following day, media containing viral particles was transferred to Falcon™

15 ml conical centrifuge tubes (Thermo Fisher Scientific, No. 352097), centrifuged and stored at -80ºC.

Table 2.3. Human TRAF6 shRNA constructs and target sequences.

NAME	CONSTRUCT	TARGET SEQUENCE
TRAF6^{KD1}	TRCN0000007348	GCCACGGGAAATATGTAATAT
TRAF6^{KD2}	TRCN0000007352	CCTGGATTCTACACTGGCAAA
TRAF6^{KD3}	TRCN0000007349	CGGAATTTCCAGGAAACTATT

2.4.1.1. Transduction of TRAF6 short hairpin RNA (shRNA)

The human DU145 and PC3 were seeded (80×10^4 cells/ml) in 25 cm^2 flasks in standard media and after 24 hours, the media was replaced with media filtered with Acrodisc® Syringe filter pore size of 0.45 µm consisting of 1:10 viral supernatant in complete DMEM and 10 µl of polybrene (5 µg/ml) (Sigma-Aldrich, No. TR-1003). The following day, media was replaced with selection medium consisting of 1 µg/ml puromycin (Gibco, No. A1113803) in standard DMEM. The concentration used was chosen based on the effects of puromycin on the viability of non-transfected PC3 cells (data not shown). This allowed the selection of cells that stably express TRAF6 shRNA. Each time cells were thawed, mock or TRAF6 shRNA DU145 and PC3 were treated with selection medium for at least two passages. In addition, elimination of non-transduced cells treated with selection medium was used as reference. The expression of TRAF6 in transfected cells was determined using Western Blot (see **2.4.5. Western Blot**).

2.4.2. Growth, motility and invasion assays

2.4.2.1. Assessment of cell viability

Cell viability was assessed by the Alamar Blue™ assay. Alamar Blue™ (Thermo Fisher Scientific, No. DAL1100) is a non-toxic and cell-permeable reagent that measures the metabolic activity of living cells (Rampersad, 2012).

Alamar Blue™ was used to evaluate the effects of TRAF6 manipulation on the viability of murine RM1-BM ($0.1x10^4$ cells) and the human prostate cancer cells LNCaP, C42-B4, DU145 and PC3 ($0.3x10^4$ cells) cultured in standard media in a 96-well plate (Corning, No. 3595). To assess the effects of 6877002 and FSAS 1-6 on cell viability, the media was replaced after 24 hours with a final volume of 100 μl of drug treatments in serum-free DMEM at a linear range of concentrations from 0.1-100 μM of 6877002 and logarithmic range of concentrations of FSAS 1-6 from 0.01-100 μM, using vehicle (DMSO) as a control.

To assess the effects of TRAF6 knockdown (as described in **section 2.4.1.1**) on viability of prostate cancer cells, human DU145 and PC3 cells transduced with mock or TRAF6 knockdown constructs ($0.1x10^4$ cells) were seeded in a 96-well plate in standard media. After 24 hours, an initial value was measured (used as a "Day 0" reading) and was assumed as 100% viability of each cell population under normal growth. To investigate the effects of treatment with the novel FSAS3, PC3-TRAF6 knockdown cells were treated with logarithmic range of concentrations of FSAS3 from 0.01-100 μM or vehicle (DMSO), as control, in 100 μl serum-free DMEM after 24 hours from seeding.

To determine the effects of macrophage conditioned media and FSAS3 treatment on prostate cancer cell viability, human PC3 prostate cancer cells ($0.2x10^4$ cells) were seeded in a 96-well plate in standard media. After 24 hours, media was replaced with complete RPMI or 100% conditioned media from Mø, M1 or M2 macrophage phenotypes derived from THP-1 cells and treated with FSAS3 or vehicle (DMSO), as control.

To assess the effects of prostate cancer cells on monocyte viability, human monocyte-like THP-1 cells (2×10^4 cells per well) were seeded in 96-well plates. After 24 hours, THP-1 cells were treated with the novel FSAS3 or vehicle (DMSO), as control, in the presence and absence of 50% PC3- or RM1-BM-conditioned media.

To determine the effects of prostate cancer cells on macrophage viability, murine RAW 264.7 macrophage-like cells (0.2×10^4 cells per well) were seeded in 96-well plates. After 24 hours, RAW 264.7 cells were treated with the novel FSAS3 or vehicle (DMSO), as control, in the presence and absence of 50% PC3- or RM1-BM-conditioned media.

At 48, 72 and 96 hours after seeding, cell viability was measured after a 2-hour incubation with Alamar Blue™ (10% v/v) at excitation of 530 nm and emission of 590 nm using a SpectraMax M5® microplate reader (Molecular Devices), as shown in **Figure 2.2**. A blank absorbance value (from wells containing media and Alamar Blue™ only) was subtracted from all values to eliminate background fluorescence, and the percentage of viability was calculated by dividing each reading over the initial absorbance value of cells. Media was replaced with 100 µl of 10% neutral buffered formalin for cell fixation. Images for each group of cells were taken by Leica DMI4000 B inverted microscope with 10X.
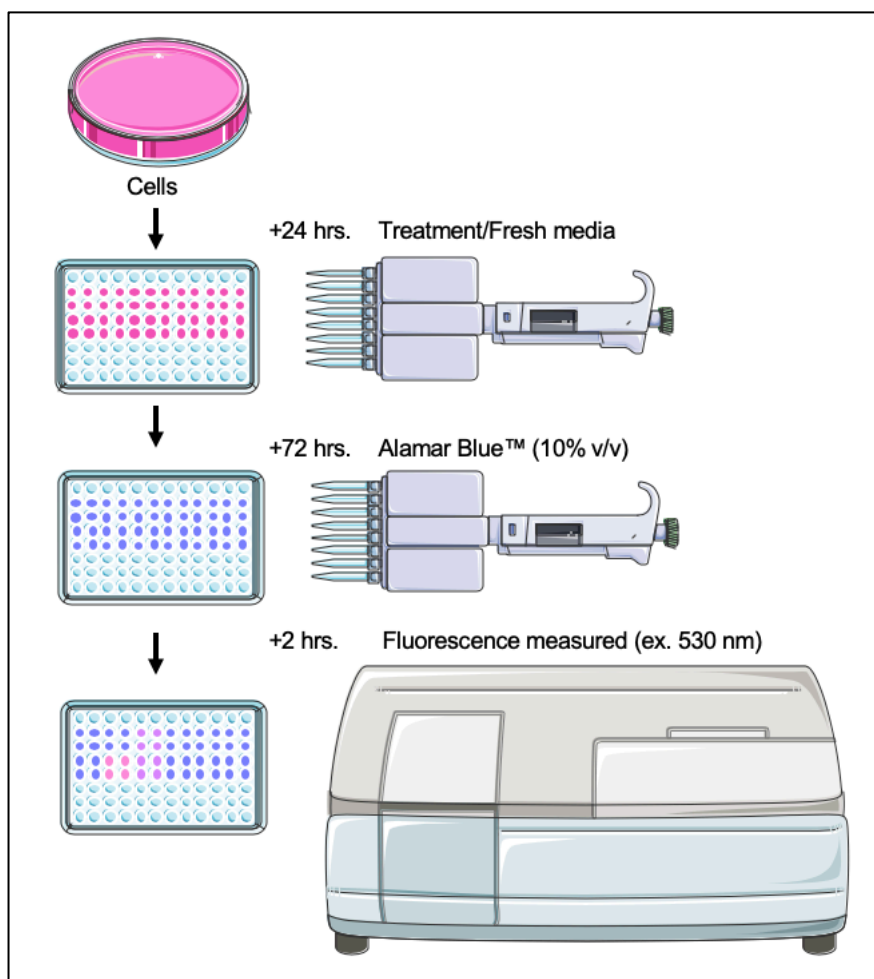
Figure 2.2. Cell viability assessed by the Alamar Blue™ assay. Cells are plated in 96-well plates, according to their respective seeding density. After 24 hours, cells are treated with compounds or vehicle or with fresh media. After the incubation period, cells are exposed to Alamar Blue™ (10% v/v) for 2 hours. Fluorescence is measured with excitation of 530 nm and emission of 590 nm using a SpectraMax M5® microplate reader. hrs.=hours.

2.4.2.2. Cell migration assessed by the wound-healing assay

The wound-healing assay was used to assess the effects of TRAF6 manipulation on the migration of prostate cancer cells (Moutasim, Nystrom and Thomas, 2011). Human prostate cancer cells DU145 and PC3 transduced with mock or TRAF6 shRNA ($20x10^4$ cells/well) (as described in **section 2.4.1.1**) were seeded in a 24-well plate (Corning, No. 3524) in standard media for 24 hours. The confluent cell monolayer was scratched using a 10 µl pipette tip in the middle region of the well to generate a wound. The cell monolayer was washed twice with serum-free DMEM to remove detached cells and incubated in DMEM medium supplemented with 1% serum DMEM for TRAF6 knockdown cells, or with serum-free DMEM and 6877002, FSAS3 or vehicle (DMSO) (0.1% v/v). The plates were placed in a humified microscope housed in a temperature controlled environment at 37ºC supplied with 5% CO_2 for the desired period. To evaluate the effects on motility of macrophage-derived conditioned media on prostate cancer cells, human PC3 prostate cancer cells ($20x10^4$ cells/well) were seeded in a 24-well plate in standard media for 24 hours. The wound was created as described above, the cell monolayer was washed twice with serum-free DMEM and cells were cultured in complete RPMI medium or 100% conditioned media from Mø, M1 or M2 macrophage phenotypes derived from THP-1 cells in the presence of vehicle or FSAS3 (1 µM). The plates were placed in a humified microscope housed in a temperature controlled environment at 37ºC supplied with 5% CO_2 for the desired period.

Cell migration across the wound was monitored by recording four randomly selected positions per well each 15 minutes for 14 hours using time-lapse video on a Leica AF6000LX inverted microscope (10X magnification). Additionally, cell viability was assessed by the Alamar Blue™ assay as described in **section 2.4.2.1**. TScratch software (ETH, Zurich) was used to analyse the time-lapse images and to obtain the percentage of wound closure (**Figure 2.3A**).

2.4.2.3. Cell invasion assessed by Transwell® invasion assay

The Transwell® assay was used to assess the effects of TRAF6 manipulation on the invasion of prostate cancer cells (Moutasim, Nystrom and Thomas, 2011). Briefly, Corning® Costar® Transwell® cell culture insert (6.5 mm with 8 µm pore polycarbonate filter; Corning, No. 3422) was coated with 20 µl of Phenol Red-Free Corning® Matrigel® Basement membrane matrix (1.5 mg/ml; Corning, No. 356237) and incubated at 37ºC supplied with 5% CO_2 for 2 hours. To determine the effects of knockdown and pharmacological inhibition of TRAF6 on prostate cancer cell invasion, PC3 ($5x10^4$ cells/well) and DU145 ($2.5x10^4$ cells/well) cells transduced with mock or TRAF6 knockdown shRNA (as previously described) were cultured in serum-free DMEM in the presence of 6877002, FSAS3 or vehicle (DMSO) (0.1% v/v) in the upper part of the Transwell® insert. Supplemented DMEM medium (500 µl) was added to the bottom chamber of the well to act as a chemoattractant. To assess the effects of macrophage-derived conditioned media on prostate cancer cell invasion, RM1-BM and PC3 cells ($5x10^4$ cells/well) were treated with vehicle (DMSO) (0.1% v/v) or FSAS3 (0.3 µM) in serum-free RPMI in the upper part of the Transwell® insert. Supplemented RPMI or conditioned media from Mø, M1 or M2 macrophages (500 µl) was added to the bottom chamber of the well to act as a chemoattractant.

After 72 hours, the media in the Transwell® was removed with a cotton tip applicator and the inserts were incubated with 100% ethanol for 5 minutes, 1% eosin Y solution (Sigma-Aldrich, No. HT110280) for 1 minute, washed with distilled water, dried and then, incubated in hematoxylin solution modified according to Gill II (Sigma-Aldrich, No. 105175) for 5 minutes. After washing with distilled water, the membrane was removed from the Transwell® and placed on a slide over one drop of Faramount aqueous mounting medium (Agilent, No. S3025) and covered by rectangular cover glasses (VWR, No. 631-0137) to avoid the generation of air bubbles (**Figure 2.3B**). Images of the insert were taken with Pannoramic 250 Flash III Slide

Scanner (3D Histech) (20X magnification) and the percentage of invading cells was quantified using Image Processing and Analysis in Java software (ImageJ; NIH, USA) as previously described (Schindelin, J. *et al.*, 2012).
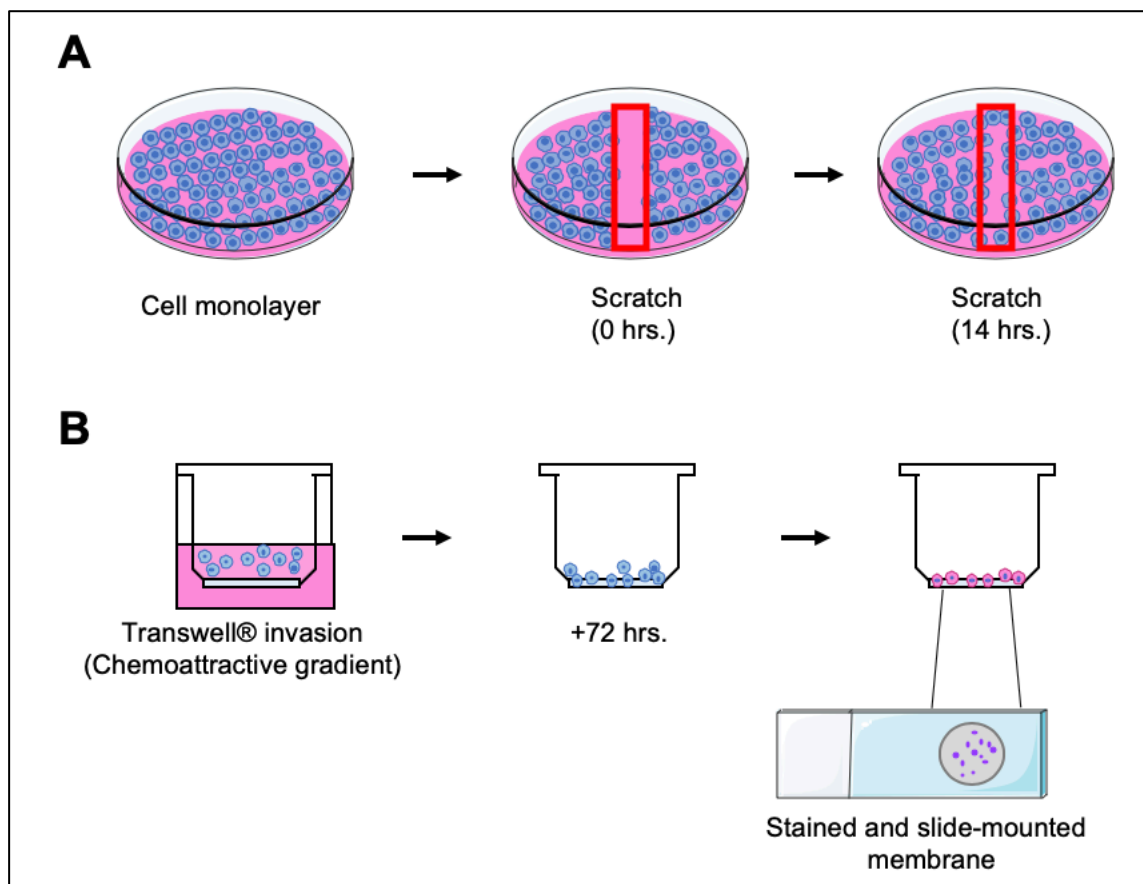
Figure 2.3. Cell migration assessed by the wound-healing assay and cell invasion assessed by Transwell® invasion assay. (A) Cells were plated to generate a monolayer and a wound was produced by scratching the middle part of the well. Migration was analysed using time-lapse video of the region of interest after 14 hours. (B) Prostate cancer cells were seeded in FBS-free media and placed in a Transwell® with Matrigel® coat inside a well containing complete media, to generate a chemoattractive gradient. After 72 hours, the Transwell® membrane was stained with Hematoxilin/Eosin and mounted in a slide for analysis. hrs.=hours.

2.4.3. Assessment of prostate cancer-induced osteoclastogenesis

The effects of prostate cancer cells and their derived factors on osteoclast formation were assessed using tartrate resistant acid phosphatase (TRAcP) staining (Yuen *et al.*, 2010). First, murine RAW 264.7 macrophage-like cells were seeded (0.2×10^4 cells/well) in a 96-well plate in supplemented media. After 24 hours, RANKL (100 ng/ml; batch No. 1044-101P donated by Dr. Patrick Mollat) was added (Rafiei and S. V. Komarova, 2013). The following day, 50 µl of media was removed and replaced with 150 µl differentiation media containing small-molecule inhibitors 6877002, FSAS3 or vehicle (DMSO) (0.1% v/v) and RANKL (100 ng/ml) in the presence and absence of RM1-BM cells (200 cells per well) or conditioned media from Mø, M1 or M2 macrophage phenotypes, or from LNCaP, C42-B4, RM1-BM, PC3 and DU145 mock or TRAF6 knockdown prostate cancer cells (10% v/v). Cells not exposed to conditioned media or prostate cancer cells were used as a negative control. Cells were treated every 48 hours for 6 days by replacing 2/3 of standard media with differentiation media. On day 6, cell viability was measured as described in **section 2.4.2.1** and cells were fixed with 100 µl of neutral buffered formalin (10% v/v). Cultures were stained with 100 µl of TRAcP staining solution (**Scientific Appendix**), washed with PBS and 200 µl 70% Ethanol was added to each well. TRAcP-positive cells with three or more nuclei were counted as osteoclasts by using a phase-contrast microscope. Representative images for each group of cells were taken by Leica DMI4000 B inverted microscope with 10X.

2.4.4. Assessment of prostate cancer-induced osteoblast growth, differentiation and bone nodule formation

The effects of prostate cancer cells and their derived factors on osteoblast differentiation and bone nodule formation were assessed using alkaline phosphatase (ALP) and Alizarin Red S (ARS) staining, respectively (Sabokbar *et al.*, 1994; Yuen *et al.*, 2010; Moh *et al.*, 2011). Human osteosarcoma-derived cells Saos-2 (3×10^4 cells/well) were seeded in standard media

in 24-well plates. To induce bone nodule formation, cells were treated every second day for 10 days with osteogenic media consisting of DMEM with 1% FBS, L-ascorbic acid (50 µM; Sigma-Aldrich, No. A4544) and after confluence, adding β-glycerophosphate (2 mM; Sigma-Aldrich, No. G9422). Cells were also exposed to conditioned media from mock or TRAF6 shRNA DU145 or PC3 (20% v/v) and treated with 6877002/FSAS3 small-molecule inhibitors or vehicle (DMSO) (0.1% v/v). Cells not exposed to conditioned media were used as a negative control. After 5, 7 and 10 days, Saos-2 cell viability was assessed using the AlamarBlue® assay. To assess osteoblast maturation and differentiation, cells were lysed with 500 µl ALP lysis buffer (**Scientific Appendix**) for 20 minutes and adherent cells were scrapped and centrifuged in Heraeus™ Fresco™ 17 microcentrifuge (Thermo Fisher Scientific) at 13,300g for 10 minutes at 4ºC. The supernatant was collected and 50 µl of the sample was mixed with 5 µl of 4-nitrophenyl phosphate disodium salt hexahydrate (4 mM, Sigma-Aldrich, No. N4645), measuring absorbance (405 nm) with a SpectraMax M5® microplate reader (Molecular Devices) at 37ºC every 15 minutes for 1 hour. The ability of osteoblasts to form bone nodules was assessed by fixing cells with 70% ethanol and after 24 hours, the plates were washed with PBS, incubated with 500 µl of ARS solution (**Scientific Appendix**) to stain calcium deposits and washed again with PBS. The plates were air-dried and scanned for representative images. To quantify bone nodule formation, the cell monolayer was destained by exposure to 1 ml destaining solution (10% (w/v) cetylpyridinium chloride monohydrate, Sigma-Aldrich, No. C0732) in 10 mM sodium phosphate (pH 7.0; Sigma-Aldrich, No. 342483) for 15 minutes at room temperature on a rocker. ARS was determined by absorbance measured at 562 nm on a Bio-Tek Synergy HT microplate reader (BioTek® Instruments) and the percentage of ARS was determined by ImageJ.

2.4.5. Western Blot

Protein expression and phosphorylation in cultures of prostate cancer cells, bone cells and macrophages was assessed using Western Blot as previously described (Idris, 2012) (**Figure

2.4). Murine RM1-BM ($25x10^4$ cells) and RAW 264.7 ($50x10^4$ cells), human differentiated and polarised THP-1 Mø, M1 and M2 ($80x10^4$ cells) (see **section 2.3.**), human LNCaP, C42-B4 ($50x10^4$ cells) and transduced with control or TRAF6 shRNA constructs PC3 and DU145 prostate cancer cells ($40x10^4$ cells/well) were seeded in a 6-well plate in standard media and maintained for 48 hours before lysis.

2.4.5.1. Assessment of NFκB activation using RANKL, TNF-α and M2-macrophage conditioned media

To assess the effects of TRAF6 manipulation on NFκB signalling pathway, RAW 264.7 and PC3 cells transduced with mock or TRAF6 knockdown constructs ($7.5x10^4$ cells) were seeded in a 12-well plates (Corning, No. 3513) in standard media. After 24 hours, media was replaced with serum-free DMEM. After 16 hours, RAW 264.7 and PC3 cells (mock or TRAF6 knockdown) were treated with compounds 6877002, FSAS3 or DMSO as control for 1 hour. After incubation, RANKL (100 ng/ml) was added to cultures of RAW 264.7 as stimulus, and RANKL (100 ng/ml), TNF-α (10 ng/ml; R&D Systems, No. 210-TA) or 20% M2-macrophage conditioned medium were added to PC3 cells as stimuli. All cells were lysed (as described in **section 2.4.5.2**) after 30 minutes of incubation with RANKL and after 6 hours for the other stimuli.

2.4.5.2. Preparation of cell lysates

Cells were washed with 1 ml of ice-cold PBS and treated with 100 μl RIPA lysis buffer (**Scientific Appendix**) supplemented with 2% (v/v) protease inhibitor (Sigma-Aldrich, No. P8340) and 0.4% (v/v) phosphatase inhibitor (Sigma-Aldrich, No. P0044) for 5 minutes. After incubation, cells were scraped, transferred into an Eppendorf tube and centrifuged in Heraeus™ Fresco™ 17 microcentrifuge (Thermo Fisher Scientific) at 13,300g for 10 minutes at 4ºC. The supernatant was collected and stored in -20ºC (**Figure 2.4A**).

2.4.5.3. Protein quantification

Pierce™ Bicinchoninic acid (BCA) protein assay was used to quantify protein amount in cell lysates, according to the manufacturer's instructions. Protein concentrations were assessed using the Pierce™ bovine serum albumin (BSA) standard prediluted set as reference (Thermo Scientific, No. 23208), by adding 10 µl of each of the serial dilutions (0-2000 µg/ml) in duplicates in a 96-well plate along with the cell lysate samples diluted 1:4 in distilled water. BCA solution (200 µl) consisting of 1 in 50 copper sulphate (Sigma-Aldrich, No. C2284) diluted in BCA (Sigma-Aldrich, No. B9643) was added to all wells. After 25 minutes of incubation at 37ºC, the absorbance was measured at 562 nm on a SpectraMax M5® microplate reader (Molecular Devices) (**Figure 2.4B**). From the known concentrations of BSA, a standard curve was constructed to assess the total protein concentration of each lysate and determine the volume of protein extract to obtain 70 µg.

2.4.5.4. Gel electrophoresis and electrophoretic transfer

Denatured proteins were separated by electrophoresis using 12% Criterion™ TGX™ Precast Midi protein gels (Bio-Rad Laboratories, No. 5671043) placed inside a vertical electrophoresis chamber filled with 1X TGS running buffer (obtained from 1 in 10 dilution of 10X TGS; Bio-Rad Laboratories, No. 161-0772, with distilled water). Before loading the gel, the quantified samples were mixed with 5X loading buffer (**Scientific Appendix**) and heated for 5 minutes at 95ºC (**Figure 2.4C**). As a reference for molecular weights, Magic Marker XP Western Protein Standard (Thermo Fisher Scientific, No. LC5602) was used. After 1 hour with 180 V, the proteins on the gel were transferred to a polyvinylidene (PVDF; Bio-Rad Laboratories, No. 1704273) membrane, previously activated in 100% methanol and equilibrated in transfer buffer (Bio-Rad Laboratories, No. 1704273) for 5 minutes. The gel was placed over the PVDF membrane, assembled together between filter papers (Bio-Rad Laboratories, No. 1704273) (**Figure 2.4D**) pre-soaked in transfer buffer, and all was placed in the Transblot Turbo® transfer system (Bio-Rad Laboratories) for 7 minutes at a constant current of 2.5 A and 21 V.

2.4.5.5. Membrane blocking and antibody incubation

The PVDF membrane was blocked to avoid unspecific binding by incubation in 5% (w/v) milk blocking solution (non-fat milk powder in Tris buffer saline solution (**Scientific Appendix**) with 0.1% TWEEN® 20 (Sigma-Aldrich, No. P9416), known as TBST) for 1 hour on a rocker with low speed in room temperature. The membrane was washed three times with TBST for 10 minutes on a rocker with medium speed and incubated overnight at 4ºC on a rocker in low speed with each primary antibody. Subsequently, the membrane was washed three times with TBST on a rocker with medium speed for 15 minutes and incubated with the secondary antibody peroxidase AffiniPure donkey Anti-Rabbit IgG (H+L) (Jackson ImmunoResearch, No. 711-035-152) in a 7:50000 dilution using 5% milk blocking solution for 1 hour on a rocker with low speed. Next, the membrane was washed three times with TBST for 10 minutes and it was visualised using Clarity™ western ECL substrate (Bio-Rad Laboratories, No. 170-5061) with the chemiluminescent detection system on ChemiDoc™ Imaging System (Bio-Rad Laboratories) (**Figure 2.4E**). Band quantification was performed with the use of Image Lab 6.0 software (Bio-Rad Laboratories). The primary antibodies used were Anti-rabbit CD40 (C-20; Santa Cruz Biotechnology, No. sc-975), Anti-rabbit RANK (H-300; Santa Cruz Biotechnology, No. sc-9072), Anti-rabbit p-IκB-α (Ser32; Cell Signalling Technology, No. 2859), Anti-rabbit IκB-α (Cell Signalling Technology, No. 9242), Anti-rabbit TRAF2 (Cell Signalling Technology, No. C192), TRAF6 rabbit mAb (Cell Signalling Technology, No. 8028), Anti-rabbit p65 (C-20, Santa Cruz Biotechnology, No. sc-372) and β-Actin rabbit mAb (D3A8; Cell Signalling Technology, No. 8457). All primary antibodies were prepared in a concentration of 1:1000 in 5% (w/v) BSA (Sigma-Aldrich, No. A7906) in TBST.
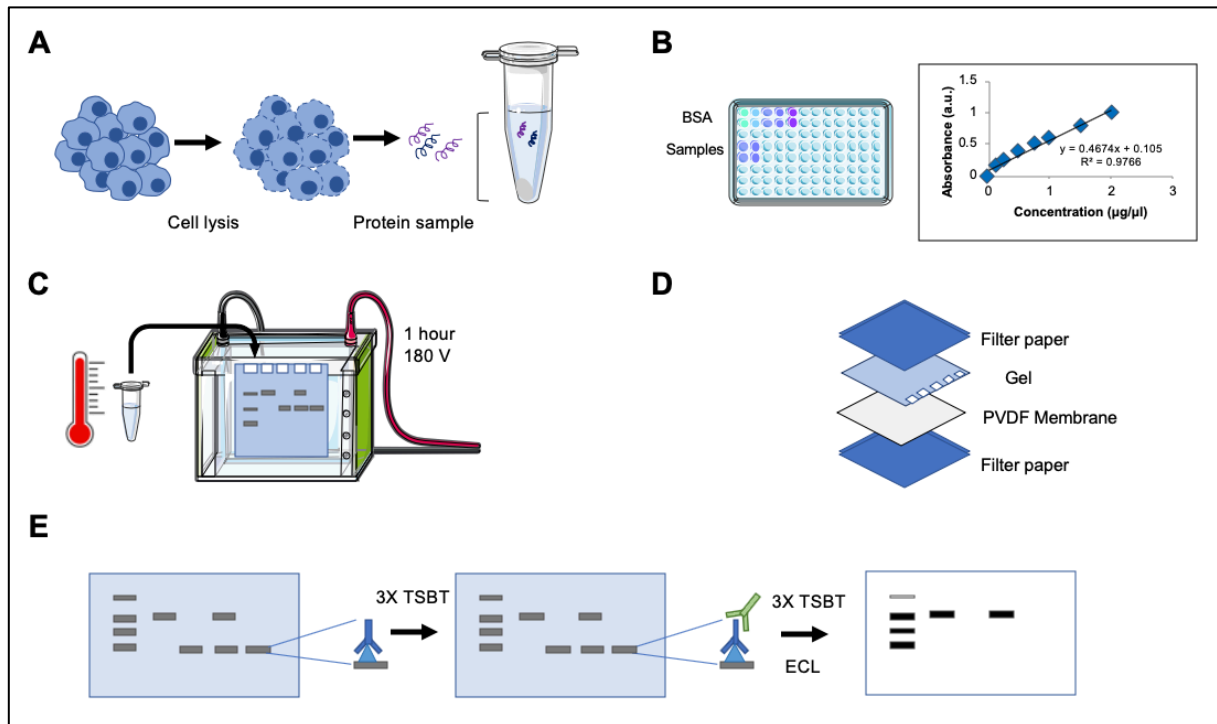
Figure 2.4. Western Blot technique. (A) Protein is obtained from whole cell lysates with RIPA buffer. (B) Protein concentrations are assessed by BCA, based on the standard curve of the Pierce™ bovine serum albumin (BSA) standard prediluted kit. (C) Cell samples are prepared, heated and separated by electrophoresis for 1 hour with 180 V. (D) The gel is placed over the PVDF membrane, assembled together between filter papers (pre-soaked in transfer buffer). The PVDF membrane is blocked in 5% (w/v) milk blocking solution, washed with TBST and (E) incubated with each primary antibody. The membrane is washed with TBST and incubated with the secondary antibody peroxidase AffiniPure donkey Anti-Rabbit IgG (H+L) and washed before visualization using Clarity™ western ECL substrate with the chemiluminescent detection system on ChemiDoc™ Imaging System. BSA=Bovine Serum Albumin. R^2=Square of the correlation.

2.5.   *In vivo* studies

The intratibial injection mouse model was used to study the effects of knockdown and pharmacological inhibition of TRAF6 on osteolysis in mice bearing human PC3 prostate cancer cells. All mice were placed in a 12-hour light-dark cycle with access to food and water *ad libitum*.

2.5.1.   Ethics

All experimental protocols were approved and performed in accordance with Italian Legislative Decree 116/9 and Gazzetta Ufficiale della Repubblica Italiana No. 40, February 18th, 1992.

2.5.2.   Intratibial injection of human PC3 prostate cancer cells in immunodeficient mice

The effects of cancer-specific inhibition of TRAF6 on osteolysis were investigated by intratibial injection of human PC3 cells, performed at the University of L'Aquila (Italy) by staff of the biological service unit under the supervision of Mattia Capulli, PhD and Student Antonio Maurizi, PhD. Animals were divided into treatment groups (n=7 per group) as follows (**Table 2.4**): (1) human mock PC3 cells and 10% DMSO in water, (2) human mock PC3 cells and TRAF6 inhibitor 6877002, (3) and (4) human TRAF6 knockdown PC3 cells from two different DNA constructs (KD1 and KD2, as described in **section 2.4.1.1.**) and 10% DMSO in water. Group (2) was pre-treated with the TRAF6 inhibitor 6877002 (20 mg/kg) one day before injecting cancer cells, based on previous findings obtained by our lab group (Bishop *et al.*, 2020). All male 4-week old BALB/c-nu/nu athymic mice were anesthetized with intraperitoneal injections (IP) of pentobarbital (60 mg/kg) and received intratibial injection on the left limb of the corresponding prostate cancer cells (20,000 cells/100 µl), based on the osteolytic nature of the cells as suggested in (Dai *et al.*, 2016). After 10 days, the formation of osteolytic lesions was monitored weekly by anesthetizing the mice as previously described and subjecting them to X-ray analysis (36 kVp for 10 seconds) using Cabinet X-ray system (Faxitron model No. 43855A Buffalo Grove). The experiment was terminated after observing osteolysis. Animals

were sacrificed after 20 days by carbon dioxide inhalation and cervical dislocation. Treated hind limbs were trimmed of excess of muscle and soft tissue and fixed in 10% buffered formalin. Next, samples were washed with PBS, placed in 70% ethanol (v/v) and stored at 4ºC.

Table 2.4. Treatment regimens for the intratibial injection mouse model.

Group	Injected cells	Treatment [100 μl]
Control/Vehicle	Human mock PC3 cells	10% DMSO in water IP daily.
TRAF6 inhibitor 6877002	Human mock PC3 cells	6877002 (20 mg/kg) IP daily.
TRAF6 knockdown1	Human TRAF6 shRNA1 transduced PC3 cells	10% DMSO in water IP daily.
TRAF6 knockdown2	Human TRAF6 shRNA2 transduced PC3 cells	10% DMSO in water IP daily.

2.5.3. Micro-computed tomography (micro-CT) analysis

Ex vivo micro-CT scanning was used to evaluate the effects of TRAF6 manipulation on bone architecture in mice bearing the human prostate cancer cell line PC3. Tibias of the hind limbs were scanned using X-ray radiation source to 50 kV and 800 μA with *ex vivo* SkyScan 1174 system (Bruker). Briefly, hind limbs were wrapped in cellophane and placed in an upright position in the scanner. The pixel size was set to 6.741 μM. To generate three-dimensional images, X-ray scans were reconstructed using Skyscan NRecon software (Bruker) with a beam hardening correction of 20%. The regions of interest were designated by 0.5 mm below the growth plate (Campbell, Ominsky and Boyd, 2011) (200 frames total). Total, trabecular and cortical bone formation were evaluated with Skyscan CTAn software (Bruker) (Campbell and Sophocleous, 2014) and representative images were obtained using CTVol software (Bruker).

2.6.   *In silico* studies

Online tools with publicly available databases were used for the analysis of protein expression and genetic alterations in prostate cancer patients. Protein interaction and function was determined using curated interaction records from Gene Ontology (GO) and Kyoto Encyclopedia of Genes and Genomes (KEGG) from the Search tool for retrieval of interacting genes/proteins (STRING) database (https://string-db.org/; Szklarczyk et al., 2018). To compare gene expression between tumour and normal tissue, the University of California Santa Cruz (UCSC) Xena platform for cancer genomics data visualization and interpretation was used (https://xena.ucsc.edu/; Goldman *et al.*, 2018). Heatmap of the expression pattern of TRAF proteins in normal and cancer tissue was obtained using The Cancer Genome Atlas (TCGA) analysis in UALCAN (http://ualcan.path.uab.edu/index.html; Chandrashekar *et al.*, 2017).

To study the association between the expression of TRAF proteins and androgen receptor at different stages of prostate cancer, Spearman correlation was obtained using cBioPortal for cancer genomics (https://www.cbioportal.org/; Cerami et al., 2012; Gao et al., 2014). The dataset Prostate Adenocarcinoma (TCGA, PanCancer Atlas) was used for studying primary tumour stage (488 patients total), and Metastatic Prostate Adenocarcinoma SU2C/PCF Dream Team (PNAS, 2019) dataset to study metastatic prostate cancer (212 patients total). Furthermore, to explore the link between immune infiltration in the prostate tumour microenvironment and the expression of TRAF proteins, web-accessible data was analysed with Tumour Immune Estimation Resource (TIMER) (cistrome.shinyapps.io/timer; Li *et al.*, 2017) using Spearman correlation. This software evaluates the association of mRNA expression with tumour-infiltrating immunologic data. Data obtained is adjusted based on the negative correlation of mRNA expression with the percentage of cancer cells in a tumour sample, allowing the measurement of expression in immune cells only. TIMER was also used to generate Kaplan-Meier survival curves and obtain hazard ratios (HR) of all TRAF proteins

using the prostate cancer adenocarcinoma TCGA database. Gene Expression Profiling Interactive Analysis (GEPIA) (http://gepia.cancer-pku.cn/; Tang *et al.*, 2017) was used to study disease-free survival curves and obtain hazard ratios of all TRAF proteins with the prostate cancer adenocarcinoma TCGA database.

To analyse genetic alterations in prostate cancer progression, cancer studies were accessed using cBioPortal. Briefly, datasets were selected based on disease stage: Prostate Adenocarcinoma (TCGA, PanCancer Atlas) study for primary tumour stage (494 patients total) and Metastatic Prostate Adenocarcinoma SU2C/PCF Dream Team (PNAS, 2019) in combination with Metastatic Prostate Cancer Project (Provisional, December 2018) datasets to study advanced stages (463 patients total).

The expression of TRAF6 in osteoblast-like cell lines Saos-2 and MG-63 was determined using the experiment "RNA-seq of 934 human cancer cell lines from the Cancer Cell Line Encyclopedia" available in the Expression Atlas (https://www.ebi.ac.uk/gxa/home).

2.7. Statistical analysis

Results presented are mean ± standard deviation (SD) from three independent experiments. All calculations were performed using GraphPad Prism version 7.0 software (GraphPad Software, Inc., La Jolla, CA, USA). Statistical analysis for two groups of data from a single experiment were determined by unpaired *T* test and differences between more than two groups and one independent variable were assessed by an ordinary one-way analysis of variance (ANOVA) followed by Tukey *post hoc* test with multiple comparisons between groups. The inhibitory concentration 50% (IC_{50}) was assessed by log 10 transformation, followed by non-linear regression analysis using variable slope fit equation for normalized dose-inhibitory response and a two-way ANOVA followed by Dunnet *post hoc* test for multiple comparisons between groups with two independent variables. In all cases, *P* values less than 0.05 were considered statistically significant.

Chapter 3. Altered TRAF6 gene expression in advanced prostate cancer

3.1.　Summary

TRAF proteins (TRAF1-7) are key regulators of many biological activities and alterations in their expression are commonly found in different types of cancer. Previous studies have reported the involvement of TRAF2, TRAF4 and TRAF6 in prostate cancer progression; however, the role of TRAF6 in the initiation and promotion of prostate cancer metastasis, particularly to bone, remains unexplored. In the present chapter, retrospective analysis of publicly-available resources and Western Blot analysis were used to study the expression of TRAF proteins in prostate cancer patients and cell lines, respectively. First, the involvement of TRAF proteins in various cancer-related biological activities was confirmed. The expression of all TRAFs was significantly altered in prostate cancer patients compared to healthy individuals and a positive correlation was found between expression of TRAF6 and androgen receptor, and TRAF6 and the number of tumour-infiltrating immune cells in prostate cancer patients. Additionally, DNA amplifications of TRAF6 were mainly observed in prostate cancer patients with bone metastasis and Western Blot analysis showed that highly metastatic, androgen-insensitive and osteotropic prostate cancer cell lines expressed higher levels of TRAF6 and CD40 and RANK receptors when compared to androgen-sensitive LNCaP cells. In addition, TRAF6 expression was significantly reduced in the anti-tumorigenic M1 phenotype, suggesting a possible involvement in macrophage anti-tumour immunity in prostate cancer. Collectively, these findings suggest that TRAF6, among other TRAFs, may be of value as a potential therapeutic target for the treatment of prostate cancer metastasis, particularly to the skeleton.

3.2.   Introduction

Prostate cancer is a heterogenous adenocarcinoma triggered by a number of genetic alterations that accumulate as the disease progresses (Hieronymus *et al.*, 2014; Arora and Barbieri, 2018). Based on its diverse molecular and genetic profiles, prostate cancer is classified as: localised, aggressive metastatic/hormone sensitive and lethal/hormone insensitive (Arora and Barbieri, 2018). A wide range of genomic alterations are detected at different stages of the disease and several studies have identified multiple DNA copy number alterations (CNAs) in a plethora of tumour-promoter and suppressor genes. These include mutations and amplifications in genes for *AR*, overexpression of *MYC,* loss of *PTEN*, mutations in *TP53*, among others (Robinson *et al.*, 2017; Hamid *et al.*, 2019; Sun *et al.*, 2019). Hence, dysregulations in a number of transduction signalling pathways have been linked to the initiation and progression of prostate cancer.

A number of studies have reported that constitutive activation of canonical and non-canonical NFκB signalling is linked to the initiation and progression of prostate cancer (Jin *et al.*, 2008; Naugler and Karin, 2008; L. Zhang *et al.*, 2009; Garg *et al.*, 2012; R. Jin *et al.*, 2013). The activation of canonical NFκB is predominantly initiated by TRAF proteins (TRAFs) (Hoesel and Schmid, 2013; Xie, 2013). All TRAFs are implicated in cancer (Zapata *et al.*, 2000; Jackson-Bernitsas *et al.*, 2007; Starczynowski *et al.*, 2011; Yamamoto *et al.*, 2017; Hyeon *et al.*, 2018; Zhu *et al.,* 2018) and, in particular, TRAF2, TRAF4 and TRAF6 play an important role in prostate cancer initiation and progression (Gudey *et al.*, 2014; Sundar *et al.*, 2015; Wei, Ruan, *et al.*, 2017; Singh *et al.*, 2018). Prostate cancer commonly metastasises to bone and several findings indicate that TRAF6/NFκB plays a substantial role in bone remodelling (Lomaga *et al.*, 1999) and in the differentiation of various immune cell types (Kobayashi *et al.*, 2003; Konno *et al.*, 2009; Walsh, Lee and Choi, 2015; Seijkens *et al.*, 2018). Thus, identifying the various abnormalities in gene expression of the TRAF/NFκB axis would aid with the development of novel treatments of advanced prostate cancer.

3.3.   Aims

The aim of this chapter was to investigate the genetic changes in TRAFs in prostate cancer.

Using publicly-available databases, this aim was achieved by examining:

- The genetic changes in TRAF1-7 in normal and tumour tissue from prostate cancer patients.

- The correlation of the expression of TRAF1-7 with AR expression in prostate cancer patients with primary adenocarcinoma and metastasis.

- The DNA copy number alterations (CNAs) in TRAF proteins in prostate cancer patients.

- The protein expression of TRAF6 in immune and prostate cancer cell lines.

3.4. Results

3.4.1. Altered expression of TRAF proteins in prostate cancer

To investigate the association of TRAF proteins with prostate cancer progression, a variety of publicly-available resources containing The Cancer Genome Atlas (TCGA) prostate cancer cohort were used. First, it was confirmed that all TRAFs, except TRAF7, are involved in pathways related to cancer. In agreement with previous findings, this analysis confirmed that TRAF2 and TRAF6 are involved in osteoclast differentiation (Lomaga *et al.*, 1999; Peramuhendige *et al.*, 2018) (**Figure 3.1A**), and as shown in **Figure 3.1B**, TRAF2, TRAF3 and TRAF6 contribute to immune activity and cytokine production. It was also found that TRAFs, except TRAF3, are implicated in signalling pathways involved in prostate cancer progression (Mukherjee *et al.*, 2011; Jin *et al.*, 2014) (**Figure 3.1C**). NFκB activation relies on TRAF1, TRAF2, TRAF5 and TRAF6 and from this pathway, TRAF2 and TRAF6 are directly involved in kinase activity (Oeckinghaus, Hayden and Ghosh, 2011). In particular, it is shown that MAPK signalling pathway is activated by TRAF2, TRAF4, TRAF6 and TRAF7 and JNK pathway is positively regulated by TRAF2, TRAF4 and TRAF6 (**Figure 3.1C**).
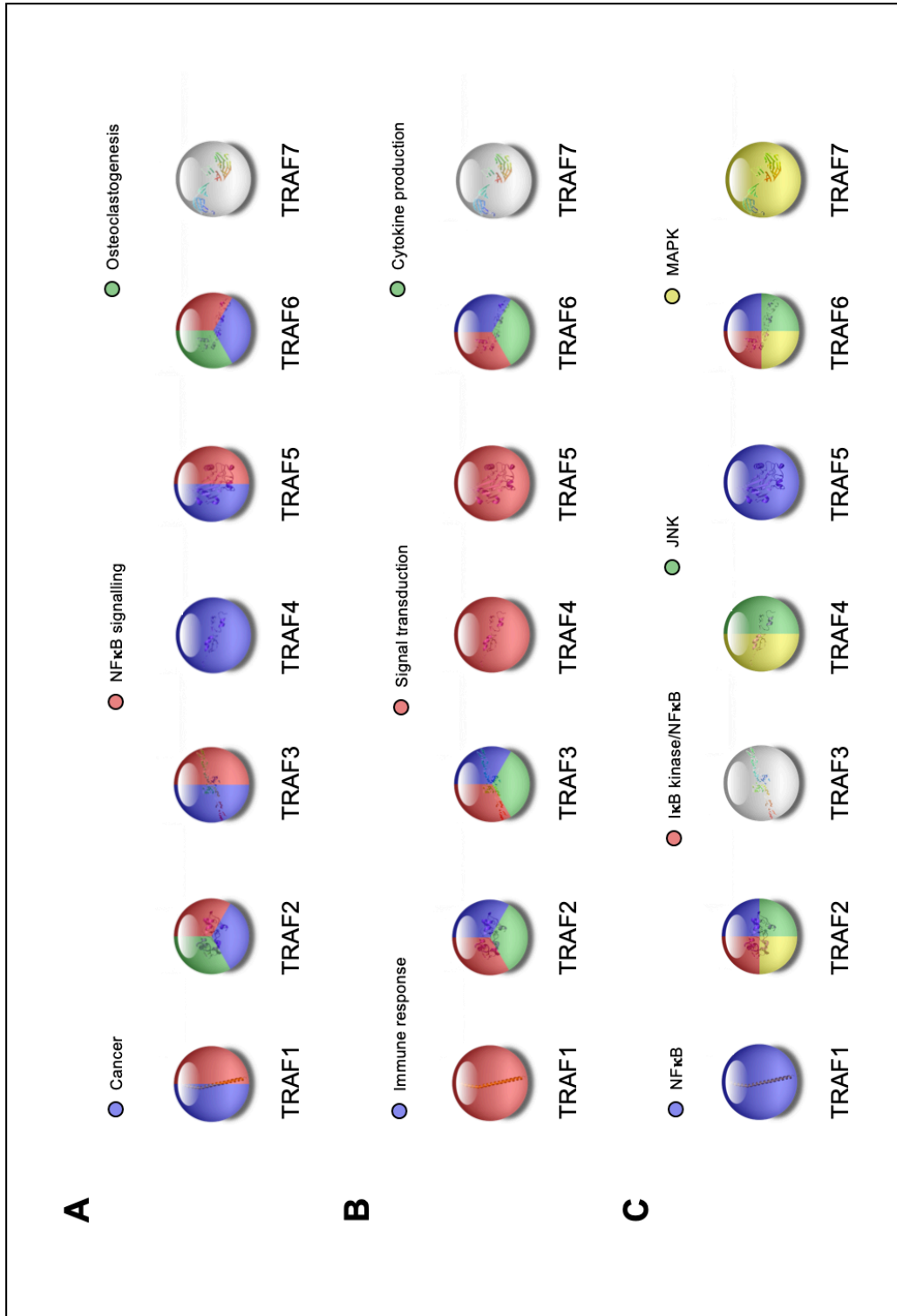
Figure 3.1. Relevant biological functions of TRAF proteins reported in STRING database. (A) Involvement of TRAF proteins established in KEGG pathways, (B) Association of TRAFs to specific biological functions related to inflammation in gene ontology database, (C) Role of TRAF proteins as mediators and activators of several signalling pathways. Non-coloured spheres have no link to activities addressed.

Next, I studied the gene expression of the TRAFs in normal and prostate cancer patients using the online databases UALCAN and UCSC Xena. **Figure 3.2** shows the heatmap expression pattern obtained from UALCAN that reveals a non-significant reduction in TRAF1 expression and an evident amplification in the expression of TRAF2, TRAF4 and TRAF7 proteins in prostate cancer patients as compared to healthy individuals. Furthermore, quantitative data obtained from UCSC Xena shows a significant difference in the expression of all TRAFs, comparing the expression of healthy and prostate cancer patients (**Figure 3.3**). Consistent with previous findings (Wei, Ruan, *et al.*, 2017; Singh *et al.*, 2018; Zhu *et al.*, 2018), the current analysis confirmed that the expression of TRAF2, TRAF4 and TRAF7 is amplified in prostate cancer tumours when compared to normal tissue. Additionally, the expression levels of TRAF1, TRAF3, TRAF5 and TRAF6 are notably reduced in prostate cancer patients. Regarding this, both databases show consistent results involving the altered expression of all TRAF proteins in prostate cancer.
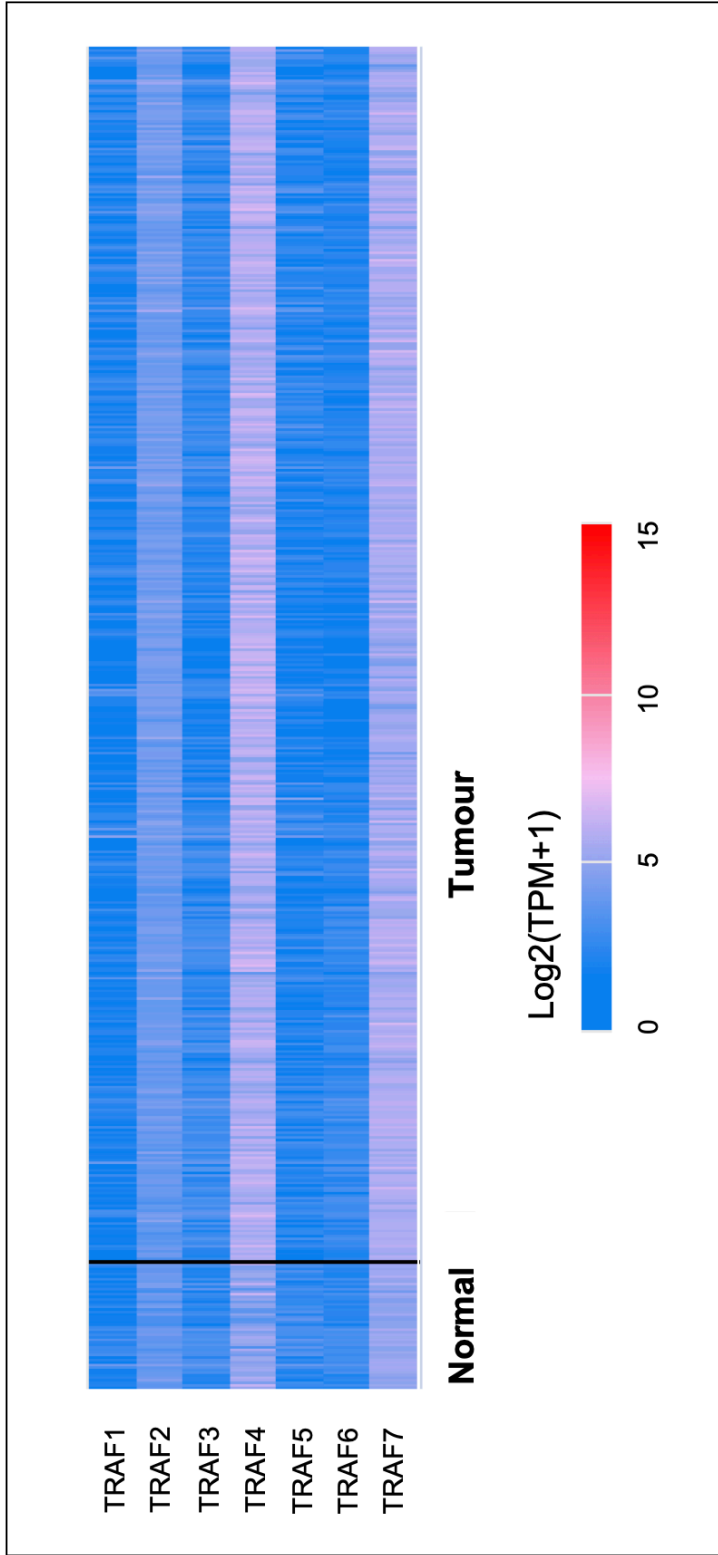
Figure 3.2. Expression pattern of TRAF proteins from healthy and prostate cancer patients, obtained from UALCAN. Data obtained from TCGA database of normal (n=52) and tumour (n=497) samples from prostate cancer patients. Blue colour represents least expression, pink represents moderate expression and red colour indicates highest expression. TPM=Transcripts Per Million.
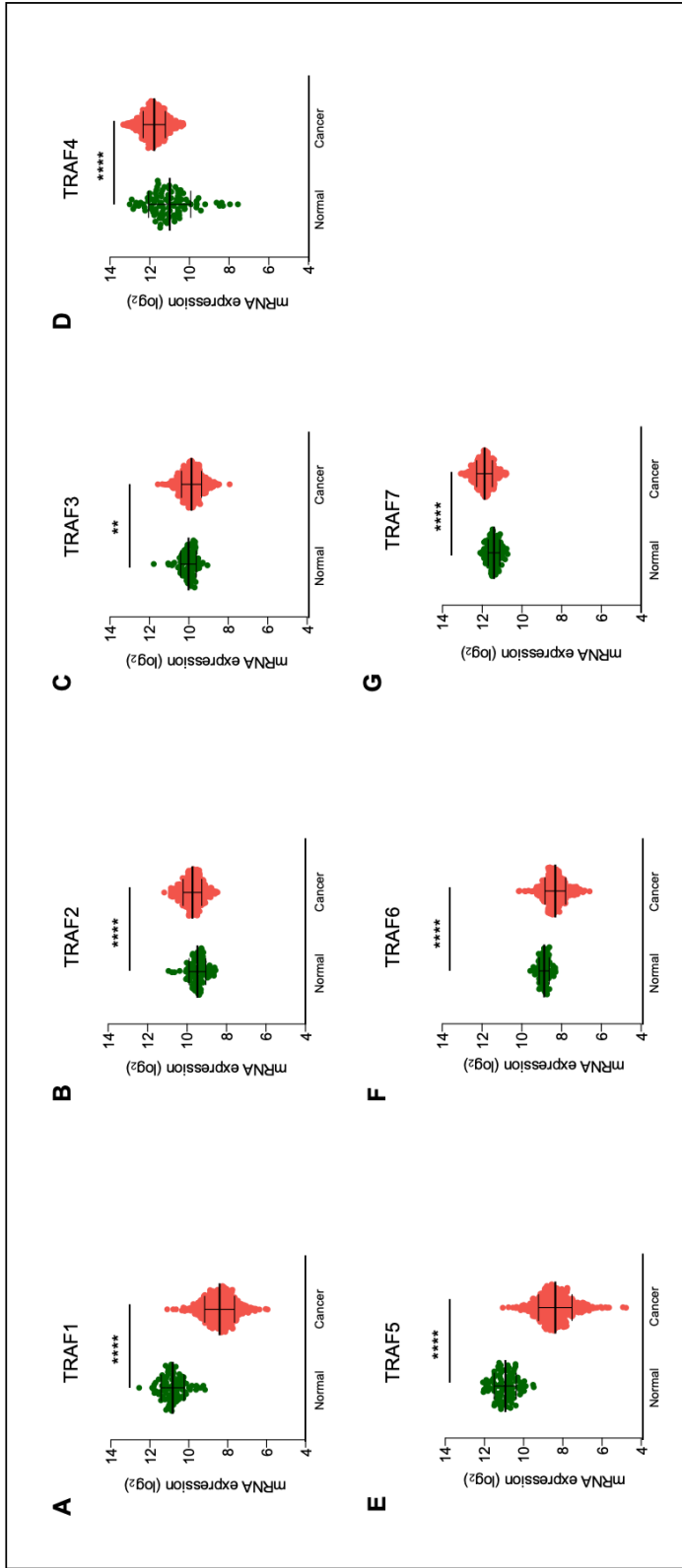
Figure 3.3. Gene expression of TRAF proteins acquired from UCSC Xena genome browser. (A-G) Expression of TRAF1-7 in TCGA prostate cancer samples (n=495) compared to normal prostate tissue (n=100). Each dot represents a single tissue sample. Black lines indicate mean and standard deviation. p-values were determined using unpaired T-test. ****p<0.0001, **p<0.005 compared to healthy gene expression.

Using the online tool TIMER, the prognostic effects of TRAF expression were examined in prostate adenocarcinoma (PRAD) by generating overall survival curves split in high and low groups via a median split (**Figure 3.4**). With the exception of TRAF1 and TRAF5, high expression of TRAFs, particularly TRAF2 ($p=0.0824$), was found to be associated with high-risk prostate cancer. Additionally, disease-free survival was significantly improved with low expression of TRAF1 ($p<0.0005$) and TRAF2 ($p<0.001$), as assessed with the online tool GEPIA (**Figure 3.5**). Overall, these results confirm the involvement of TRAF proteins in prostate cancer progression compared to healthy individuals.
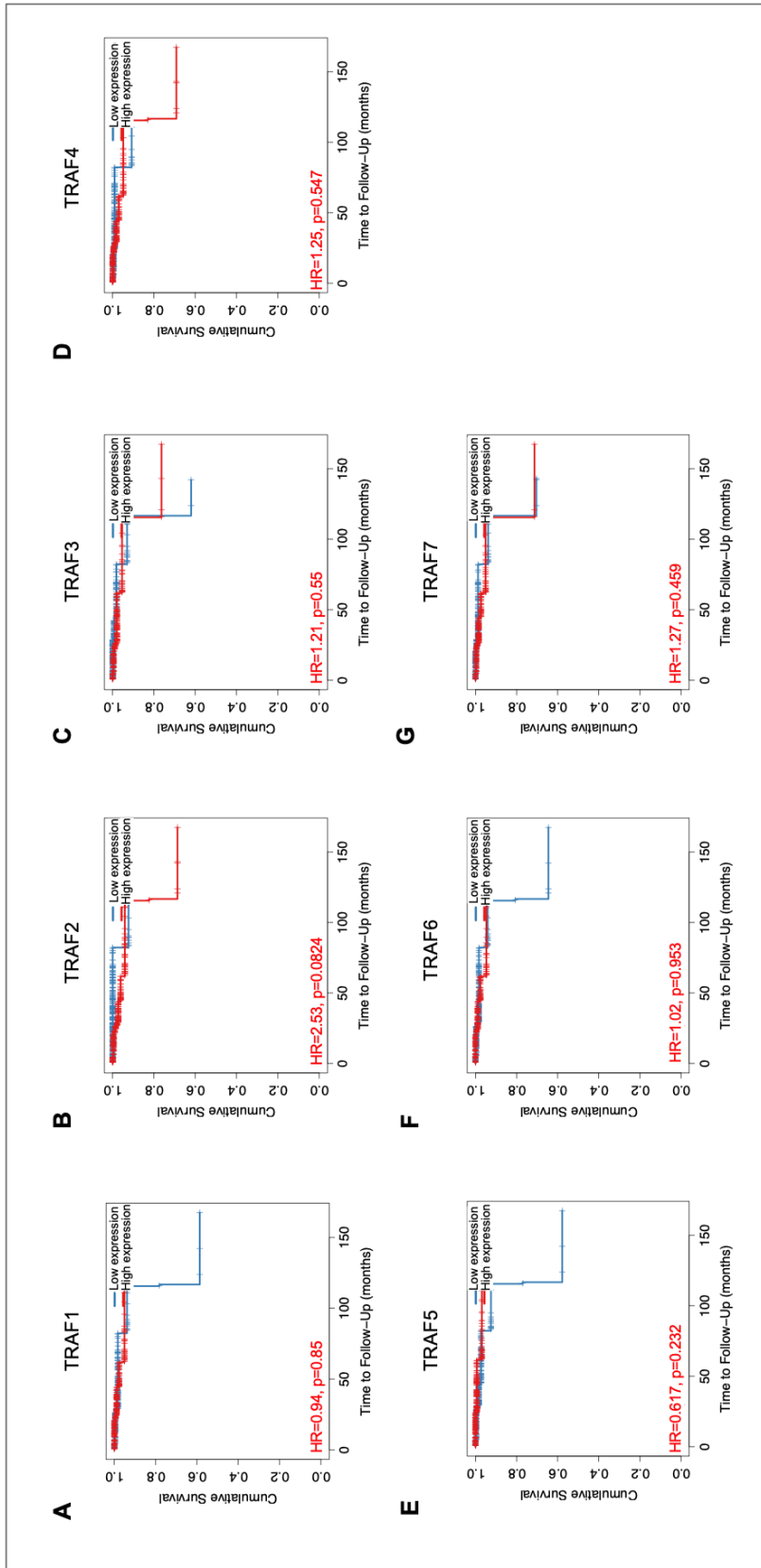
Figure 3.4. Kaplan-Meier estimator curves of overall survival of prostate cancer with altered expression of TRAFs, obtained with TIMER tool. (A-G) Kaplan-Meier overall survival plots in prostate adenocarcinoma patients of the TCGA PRAD dataset (n=498) with low (blue line) and high (red line) expression of TRAF1-7. p-values were obtained with the online tool from log-rank test to compare expression of each TRAF. HR=Hazard ratio.

71
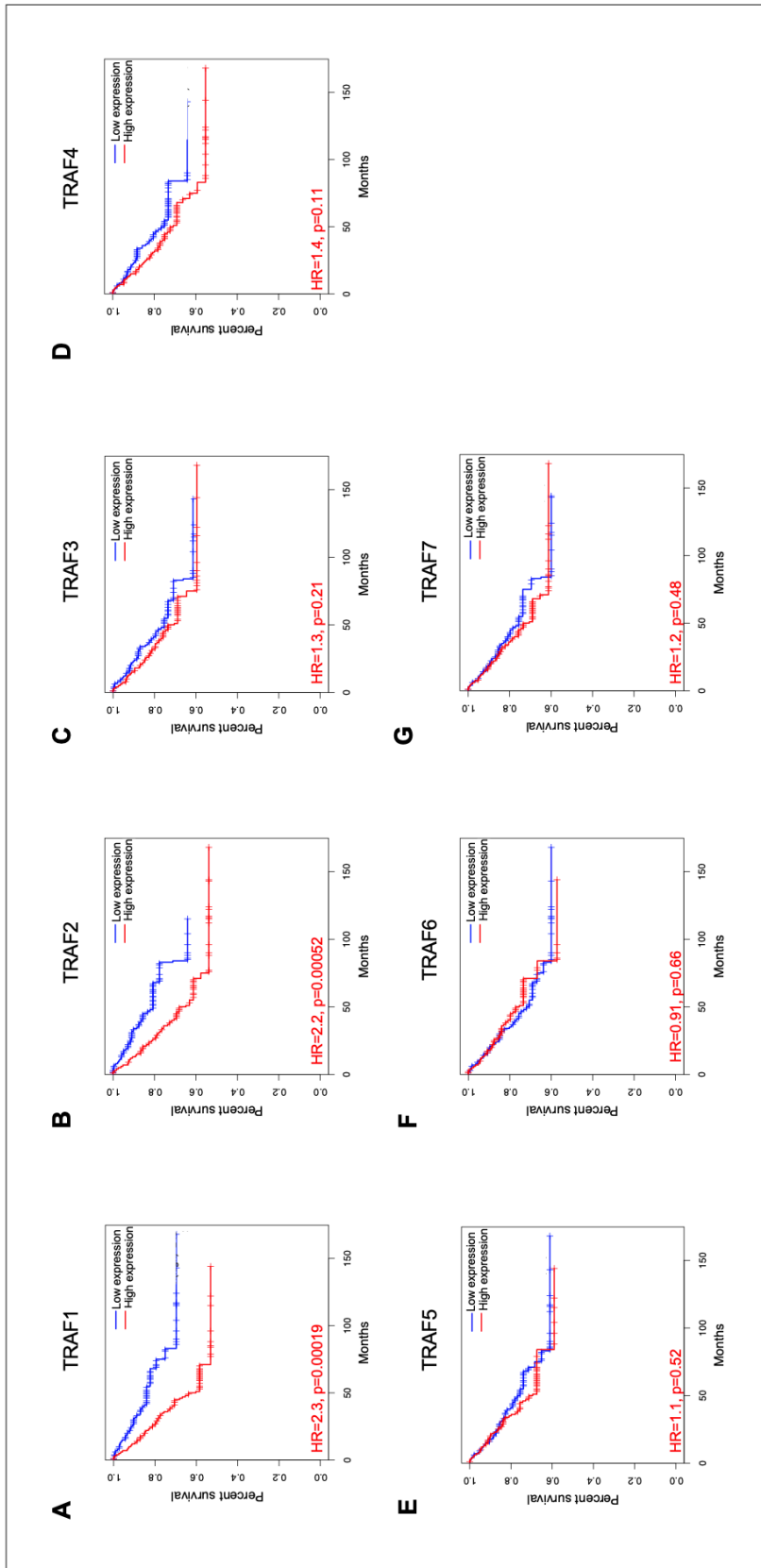
Figure 3.5. Kaplan-Meier estimator curves of disease-free survival of prostate cancer in altered expression of TRAFs, obtained with GEPIA database. (A-G) Kaplan-Meier disease-free survival plots in prostate adenocarcinoma patients of the TCGA PRAD dataset (n=498) with low (blue line) and high (red line) expression of TRAF1-7. p-values were obtained with the online tool from log-rank test to compare expression of each TRAF. HR=Hazard ratio.

3.4.2. Association of TRAFs with identified contributors of prostate cancer

Inflammation plays a substantial role in the initiation and promotion of prostate cancer (Sfanos and Marzo, 2014). Previous studies have reported that infiltration of pro-inflammatory immune and bone-marrow cells in prostate tumours and distant organs, particularly bone, supports prostate cancer progression and spread (Zhao *et al.*, 2012; Fang *et al.*, 2013; Martinez-Marin *et al.*, 2017). Androgen receptor (AR) is a well-known contributor to various aspects of prostate cancer (Fang *et al.*, 2013), and elevated activity of the pro-inflammatory NFκB pathway is implicated in the regulation of expression and activity of AR (L. Zhang *et al.*, 2009; Xia, L., Shen, S., 2014).

To assess the association of key components of the TRAF/NFκB pathway to AR expression, the correlation between TRAFs and AR expression was examined in primary tumour and metastatic prostate cancer datasets using cBioPortal online tool. In previous publications, positive correlations with AR have been studied to identify potential promoters of prostate cancer (L. Zhang *et al.*, 2009; Nabbi *et al.*, 2017). The strength of association was determined by the correlation coefficient, namely R value (Mukaka, 2012), and data showed that TRAF3 and TRAF6 have a significantly positive correlation with AR at initial stages of prostate cancer (**Figure 3.6**). In patients with metastatic prostate cancer, AR expression showed a positive correlation with TRAF3 and TRAF7, being negligible or negative for all other TRAFs (**Figure 3.7**). The R values obtained from primary prostatic tumours and metastatic prostate cancer are summarised in **Table 3.1.**
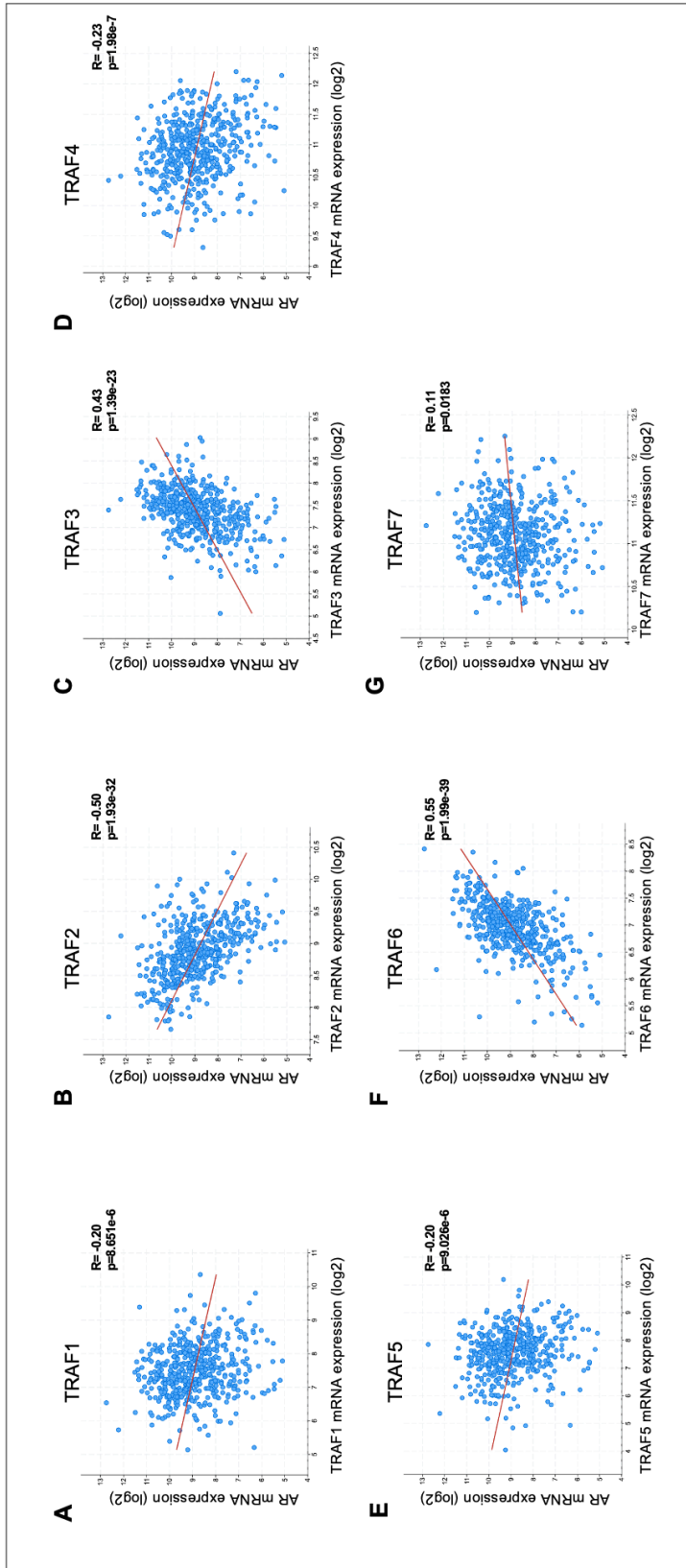
Figure 3.6. Spearman Correlation of mRNA expression between androgen receptor and TRAF proteins in prostate adenocarcinoma patients using cBioPortal. (A-G) TRAF1-7 mRNA expression correlated with androgen receptor expression. Data obtained from TCGA dataset of adenocarcinoma (n=488) prostate cancer patients. R is the correlation coefficient representing the strength of association with values between -1 and +1, showing a direct link for positive values. Each dot represents a single sample. p-values represent significance and were determined with the online tool.
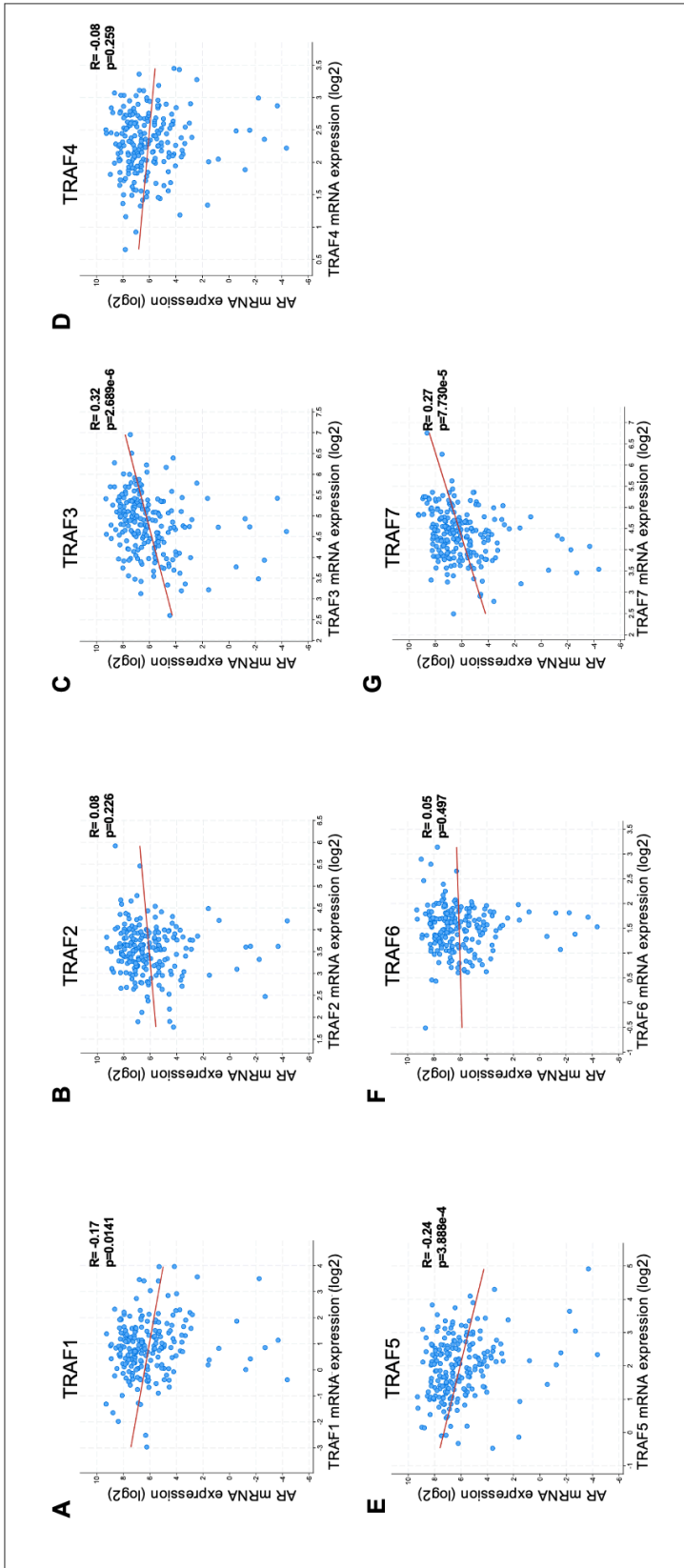
Figure 3.7. Spearman Correlation of mRNA expression between androgen receptor and TRAF proteins in metastatic prostate cancer patients using cBioPortal. (A-G) TRAF1-7 mRNA expression correlated with androgen receptor expression. Data obtained from TCGA dataset of metastatic (n=212) prostate cancer patients. R is the correlation coefficient representing the strength of association with values between -1 and +1, showing a direct link for positive values. Each dot represents a single sample. p-values represent significance and were determined with the online tool.

Table 3.1. Spearman correlation R values of AR expression with TRAFs in primary tumour and metastatic prostate cancer. PCa=Prostate cancer.

	PCa patients (n=488)	PCa patients with metastasis (n=212)
TRAF1	-0.20	-0.17
TRAF2	-0.50	0.08
TRAF3	0.43	-0.08
TRAF4	-0.23	0.32
TRAF5	-0.20	-0.24
TRAF6	0.55	0.05
TRAF7	0.11	0.27

Next, the online software TIMER was used to investigate the link between the infiltration of immune cell populations and TRAF expression in prostate cancer (**Figure 3.8** and **Supplementary Figure 1** for original graphs). Notably, the expression of TRAF2, TRAF4 and TRAF7 showed a negative correlation with the presence of tumour-infiltrating immune cells. Interestingly, TRAF2 had the most negative correlation with CD8+ T cells and also, a positive correlation with CD4+ T cells. In contrast, a positive and uniform association of the infiltrating immune cell populations is observed with the expression of TRAF3 and TRAF6. In particular, TRAF6 exhibited the strongest positive correlation with CD8+ cytotoxic T cells (R=0.6, p<0.0001). Similarly, TRAF1 and TRAF5 shared a resembling infiltrating immune cell profile that shows high association between TRAF1 and TRAF5 expression and CD4+ T cells and neutrophils. A weak correlation of TRAF1 and TRAF5 expression with CD8+ T cells and a moderate association with the other immune cells was also observed (**Figure 3.8A and E**, respectively). Interestingly, no association between TRAF2 and AR or TRAF2 with immune cell infiltration was found.
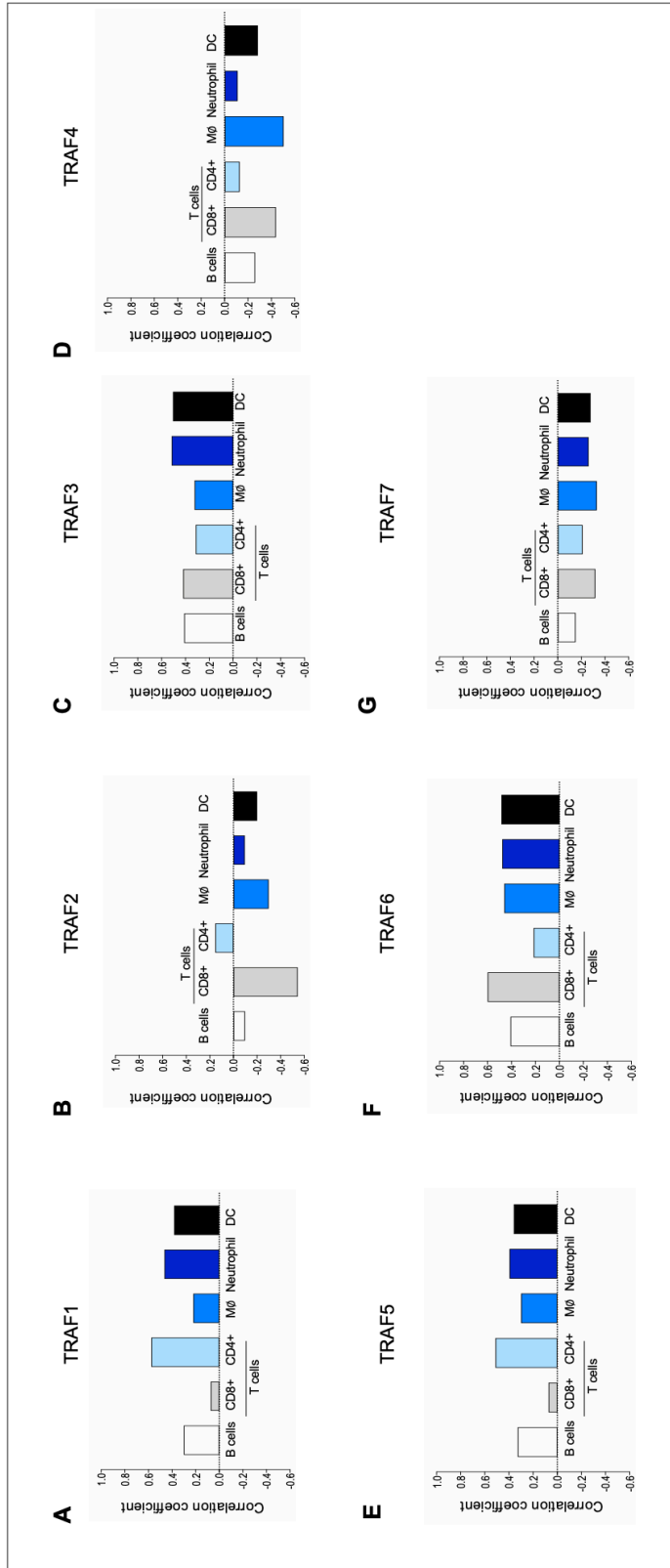
Figure 3.8. Pearson correlation coefficient of tumour-infiltrating immune cells with TRAF1-7 expression in prostate cancer assessed by TIMER. Correlation coefficient of TRAF1-7 (A-G) with the specified tumour-infiltrating immune cells. Data obtained from TCGA database of prostate cancer patients (n=497). Correlation values displayed in the graphs are based on the negative association with tumour purity in order to determine the gene expression of the immune cells in the environment. CD=Cluster of differentiation, DC=Dendritic cells. MØ=Macrophages.

3.4.3. TRAF6 and related NFκB components are highly amplified in metastatic prostate cancer

Genetic alterations in TRAF proteins are commonly found in different types of cancer (Zhu *et al.*, 2018) and upregulated expression of TRAF2 and TRAF4 has been previously reported in prostate cancer (Yang *et al.*, 2009; Wei, Ruan, *et al.*, 2017; Singh *et al.*, 2018). To gain a better understanding of the complex interactions between the TRAFs involved in the progression of prostate cancer, I first studied the interactions between different TRAF proteins using STRING.

As shown in **Figure 3.9,** most interactions between the TRAFs have been confirmed experimentally and with curated databases. TRAF7 has no reported interaction with other TRAFs. On the other hand, TRAF6 interacts with TRAF1 to 5 and TRAF2 and TRAF3 interact with all TRAFs, except TRAF4 and TRAF7.
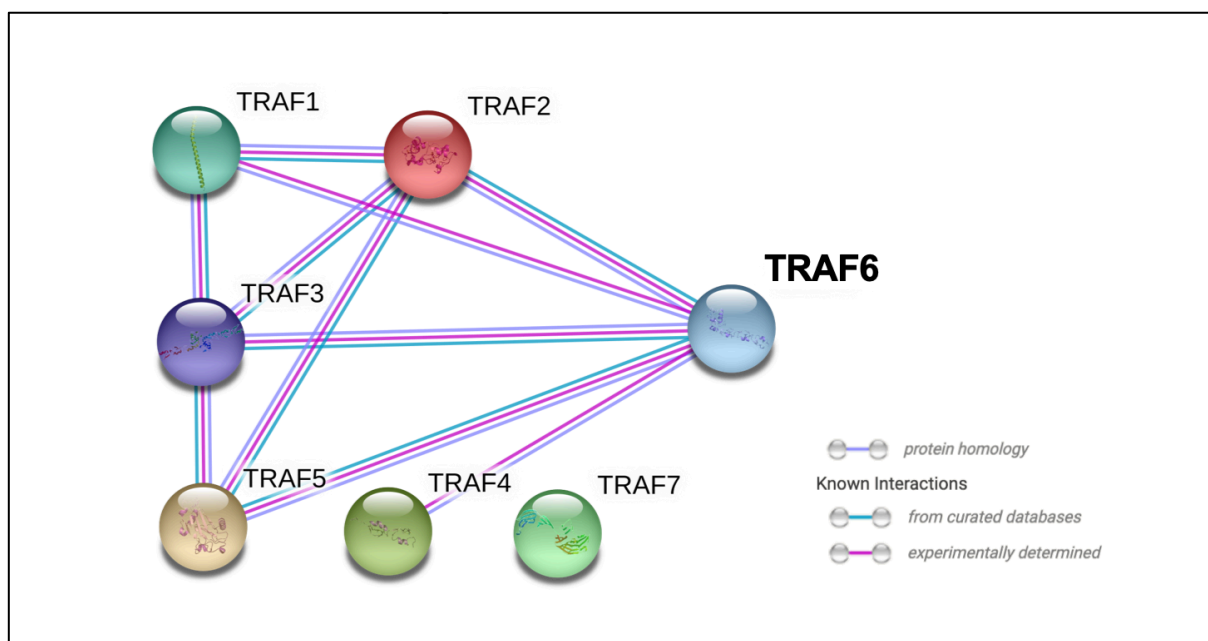
Figure 3.9. Reported interactions of TRAF proteins found in STRING database. TRAFs 1-7 predicted and experimentally confirmed interactions between each other. Purple line indicates protein homology, blue line represents information from curated databases and pink is based on experimentally determined interactions.

Next, CNAs in prostate cancer patients were investigated to determine acquired modifications at DNA-level regarding the expression of TRAF proteins. Briefly, correct selection of databases was confirmed by using commonly altered genes in prostate cancer as inputs (see **Supplementary Figure 2.**) (Taylor *et al.*, 2010; Rubin and Demichelis, 2018). As shown in **Figure 3.10**, the most common CNA of TRAF proteins found in primary prostate tumours is amplification, particularly of TRAF7, followed by TRAF2 and TRAF5, and all TRAF proteins mostly present amplified CNAs at a metastatic stage. Little or no modifications in the percentage of deletions in TRAF1, TRAF3, TRAF4 and TRAF5 were found at the primary and advanced stages. Deletions of TRAF2 and TRAF7 augmented in metastasis and, in contrast, TRAF6 deletions reduced. Mutations at metastatic stages of prostate cancer were found to be increased in TRAF1, TRAF3 and TRAF5, decreased in TRAF2 and TRAF7, and remained unmodified in TRAF4 and TRAF6. The effects of CNAs were confirmed by studying mRNA expression of the TRAFs at primary and metastatic stages of prostate cancer (**Supplementary Figure 3**).

Then, the chromosomal alterations of TRAF proteins were studied in patients with bone metastasis. As observed in **Figure 3.11**, prostate cancer patients with bone metastasis present deletions of TRAF3 and TRAF7 and gains or amplifications of TRAF1, TRAF2 and particularly, TRAF6, which in fact was found in approximately 30% of patients.
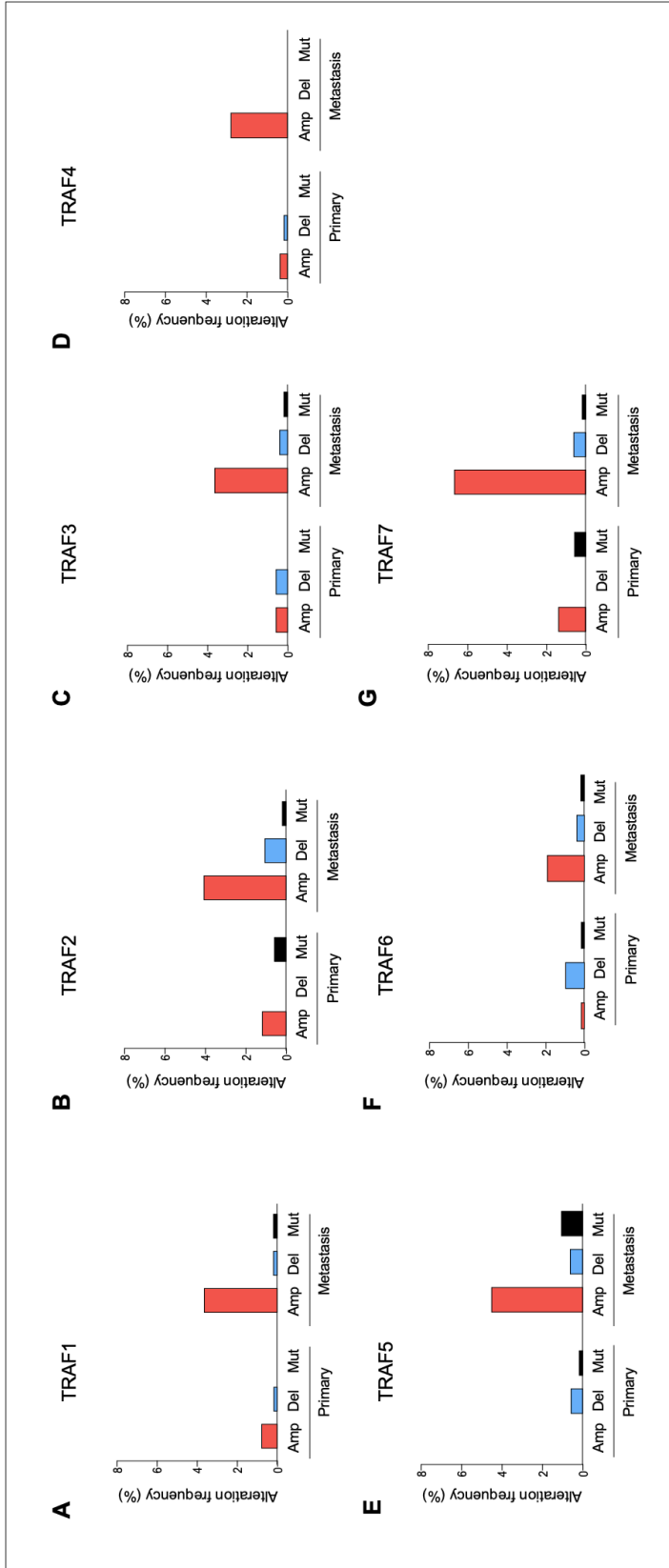
Figure 3.10. Copy-number alterations of TRAF proteins in primary and metastatic prostate cancer patients using cBioPortal. Percentage of alteration frequency involving amplification (Amp), deletion (Del) and mutation (Mut) found in TRAF1-7 (A-G) from different stages of prostate cancer. Data obtained from TCGA databases of primary (n=494) and metastatic (n=463) prostate cancer patients.
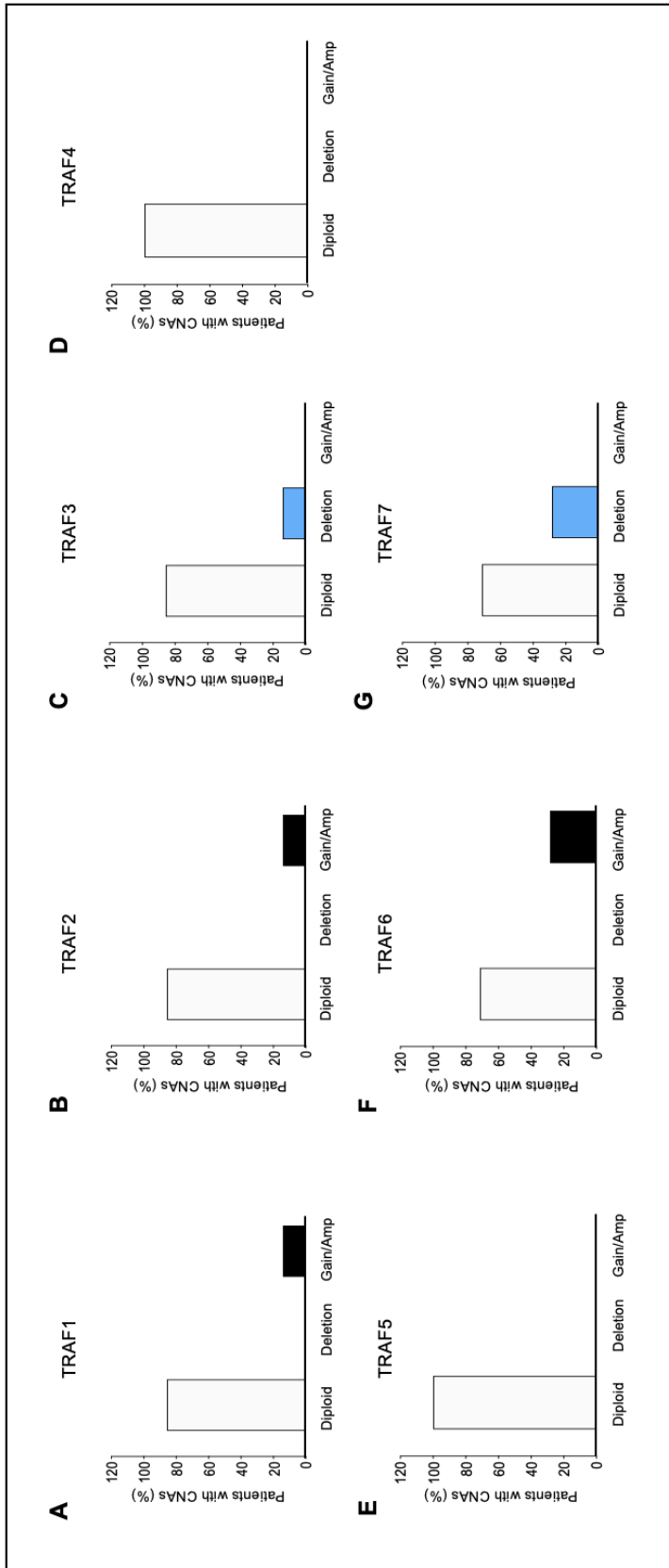
Figure 3.11. Expression of TRAF proteins in prostate cancer bone metastasis using cBioPortal. Percentage of patients with diploid or copy-number alterations involving deletions and gain/amplifications (Gain/Amp) in TRAF1-7 (A-G). Data obtained was accessed with cBioPortal from the publicly available TCGA database " The Metastatic Prostate Cancer Project" (n=30).

As several NFκB components have been linked to dysregulation of the MAPK pathway in prostate cancer (Gasparian *et al.*, 2002; L. Zhang *et al.*, 2009), amplifications in MAPK- and NFκB-related receptors upstream of TRAF6 (**Figure 3.12A**) and downstream signalling proteins (**Figure 3.12B**) were investigated. The ratio of metastatic and primary prostate cancer CNAs showed elevated amplifications in the expression of several receptors, specifically CD40, TNF-α Receptor (TNFRSF1A), Transforming Growth Factor β Receptor (TGFR-β) and insulin growth-like factor 1 receptor (IGF-1R), and in various ligands, particularly CD40L and TNF-α. In addition, various signalling proteins downstream of TRAF6, including p38, JNK, p65 (RELA) and Akt, were found to be highly expressed in patients with metastatic disease.
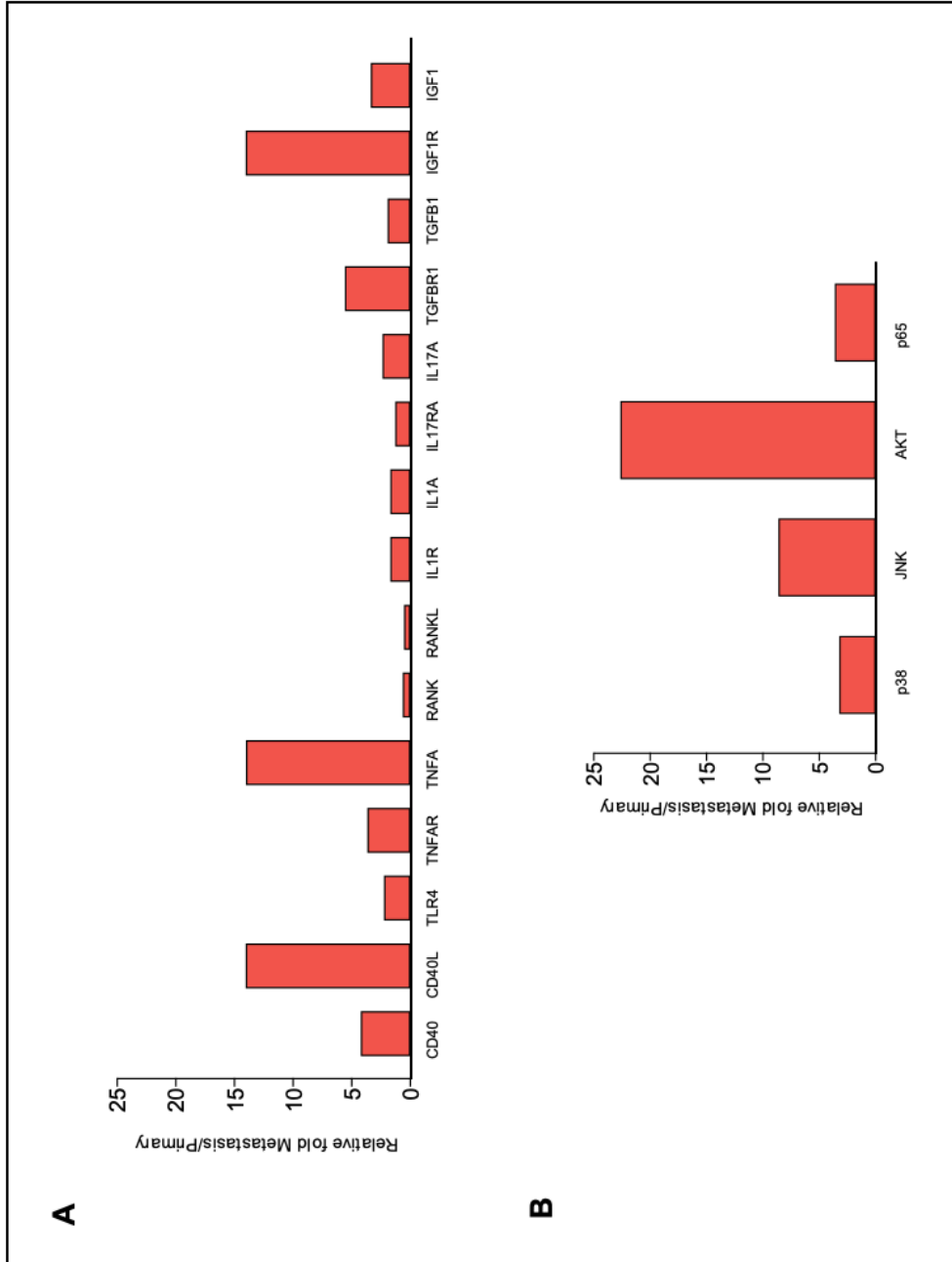
Figure 3.12. Metastasis/Primary prostate cancer ratio of upstream and downstream components of the TRAF6/NFKB pathway. Ratio of metastatic/primary prostate cancer alterations involving amplification (Amp), deletion (Del) and mutation (Mut) found in (A) upstream molecules involved in TRAF6 recruitment and (B) downstream effectors activated by TRAF6. Ratio was calculated based on the percentages of amplifications obtained from TCGA databases of metastatic (n=463) over primary (n=494) prostate cancer patients.

3.4.4. TRAF6 protein expression levels and of receptors CD40 and RANK in a panel of human and mouse prostate cancer cell lines and in different macrophage subtypes

RANK and CD40 receptors have a unique binding site for TRAF6 (Park, 2018). Thus, the expression of TRAF6 and these receptors was assessed in a panel of mouse and human prostate cancer cells with different growth and metastatic capabilities by using Western Blot analysis. The human C42-B4 and the osteotropic and castration-resistant murine RM1-BM and human DU145 and PC3 prostate cancer cells expressed higher levels of CD40, RANK (**Figure 3.13**) and TRAF6 (**Figure 3.14A and C**) when compared to the parental androgen-sensitive LNCaP.

Furthermore, given the involvement of macrophages in prostate cancer progression and the important role of TRAF6 in macrophage differentiation and lineage commitment, I next assessed TRAF6 expression in uncommitted macrophage-osteoclast precursors (MØ) and in anti-tumorigenic M1 and pro-tumorigenic M2 macrophage subtypes, derived from differentiated monocyte-like THP-1 cells and by previously confirming their phenotypes using flow cytometry (**Supplementary Figure 4**). As shown in **Figure 3.14B and D**, the anti-tumorigenic M1 phenotype showed a significant decrease in TRAF6 expression compared to uncommitted MØ and pro-tumorigenic M2 macrophage subtypes.
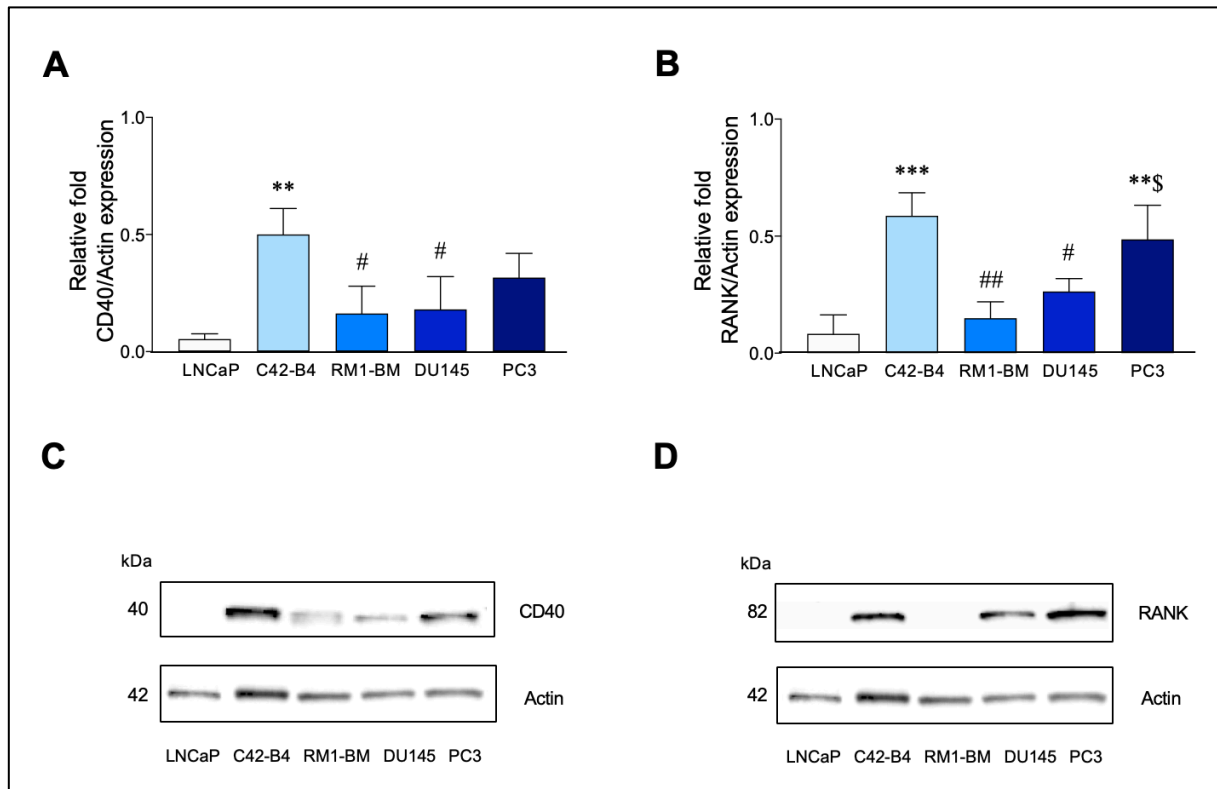
Figure 3.13. Expression of TRAF6 receptors, CD40 and RANK, in a panel of human prostate cancer cell lines. Relative fold of CD40/Actin (A) and RANK/Actin (B) expression from LNCaP and its derivative C42-B4 and highly metastatic mouse RM1-BM and human DU145 and PC3 prostate cancer cells. Representative Western Blot images of expression of CD40 (C) and RANK (D). The data are mean $\pm$ standard deviation (n=3). p-values were obtained from ordinary ANOVA test followed by Tukey *post hoc* test. ***$p<0.0005$, **$p<0.005$, *$p<0.05$ compared to LNCaP, ##$p<0.005$, #$p<0.05$ compared to C42-B4, \$$p<0.05$ compared to RM1-BM.

Figure 3.14. TRAF6 expression in a panel of human prostate cancer cell lines and in different macrophage subtypes. Relative fold of TRAF6/Actin expression in (A) LNCaP and its derivative C42-B4 and highly metastatic mouse RM1-BM and human DU145 and PC3 and (B) uncommitted (MØ), anti-tumorigenic (M1) and pro-tumorigenic (M2) macrophage subtypes. Representative Western Blot images of expression of prostate cancer cells (C) and macrophages (D). The data are mean ± standard deviation (n=3). p-values were obtained from ordinary ANOVA test followed by Tukey *post hoc* test. ****$p<0.0001$, **$p<0.01$, *$p<0.05$ compared to control (LNCaP or MØ), ++$p<0.01$, +$p<0.05$ compared to PC3, \$$p<0.05$ compared to M2.
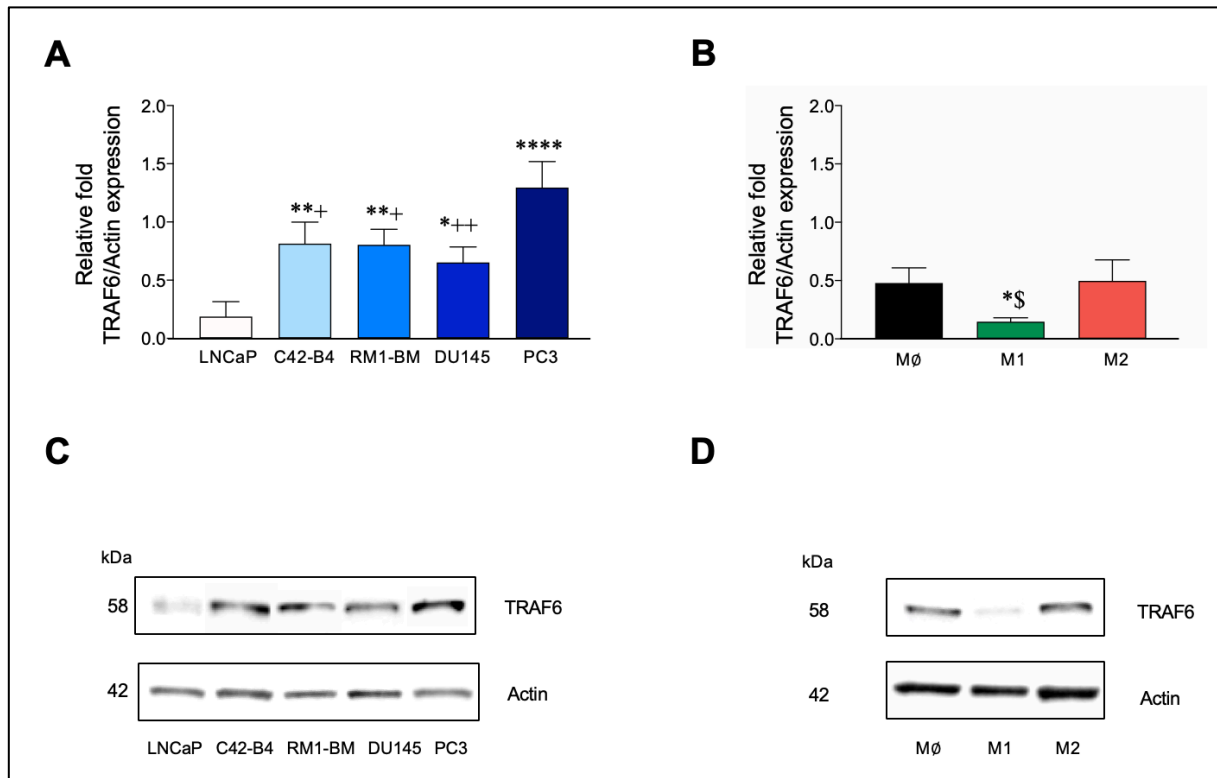
3.5.   Discussion

TRAF proteins are key modulators of several biological processes and their genetic alterations have been linked to cancer progression (Zhu *et al.*, 2018). Previous findings have confirmed the involvement of TRAF2, TRAF4 and TRAF6 in prostate cancer progression (Ahmed *et al.*, 2013; Sundar *et al.*, 2015; Wei, Ruan, *et al.*, 2017). In this chapter, a combination of publicly available resources and Western Blot analysis were used to examine the association between genetic modifications of TRAF proteins and prostate cancer initiation and metastasis. The initial results confirmed the involvement of all TRAFs, except TRAF7, in cancer. This finding can be attributed to the understudied signalling mechanisms of TRAF7 since it is generally not considered as a classical member of the TRAF family due to lack of the highly conserved TRAF domain and thereby, lack of interaction with members of the TNFR superfamily (Zhu *et al.*, 2018). The analysis in datasets from prostate cancer patients showed that all TRAFs exhibited modified expression compared to healthy tissue and a marked amplification was only observed in TRAF2 and TRAF4 (as described in the literature) and TRAF7. The analyses of overall survival confirmed these findings and showed that high expression of TRAF2, TRAF4 and TRAF7 was associated to high-risk prostate cancer; however, this was found not to be statistically significant. Moreover, disease-free survival was significantly affected by high expression of TRAF1 and TRAF2. Of all key factors that contribute to enhanced prostate cancer progression, AR expression was found to be positively correlated with TRAF3 and TRAF6 at initial stages of the disease and to TRAF4 and TRAF7 at a metastatic stage. The expression of TRAF3 and TRAF6 was also found to be highly associated with the number of tumour-infiltrating immune cells. Interestingly, these data suggest that even though TRAF2 is overexpressed in prostate cancer tissue, it plays a minor role in influencing the tumour microenvironment. The analysis of protein-protein interactions confirmed that TRAF6 interacts with all other TRAFs (except TRAF7, possibly due to lack of exploration) and studies on genetic modifications suggested that TRAF6 represents a potential therapeutic target for prostate

cancer metastasis since it exhibited the highest gain/amplification in prostate cancer patients with bone metastasis, along with elevated amplifications found in downstream components of oncogene Akt and JNK MAPK. Amplifications in AR were also found in the same cohort of patients (**Supplementary Figure 5**) and it is well-known that alterations in AR play a critical role throughout the development of prostate cancer and at a metastatic stage (Barfeld *et al.*, 2012; Culig and Santer, 2014). Importantly, selecting TRAF6 as a target for the study of the prostate cancer bone metastatic microenvironment was supported by previous reports implicating TRAF6 in prostate cancer progression (Sundar *et al.*, 2015; Aripaka *et al.*, 2019), the specific receptor-interaction of TRAF6 compared to other TRAFs and the requirement of TRAF6 in immune cell function and bone homeostasis, particularly in osteoclastogenesis (Kobayashi *et al.*, 2001; Kobayashi, Walsh and Choi, 2004; Lamothe *et al.*, 2007; Zhuang *et al.*, 2017; Seijkens *et al.*, 2018).

These results showed for the first time that TRAF6 and its related receptors CD40 and RANK are highly expressed in AR-insensitive, highly metastatic and osteotropic prostate cancer cells. Interestingly, a significant reduction of TRAF6 was also detected in anti-tumorigenic M1 macrophages, thereby implicating TRAF6 in macrophage anti-tumour immunity. Although some studies have failed to show that TRAF6 inhibition affects macrophage lineage commitment (Bosch *et al.*, 2019), genetic inactivation of TRAF6 is known to abolish macrophage differentiation into osteoclasts induced by the pro-inflammatory CD40L, IL-1β and LPS (Lomaga *et al.*, 1999). Thus, further analyses of the effects of TRAF6 inhibition on macrophage lineage commitment were addressed in this study.

Table 3.2 summarises the main findings of this chapter that, altogether, suggest that TRAF6 is involved in bone metastasis and anti-tumour macrophage immunity in prostate cancer. Thus, TRAF6 inhibition may be of value in the treatment of prostate cancer metastasis, particularly to the skeleton.

Table 3.2. Summary of the key findings involving the expression of TRAF proteins in prostate cancer initiation, progression and metastasis.
± indicates neutral, + indicates moderately high, ++ high and +++ very high. - indicates moderately low and - - low.

	TRAF1	TRAF2	TRAF3	TRAF4	TRAF5	TRAF6	TRAF7
Involvement in cancer and osteoclastogenesis	++	++	++	+	++	**++**	-
Activator in cancer-related signalling pathways	+	+++	-	++	++	**+++**	+
Expression in cancer vs. normal tissue	- -	+	±	+	- -	**-**	+
Increased hazard ratio in overall survival	No	Yes	Yes	Yes	No	**Yes**	Yes
Correlation with AR at initial stages of PCa	-	- -	++	-	-	**++**	+
Correlation with infiltrating immune cells	++	-	+++	-	+	**+++**	-
Increased DNA amplification in metastasis	++	++	++	+	+++	**+**	+++
Gain/Amplification in bone metastasis	+	+	++	++	-	**+++**	+

Chapter 4. Effects of cancer-specific inhibition of TRAF6 on prostate cancer cell behaviour *in vitro* and osteolysis in mice

4.1.   Summary

TRAF6, a key member of the TRAF family, plays a critical role in osteoclastogenesis and studies in the literature and in **Chapter 3** suggest that TRAF6 inhibition could be of value in the treatment of prostate cancer bone metastasis. However, the effects of manipulation of cancer-specific TRAF6 on prostate cancer-induced bone disease have not been investigated. In this chapter, the role of cancer-specific TRAF6 on prostate cancer cell growth, motility and ability to influence bone cell activity and to cause osteolysis was investigated. To achieve this, I successfully knocked down TRAF6 in the highly metastatic human DU145 and PC3 prostate cancer cells by lentiviral transduction using three shRNA constructs. The DU145 and PC3 cell colonies with the lowest expression of TRAF6 were chosen for following experiments. Further mechanistic Western Blot analysis of NFκB signalling showed that TRAF6 knockdown caused a significant reduction in the expression of transcriptional factor p65 when compared to control cells. Furthermore, TRAF6 knockdown in DU145 and PC3 cells showed a significant reduction in cell growth, migration and invasion and a modest decrease in their ability to influence osteoclast formation and osteoblast maturation *in vitro*. *In vivo*, no differences were found in either cortical or trabecular bone volume in nude mice inoculated with mock or TRAF6-deficient PC3 cells by intratibial injection. Altogether, these findings suggest that TRAF6 knockdown reduces the ability of the human PC3 and DU145 prostate cancer cells to grow, move and influence bone cells *in vitro*. However, the results of the *in vivo* experiment showed that cancer-specific inhibition of TRAF6 was not sufficient to protect against osteolysis in the human PC3 model of immunodeficient mice.

4.2.   Introduction

Constitutive activation of the NFκB pathway has been implicated in prostate cancer progression (S. Huang *et al.*, 2017; Zhu *et al.*, 2018), and TRAF2, TRAF4 and TRAF6, key components of NFκB signalling, have been found to be upregulated in prostate tumours (Wei, Ruan, *et al.*, 2017; Singh *et al.*, 2018; Aripaka *et al.*, 2019). Knockdown of TRAF2 (Wei, Ruan, *et al.*, 2017) and TRAF4 (Ahmed *et al.*, 2013) reduced the growth and migration of prostate cancer cells *in vitro*. Several studies have examined the involvement of TRAF6 in the growth and motility of prostate cancer cells *in vitro* (Gudey *et al.*, 2014; Sundar *et al.*, 2015; Aripaka *et al.*, 2019) and *in vivo,* as Yang and colleagues (2009) showed that subcutaneous injection with TRAF6-deficient PC3 in mice had reduced tumour growth compared to control mice (Yang *et al.*, 2009).

TRAF6 is a key regulator of RANKL-induced osteoclast formation, survival and bone resorption (Gohda *et al.*, 2005) and TRAF6-deficiency is linked to osteopetrosis and reduced osteoclast formation (Lomaga *et al.*, 1999; Naito *et al.*, 1999). CD40-TRAF6 signalling is implicated in the maturation and activation of various immune cells including dendritic cells, macrophages and B cells (Dainichi *et al.*, 2019). TRAF6 plays an important role in these functions as a result of its involvement in the signalling of various systematic and bone- and tumour-derived pro-inflammatory mediators that include RANKL, TNFα, IL-1β, TGF-β (Lamothe *et al.*, 2007; Lu *et al.*, 2014; Sundar *et al.*, 2015) and others immune modulators such as CD40L and LPS (Kobayashi *et al.*, 2003).

To have a better understanding of the role of TRAF6 in prostate cancer cell behaviour in bone, the effects of TRAF6 inhibition were studied on prostate cancer cell growth, motility and ability to influence bone cell activity and to cause osteolysis in models of human prostate cancer.

4.3.   Aims

The aim of this chapter was to successfully knockdown TRAF6 in the highly metastatic human prostate cancer cells DU145 and PC3 cells and investigate the effects of cancer-specific inhibition of TRAF6 on:

- The expression of TRAF6 and NFκB p65.

- The *in vitro* viability, migration and invasion of prostate cancer cells*.*

- The ability of prostate cancer cells to influence

    o   Osteoclast formation *in vitro.*

    o   Osteoblast differentiation and bone nodule formation *in vitro.*

- The osteolysis in immunodeficient mice bearing the human prostate cancer cells PC3*.*

4.4.   Results

4.4.1.   Confirmation of successful knockdown of TRAF6 in human DU145 and PC3 prostate cancer cells

In **chapter 3**, I confirmed that the highly metastatic human DU145 and PC3 prostate cancer cells express high levels of TRAF6 when compared to hormone-dependent LNCaP cells. Here, stable TRAF6 knockdown was performed in the human DU145 and PC3 cells using lentiviral vectors expressing three TRAF6 shRNA individual clones and one empty vector (mock), as control. Successful TRAF6 knockdown was confirmed by analysing TRAF6 protein expression with the use of Western Blot. As shown in **Figure 4.1**, TRAF6 expression was significantly reduced in all three colonies of DU145 and PC3 prostate cancer cells when compared to the mock group, with approximately over 70% reduction of TRAF6 detected in colonies shRNA TRAF6 knockdown 1 (shT6KD[1]) and shT6KD[2] of each cell line. Thus, these two colonies were chosen for following experiments.

TRAF6 plays an important role in the activation of canonical NFκB signalling (Lalani *et al.*, 2018) and previous studies have shown that TRAF6 associates with TRAF2 to coordinate the activation of this pathway (Jabara *et al.*, 2002). To further confirm the successful knockdown of TRAF6 in human DU145 and PC3 cells, I assessed the expression of TRAF2 and downstream components of the NFκB pathway, namely IκB-α and NFκB p65, using Western Blot analysis. As shown in **Figure 4.2**, TRAF6 knockdown significantly reduced the constitutive expression of NFκB p65 in human DU145 and PC3 without significantly affecting TRAF2 expression. In addition, no significant decrease was detected in IκB-α expression in TRAF6-deficient human DU145 and PC3 cells, indicative of inhibition of canonical NFκB signalling in these cells.
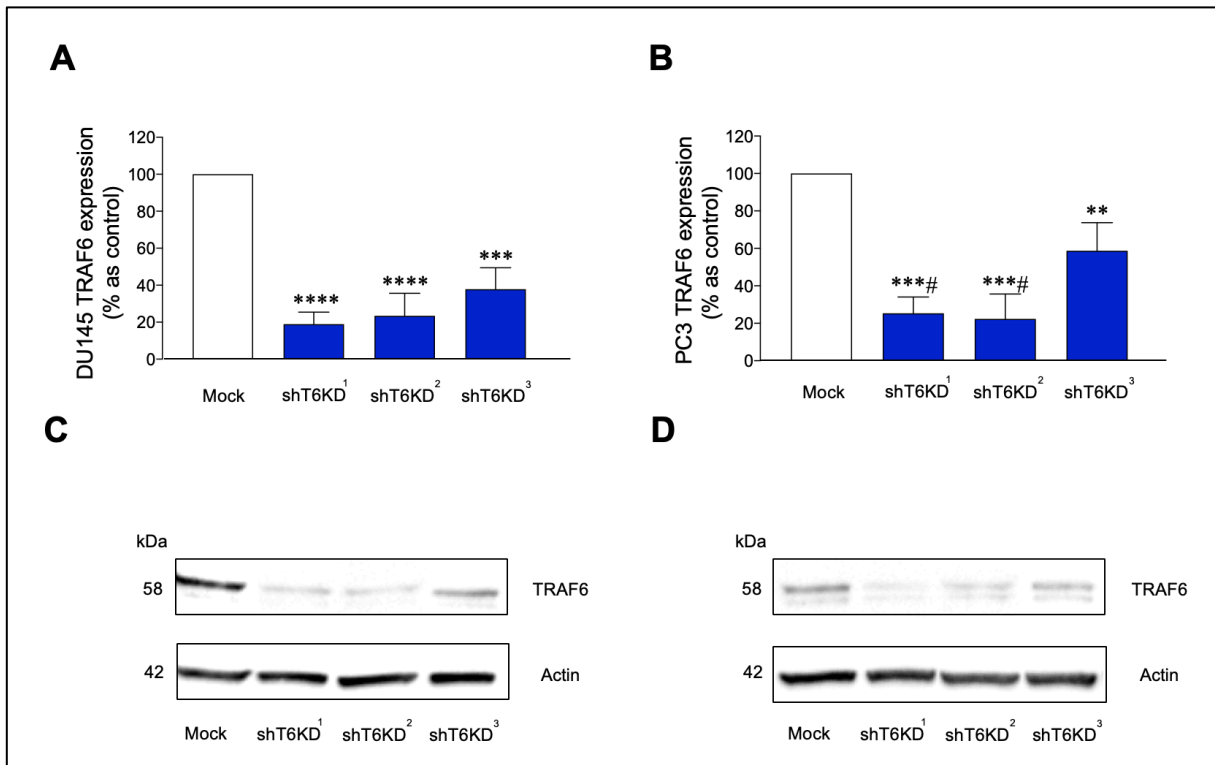
Figure 4.1. Successful TRAF6 knockdown expression in metastatic DU145 and PC3 prostate cancer cells. Percentage of relative TRAF6 expression from the three shRNA TRAF6 constructs using DU145 (A) and PC3 (B) prostate cancer cells. Representative images of DU145 (C) and PC3 (D) cell samples by Western Blot. Data obtained from three independent experiments. p-values were obtained from ordinary ANOVA test followed by Tukey *post hoc* test. ****p<0.0001, ***p<0.0005, **p<0.01 compared to mock transfected cells; #p<0.05 compared to shT6KD[3]. KD=Knockdown.
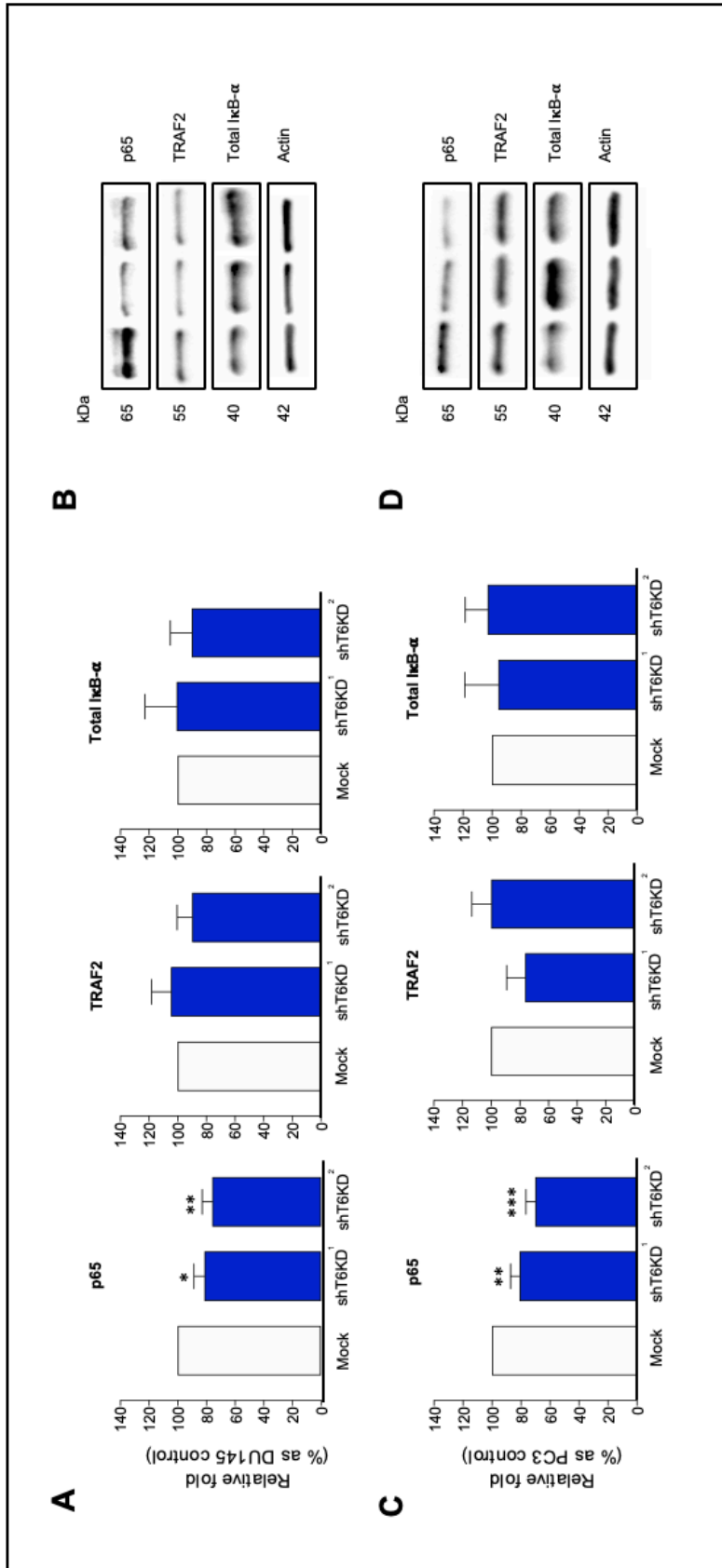
Figure 4.2. Expression of NFKB components associated with TRAF6 in DU145 and PC3 TRAF6 knockdown cells assessed by Western Blot analysis. Percentage of relative p65, TRAF2 and IκB-α expression from the two selected shRNA TRAF6 constructs using DU145 (A) and PC3 (C) prostate cancer cells. Representative images of DU145 (B) and PC3 (D) cell samples by Western Blot. Data obtained from three independent experiments. p-values were obtained from one-way ANOVA test followed by Tukey *post hoc* test. ***p<0.0005, **p<0.01 and *p<0.05 compared to mock transfected cells.

4.4.2. TRAF6 knockdown reduces prostate cancer cell growth *in vitro*

Next, the viability of human DU145 and PC3 prostate cancer cells transduced with control or TRAF6 shRNAs was analysed using AlamarBlue™ cell viability assay, as described in **section 2.4.2.1.** As shown in **Figure 4.3**, TRAF6 knockdown significantly decreased the number of DU145 cells after 72 hours (**Figure 4.3A and C**) and PC3 cells after 48 and 72 hours (**Figure 4.3B and D**), compared to control group. Interestingly, TRAF6 knockdown caused 51-52% reduction in the viability of PC3 after 72 hours compared to 32-38% reduction in DU145 cell viability after the same period of culture.
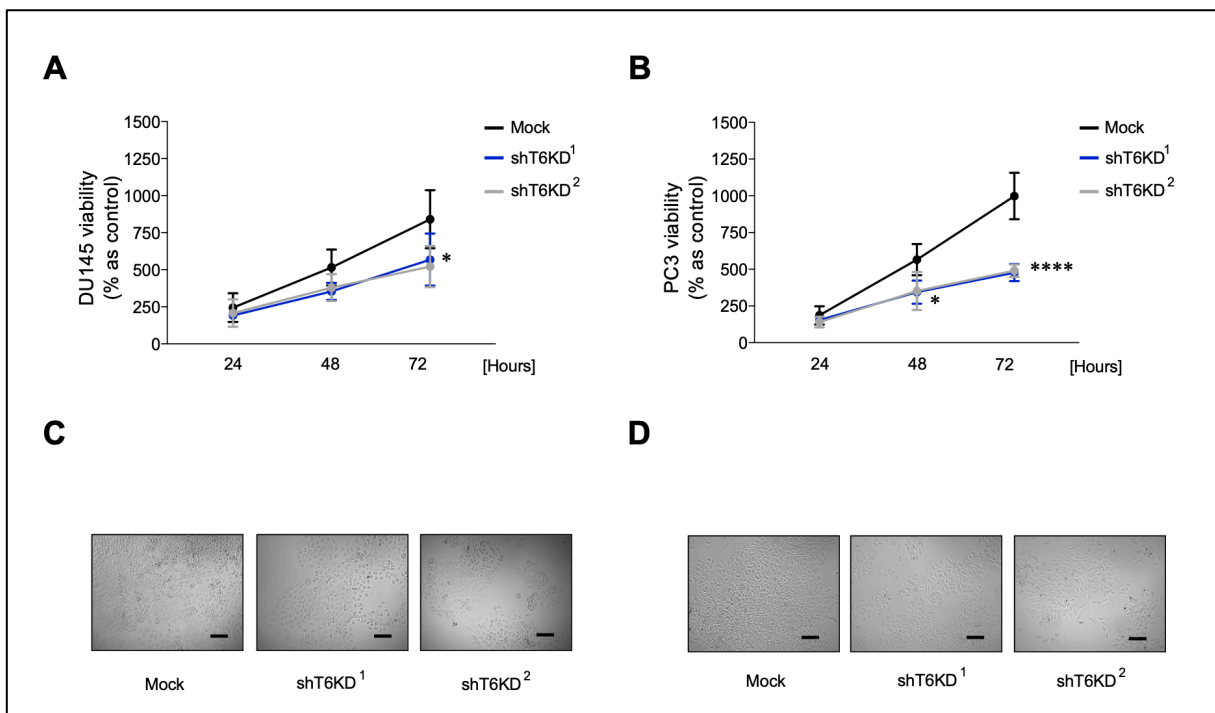
Figure 4.3. TRAF6 knockdown in highly metastatic prostate cancer cells reduces cell growth *in vitro*. Percentage of viability of DU145 (A) and PC3 (B) TRAF6 knockdown prostate cancer cells compared to cells silenced with control shRNA. Representative images of viability after 72 hours from DU145 (C) and PC3 (D) cells. Data obtained from three independent experiments. p-values were obtained from two-way ANOVA test followed by Tukey *post hoc* test. ****p<0.0001 and *p<0.05 compared to mock transduced cells. Scale bar=100 µM.

4.4.3. TRAF6 knockdown reduces the motility of prostate cancer cells *in vitro*

Various studies have implicated TRAF6 in the promotion of the invasion of prostate cancer cells (Gudey *et al.*, 2014; Sundar *et al.*, 2015) and downregulation of TRAF6, by overexpression of miR-146a-5p, inhibited the motility of P69 and PC3 prostate cancer cells *in vitro* (Paik *et al.*, 2011; Sun *et al.*, 2014)*.* Here, the effects of TRAF6 knockdown on DU145 and PC3 migration and invasion *in vitro* were assessed by the wound healing assay (See **2.4.2.2. Cell migration assessed by the wound-healing** assay) and Transwell® invasion assay (See **2.4.2.3. Cell invasion assessed by Transwell® invasion assay**) respectively (Moutasim, Nystrom and Thomas, 2011). As shown in **Figure 4.4**, TRAF6 knockdown in DU145 and PC3 significantly reduced cell migration after 14 hours when compared to mock control. As shown in **Supplementary Figure 6**, TRAF6 knockdown in PC3 had no effect on cell viability after 14 hours of culture period; however, DU145 cell viability decreased approximately 10-20%. In addition, TRAF6 knockdown in PC3, but not in DU145, significantly reduced cell invasion compared to mock cells (**Figure 4.5**).
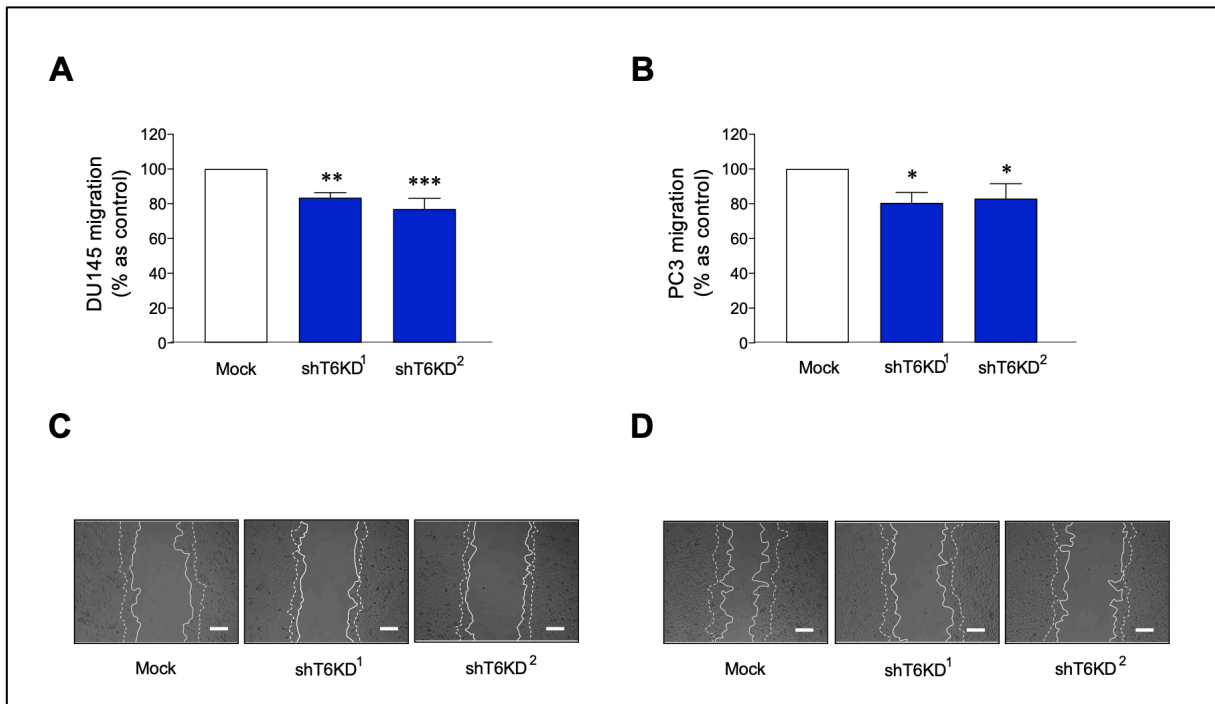
Figure 4.4. TRAF6 knockdown decreased DU145 and PC3 cell migration *in vitro*. Percentage of cell migration from prostate cancer cells silenced with control shRNA compared to TRAF6 knockdown DU145 (A) and PC3 (B) prostate cancer cells. Representative images showing initial and final positions of motility in timepoints 0 (dotted lines) and 14 hours (continuous lines) from DU145 (C) and PC3 (D) cells. Data obtained from three independent experiments. p-values were obtained from one-way ANOVA test followed by Tukey *post hoc* test. ***p<0.0005, **p<0.01 and *p<0.05 compared to mock transfected cells. Scale bar=100 µM.
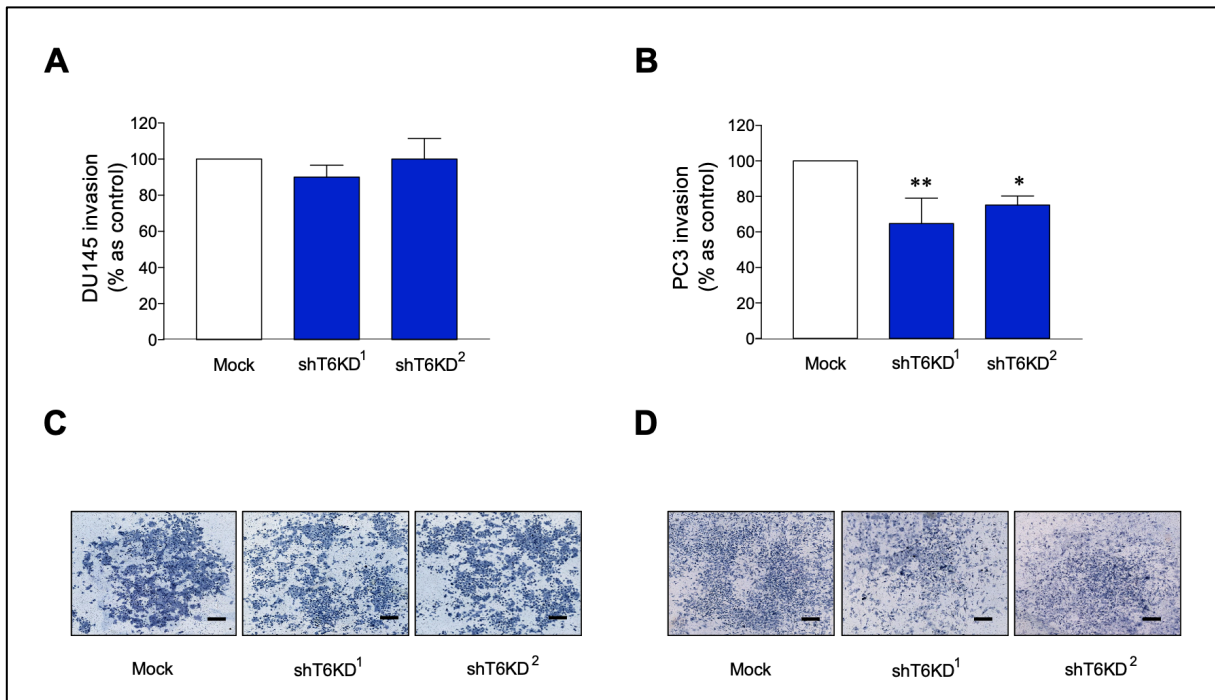
Figure 4.5. TRAF6 knockdown reduced DU145 and PC3 cell invasion *in vitro*. Percentage of cell invasion from prostate cancer cells silenced with control shRNA compared to TRAF6 knockdown DU145 (A) and PC3 (B) prostate cancer cells. Representative images of cell invasion after 72 hours from DU145 (C) and PC3 (D) cells. Data obtained from three independent experiments. p-values were obtained from one-way ANOVA test followed by Tukey *post hoc* test. **p<0.01 and *p<0.05 compared to mock transfected cells. Scale bar=200 µM.

4.4.4. TRAF6 knockdown in prostate cancer cells had no effect on RANKL-induced osteoclast formation *in vitro*

Prostate cancer cells produce and respond to several NFκB-activating pro-inflammatory factors including RANKL, CD40L and IL-1β, that directly or indirectly enhance bone cell activity and contribute to the formation of osteoblastic and osteolytic lesions (Vela *et al.*, 2007; Liu *et al.*, 2013; Roodman and Silbermann, 2015). In this project, the effect of TRAF6 knockdown prostate cancer cells on RANKL-induced osteoclast formation was tested (See **section 2.4.3**). Briefly, cultures of the murine macrophage-like cell line RAW264.7 were exposed to RANKL (100 ng/ml) in the presence and absence of conditioned medium from mock or TRAF6 shRNA DU145 or PC3 for 6 days. RAW264.7 cells exposed to RANKL alone were used as control.

Figure 4.6 shows that addition of conditioned media from mock or TRAF6-deficient DU145 and PC3 cells had no effect on the number of TRAcP-positive osteoclasts with three or more nuclei as compared to control cultures. Additionally, in all cell cultures and conditions, no difference was observed in cell number assessed by AlamarBlue™ assay (**Supplementary Figure 7**).
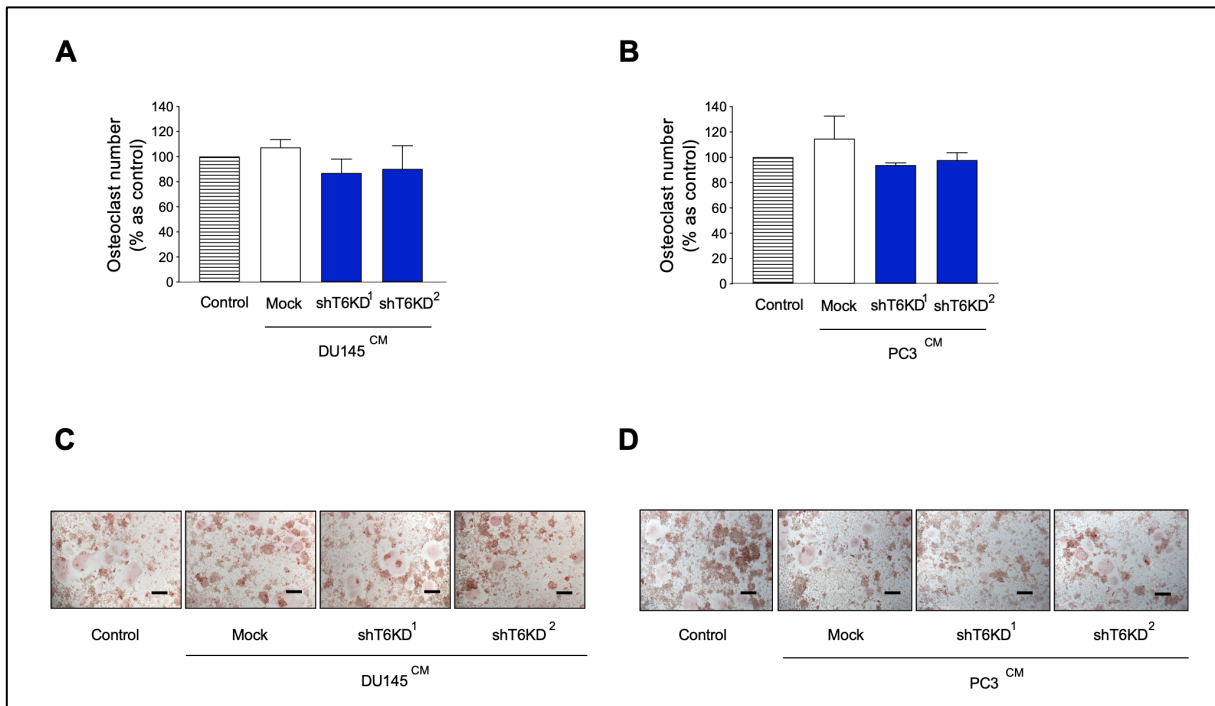
Figure 4.6. TRAF6 knockdown in DU145 and PC3 had no effect on RANKL-induced osteoclast formation in RAW 264.7 macrophage cultures *in vitro*. Percentage of osteoclast formation from RAW 264.7 cells stimulated by RANKL in the presence and absence of soluble factors produced by prostate cancer cells silenced with control shRNA compared to TRAF6 knockdown DU145 (A) and PC3 (B). Representative images of multinucleated TRAcP-positive control cells exposed to conditioned medium from control or TRAF6 shRNA transduced DU145 (C) and PC3 (D) cells. Data obtained from three independent experiments. Statistical analysis was performed with one-way ANOVA test followed by Tukey *post hoc* test. Scale bar=100 µM.

4.4.5.   TRAF6 knockdown prostate cancer cells alter osteoblast activity *in vitro*

Prostate cancer cells promote both osteoclastic and osteoblastic features; however, osteoblastic lesions are more commonly observed in patients (Armstrong *et al.*, 2008; Rafiei and S. V Komarova, 2013). Due to this, osteoblast differentiation and nodule formation was studied in cultures of the human osteoblast-like cells Saos-2 exposed to conditioned medium from TRAF6 knockdown and control DU145 and PC3 cells by assessing alkaline phosphatase activity and alizarin red assay, respectively (See **section 2.4.4**). 7-day exposure of Saos-2 cells to conditioned medium from TRAF6 knockdown DU145 cells reduced alkaline phosphatase activity and increased bone nodule formation when compared to mock control, suggesting reduced osteoblast differentiation and enhanced bone-forming activity (**Figure 4.7A and B**). Interestingly, exposure to conditioned medium from TRAF6 knockdown DU145 also reduced the total number of osteoblasts in culture when compared to cells exposed to media from mock (**Figure 4.7C**). In contrast, conditioned medium from TRAF6 knockdown PC3 cells caused a reduction in bone nodule formation compared to cells exposed to media from mock, without significantly affecting alkaline phosphatase activity or osteoblast viability (**Figure 4.8**).
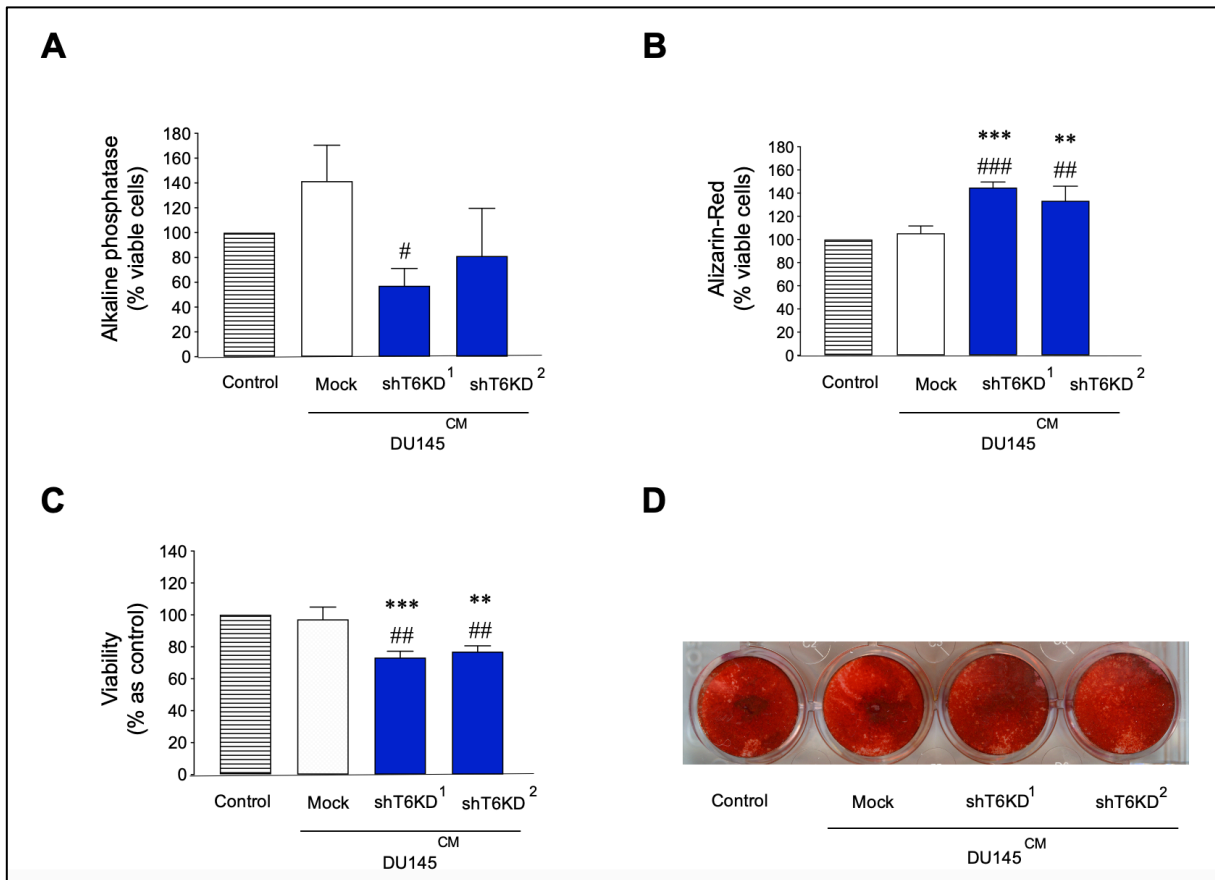
Figure 4.7. Conditioned medium from TRAF6 knockdown DU145 prostate cancer cells enhanced bone nodule formation *in vitro*. Percentage of alkaline phosphatase after 7 days (A) and after 10 days, marker for nodule formation alizarin red (B) and cell viability (C) of Saos-2 cells with or without exposure to conditioned medium from DU145 cells silenced with TRAF6 or control. (D) Representative images of Saos-2 mineralisation in the presence and absence of conditioned medium from mock or TRAF6 knockdown DU145 cells. Data obtained from three independent experiments. p-values were obtained from one-way ANOVA test followed by Tukey *post hoc* test. ***$p<0.005$, **$p<0.01$, *$p<0.05$ compared to control Saos-2 without exposure to conditioned medium, ###$p<0.005$, ##$p<0.01$, #$p<0.05$ compared to DU145 mock transduced cells.
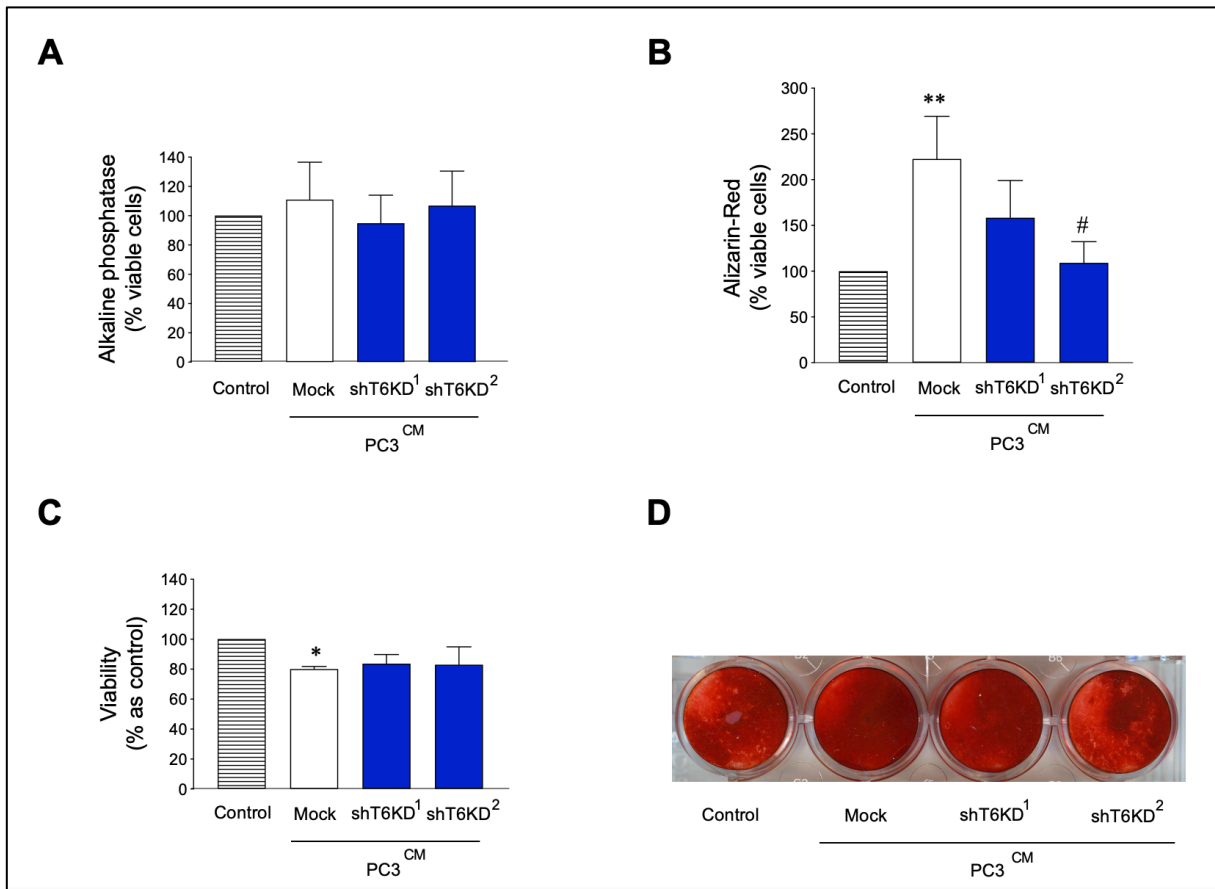
Figure 4.8. Conditioned medium from TRAF6 knockdown PC3 prostate cancer cells reduced bone nodule formation *in vitro*. Percentage of alkaline phosphatase after 7 days (A) and after 10 days, marker for nodule formation alizarin red (B) and cell viability (C) of Saos-2 cells with or without exposure to conditioned medium from PC3 cells silenced with TRAF6 or control. (D) Representative images of Saos-2 mineralisation in the presence and absence of conditioned medium from mock or TRAF6 knockdown PC3 cells. Data obtained from three independent experiments. p-values were obtained from one-way ANOVA test followed by Tukey *post hoc* test. **p<0.01, *p<0.05 compared to control Saos-2 without exposure to conditioned medium, #p<0.05 compared to PC3 mock transduced cells.

4.4.6. Cancer-specific TRAF6 knockdown in human PC3 had no significant effect in osteolysis in nude mice

Yang and colleagues (2010) have previously reported that TRAF6 knockdown in human PC3 cells reduced tumour growth in mice (Yang *et al.*, 2010). Here, the effects of cancer-specific knockdown of TRAF6 were tested on the ability of prostate cancer cells to influence bone cell activity and to cause osteolysis after injection of human PC3 cells in the left tibia of nude mice, as described in **2.5.2. Intratibial injection of human PC3 prostate cancer cells in immunodeficient mice.**

Detailed micro-computed tomography (micro-CT) analysis (described in **section 2.5.3.**) of the tibia metaphysis of mice showed no significant difference in trabecular bone volume, trabecular number, thickness, separation, porosity or structure model index between mice bearing mock or TRAF6 knockdown PC3 cells (**Figure 4.9**). Similarly, no significant difference in cortical bone volume or porosity was observed in mice bearing mock or TRAF6 knockdown PC3 cells (**Figure 4.10**).
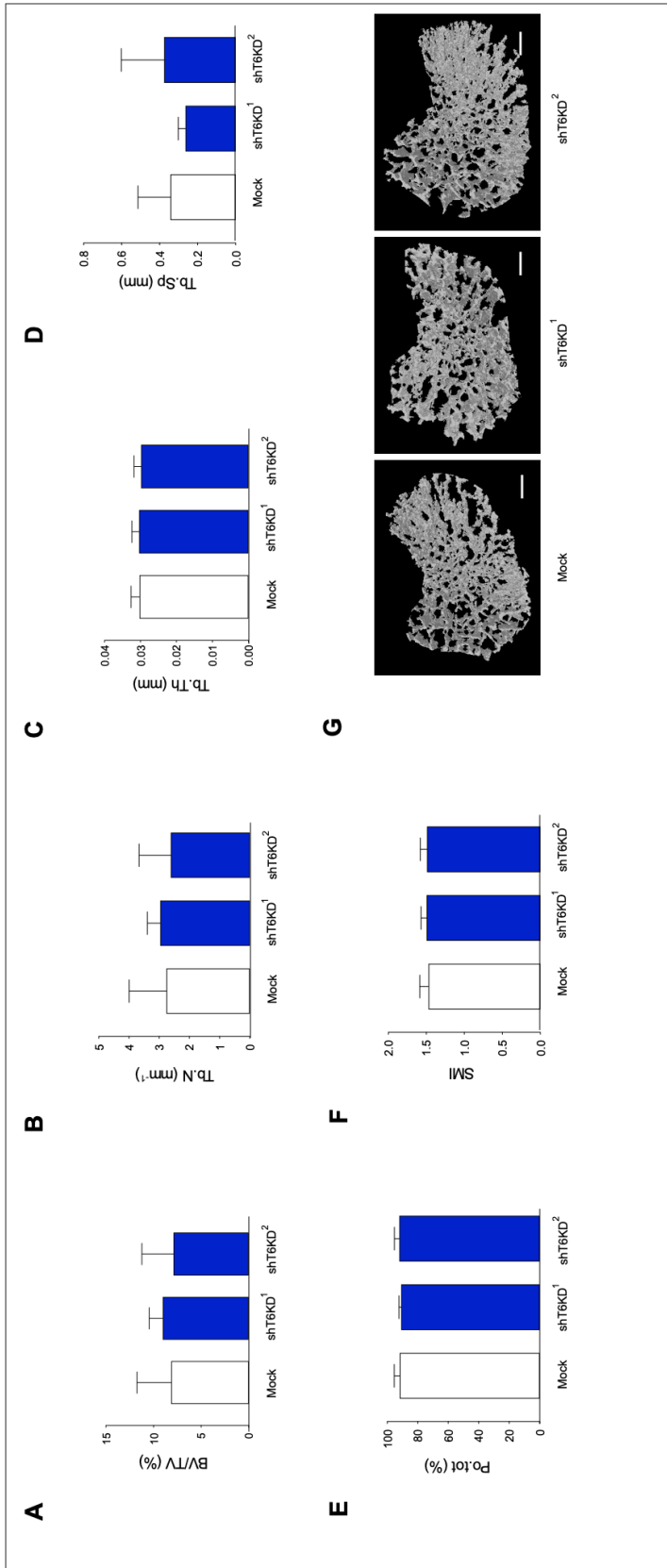
Figure 4.9. PC3 TRAF6 knockdown cells present no effect in trabecular bone parameters in mice. 4-week old BALB/c-nu/nu athymic mice (n=7/per group) received intratibial injection of 2×10^4 PC3 mock or TRAF6 knockdown human prostate cancer cells. Trabecular parameters bone volume/tissue volume (BV/TV%; A), trabecular number (Tb.N; B), thickness (Tb.Th; C), separation (Tb. Sp; D), porosity (Po.tot%; E) and Structure Model Index (SMI; F) were measured with microcomputed tomography using CTAn software. (G) Representative 3D reconstructions of the cortical bone were obtained with microcomputed tomography using CTVol software. Scale bar=1 mm.
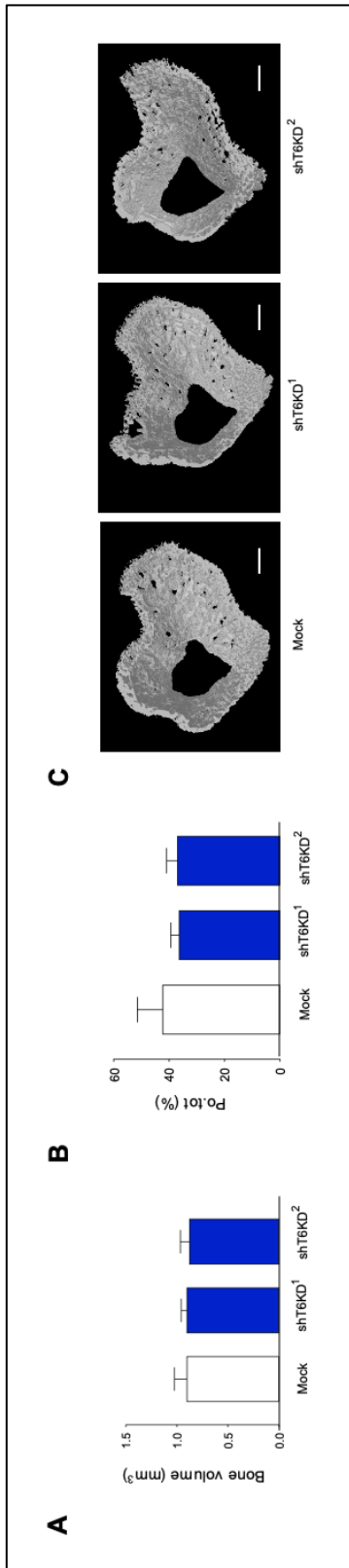
Figure 4.10. TRAF6 knockdown has no effect in PC3 induced cortical osteolysis in immunodeficient mice. 4-week old BALB/c-nu/nu athymic mice (n=7/per group) received intratibial injection of 2×10^4 PC3 mock or TRAF6 knockdown human prostate cancer cells. Bone volume (A) and percentage of total porosity (B) were measured with microcomputed tomography using CTAn software. (C) Representative 3D reconstructions of the cortical bone were obtained with microcomputed tomography using CTVol software. Scale bar=1 mm.

4.5.　Discussion

In **chapter 3**, I showed that the expression of TRAF6 is linked to prostate cancer bone metastasis and that TRAF6 is highly expressed in metastatic and osteotropic mouse and human prostate cancer cells (**Figure 3.14**). Several studies have shown that TRAF6, a downstream regulator of NFκB activation, has been linked to the promotion of prostate cancer progression (Gudey *et al.*, 2014; Sundar *et al.*, 2015; Aripaka *et al.*, 2019). The aim of this chapter was to investigate the effects of cancer-specific TRAF6 knockdown on the ability of highly metastatic human prostate cancer cells to influence bone cell activity and to cause osteolytic bone damage.

First, TRAF6 knockdown expression was successfully generated in moderately and highly metastatic DU145 and PC3 cells, respectively. The constructs showing the lowest reduction in TRAF6 expression were selected for further experiments. Next, a number of *in vitro* experiments were conducted to study the effects of TRAF6 knockdown in DU145 and PC3 cells on NFκB signalling and the ability of these cells to grow, migrate, invade and influence the differentiation of osteoblasts and osteoclasts. As the analysis shown in **chapter 3**, TRAF6 interacts with all other TRAFs, possibly influencing the expression of closely related TRAFs, such as TRAF2, in TRAF6 knockdown cell lines. In addition, ubiquitination and degradation of IκB-α are important processes in the activation of NFκB signalling and higher levels of expression of IκB-α indicate a reduction in NFκB activation. The experiments described in this chapter confirm that TRAF6 knockdown in DU145 and PC3 cells reduced the expression of the transcriptional factor p65 without affecting TRAF2 expression.

Encouraged by these findings, it was shown that prostate cancer cell viability was significantly reduced in DU145- and PC3-TRAF6 knockdown cells compared to control. These findings are consistent with previous reports that have shown the important role of TRAF6 in the activation of signalling pathways that are involved in cancer cell proliferation and survival. Gudey and

collaborators (2014) showed that inhibition of a protein complex (γ-secretase) activated by TRAF6 decreased tumour growth in a xenograft prostate cancer model (Gudey *et al.*, 2014). Additionally, by studying the E3 ligase function of TRAF6 in the activation of the cell survival pathway Akt, Yang and colleagues (2009) reported that TRAF6 knockdown in PC3 cells reduced their tumorigenic potential in nude mice (Yang *et al.*, 2009). Together, these findings suggest that TRAF6 inhibition reduces the growth of human prostate cancer cells.

In vitro studies have shown that TRAF6 promotes prostate cancer cell invasiveness, induced by TGF-β (Gudey *et al.*, 2014; Sundar *et al.*, 2015). In this project, the effects of TRAF6 inhibition were studied on the metastatic abilities of prostate cancer cells by examining the ability of mock and TRAF6-deficient cells to migrate and invade *in vitro*. These experiments showed that TRAF6 knockdown in PC3 caused a significant reduction in cell migration and invasion, whereas TRAF6 knockdown in DU145 had a significant reduction in migration but their invasion capability was relatively unaffected despite of exhibiting significantly lower expression of TRAF6 after knockdown. This might be due to the different origin of DU145 cells (derived from brain metastasis) or possibly to reduced expression of TRAF6-related receptors such as RANK and CD40 compared to the highly metastatic PC3, as previously discussed in **section 3.4.4.**

In this study, the role of cancer-specific TRAF6 inhibition in prostate cancer – bone cell interaction was assessed. Previous work has shown that TRAF6 enhances bone volume in mice by inhibition of osteoclasts (Lomaga *et al.*, 1999). Given the high incidence of skeletal-related events in advanced prostate cancer patients and the propensity of prostate cancer cells to metastasise to bone, the effects of TRAF6 inhibition in prostate cancer cells were addressed on osteoclast precursors and osteoblasts. *In vitro* studies showed that TRAF6 knockdown in prostate cancer cells exerted a modest effect on RANKL-induced osteoclast formation in the described models of DU145 and PC3. This suggests that TRAF6 in prostate cancer cells plays

a minor role in RANKL-induced osteoclast formation. It is also important to note that previous *in vitro* studies showed that prostate cancer cells-derived factors induced a modest, non-significant increase in osteoclast number in RANKL-stimulated RAW 264.7 cultures (Yuen *et al.*, 2010; Rafiei and S. V. Komarova, 2013). Due to this, future studies should identify, examine and compare the expression levels of tumour-derived factors produced by mock and TRAF6 knockdown prostate cancer cells.

Osteoblast number and activity is enhanced during the osteoblastic phase of prostate cancer and osteoblastic lesions are a major feature of prostate cancer-induced bone disease (Vela *et al.*, 2007). Interestingly, a differential effect in the ability of Saos-2 cells to grow, mature and to form bone nodules was observed in the presence of conditioned medium from TRAF6 knockdown DU145 and PC3. TRAF6 knockdown PC3 cells had reduced ability to form bone nodules *in vitro*, as opposed to DU145-TRAF6 knockdown cells. This suggests that TRAF6 inhibition in highly metastatic prostate cancer cells could be of value in the treatment of osteoblastic prostate cancer bone metastasis. In addition, similar to exposure to control conditioned medium of PC3, soluble factors from DU145-TRAF6 knockdown significantly reduced viability of osteoblast-like Saos-2 cells. Even though the results obtained from the use of both cell lines are contrasting, it is important to note that TRAF6 knockdown in prostate cancer cells did indeed alter osteoblast differentiation and viability. The animal study carried out to further confirm these findings, showed that TRAF6 knockdown in PC3 cells injected intratibially failed to protect mice against bone loss in both trabecular and cortical compartments. Although further histological and histomorphometrical analysis are needed, the present detailed micro-CT analysis indicates that cancer-specific inhibition of TRAF6 is not sufficient to reduce prostate cancer induced osteolysis.

Overall, the results of the *in vitro* studies in this chapter suggest that inhibition of cancer-specific TRAF6 reduces the ability of highly metastatic cells, namely PC3 and DU145, to grow,

migrate, invade and influence osteoclast formation and osteoblast differentiation *in vitro*; yet it had no significant effect against PC3 cell-induced osteolysis in immunodeficient mice. Given the important role that the TRAF/NFκB pathway plays in cancer, future studies should examine the effects of cancer-specific inhibition of TRAF6 on prostate cancer-associated bone disease in immunocompetent mice and test the hypothesis that inhibition of TRAF6 in both tumour and host cells is required for the reduction of skeletal-related events associated with advanced prostate cancer in bone.

Chapter 5. Effects of pharmacological inhibition of TRAF6 on prostate cancer cell behaviour *in vitro* and osteolysis in mice

5.1.   Summary

TRAF6 expression in osteoclasts and immune cells plays an important role in the regulation of bone remodelling and immunity. In **Chapter 4**, it was shown that cancer-specific inhibition of TRAF6 in human PC3 prostate cancer cells influenced bone-cell activity *in vitro* but failed to protect mice against osteolysis. In this chapter, a pharmacological approach was used to test the effects of TRAF6 inhibition in both host and prostate cancer cells on bone cell activity and osteolysis. Our collaborator Nicolaes and colleagues (University of Maastricht, Netherlands) designed and verified the targeting and inhibition of CD40-TRAF6 interaction with the compound 6877002, used in these studies. 6877002 showed anti-tumour and anti-metastatic properties by significantly inhibiting the *in vitro* viability of a panel of human and mouse prostate cancer cells and reducing the ability of human PC3 and DU145 prostate cancer cells to migrate and invade *in vitro*. Furthermore, treatment with 6877002 significantly reduced the ability of RANKL-stimulated RAW264.7 cells to form osteoclasts and of Saos-2 to form bone nodules in the presence of prostate cancer cell-derived factors. *In vivo*, administration of 6877002 (20 mg/kg/daily) in nude mice failed to enhance bone volume at both trabecular and cortical compartments following the intratibial injection of the human PC3 prostate cancer cell line. Altogether, these findings imply that inhibition of TRAF6, at the level of CD40/RANKL binding site, by 6877002 in the tumour microenvironment was insufficient to protect against osteolysis after local injection of human PC3 in immunodeficient mice.

5.2. Introduction

Osteoblast and osteoclast activity plays an important role in the pathogenesis of prostate cancer-associated bone disease (Yuen *et al.*, 2010). TRAF6 is essential for osteoclast formation, survival and activity and it is the main regulator of RANKL-induced signalling (Lomaga *et al.*, 1999; Lamothe *et al.*, 2007). Upon activation, TRAF6 is recruited by members of the TNF receptor superfamily including CD40 and RANK (Moriya *et al.*, 2015). This results in the activation of a cascade of intracellular signalling events including the phosphorylation of IκB-α by the IκB-α kinase (IKK) complex, followed by the proteasomal degradation of IκB-α and subsequently, leads to NFκB nuclear translocation and DNA binding (Davies *et al.*, 2005; Lamothe *et al.*, 2007; Seijkens *et al.*, 2018)

Studies performed by Chatzigeorgiou and colleagues in 2014 led to the discovery of the small-molecule inhibitor of CD40-TRAF6 interaction, 6877002 (Antonios Chatzigeorgiou *et al.*, 2014). The compound 6877002 selectively inhibited the CD40-TRAF6 pathway and not CD40-TRAF2/3/5, showing promising results in the improvement of insulin sensitivity and in the decrease of inflammatory cell recruitment *in vivo*, as confirmed by other studies (Aarts *et al.*, 2017; Seijkens *et al.*, 2018). In addition, 6877002 along with six TRAF6 small-molecule inhibitors were used to reduce inflammation of the peritoneum in an *in vivo* model. Consequently, 6877002 and one of its derivatives were selected in studies that showed that inhibition of TRAF6 increased the survival rate of mice bearing systemic inflammation by polymicrobial sepsis (Zarzycka *et al.*, 2015). More recently, findings from our group have shown that the verified TRAF6 inhibitor 6877002 decreases the ability of breast cancer cells to induce osteoclastogenesis (Bishop *et al.*, 2020).

TRAF6 plays a role in the promotion of prostate cancer cell invasion (Gudey *et al.*, 2014; Sundar *et al.*, 2015) and tumorigenesis in mice (Yang *et al.*, 2009). Due to this and encouraged by the results in **chapter 4** showing that cancer-specific TRAF6 inhibition had no effects on prostate cancer-associated osteolysis in mice bearing the human PC3, the compound

6877002 was utilised to test the effects of pharmacological inhibition of TRAF6 on prostate cancer-associated bone cell activity and osteolysis.

5.3. **Aims**

The aims of this chapter were to test the hypothesis that TRAF6 inhibition in both host and prostate cancer cells reduces the ability of prostate cancer cells to grow, move, influence bone cell activity and cause osteolysis. To test this hypothesis, I assessed the effects of the verified TRAF6 inhibitor 6877002 on:

- The viability of a panel of human and mouse prostate cancer cells *in vitro.*

- The migration and invasion of the human metastatic prostate cancer cell lines DU145 and PC3 *in vitro.*

- The ability of the human metastatic prostate cancer cells DU145 and PC3 to influence:

  - ○ Osteoclast formation *in vitro.*

  - ○ Osteoblast differentiation and bone nodule formation *in vitro.*

- Osteolysis in immunodeficient mice bearing the human prostate cancer cells PC3*.*

5.4.   Results

5.4.1.   The verified 6877002 TRAF6 compound reduced human and mouse prostate cancer cell viability *in vitro*

First, the effects of the verified small-molecule inhibitor of CD40-TRAF6 (6877002) were studied on cell viability in a panel of prostate cancer cell lines using the Alamar Blue® assay (See **section 2.4.2.1**). As shown in **Figure 5.1**, 6877002 reduced the viability of a panel of human and murine prostate cancer cells in a concentration-dependent manner. The half maximal inhibitory concentrations (IC_{50}) for 6877002 were not significantly different in cultures of the human PC3 and DU145 (**Table 5.1**). Interestingly, 6877002 was more potent in inhibiting the growth of the syngeneic and osteotropic prostate cancer cell line RM1-BM.
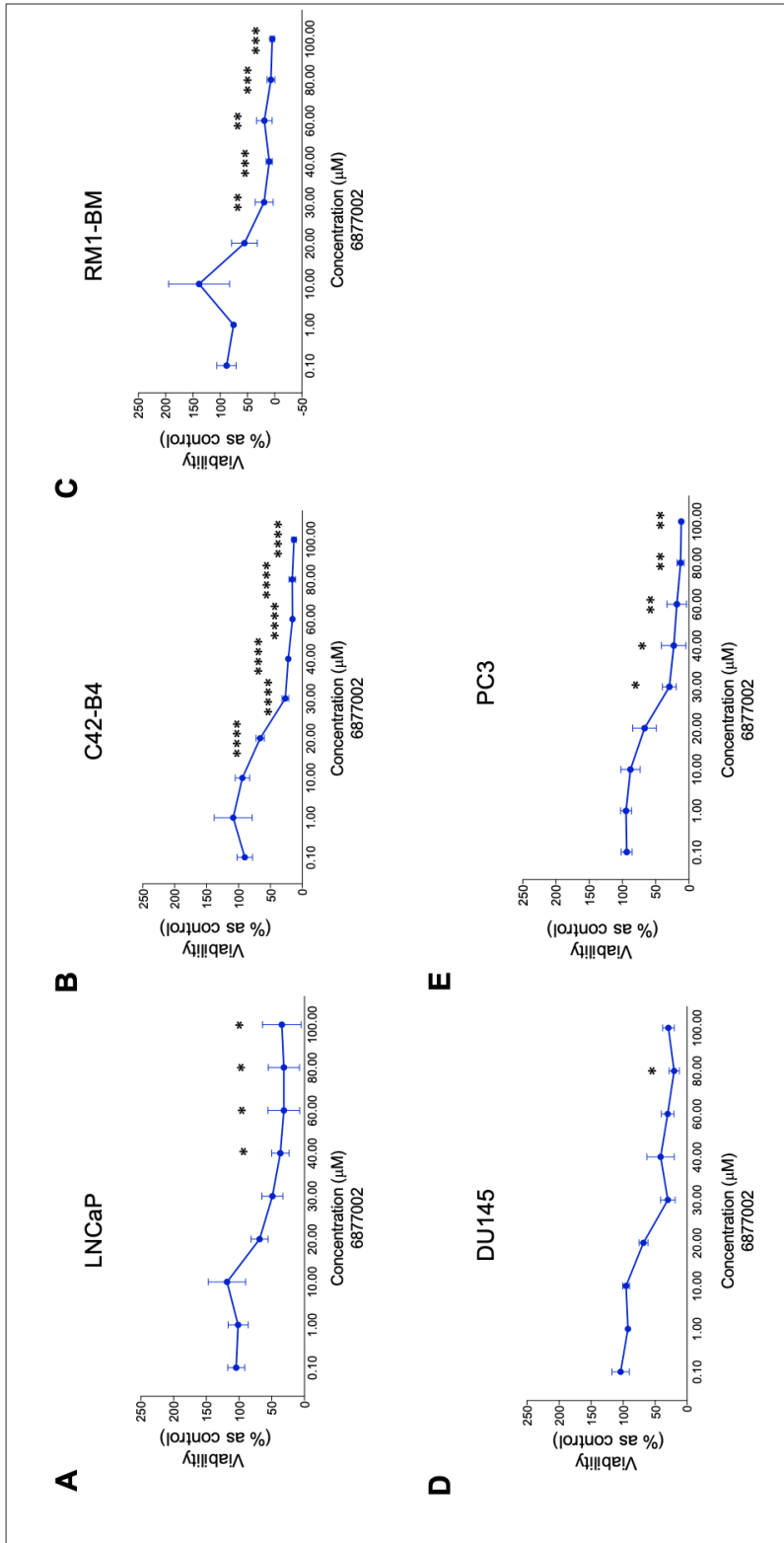
Figure 5.1. Effects of the verified TRAF6 inhibitor 6877002 on the viability of human and mouse metastatic prostate cancer cells *in vitro*. Dose-response curves of the verified 6877002 on the viability of parental LNCaP (A) and sub-clone LNCaP-C4-2B4 (B), the murine and highly metastatic RM1-BM (C) and human highly metastatic DU145 (D) and PC3 (E) prostate cancer cells after 72 hours, assessed by Alamar Blue™ assay. Data obtained from three independent experiments. p-values were obtained from two-way ANOVA test followed by Dunnett *post hoc* test.*p<0.05, **p<0.01, ***p<0.005 and ****p<0.001 compared to cells treated with vehicle.

Table 5.1. Effects of the verified TRAF6 inhibitor 6877002 on the viability of a panel of human and murine prostate cancer cells with different metastatic abilities *in vitro*. Cell viability was measured after 72 hours of continuous exposure to the verified 6877002 (0-100 µM). Calculation of half maximal inhibitory concentrations (IC_{50}) was performed as described in **section 2.7.** Values are expressed as means ± SD and were obtained from three independent experiments.

		Half maximal inhibitory concentration (IC_{50}) in µM after 72 hours
Cell type	Classification	6877002
LNCaP	Human Androgen sensitive	38.19±3.90
C42-B4	Human Androgen insensitive- Bone trophic	37.54±12.11
RM1-BM	Mouse Androgen insensitive- Bone trophic	21.18±2.59
DU145	Human Androgen insensitive- Bone trophic	34.08±12.67
PC3	Human Androgen insensitive- Bone trophic	38.49±14.3

5.4.2. The verified TRAF6 inhibitor 6877002 decreases prostate cancer cell motility *in vitro*

The involvement of TRAF6 in prostate cancer progression has been confirmed by numerous studies (Gudey *et al.*, 2014; Sundar *et al.*, 2015; Aripaka *et al.*, 2019). Moreover, previous studies have shown that treatment with the verified TRAF6 inhibitor 6877002 reduced monocyte migration in a dose-dependent manner (Aarts *et al.*, 2017). With this in mind, the effects of pharmacological inhibition of TRAF6 on the migration of human metastatic prostate cancer cells DU145 and PC3 were assessed. In **Figure 5.2**, treatment with the verified TRAF6 inhibitor 6877002 (10 µM) decreased the 2D migration of DU145 and PC3 prostate cancer cells after 14 hours, as assessed by the wound-healing assay (See **section 2.4.2.2.**); however, only significant inhibition of cell migration was observed in PC3 cancer cells (**Figure 5.2B**). The used concentration of the TRAF6 inhibitor was selected based on the values obtained from the IC$_{50}$ analysis, in which 10 µM had no effect on cell viability. This was confirmed by assessing cell viability with the AlamarBlue™ assay (See **section 2.4.2.1**) after 14 hours (**Supplementary Figure 8**). Representative images of DU145 and PC3 cells are shown in **Figure 5.2C** and **D**, respectively.
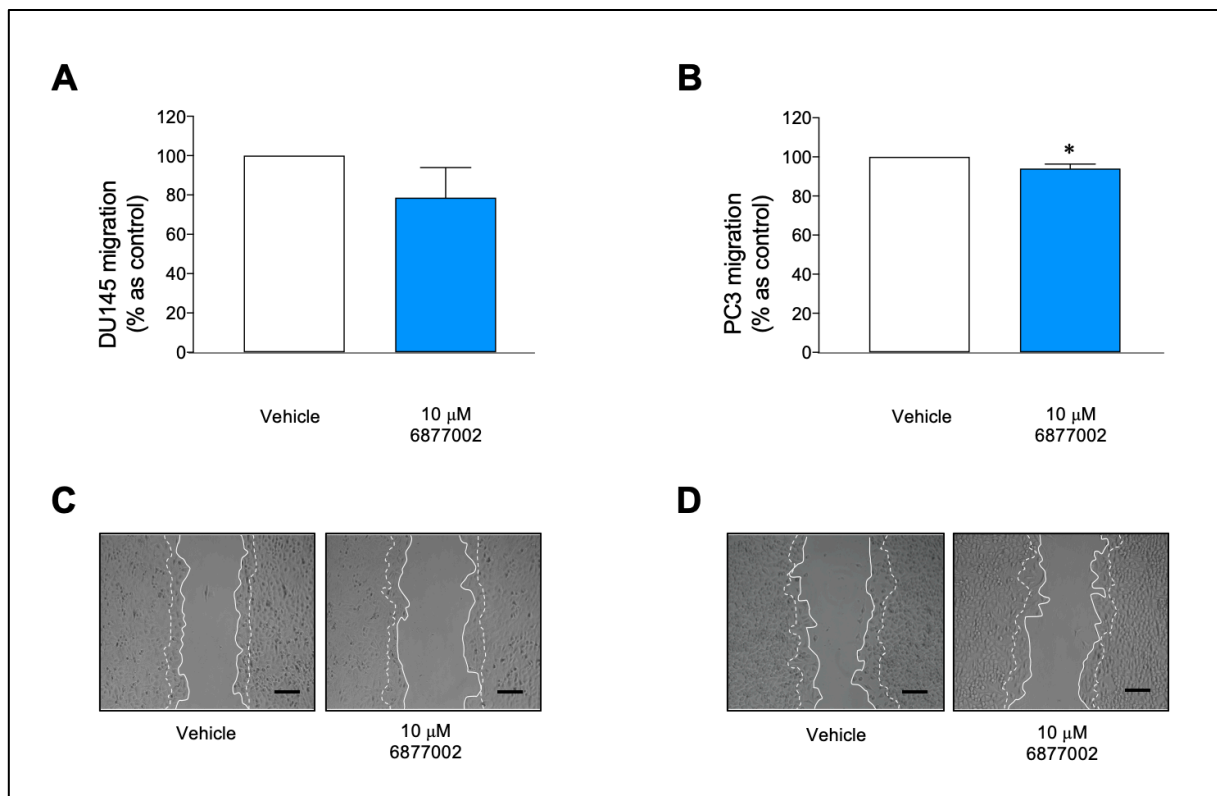
Figure 5.2. 6877002 reduced DU145 and PC3 cell migration *in vitro*. Percentage of cell migration of prostate cancer cells DU145 (A) and PC3 (B) treated with vehicle or 10 µM of the verified TRAF6 inhibitor 6877002. Representative images showing initial and final positions of motility in timepoints 0 (dotted lines) and 14 hours (continuous lines) of DU145 (C) and PC3 (D) cells. Data obtained from three independent experiments. p-values were determined using unpaired T-test. *p<0.05 compared to cells treated with vehicle. Scale bar=100 µM.

Next, cell invasion was assessed with the Transwell® invasion assay (See **section 2.4.2.3.**) to study the effects of 6877002 on the invasive capabilities of human DU145 and PC3 prostate cancer cells (Carrasco Gonzalez, MSc Thesis, 2017). As shown in **Figure 5.3**, 6877002 (10 µM) exerted a significant decrease in invasion of the human DU145 and, particularly, of PC3 prostate cancer cells.
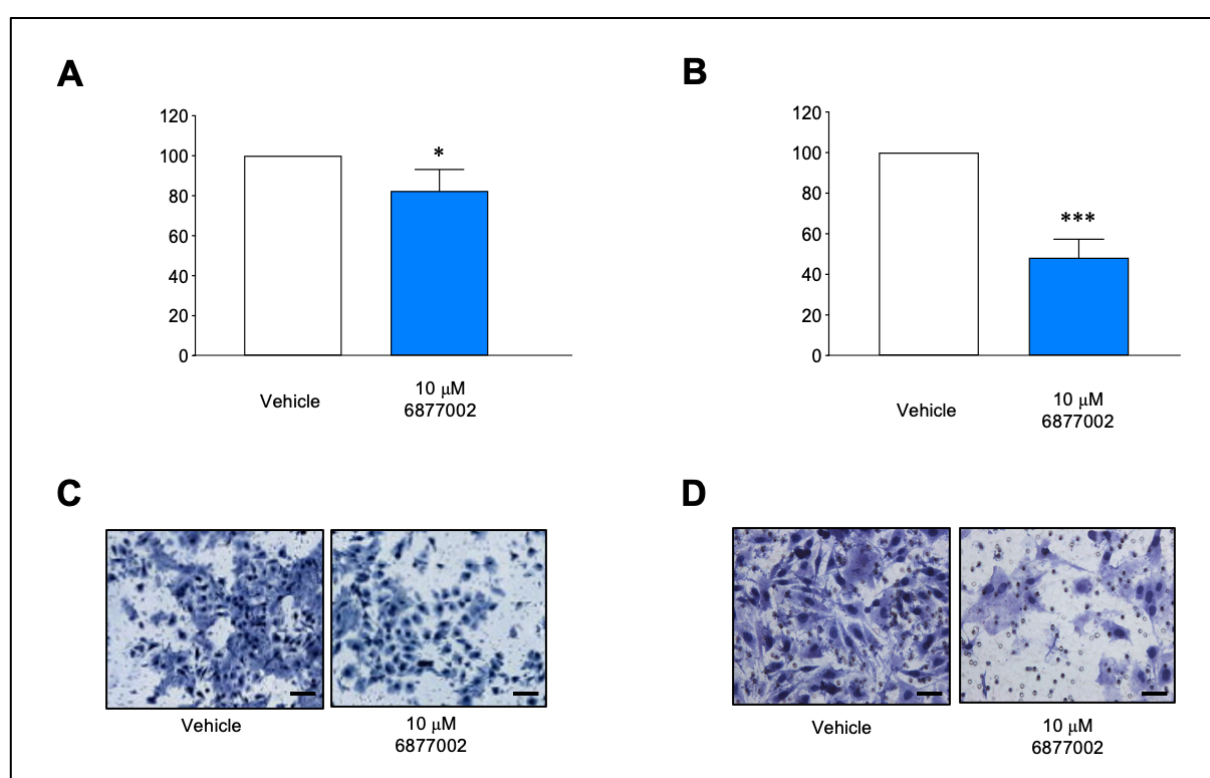
Figure 5.3. Pharmacological inhibition of TRAF6 using 6877002 reduced DU145 and PC3 cell invasion *in vitro*. Percentage of cell invasion of DU145 (A) and PC3 (B) prostate cancer cells treated with vehicle or 10 µM of the TRAF6 inhibitor 6877002. Representative images of invading DU145 (C) and PC3 (D) cells stained with Hematoxilin and Eosin after 72 hours. Scale bar=100 µM for (C) and Scale bar=50 µM for (D). Panel B and D were originally presented in MSc thesis "The role of TRAF6/NF-Kappa B in prostate cancer metastasis". Data obtained from three independent experiments. p-values were determined using unpaired T-test. *p<0.05, ***p<0.005 compared to cells treated with vehicle.

5.4.3. The verified 6877002 compound inhibits prostate cancer- and RANKL-induced osteoclast formation *in vitro*

TRAF6 plays a critical role in RANKL-induced signalling and TRAF6-deficient mice have exhibited high bone volume due to absence of mature osteoclasts (Lomaga *et al.*, 1999). In the present chapter, the effects of TRAF6 inhibition on bone cell activity in the presence of the derived factors of prostate cancer cells were studied as described in **section 2.4.3.** First, the concentration range for 6877002 was determined based on observing no effects on the viability of the osteoclast precursors and murine macrophage-like cells RAW264.7. As shown in **Figure 5.4A**, 6877002 had no significant effect in the number of RAW264.7 cells at 0.1 µM and induced a modest, non-significant increase at 1 µM and 10 µM. Next, cultures of RAW264.7 cells were stimulated with RANKL (100 ng/ml) and treated with the verified 6877002 TRAF6 inhibitor in a dose-dependent manner (**Figure 5.4**). Osteoclast precursors, RAW264.7 cells, were exposed to DU145- and PC3-conditioned media and treated with vehicle (DMSO) or the TRAF6 inhibitor 6877002 (0.1 µM) and RANKL (100 ng/ml) every 48 hours for 6 days. RAW264.7 cells only exposed to RANKL were used as control. The verified TRAF6 inhibitor 6877002 significantly reduced the formation of TRAcP-positive multi-nucleated osteoclasts in the presence of RANKL only (**Figure 5.4B**) and in combination with conditioned medium from the human DU145 and PC3 prostate cancer cell lines (**Figure 5.5**), without affecting RAW264.7 cell viability (**Supplementary Figure 9**). Representative images of TRAcP-positive cells from the described experiment are shown in **Figure 5.5**, **Panel C** and **D**.
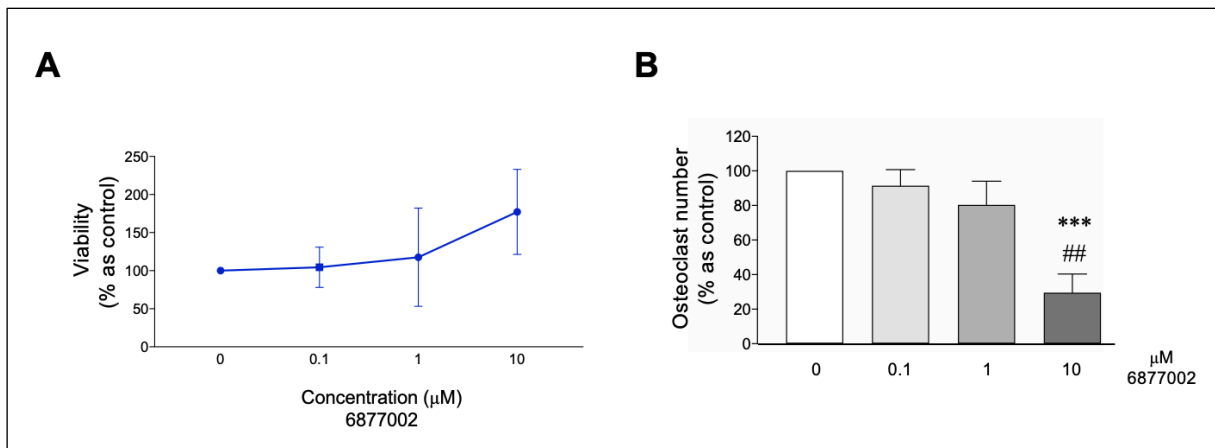
Figure 5.4. Effects of the verified TRAF6 inhibitor 6877002 in cell viability and osteoclast formation in RAW 264.7 cells. Viability (A) and osteoclast formation (B) of RAW264.7 cells stimulated with RANKL and treated with 678002 in a dose-response manner, assessed by Alamar Blue™ and TRAcP staining, respectively. Data obtained from three independent experiments. p-values were obtained from one-way ANOVA test followed by Tukey *post hoc* test. ***p<0.005 compared to cells treated with vehicle, ##p<0.01 compared to cells treated with 0.1 µM of 6877002.
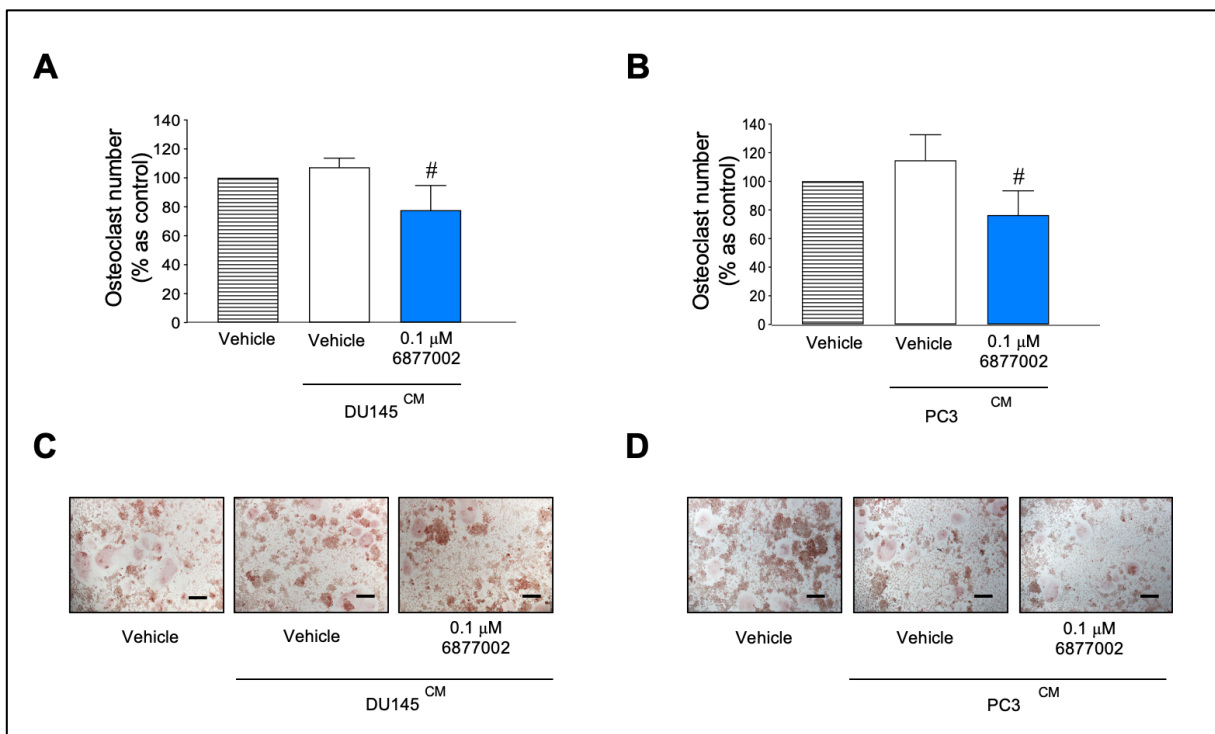
Figure 5.5. Pharmacological TRAF6 inhibition reduced osteoclast formation in RAW 264.7 cultures exposed to conditioned medium from DU145 and PC3 *in vitro*. Percentage of osteoclast formation in RANKL-stimulated RAW 264.7 cells in the presence and absence of conditioned medium from prostate cancer cells DU145 (A) and PC3 (B) treated with vehicle or 0.1 µM TRAF6 inhibitor 6877002. Representative images of multinucleated TRAcP-positive control cells exposed to conditioned medium from DU145 (C) and PC3 (D) cells and treated with the TRAF6 inhibitor or vehicle. Data obtained from three independent experiments. p-values were obtained from one-way ANOVA test followed by Tukey *post hoc* test. #p<0.05 compared to cells treated with vehicle and exposed to conditioned medium. Scale bar=100 µM.

5.4.4. Pharmacological inhibition of TRAF6 using 6877002 alters osteoblast activity

Bone metastatic prostate cancer presents a mix of osteoblastic and osteolytic lesions (Hirata *et al.*, 2016) and osteoblasts play a key role in this process by producing osteolytic RANKL and promoting bone matrix mineralization (Rucci and Angelucci, 2014). Here, the effects of the verified TRAF6 inhibitor 6877002 on osteoblast viability, differentiation and nodule formation were studied by Alamar Blue™, alkaline phosphatase (ALP) activity and alizarin red assay, respectively (See **section 2.4.4**). The used concentration of 6877002 (0.1 µM) was chosen to ensure consistency with the effects of this compound on osteoclast formation (**Figure 5.5**). As shown in **Panel A** of **Figure 5.6** and **Figure 5.7**, exposure of the human osteoblast-like Saos-2 cells to conditioned medium from DU145 and PC3 prostate cancer cells caused a modest increase in alkaline phosphatase activity and moderately reduced cell viability (**Figure 5.6C and Figure 5.7C,** respectively). Treatment with 6877002 (0.1 µM) significantly enhanced bone nodule formation and reduced cell number without significantly affecting alkaline phosphatase activity on cells exposed to soluble factors from DU145 (**Figure 5.6**). Similar effects of 6877002 on alkaline phosphatase activity and cell viability were observed in cultures of PC3 prostate cancer cells; however, there was a moderate decrease in bone nodule formation (**Figure 5.7**). Representative images of bone nodule formation from the described experiment are shown in **Panel D** of **Figure 5.6** and **Figure 5.7**.
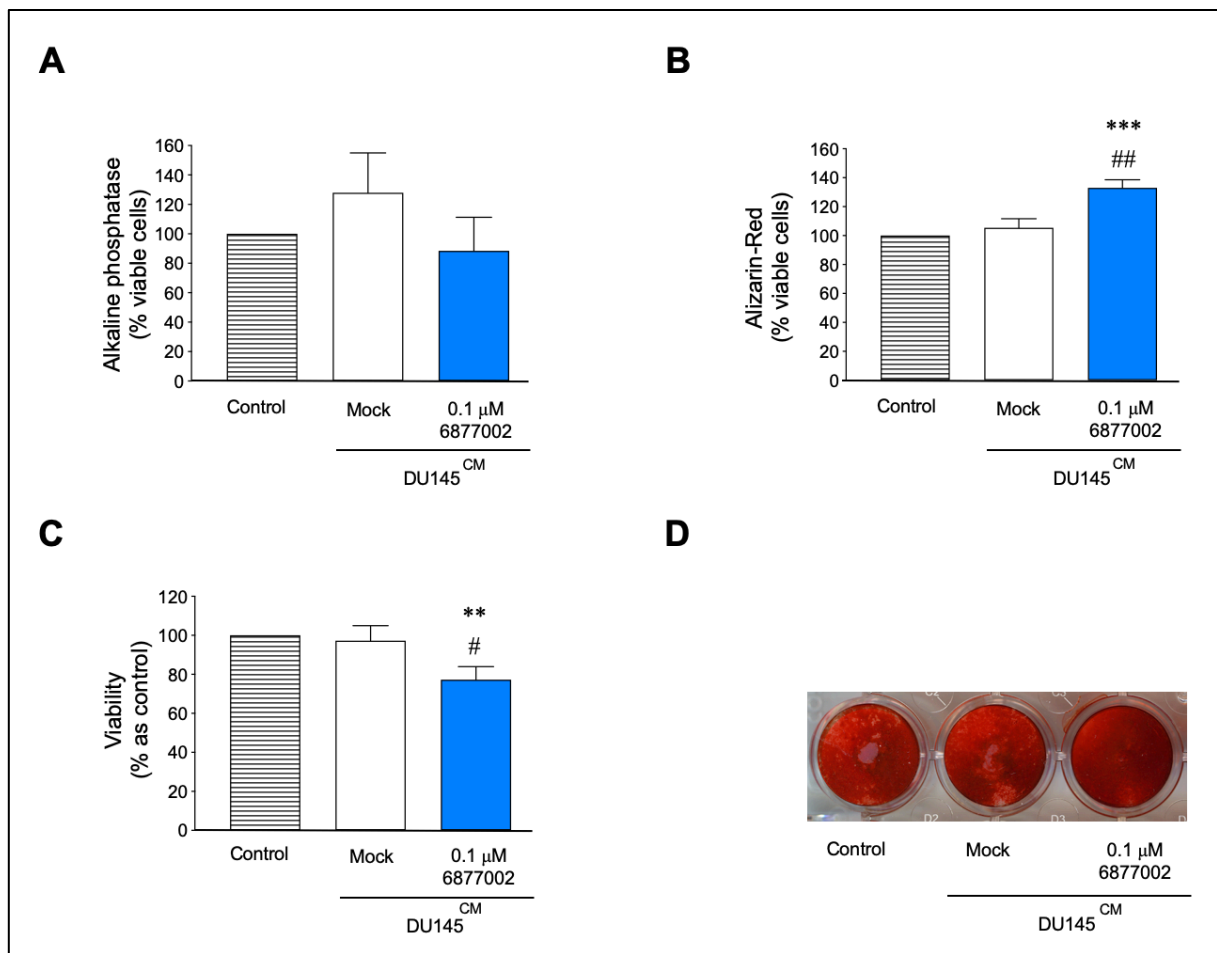
Figure 5.6. Pharmacological TRAF6 inhibition using the verified 6877002 reduced viability and increased bone nodule formation of osteoblast-like cells Saos-2 exposed to DU145-conditioned medium *in vitro*. Percentage of alkaline phosphatase (A), marker for nodule formation alizarin red (B) and cell viability (C) of Saos-2 cells exposed to conditioned medium from DU145 and treated with vehicle or TRAF6 inhibitor 6877002. (D) Representative images of Saos-2 mineralisation in the presence and absence of conditioned medium from DU145 cancer cells and treatment with vehicle or TRAF6 inhibitor 6877002. Data obtained from three independent experiments. p-values were obtained from one-way ANOVA test followed by Tukey *post hoc* test. ***$p < 0.005$ and **$p < 0.01$ compared to control without exposure to conditioned medium, ##$p < 0.01$, #$p < 0.05$ compared to cells exposed to DU145 conditioned media and treated with vehicle.
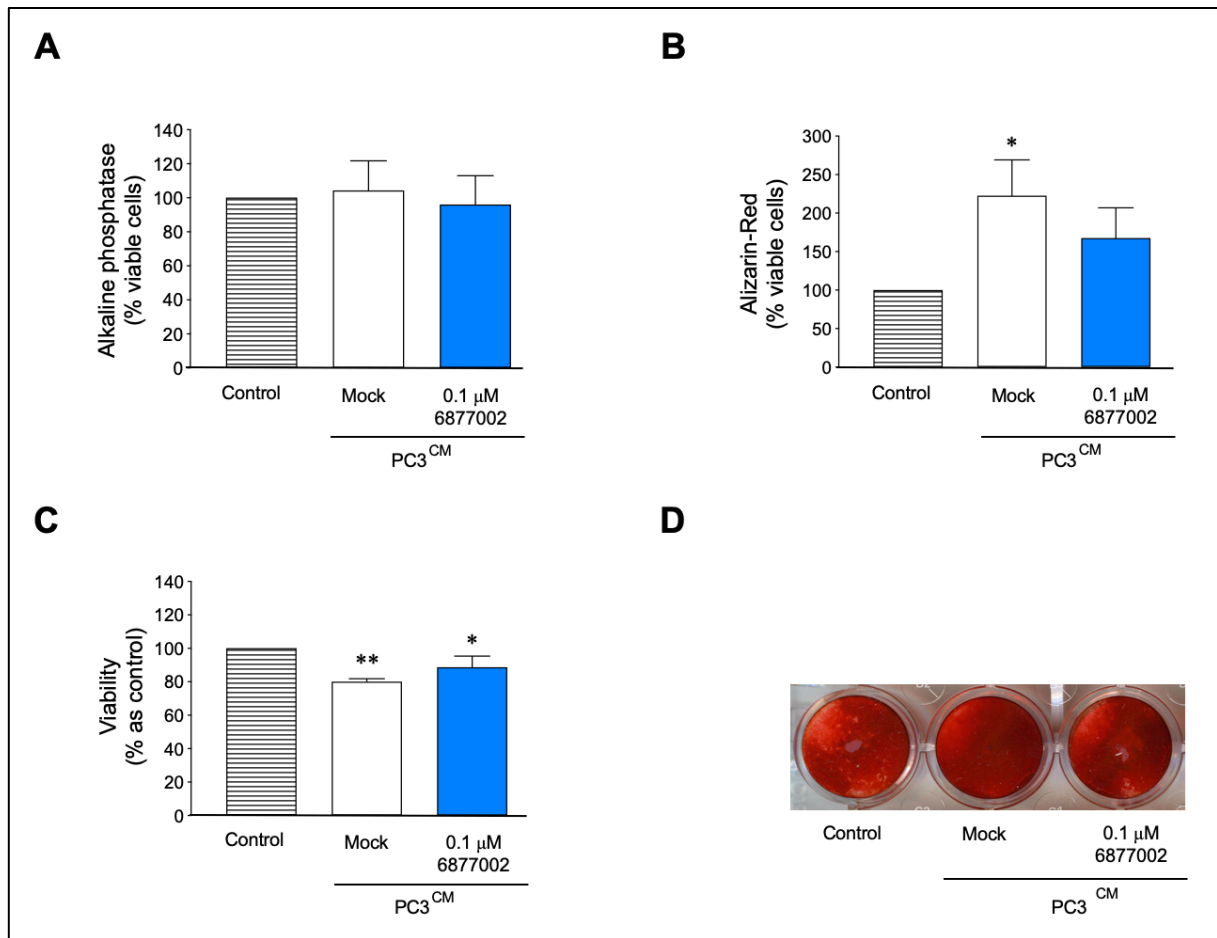
Figure 5.7. Pharmacological TRAF6 inhibition using the verified 6877002 decreased bone nodule formation of osteoblast-like cells Saos-2 exposed to PC3-conditioned medium *in vitro*. Percentage of alkaline phosphatase (A), marker for nodule formation alizarin red (B) and cell viability (C) of Saos-2 cells exposed to conditioned medium from PC3 prostate cancer cells and treated with vehicle or TRAF6 inhibitor 6877002. (D) Representative images of Saos-2 mineralisation in the presence and absence of conditioned medium from PC3 and treatment with vehicle or TRAF6 inhibitor 6877002. Data obtained from three independent experiments. p-values were obtained from one-way ANOVA test followed by Tukey *post hoc* test. **p<0.01 and *p<0.05 compared to control Saos-2 without exposure to conditioned medium.

5.4.5. The verified TRAF6 inhibitor 6877002 had no significant effects in osteolysis in mice bearing human PC3 cells

RANKL- and CD40-induced TRAF6 activation regulates osteoclast formation and bone loss in mice (Lomaga *et al.*, 1999) and it has been previously confirmed that the verified TRAF6 inhibitor 6877002 targets the binding pocket of the TNF superfamily receptor peptide due to the unique interaction of TRAF6 with CD40 and RANK (Moriya *et al.*, 2015). To study the effects of TRAF6 inhibition on osteolysis caused by prostate cancer cells *in vivo*, PC3 cells were injected in the left tibia of nude mice, as described in **2.5.2. Intratibial injection of human PC3 prostate cancer cells in immunodeficient** mice. PC3 cells were used due to their potential to induce osteolytic lesions (Alsulaiman, Bais and Trackman, 2016), their high expression of TRAF6 and based on the previous results *in vitro*, showing significant decrease in the metastatic behaviour of PC3 cells when treated with the TRAF6 inhibitor 6877002 (10 µM). Lesions in the trabeculae, cortex and total bone volume were assessed with the use of micro-computed tomography (Micro-CT; **2.5.3. Micro-computed tomography (micro-CT) analysis**). As shown in **Figure 5.8**, administration of the verified TRAF6 inhibitor 6877002 in mice (20 mg/kg/daily) had no significant effects on trabecular bone volume and trabecular number, consistent with the lack of effects on trabecular separation, thickness, porosity or structure model index. Similarly, treatment with 6877002 failed to exert any significant changes in cortical bone volume nor porosity (**Figure 5.9**).
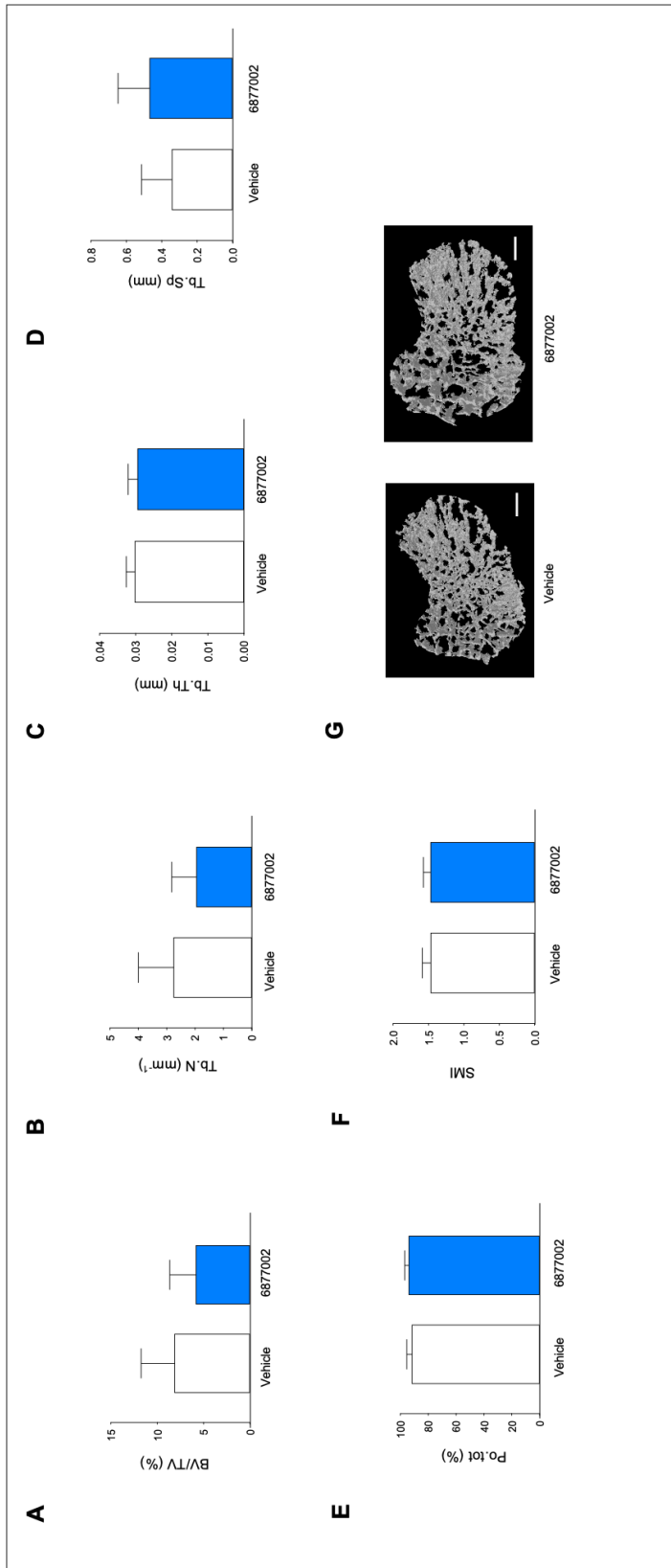
Figure 5.8. Pharmacological inhibition of TRAF6 had no effect in bone-destruction caused by PC3 in trabecular osteolysis in immunodeficient mice. 4-week old BALB/c-nu/nu athymic mice (n=7/per group) received intratibial injection of 2x10^{4} PC3 human prostate cancer cells and were treated with vehicle or with the small-molecule inhibitor 6877002 thrice/week. Trabecular parameters bone volume/tissue volume (BV/TV%; A), trabecular number (Tb.N; B), thickness (Tb.Th; C), separation (Tb. Sp; D), porosity (Po.tot%; E) and Structure Model Index (SMI; F) were measured with microcomputed tomography using CTAn software. (G) Representative 3D reconstructions of the cortical bone were obtained with microcomputed tomography using CTVol software. Scale bar=1 mm.
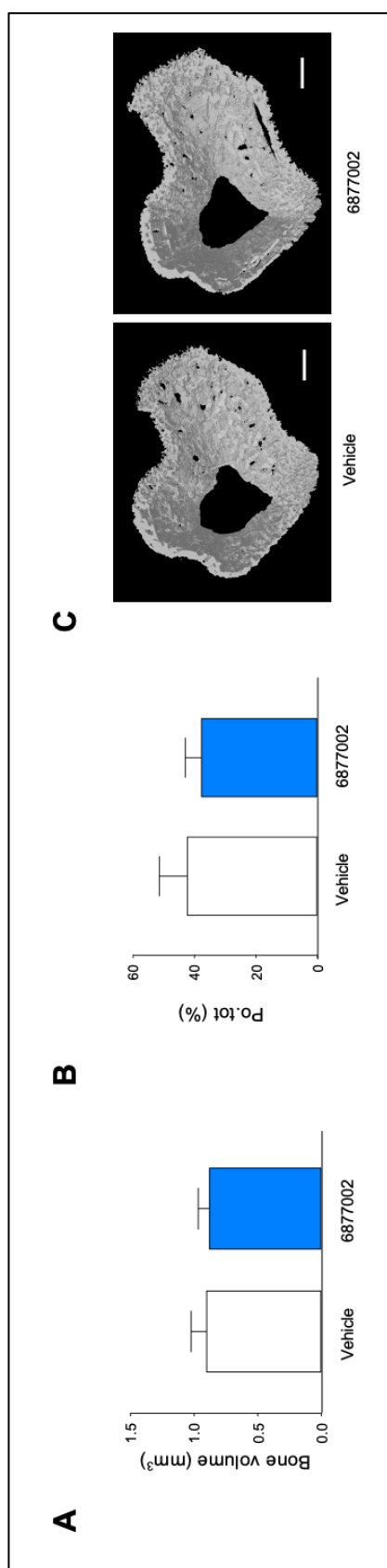
Figure 5.9. Pharmacological inhibition of TRAF6 using the verified TRAF6 inhibitor 6877002 in PC3 tumour growth had no effect in cortical bone parameters in immunodeficient mice. 4-week old BALB/c-nu/nu athymic mice (n=7/per group) received intratibial injection of 2x10⁴ PC3 human prostate cancer cells and were treated with vehicle or with the small-molecule inhibitor 6877002 thrice/week. Bone volume (A) and percentage of total porosity (B) were measured with microcomputed tomography using CTAn software. (C) Representative 3D reconstructions of the cortical bone were obtained with microcomputed tomography using CTVol software. Scale bar=1 mm.

5.5.   Discussion

TRAF6 has a unique binding motif that allows the recruitment of a subset of pro-inflammatory mediators from the TNFR superfamily that includes CD40 and RANK (Park, 2018). Among all TRAFs, TRAF6 has been widely investigated in inflammation (Lalani *et al.*, 2018) and, subsequently, the TRAF6 inhibitor 6877002, which disrupts the interaction between CD40 and TRAF6, was developed to treat obesity-metabolic complications (Antonios Chatzigeorgiou *et al.*, 2014). The specificity of 6877002 to target the unique interaction of CD40-TRAF6 and not CD40 TRAF2/3/5 has been verified *in vitro* and *in vivo* (Antonios Chatzigeorgiou *et al.*, 2014; Aarts *et al.*, 2017). Studies using the verified 6877002 inhibitor have shown promising results in the reduction of macrophage recruitment and inflammation (Aarts *et al.*, 2017; Seijkens *et al.,* 2018). In addition, work from our group have shown that administration of 6877002 reduced metastasis in the syngeneic and osteotropic 4T1-Luc2 breast cancer bone metastasis model (Bishop *et al.*, 2020). Altogether, this suggests that TRAF6 inhibitors such as 6877002 have the potential of influencing cells in the tumour microenvironment and could be of value in the treatment of cancer-associated bone disease.

Due to the involvement of TRAF6 in prostate cancer progression (Sundar *et al.*, 2015; Aripaka *et al.*, 2019) and based on the findings described in **Chapter 4** that showed that cancer-specific TRAF6 knockdown had no effects on PC3-induced osteolysis, the effects of 6877002 were tested on bone cell activity *in vitro* and local osteolysis in a mouse model of human prostate cancer. The *in vitro* investigation showed that exposure to 6877002 reduced the viability of various human and mouse prostate cancer cells in a dose-response manner. Among the human prostate cancer cells, marked concentration-dependent inhibition of cell number was observed in cultures of human C42-B4 and PC3 prostate cancer cells. This was consistent with their high expression of TRAF6 demonstrated in the western blot analysis in **Chapter 3**. In pursuit of assessing the effects of this agent on the migratory and invasive abilities of human prostate cancer cells, the wound-healing migration assay and the Transwell® invasion assay

were performed, respectively. Treatment with the 6877002 compound had a moderate effect in reducing DU145 cell migration and significantly decreased migration and invasion of DU145 and PC3 cells. The results presented here are in agreement with the findings described in **Chapter 4**, where knockdown of TRAF6 in human PC3 and DU145 prostate cancer cells caused a significant reduction in cell growth, migration and invasion. Moreover, TRAF6 inhibition using the verified 6877002 compound had a significant effect in decreasing osteoclast formation enhanced by the presence of soluble factors produced by DU145 and PC3 prostate cancer cells. This is consistent with the modest reduction in osteoclastogenesis observed in cultures exposed to tumour-derived factors from TRAF6-deficient DU145 and PC3 cells. Nonetheless, the decrease in osteoclast number was more evident in cultures treated with 6877002, which is attributed to inhibiting TRAF6 in the cells involved in the bone-tumour microenvironment as opposed to the genetic inactivation of TRAF6 exclusively in the prostate cancer cells. Furthermore, contrasting results were obtained when osteoblasts were exposed to conditioned medium from DU145 and PC3 prostate cancer cells. These results showed an increase in bone nodule formation and decrease in ALP expression and viability in cultures of the osteoblast-like cells Saos-2 exposed to soluble factors from DU145 prostate cancer cells with genetic inactivation or treatment with 6877002 TRAF6 inhibitor. On the other hand, conditioned media from PC3 cells significantly increased formation of nodules from Saos-2 cells and these effects were decreased when using conditioned media from TRAF6 knockdown PC3 cells or treatment with the TRAF6 inhibitor 6877002. Overall, based on the premise that PC3 cells are highly metastatic and generate osteolytic lesions (Berish *et al.*, 2018) and supported by the *in vitro* results presented in this and the previous chapters, the human PC3 cell line was selected for the *in vivo* study. As mentioned in **chapter 4**, the intratibial model was chosen to study tumour growth in the bone environment and to assess the potential improvement of bone architecture by TRAF6 inhibition with 6877002 treatment. Recent work from our lab has shown that treatment with the verified 6877002 TRAF6 inhibitor caused a significant decrease in bone metastasis and a moderate increase in bone volume in a breast

cancer model using syngeneic and osteotropic 4T1-Luc2 breast cancer cells. Surprisingly, the same compound failed to affect bone volume after intratibial injection of human PC3 cells in nude mice. It is important to note that the prostate cancer model used in the current chapter was different from the mentioned breast cancer model. The human PC3 prostate cancer cells were injected intratibially in immunodeficient mice and, in contrast, the used breast cancer cell line 4T1-Luc2 was syngeneic and these cells were injected intracardially in immunocompetent mice. Thus, the anti-cancer effects observed in the 4T1-Luc2 model could be due to the ability of 6877002 to inhibit metastasis of mouse prostate cancer cells to bone. In addition, TRAF6 is involved in cell-cell interactions between immune, bone and prostate cancer cells (Lomaga *et al.*, 1999; Gudey *et al.*, 2014; Seijkens *et al.*, 2018; Aripaka *et al.*, 2019) and due to its relevance in the activation of many immune cell types such as dendritic cells and T cells (Kobayashi *et al.*, 2003; Ni *et al.*, 2019), it is believed that TRAF6 inhibition may be more beneficial in a fully functional immune environment. A possible explanation for the discrepancies between the results of the two studies could be the ability of 6877002 to influence the activity of immune cells in immunocompetent mice used in the 4T1-Luc2 mouse study (Bishop *et al.*, 2020), in contrast with the model used in this chapter involving immunodeficient mice, which are athymic and thereby unable to produce T cells. Thus, syngeneic and osteotropic RM1-BM murine prostate cancer cells – which express TRAF6 (**Chapter 3**) and respond well to 6877002 treatment *in vitro* – will be injected intracardially in immunocompetent mice in future studies. In addition, combining and developing novel, efficient and safe TRAF/NFκB inhibitors that target different binding sites of the TNF family receptors, including RANK and CD40, could result in an increased efficacy in inhibition of cancer progression (Moriya *et al.*, 2015) and is of potential interest for approaching new therapeutic strategies.

Furthermore, another technical factor that might have contributed to these discrepancies could be the poor solubility of the 6877002 compound, thus higher doses could not be administered

in either study. Although 6877002 has been previously tested in animal studies and has been reported as soluble (Chatzigeorgiou *et al.*, 2014; Aarts *et al.*, 2017), different vehicles had to be tested to fully dissolve the amount of the compound injected, being likely that the treatment could not have been efficiently delivered. Further studies should consider the development and testing of a TRAF6 inhibitor with better solubility.

Altogether, the results of this chapter indicate that pharmacological inhibition of TRAF6 significantly reduced osteoclastogenesis and modestly decreased bone nodule formation, both enhanced by prostate cancer cells *in vitro*. Further studies will be focused on using an immunocompetent mouse model of prostate cancer to conclude whether TRAF6 inhibition in bone and prostate cancer affects osteolysis.

Chapter 6. Effects of the novel FSAS compounds on prostate cancer cell behaviour *in vitro*

6.1.   Summary

The results in **Chapter 5** showed that the verified inhibitor of TRAF6 6877002 had no effect on prostate cancer-induced bone loss in the human PC3 model. In this chapter, the effects of a panel of novel congeners of the verified TRAF6 inhibitor 6877002 were tested on prostate cancer cell growth, motility and interaction with bone and immune cells *in vitro*. The novel congeners FSAS1 to 6 were developed in collaboration with the University of Milan (Italy). First, it was shown that the novel FSAS1 to 6 reduced the *in vitro* growth of a panel of human and mouse prostate cancer cells in a dose-dependent manner. FSAS3 was significantly more potent than 6877002 and other congeners, thus it was selected for further experiments. Mechanistically, the novel FSAS3 reduced IκB-α phosphorylation induced by RANKL in macrophage-like RAW 264.7 cells and by both RANKL and TNF-α in PC3 cells, indicative of NFκB inhibition. Moreover, FSAS3 significantly reduced cell migration and invasion in the highly metastatic androgen-insensitive human PC3 and the osteotropic murine RM1-BM prostate cancer cells. Conditioned medium from tumour-associated M2 macrophages enhanced PC3 viability, migration and invasion and these effects were significantly inhibited by the novel FSAS3. Interestingly, FSAS3 treatment had no effects on the anti-tumour ability of classically-activated macrophages (M1) to reduce the metastatic behaviour of human PC3 prostate cancer cells and enhanced the ability of uncommitted monocyte/macrophages (M∅) to differentiate into M1 rather than M2, as assessed by flow cytometry. Additionally, FSAS3 significantly reduced the ability of RAW 264.7 macrophage-like cells to form bone-resorptive TRAcP-positive osteoclasts in the presence and absence of tumour-derived factors from human PC3 and mouse RM1-BM prostate cancer cells. Collectively, these findings identify the novel FSAS3 as a class of anti-tumour, anti-migratory and antiresorptive agent, which may be of value in the treatment of both skeletal and non-skeletal complications related to metastatic prostate cancer.

6.2.   Introduction

Pro-inflammatory cytokines and immune cells, in particular macrophages, play a key role in the behaviour of prostate cancer cells in bone (D'amico and Roato, 2015) and a number of studies have shown that tumour-associated macrophages (TAMs), a major cell population in the stroma of many tumours, are considered a prognostic in prostate cancer patients (Lindsten *et al.*, 2017; Santoni *et al.*, 2017). Various studies have addressed the influence of macrophages in prostate cancer progression, showing a supportive role of TAMs in prostate cancer tumorigenesis and bone metastasis in mouse models (Fang *et al.*, 2013; Soki *et al.*, 2015) and in patients with advanced castration-resistant prostate cancer (Roca *et al.*, 2009). *In vitro* studies have shown that TRAF6 inhibition using the verified 6877002 decreased the migration and activation of bone-marrow derived macrophages (Seijkens *et al.*, 2018). Altogether, these studies suggest that disruption of the influence of pro-inflammatory cytokines and macrophages in prostate cancer by TRAF6 inhibition could be of value in the treatment of advanced prostate cancer.

To date, several compounds derived from the verified CD40-TRAF6 inhibitor 6877002 have been generated with the purpose of treating inflammation (Moriya *et al.*, 2015; Zarzycka *et al.*, 2015). Based on the efficient binding activities of the verified 6877002 TRAF6 inhibitor and aiming to select and optimise ligand structures, Zarzycka and colleagues (2015) showed that 6 compounds out of 151 inhibited NFκB signalling in macrophage-like RAW264.7 cells in a dose-dependent manner. These 6 compounds were analogues of the verified 6877002 CD40-TRAF6 inhibitor and, in fact, were more potent in inhibiting the expression of cytokines IL-1β and IL-6 in bone marrow-derived macrophages (Zarzycka *et al.*, 2015). Given that the results of **Chapters 4 and 5** indicated that cancer-specific TRAF6 inhibition was insufficient to enhance bone volume in immunodeficient mice bearing the human PC3 model, we designed, synthesised and tested the effects of a series of novel congeners of the small-molecule inhibitors of TRAF6 (6877002; Zarzycka *et al.*, 2015) and NFκB (ABD56; Idris *et al.*, 2008, 2009) on models of prostate cancer cell – macrophage - bone cell interactions.

6.3.   Aims

The aims of this chapter were to study the effects of the novel FSAS family of compounds on:

- The growth of a panel of human and mouse prostate cancer cells *in vitro.*

- NFκB activation in prostate cancer cells and macrophages.

- The migration and invasion of the human metastatic PC3 and mouse osteotropic RM1-BM prostate cancer cells in the presence and absence of derived factors from different macrophage phenotypes *in vitro.*

- The ability of the metastatic mouse RM1-BM and human PC3 prostate cancer cells to influence bone cell activity and macrophage lineage commitment *in vitro*.

6.4. Results

6.4.1. The novel FSAS3 reduced the viability of a panel of human and mouse prostate cancer cells *in vitro*

In the present chapter, the effects of six structurally-related novel congeners of the inhibitors of TRAF6/NFκB, 6877002 and ABD56, on the viability of a panel of human and mouse prostate cancer cells were assessed by using the Alamar Blue™ assay (See **section 2.4.2.1**). As shown in **Table 6.1**, FSAS1 to 6, except FSAS4, inhibited the viability of all prostate cancer cells tested in a dose-dependent manner with different degrees of potency, as indicated by the IC$_{50}$ values. FSAS3 was significantly more potent than 6877002 and other congeners, thus it was selected for the following experiments (**Figure 6.1**). Interestingly, FSAS3 exerted marked inhibitory effects on the growth of mouse and osteotropic prostate cancer cell line RM1-BM when compared to the human cell lines tested (**Table 6.1**).

Table 6.1. Effects of the verified TRAF6 inhibitor 6877002 and six congeners on the viability of a panel of murine and human prostate cancer cells with different metastatic abilities *in vitro*. Cell viability was measured after 72 hours of continuous exposure to the seven profiled TRAF inhibitors. Calculation of half maximal inhibitory concentrations (IC_{50}) was performed as described in **section 2.4.2.1**. Values are expressed as mean ± SD and were obtained from three independent experiments.

Cell type	Classification	Half maximal inhibitory concentration (IC_{50}) in µM after 72 hours						
		FSAS1	FSAS2	FSAS3	FSAS4	FSAS5	FSAS6	6877002
LNCaP	Androgen sensitive	31.54±12.14	30.04±14.31	1.45±0.19	>100	65.87±13.13	1.85±0.89	38.19±3.90
C42-B4	Androgen insensitive-Bone trophic	11.46±2.72	15.31±8.13	1.7±0.46	69.64±26.55	14.22±6.48	6.00±3.91	37.54±12.11
RM1-BM	Androgen insensitive-Bone trophic	8.96±5.17	20.96±8.96	0.43±0.24	>100	45.70±15.99	1.93±1.36	21.18±2.59
DU145	Androgen insensitive-Bone trophic	80.69±12.24	39.28±19.65	6.82±3.87	>100	49.89±13.52	2.59±0.25	34.08±12.67
PC3	Androgen insensitive-Bone trophic	58.14±9.88	23.03±6.56	1.43±0.81	68.72±22.85	36.10±4.35	3.72±0.56	38.49±14.3
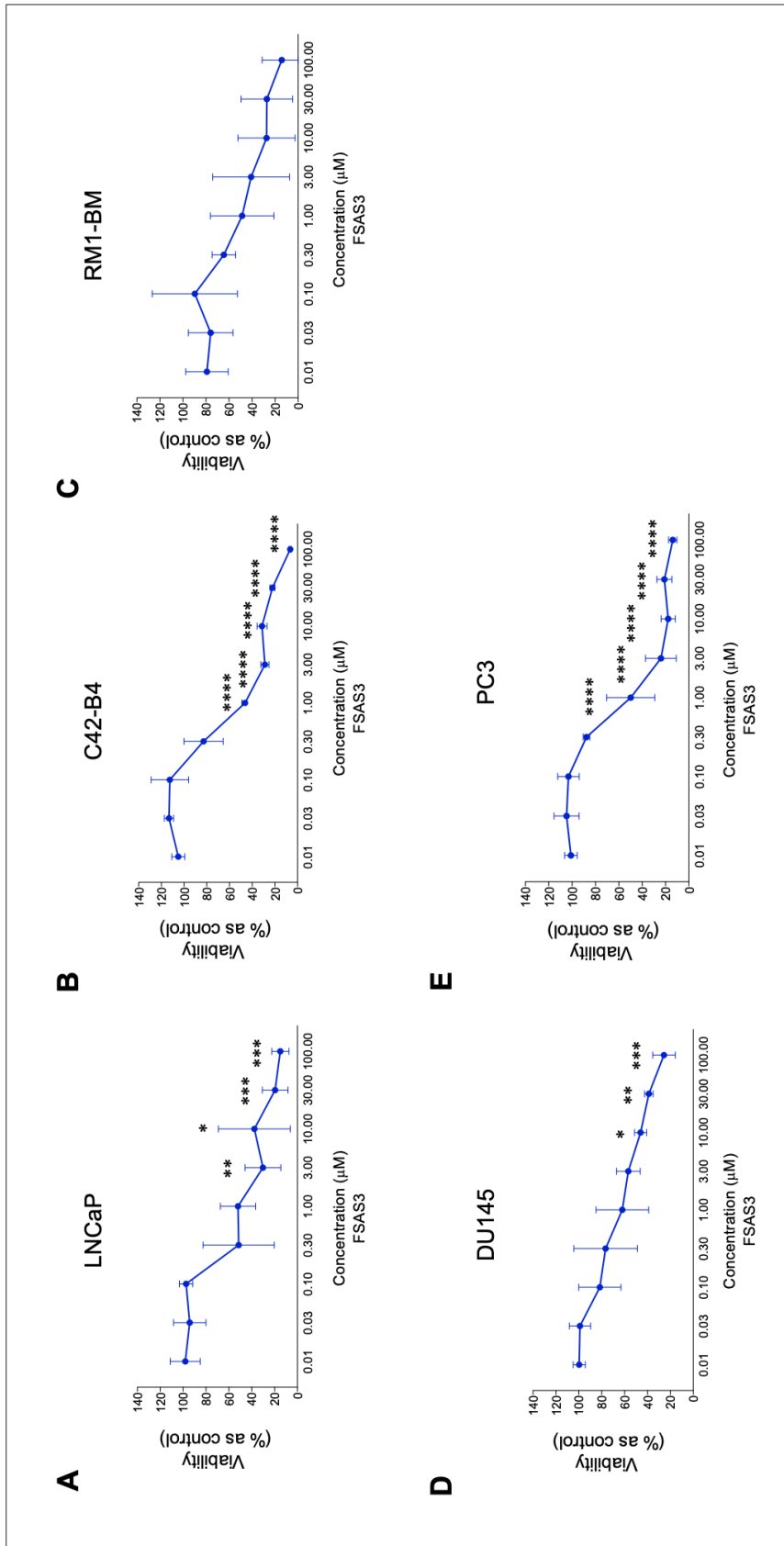
Figure 6.1. Effects on cell viability of a panel of murine and human prostate cancer cells treated with the novel TRAF inhibitor FSAS3 *in vitro*. Dose-response curves of the novel TRAF inhibitor FSAS3 on the viability of parental LNCaP (A) and sub-clone LNCaP-C4-2B4 (B), the murine and highly metastatic RM1-BM (C) and human highly metastatic DU145 (D) and PC3 (E) prostate cancer cells after 72 hours, as assessed by Alamar Blue™ assay. Data obtained from three independent experiments. p-values were obtained from two-way ANOVA test followed by Tukey *post hoc* test. ****p<0.001, ***p<0.005, **p<0.01, *p<0.05 compared to cells treated with vehicle.

6.4.2. The novel FSAS3 inhibited RANKL- and TNF-α-induced NFκB activation

As an adaptor protein, TRAF6 plays a major role in the activation of several signalling pathways in prostate cancer, bone cells and macrophages, in particular NFκB (Lomaga *et al.*, 1999; Antonios Chatzigeorgiou *et al.*, 2014; Aripaka *et al.*, 2019). Zarzycka and colleagues (2015) selected optimal CD40-TRAF6 inhibitors by studying their efficiency in disrupting NFκB activation in macrophage-like RAW 264.7 cells (Zarzycka *et al.*, 2015). With the premise that NFκB is constitutively active in prostate cancer (L. Zhang *et al.*, 2009), in this chapter, the effects of the novel FSAS3 on RANKL- and TNF-α-induced NFκB activation were investigated by assessing the expression of phosphorylated IκB-α and total IκB-α in macrophage-like RAW 264.7 cells and PC3 prostate cancer cells. Previous experiments were performed to define an optimal timepoint to study IκB-α phosphorylation in RAW 264.7 and PC3 cells (**Supplementary Figure 10** and **Supplementary Figure 11-12**, respectively). Briefly, murine macrophage-like RAW 264.7 and PC3 cells were exposed to FSAS3, 6877002 or vehicle for 1 hour and then stimulated with RANKL (100 ng/ml) or TNF-α (10 ng/ml) for the previously determined period of time. As shown in **Figure 6.2**, pre-exposure of murine macrophage-like RAW 264.7 to the novel FSAS3 (10 µM) significantly reduced and completely prevented RANKL-induced IκB-α phosphorylation without affecting the level of IκBα expression, whereas 6877002 (10 µM) had no effects.

In PC3 prostate cancer cells, the novel FSAS3 significantly reduced RANKL-induced (100 ng/ml) phosphorylation of IκB-α without affecting the level of IκB-α expression (**Figure 6.3**). In addition, exposure of PC3 cells to 6877002 (10 µM) caused a significant inhibition of IκB-α phosphorylation induced by RANKL (**Figure 6.3**). The concentrations used for both compounds were chosen based on the premise that these concentrations failed to cause significant inhibition of cell viability after 24 hours of continuous treatment (**Supplementary Figure 13**). Similarly, the novel FSAS3 caused a significant reduction in expression of phosphorylated IκB-α induced by TNF-α (10 ng/ml) after 6 hours (**Figure 6.4**).
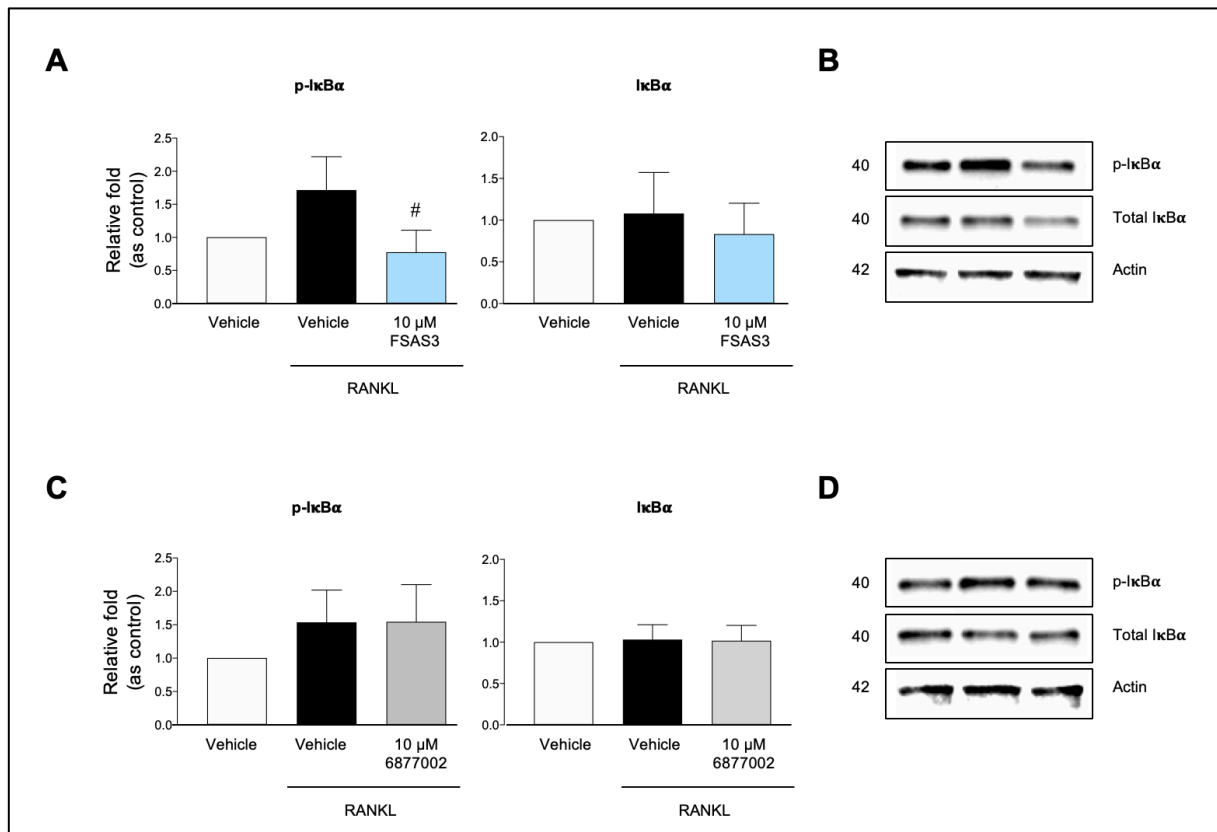
Figure 6.2. The novel FSAS3 reduced the phosphorylation of IκB-α in RAW 264.7 induced by RANKL *in vitro*. Relative fold of phosphorylated-IκB-α/Actin and IκB-α/Actin expression of murine macrophage-like RAW 264.7 cells exposed to vehicle, FSAS3 (A) or 6877002 (C) (10 µM) for 1 hour prior to stimulation with RANKL (100 ng/ml). Representative Western Blot images of expression of p-IκB-α and IκB-α of RAW 264.7 cells exposed to vehicle, FSAS3 (B) or 6877002 (D). Data presented are mean ± standard deviation (n=3). p-values were obtained from ordinary ANOVA test followed by Tukey *post hoc* test. #p<0.05 compared to RANKL-stimulated RAW 264.7.
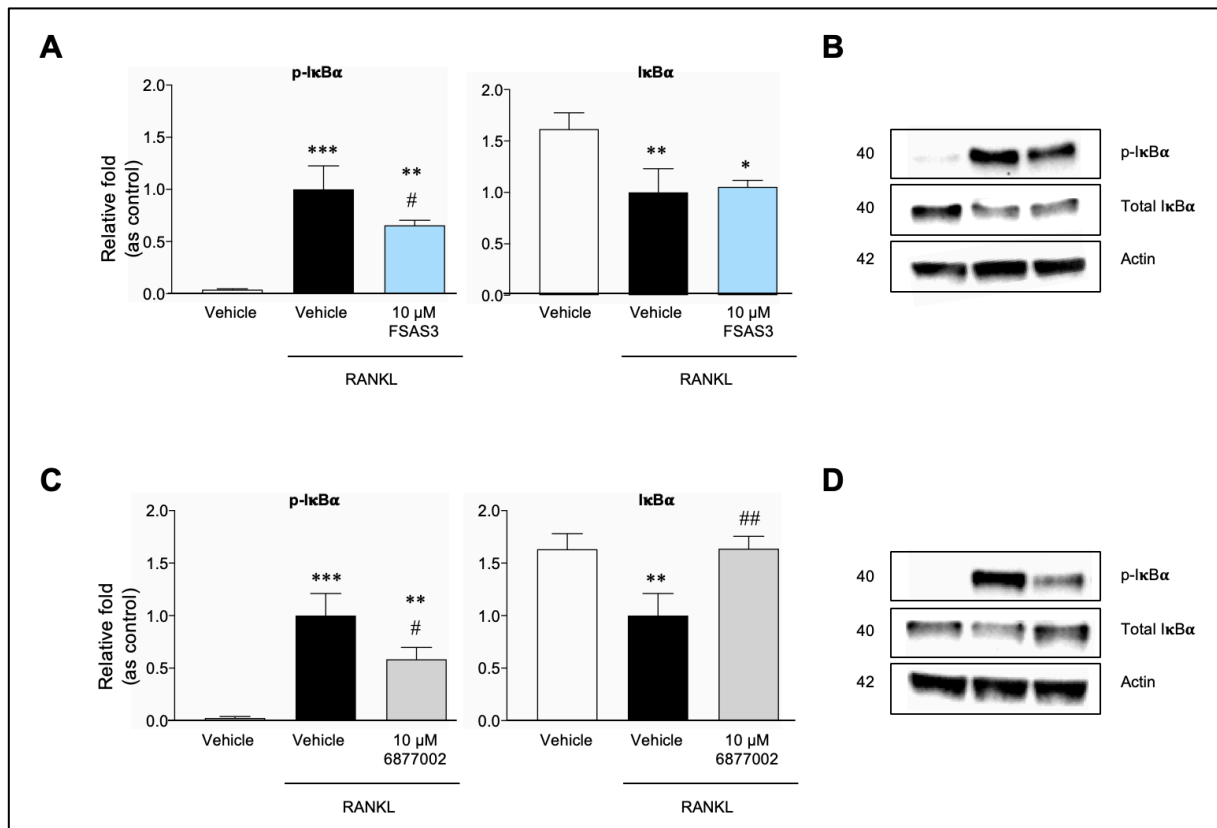
Figure 6.3. The novel FSAS3 reduced the phosphorylation of IκB-α in PC3 induced by RANKL *in vitro*. Relative fold of phosphorylated-IκB-α/Actin and IκB-α/Actin expression of human PC3 prostate cells exposed to vehicle, FSAS3 (A) or 6877002 (C) (10 µM) for 1 hour prior to stimulation with RANKL (100 ng/ml) for 0.5 hours. Representative Western Blot images of expression of p-IκB-α and IκB-α of PC3 cells exposed to vehicle, FSAS3 (B) or 6877002 (D). Data presented are mean ± standard deviation (n=3). p-values were obtained from ordinary ANOVA test followed by Tukey *post hoc* test. ***$p < 0.005$, **$p < 0.01$ and *$p < 0.05$ compared to unstimulated PC3 cells, ##$p < 0.01$ and #$p < 0.05$ compared to RANKL-stimulated PC3 cells.
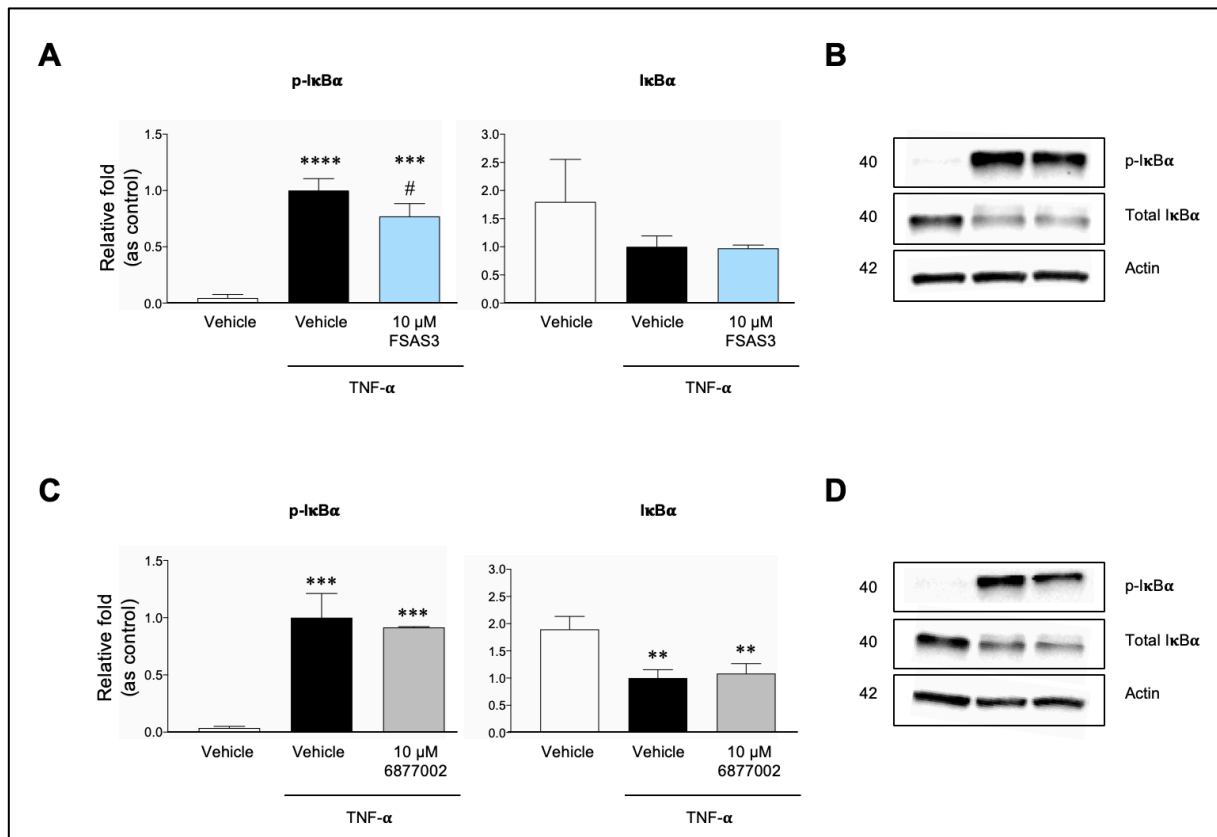
Figure 6.4. The novel FSAS3 reduced the phosphorylation of IκB-α in PC3 induced by TNF-α *in vitro*. Relative fold of phosphorylated-IκB-α/Actin and IκB-α/Actin expression of human PC3 prostate cells exposed to vehicle, FSAS3 (A) or 6877002 (C) (10 µM) for 1 hour prior to stimulation with TNF-α (10 ng/ml) for 6 hours. Representative Western Blot images of expression of p-IκB-α and IκB-α of PC3 cells exposed to vehicle, FSAS3 (B) or 6877002 (D). Data presented are mean ± standard deviation (n=3). p-values were obtained from ordinary ANOVA test followed by Tukey *post hoc* test. ****p<0.001, ***p<0.005 and **p<0.01 compared to unstimulated PC3 cells, #p<0.05 compared to TNF-α-stimulated PC3 cells.

6.4.3. The novel FSAS3 reduces prostate cancer cell viability via a TRAF6-dependent mechanism

In an attempt to examine the involvement of TRAF6 on the anti-tumour effect of the novel FSAS3, the viability of mock and TRAF6 knockdown (70% reduced expression of TRAF6 as assessed in **Chapter 4**) PC3 prostate cancer cells was assessed in the presence of different concentrations of FSAS3 (0 – 100 μM) by the Alamar Blue™ assay (See **section 2.4.2.1**). As shown in **Figure 6.5**, the novel FSAS3 reduced the viability of the mock and TRAF6 knockdown (shT6KD1 and shT6KD2) PC3 prostate cancer cells in a concentration-dependent manner. In comparison to mock control, cultures of TRAF6 knockdown (shT6KD1 and shT6KD2) PC3 prostate cancer cells were relatively resistant to treatment of FSAS3 (**Figure 6.5C and D**), thereby indicating at least in part a TRAF6-dependent effect.
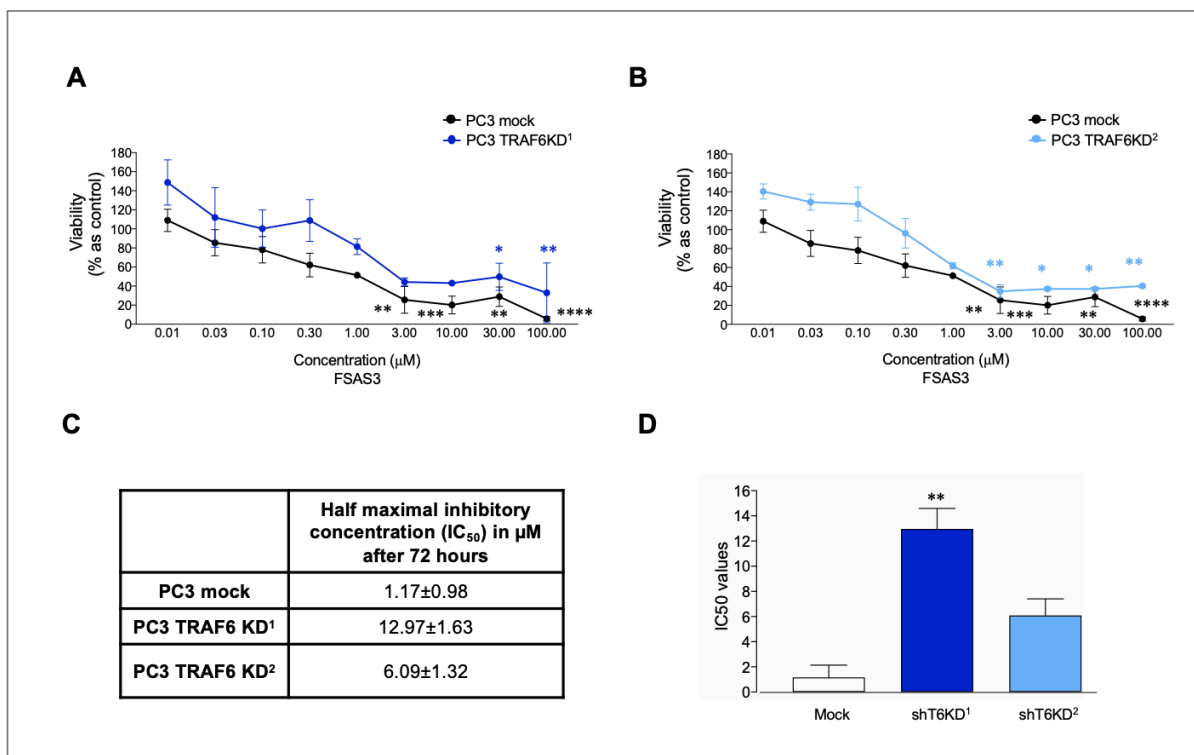
Figure 6.5. Effects of the novel FSAS3 on viability of TRAF6 knockdown PC3 prostate cancer cells *in vitro*. Dose-response curves of the novel FSAS3 on the viability of PC3 transduced with control and shRNA TRAF6 knockdown 1 (A) or TRAF6 knockdown 2 (B) constructs after 72 hours, assessed by Alamar Blue™ assay. (C and D) IC_{50} values were obtained as described in **section 2.4.2.1**. Data obtained from two independent experiments. p-values were obtained from two-way ANOVA test followed by Tukey *post hoc* test. ****p<0.001, ***p<0.005, **p<0.01, *p<0.05 compared to cells treated with vehicle.

6.4.4. The novel FSAS3 reduced cell motility in prostate cancer cells

Several studies have shown that inhibition of TRAF2, TRAF4 and TRAF6 reduced prostate cancer cell motility *in vitro* (Wei, Ruan, *et al.*, 2017; Singh *et al.*, 2018; Aripaka *et al.*, 2019) and in **Chapter 5** I showed that exposure of human PC3 and DU145 to the verified TRAF6 inhibitor 6877002 reduced both 2D migration and invasion *in vitro*. In this chapter, the effects of the novel FSAS3 on the ability of the highly metastatic human PC3 prostate cancer cell line to migrate were assessed by the wound-healing assay (See **2.4.2.2. Cell migration assessed by the wound-healing assay**). In **Figure 6.7**, treatment of human PC3 with the novel FSAS3 (1 μM) caused a significant reduction in the 2D migration of PC3 cell after 14 hours (45% inhibition, $p<0.05$). Additionally, FSAS3 caused a relatively modest but significant inhibition of PC3 cell viability (14% inhibition, $p < 0.05$) after 14 hours in these cultures (**Figure 6.7B**). Representative images of the experiment described are shown in **Figure 6.7C.**

In addition, exposure of human PC3 prostate cancer cells to FSAS3 (0.3 μM) significantly reduced cell invasion (**Figure 6.7**), as assessed by the Transwell® invasion assay (See **2.4.2.3. Cell invasion assessed by Transwell® invasion assay**). Representative images of the experiment described are shown in **Figure 6.7B.** The concentrations used in these experiments were based on previous experiments that showed FSAS3 had no significant effects of PC3 cell viability after 24 hours and 72 hours, respectively (**Supplementary Figure 13**).
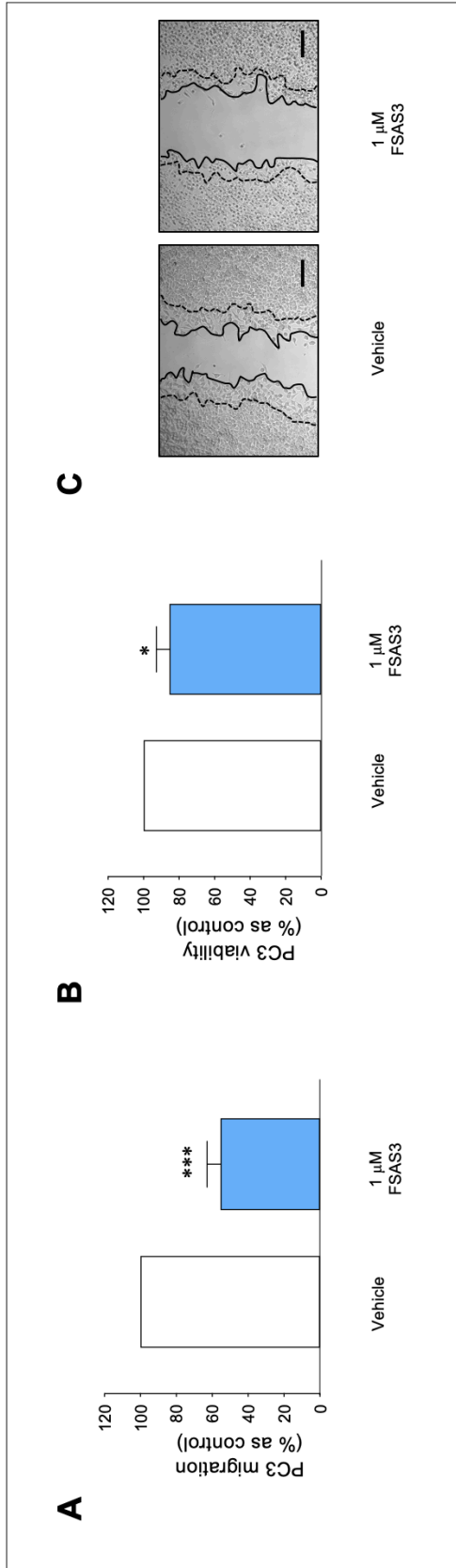
Figure 6.6. The novel FSAS3 reduced PC3 cell migration *in vitro*. Percentage of (A) cell migration of human PC3 prostate cancer cells treated with vehicle or 1 µM of the novel FSAS3 and (B) PC3 cell viability after 14 hours. (C) Representative images showing initial and final positions of motility in timepoints 0 (dotted lines) and 14 hours (continuous lines) from PC3 cells. Data obtained from three independent experiments. p-values were determined using unpaired T-test. ***p<0.005, *p<0.05 compared to cells treated with vehicle. Scale bar=100 µM.
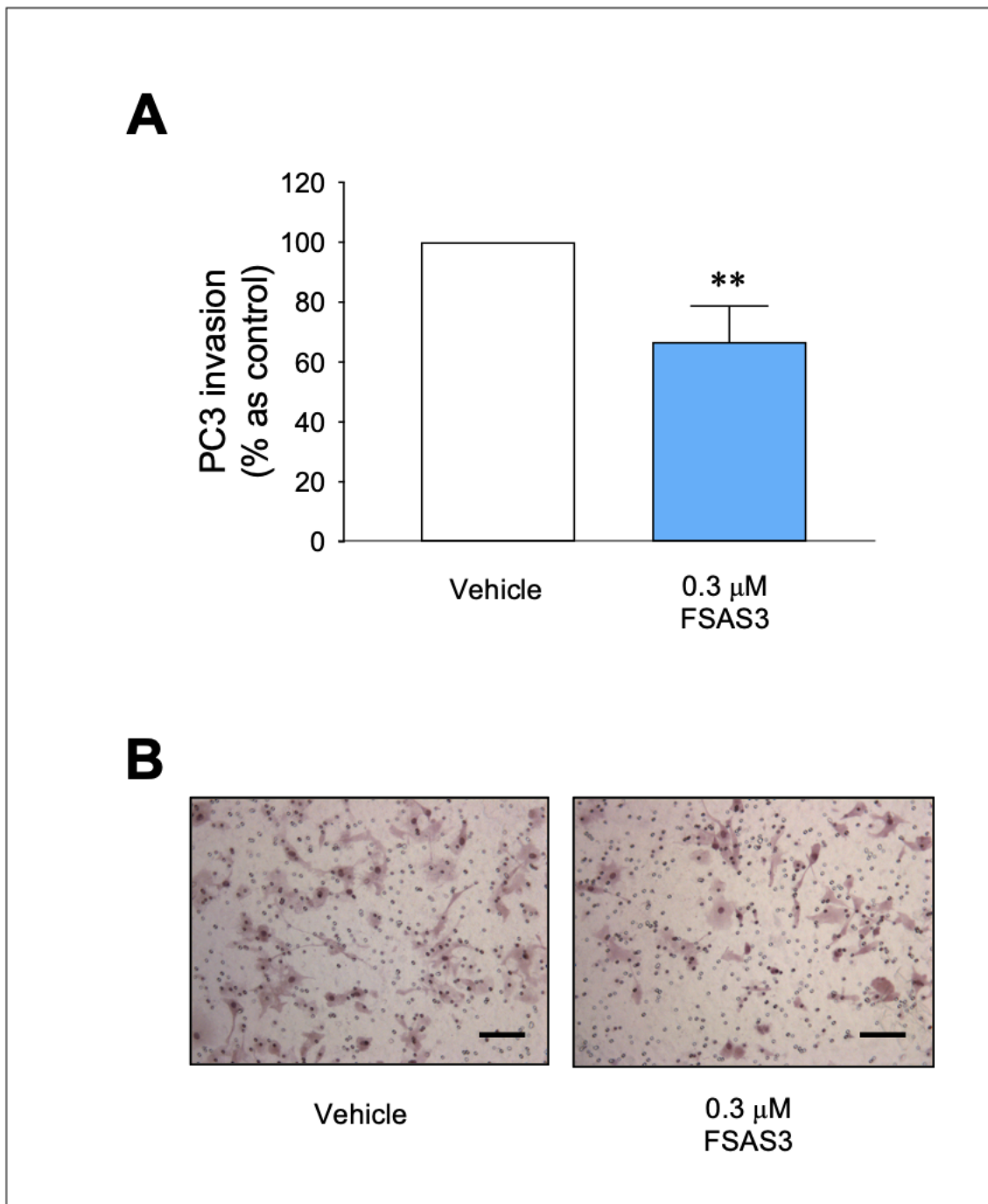
Figure 6.7. The novel FSAS3 reduced PC3 cell invasion *in vitro*. (A)Percentage of cell invasion of PC3 prostate cancer cells treated with vehicle or 0.3 µM of the novel FSAS3. (B)Representative images of invading PC3 cells stained with Hematoxilin and Eosin after 72 hours. Data obtained from three independent experiments. p-values were determined using unpaired T-test. **p<0.01 compared to cells treated with vehicle. Scale bar=100 µM.

6.4.5. The novel FSAS3 decreases the pro-tumorigenic effects of macrophages *in vitro*

In prostate cancer, the population of TAMs that infiltrate tumours in the primary site or distant organs such as bone are skewed towards a pro-tumorigenic M2 macrophage subtype (Soki *et al.*, 2015; Ylitalo *et al.*, 2017; Lo and Lynch, 2018). A number of *in vitro* studies have shown that monocytes and macrophages, and their derived factors, contribute to prostate cancer cell invasion and migration (Lindholm *et al.*, 2010; Lindsten *et al.*, 2017; Han *et al.*, 2019). Here, the effects of the novel FSAS3 on prostate cancer cell growth, migration and invasion in the presence of soluble factors produced by uncommitted (MØ), anti-tumorigenic (M1) and pro-tumorigenic (M2) macrophage subtypes were studied. Briefly, the human prostate cancer cells PC3 were exposed to conditioned medium from the different macrophage phenotypes to assess viability, 2D migration and invasion as described above. As shown in **Figure 6.8**, exposure of PC3 to conditioned medium from the pro-tumorigenic M2 macrophages significantly increased human PC3 prostate cancer cell viability (**Figure 6.8A**), migration (**Figure 6.8B**) and invasion (**Figure 6.8C**) when compared to control and cultures exposed to conditioned medium from cultures of MØ and M1 macrophage subtypes (p<0.05). Furthermore, the uncommitted MØ caused a modest increase in PC3 cell migration and significantly enhanced cell invasion without affecting cell viability (**Figure 6.8E**). In contrast, soluble factors produced by anti-tumorigenic M1 macrophages significantly decreased human PC3 cell migration and invasion in the model described and under these same conditions (**Figure 6.8**).

Treatment with the novel FSAS3 (1 µM) significantly decreased soluble factors derived from the pro-tumorigenic macrophages on PC3 cell viability (**Figure 6.9A**) and migration (**Figure 6.9B** and **Supplementary Figure 15**). Consistently, treatment with FSAS3 (0.3 µM) reduced the invasive capabilities of PC3 alone and influenced by the M2 macrophages (**Figure 6.9C**). Given that the most marked influence of MØ, M1 and M2 macrophage was observed in the ability of PC3 to invade, the effects of FSAS3 were studied on the ability of the highly metastatic and osteotropic murine prostate cancer cell line RM1-BM to invade. As shown in **Figure 6.10**, the novel FSAS3 significantly reduced the invasive capabilities of murine RM1-BM.
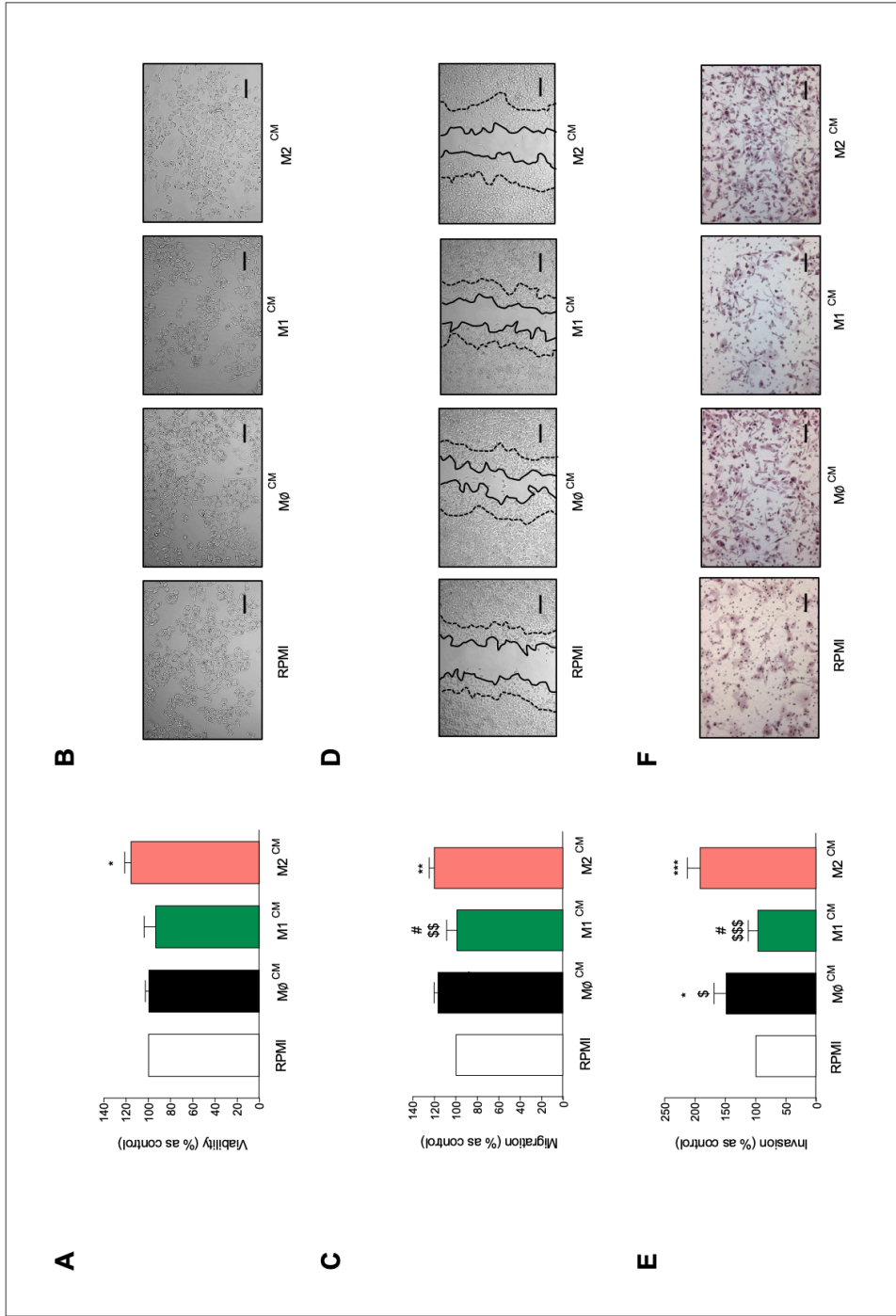
Figure 6.8. Effects of uncommitted (MØ), anti-tumorigenic (M1) and pro-tumorigenic (M2) macrophage subtypes on PC3 prostate cancer cell growth and motility *in vitro*. Percentage of PC3 cell viability assessed by Alamar Blue™ assay (A), wound-healing migration (C) and Transwell® invasion (E) from exposure to soluble factors produced by MØ, M1 and M2 macrophage subtypes. Representative images of PC3 cell growth (B), migration (D) and invasion (F). Data obtained from three independent experiments. p-values were obtained from ordinary ANOVA test followed by Tukey *post hoc* test. ***p<0.005, **p<0.01 and *p<0.05 compared to PC3 cells with RPMI control media, #p<0.05 compared to MØ-treated PC3 cells, $$$p<0.005, $$p<0.01 and $p<0.05 compared to M2-treated PC3 cells. Scale bar=100 µM.
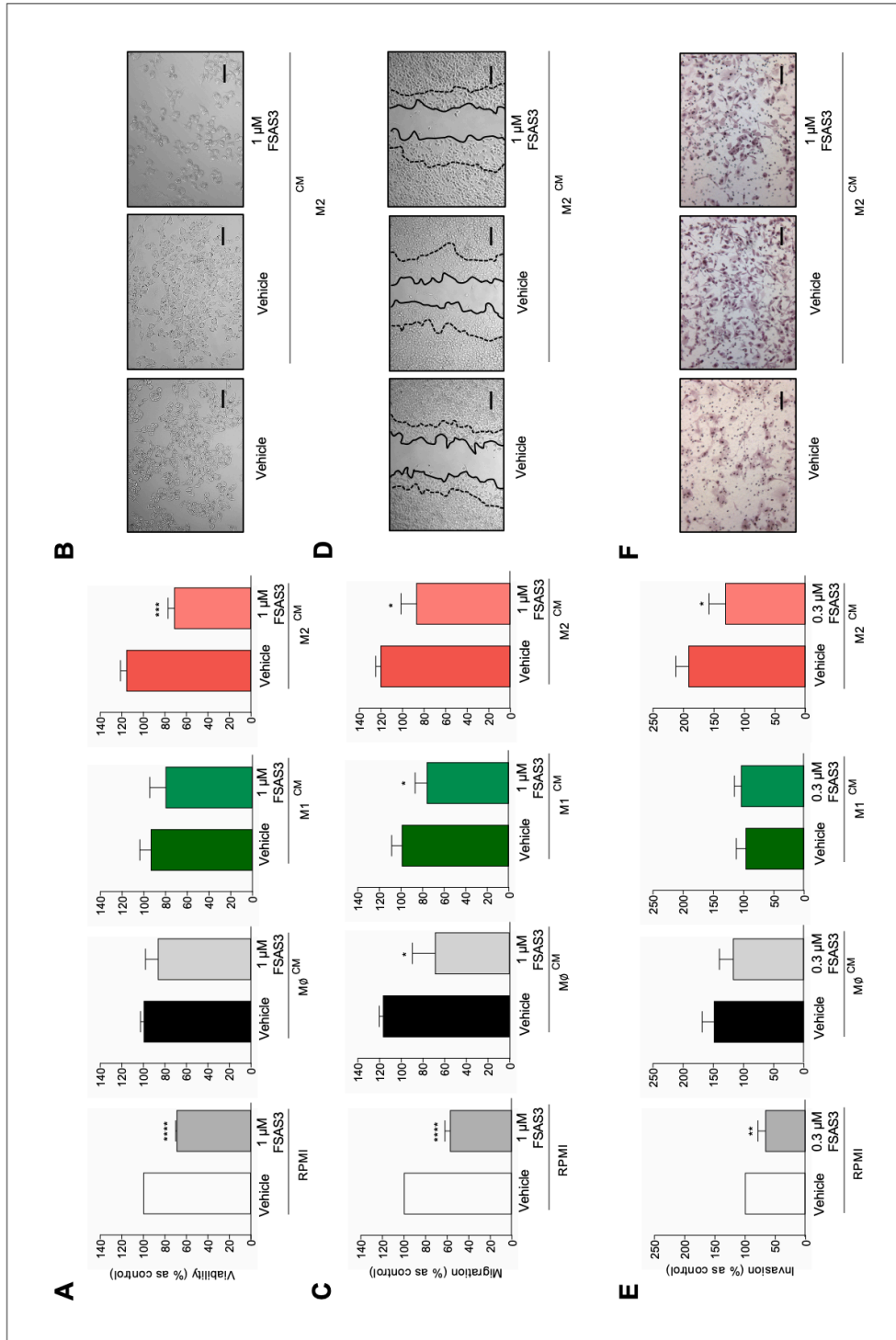
Figure 6.9. Pharmacological inhibition of TRAF/NFκB with the novel FSAS3 reduced the pro-tumorigenic effects of M2 macrophages on human PC3 prostate cancer cells. Percentage of PC3 cell viability assessed by Alamar Blue™ assay (A), wound-healing migration (C) and Transwell® invasion (E) from exposure to soluble factors produced by M∅, M1 and M2 macrophage subtypes and treatment with vehicle or FSAS3. Representative images of PC3 cell growth (B), migration (D) and invasion (F). Data obtained from three independent experiments. p-values were determined using unpaired T-test. ****p<0.001, ***p<0.005,**p<0.01 and *p<0.05 compared to own PC3 control. Scale bar=100 μM.
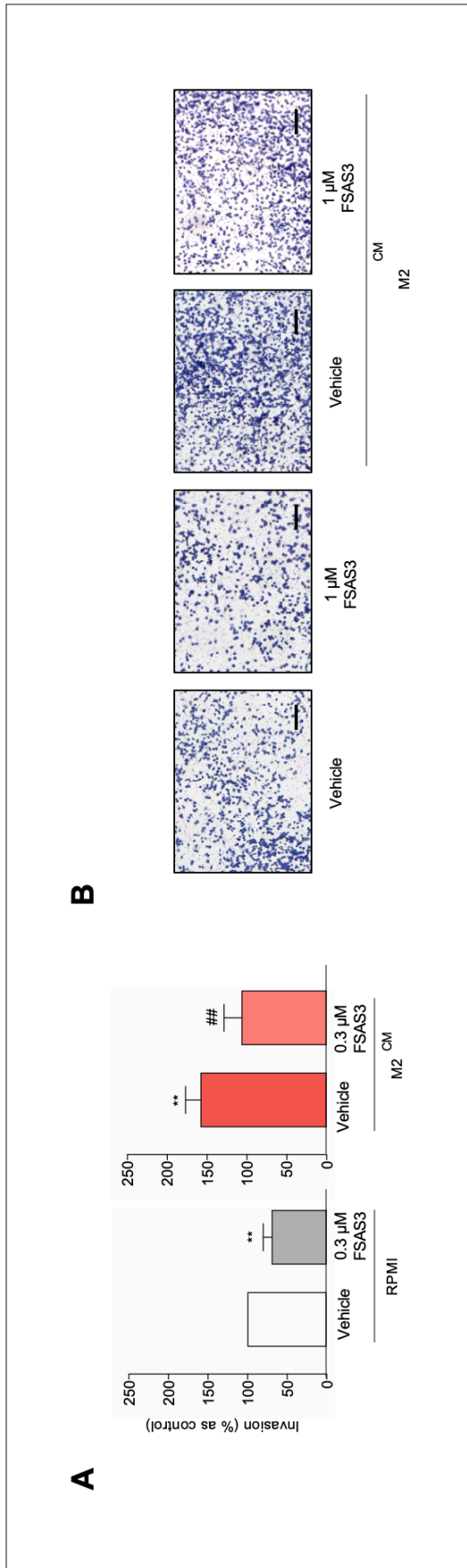
Figure 6.10.Pharmacological inhibition of TRAF/NFκB with the novel FSAS3 reduced invasion of murine RM1-BM prostate cancer cells induced by the pro-tumorigenic effects of M2 macrophages. (A) Percentage of RM1-BM cell invasion assessed by the Transwell® invasion assay from exposure to soluble factors produced by M2 macrophage subtype and treatment with vehicle or FSAS3. (B) Representative images of RM1-BM invasion. Data obtained from three independent experiments. p-values were determined using unpaired T-test for each graph. **p<0.01 compared to RM1-BM control, ##p<0.01 compared to M2-treated RM1-BM cells. Scale bar=100 µM.

6.4.6. The novel FSAS3 reduces cancer-specific NFκB activation by macrophage-derived factors *in vitro*

Mechanistic studies on the effects of the novel FSAS3 on NFκB activation were carried out in prostate cancer cells cultured in the presence and absence of soluble factors derived from pro-tumorigenic M2 macrophages. Briefly, human PC3 prostate cancer cells were pre-treated with FSAS3 for one hour and then exposed to M2-macrophage conditioned media (20%, v/v) for 6 hours. The timepoint used was selected based on mechanistic studies that showed that exposure of human PC3 prostate cancer cells to FSAS3 at this concentration had no effect on cell viability and phosphorylation of IκB-α induced by M2 macrophages was notably observed (**Supplementary Figure 13 and 14**, respectively).

As shown in **Figure 6.11**, exposure of human PC3 prostate cancer cells to conditioned medium of pro-tumorigenic M2 macrophages increased IκB-α phosphorylation and these effects were significantly inhibited by FSAS3 (3 μM), whereas treatment with the verified TRAF6 inhibitor 6877002 (3 μM) had no significant effect.
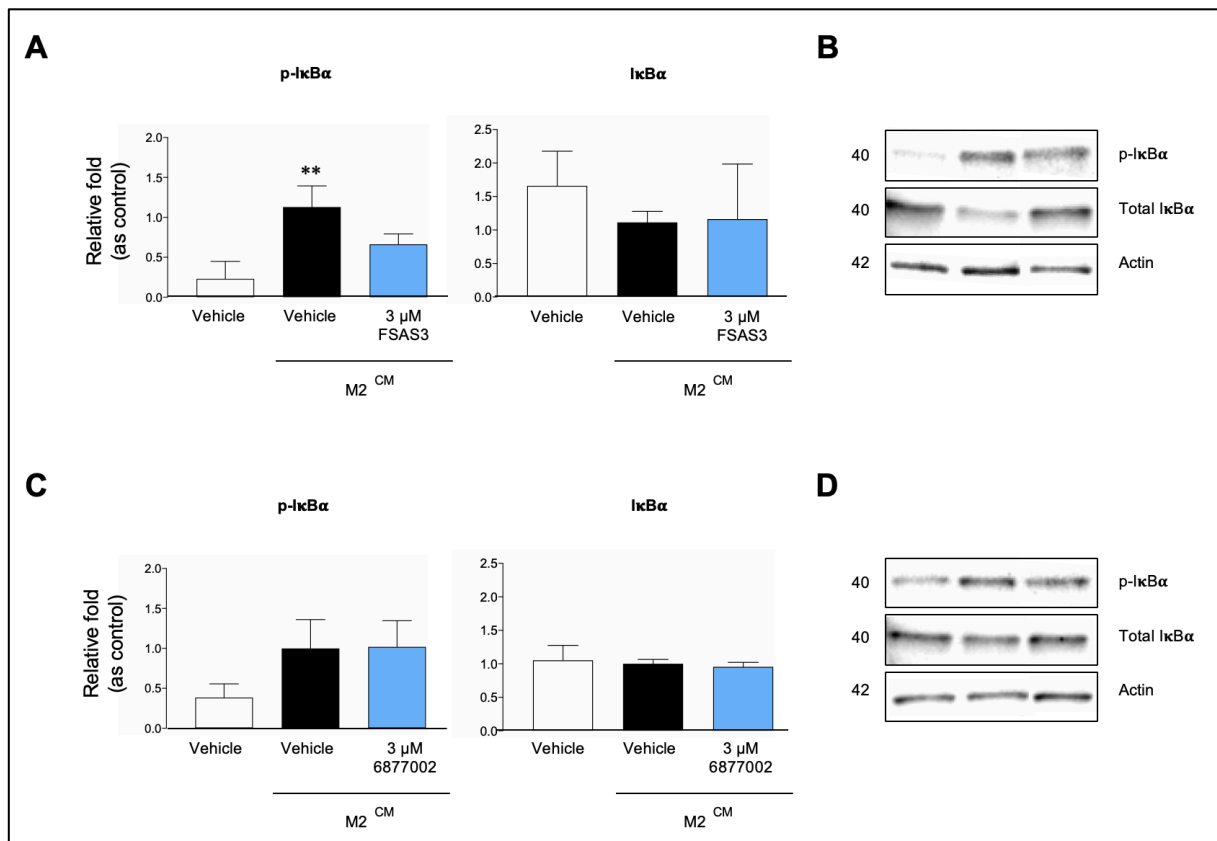
Figure 6.11. The novel FSAS3 reduced the phosphorylation of IκB-α induced by M2 macrophages in PC3 cells *in vitro*. Relative fold of phosphorylated-IκB-α/Actin and IκB-α/Actin expression of human PC3 prostate cancer cells exposed to vehicle, FSAS3 (A) or 6877002 (C) (3 μM) for 1 hour prior to stimulation with M2-conditioned media (20% v/v) for 6 hours. Representative Western Blot images of expression of p-IκB-α and IκB-α of PC3 cells exposed to vehicle, FSAS3 (B) or 6877002 (D). Data presented are mean ± standard deviation (n=3). p-values were obtained from ordinary ANOVA test followed by Tukey *post hoc* test. **p<0.01 compared to unstimulated PC3 cells.

6.4.7. The novel FSAS3 inhibits prostate cancer-related macrophage viability and differentiation into osteoclasts

A number of reports have shown that inflammatory cytokines secreted and surface markers expressed by prostate cancer cells affect macrophage polarisation and predominantly stimulate the differentiation of the pro-tumorigenic M2 subtype (Maolake *et al.*, 2017; Mazalova *et al.*, 2018). Since treatment with the verified TRAF6 inhibitor 6877002 was found to decrease monocyte recruitment (Seijkens *et al.*, 2018), the effects of the novel FSAS3 were studied on the viability and differentiation of monocyte/macrophage precursors into different macrophage subtypes and osteoclasts in the presence of derived factors from the human PC3 prostate cancer cells.

Initially, human monocyte-like cells THP-1 cells were differentiated into adherent macrophage-like cells and treated with the novel FSAS3 (**2.3.3. Macrophage polarisation influenced by treatments**). Macrophage polarisation and commitment into M1 and M2 subtypes were studied by assessing the expression of CD80 (M1 marker) and CD163 (M2 marker) with flow cytometry (**2.3.2. Macrophage phenotype identification by flow cytometry**). Briefly, the culture and detection methods for polarised M1 and M2 derived from THP-1 cultures were successfully optimised (**Supplementary Figure 4**).

As shown in **Figure 6.12**, FSAS3 significantly decreased the expression level of the M2 marker CD163 in cultures of THP-1 cells when compared to vehicle treated uncommitted macrophages. In contrast, FSAS3 treatment had no effect in the expression of M1 marker CD80; however, it is observed that THP-1 cells treated with this agent were more polarised to the anti-tumorigenic M1 phenotype compared to pro-tumorigenic M2.
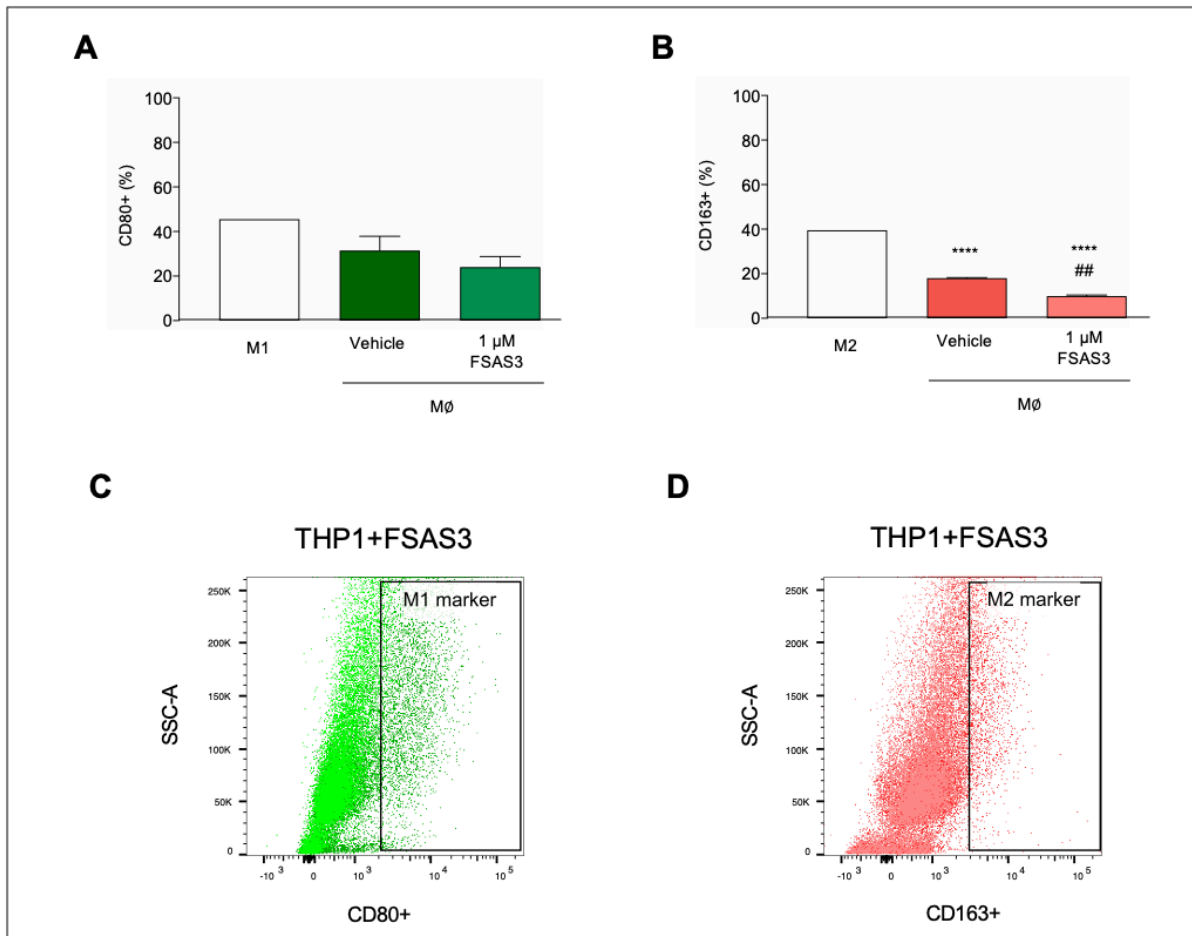
Figure 6.12. The novel FSAS3 supports M1 polarisation in monocyte-like THP-1 cells. Percentage of (A) CD80+ and (B) CD163+ expression in M1 or M2 macrophages, respectively, compared to uncommitted macrophages treated with FSAS3 or vehicle. Representative dot plots obtained by flow cytometry of (C) M1/CD80+ and (D) M2/CD163+ THP-1 cells treated with the novel FSAS3. Unstained cells are presented in light green/red and percentage of cells stained with their respective marker are gated and presented with dark green/red. Data obtained from three independent samples. p-values were obtained from one-way ANOVA test followed by Tukey *post hoc* test. ****p<0.001 compared to M1 or M2 control, ##p<0.01 compared to vehicle.

Next, human monocyte-like THP-1 and mouse macrophage-like RAW 264.7 cells were treated with the novel FSAS3 and exposed to conditioned media from human PC3 and murine RM1-BM prostate cancer cell lines. As observed in **Figure 6.13A and B**, conditioned media from PC3 significantly increased monocyte and macrophage cell viability and these effects were significantly reduced by treatment with FSAS3. In contrast, the effects of the soluble factors produced by the murine RM1-BM cell line were increased in murine RAW264.7 cells and exposure to FSAS3 had no effect in the viability of RM1-BM cells under these conditions (**Figure 6.13C and D**). Treatment with the novel FSAS3 had no effect in human monocyte-like THP-1 cells nor in the mouse macrophage-like RAW 264.7 cell line.
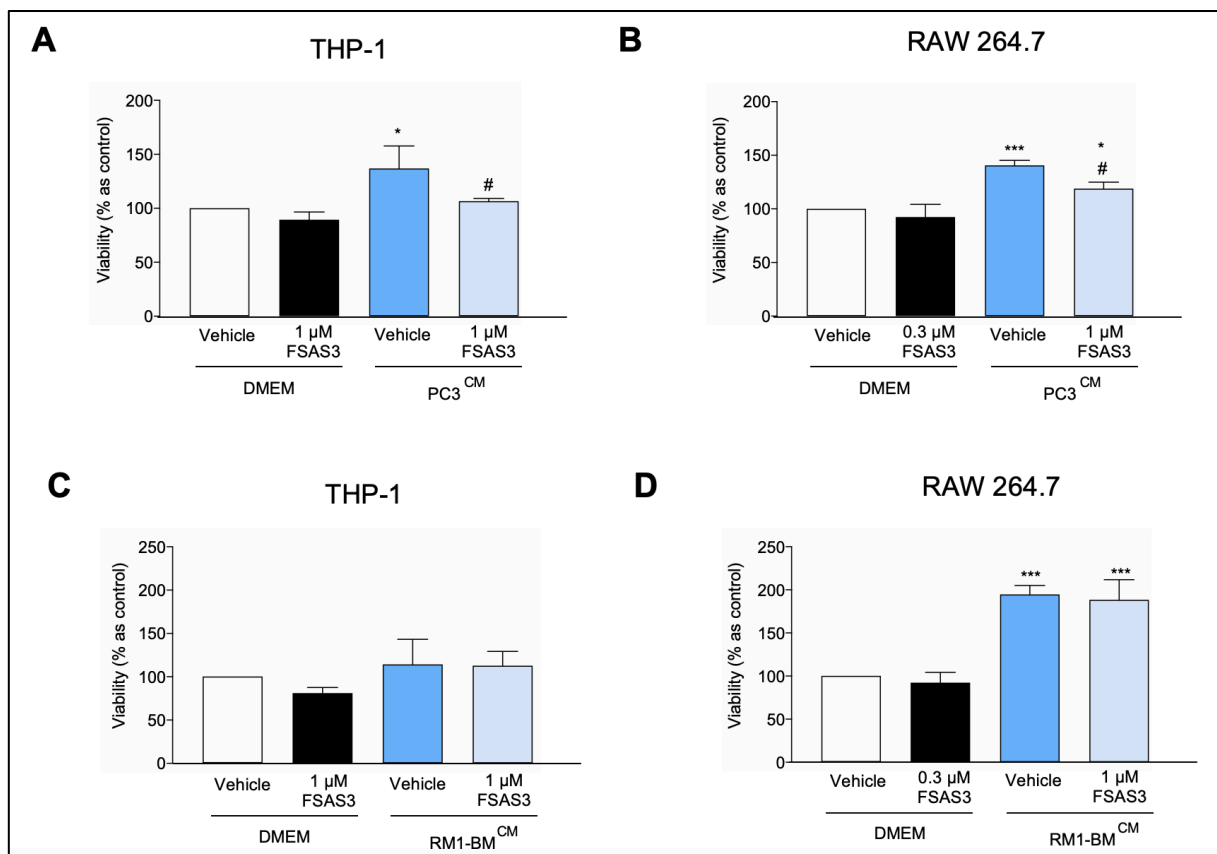
Figure 6.13. The effects of the novel FSAS3 on the viability of monocyte/macrophage cells in the presence of prostate cancer cell-conditioned medium. Human monocytic-like cells THP-1 and murine macrophage-like cells RAW 264.7 were treated with FSAS3 and exposed to conditioned media of human PC3 (A and B, respectively) and murine RM1-BM (C and D respectively) prostate cancer cell lines. p-values were obtained from ordinary ANOVA test followed by Tukey *post hoc* test. ***$p < 0.005$ and *$p < 0.05$ compared to control, #$p < 0.05$ compared to cultures stimulated with prostate cancer cells.

To study the effects of the novel FSAS3 on the ability of prostate cancer cells to influence macrophage differentiation in multi-nucleated osteoclasts, murine RAW264.7 cells were treated with the novel FSAS3 and then stimulated by RANKL in the presence of murine RM1-BM cells or conditioned media from human PC3 or RM1-BM. As shown in **Figure 6.14**, the murine RM1-BM prostate cancer cells (**Figure 6.14A**) and their conditioned medium (**Figure 6.14B**) enhanced RANKL-induced osteoclast formation and these effects were diminished by treatment with FSAS3 (0.1 µM). Similar anti-osteoclast effects by FSAS3 were observed in cultures exposed to conditioned media from human PC3 prostate cancer cells (**Figure 6.14C**) without affecting viability (**Supplementary Figure 17**).
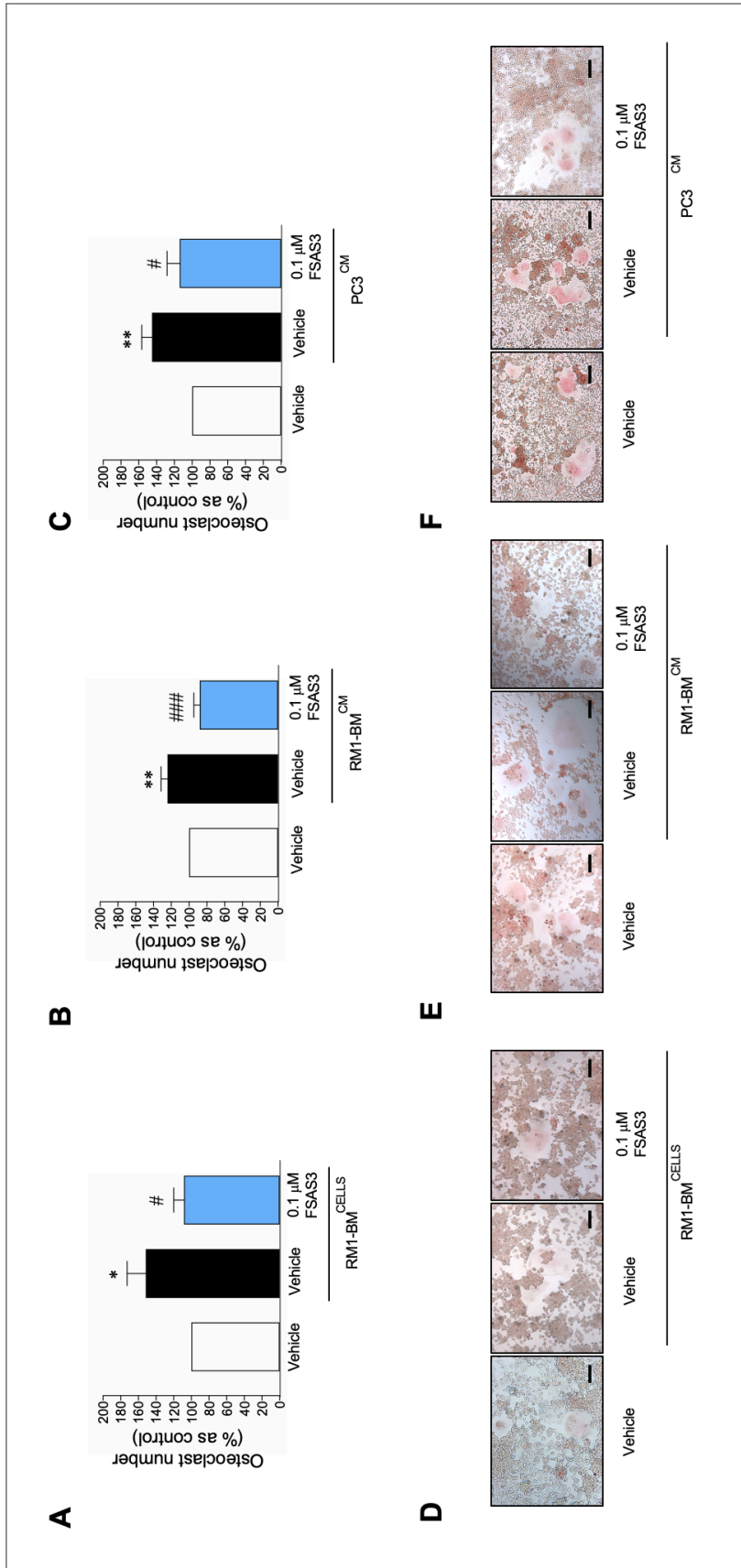
Figure 6.14. Pharmacological TRAF inhibition using FSAS3 reduced osteoclast formation in RAW 264.7 cultures exposed to RM1-BM cells or conditioned medium from RM1-BM and PC3 *in vitro*. Percentage of osteoclast formation in RAW264.7 cells stimulated with RANKL and in the presence and absence of murine RM1-BM cells (A) or conditioned medium from RM1-BM (B) or human PC3 (C) prostate cancer cells, treated with vehicle or FSAS3. Representative images of osteoclast formation using RM1-BM cells (D) or conditioned media (E) and soluble factors produced by PC3 cells (F). Data obtained from three independent experiments. p-values were obtained from ordinary ANOVA test followed by Tukey *post hoc* test. **p<0.01 and *p<0.05 compared to RANKL-stimulated RAW 264.7 cells, ###p<0.005 and #p<0.05 compared to cultures stimulated with prostate cancer cells. Scale bar=100 μM.

161

The effects of FSAS3 were also studied on the ability of different macrophage subtypes to influence RANKL-induced osteoclast formation. As shown in **Figure 6.15**, conditioned medium from MØ, M1 and M2 enhanced RANKL induced osteoclast formation; however, FSAS3 only prevented the increase in osteoclast number generated by conditioned medium from the tumour-promoting M2 macrophages.
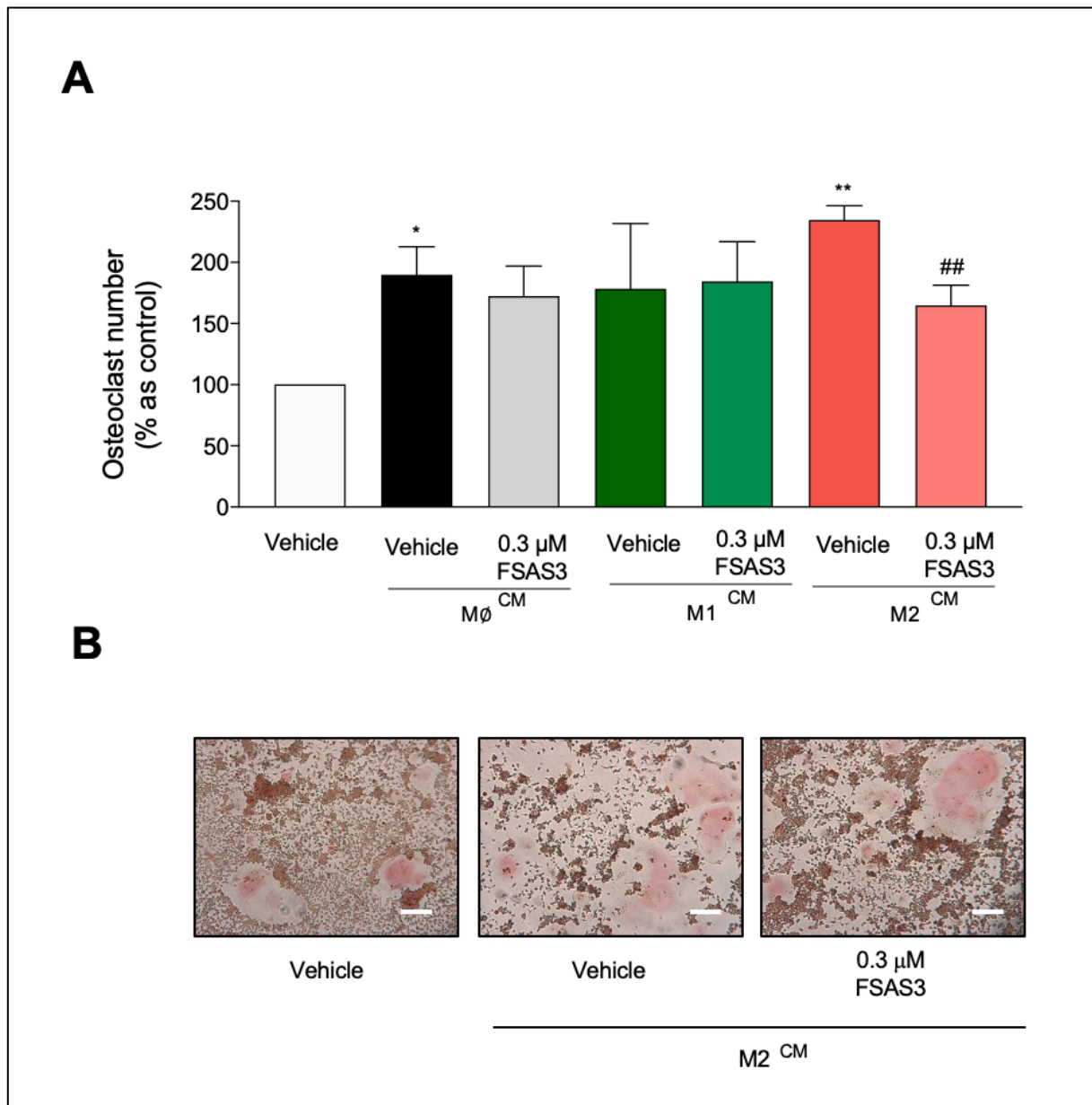
Figure 6.15. The novel FSAS3 reduced osteoclast formation in RAW 264.7 cultures exposed to conditioned medium from different macrophage subtypes *in vitro*. (A)Percentage of osteoclast formation in RAW264-7 cells stimulated with RANKL and exposed to conditioned media from MØ, M1 and M2 macrophage subtypes and treated with vehicle or FSAS3. (B) Representative images of osteoclast formation using MØ, M1 and M2 soluble factors. Data obtained from two independent experiments. p-values were obtained from ordinary ANOVA test followed by Tukey *post hoc* test. **$p < 0.01$ and *$p < 0.05$ compared to RANKL-stimulated RAW 264.7 cells, ##$p < 0.01$ compared to cultures stimulated with M2 macrophages. Scale bar=100 µM.

6.5.   Discussion

In this chapter, the effects of the novel class of NFκB inhibitors that are structurally related to the verified TRAF6 inhibitor 6877002 were validated on prostate cancer cell growth, motility and ability to influence macrophage lineage commitment *in vitro*. In view of the role of the TRAF6/NFκB pathway in prostate cancer and based on the results in **Chapter 5** showing that a verified TRAF6 inhibitor reduced prostate cancer growth, it was confirmed that the six FSAS congeners of 6877002 reduced the *in vitro* viability of a panel of human and mouse prostate cancer cell lines. FSAS3, followed by FSAS6, had the lowest IC_{50} values in all prostate cancer cells tested, showing a strong potency in the reduction of cell viability. The human prostate cancer cells C42-B4 and PC3 exhibited more sensitivity towards FSAS treatment, likely due to their high expression of TRAF6 (**Chapter 3**) and possibly their ability to metastasise and colonise bone, an environment rich in pro-inflammatory TRAF6-activating factors including RANKL and CD40L. In support to this hypothesis, it was observed that the osteotropic mouse RM1-BM cell line was highly susceptible to most compounds tested and in particular the novel FSAS3.

To investigate the involvement of NFκB activation in the effects of the novel FSAS3, a head-to-head comparison of the effects of FSAS3 and the verified TRAF6 inhibitor 6877002 on IκB-α phosphorylation was performed in murine macrophage-like RAW 264.7 cells and human PC3 prostate cancer cells using Western Blot analysis. These results confirmed that the novel FSAS3 reduced both RANKL- and TNF-α-induced IκB-α phosphorylation in RAW 264.7 and PC3 cells. In contrast, the verified 6877002 failed to affect RANKL-stimulated IκB-α phosphorylation in human PC3, which can be attributed to mutations in RANK in prostate cancer cells (Chen *et al.*, 2006). Interestingly, the novel FSAS3 significantly decreased the effects of both RANKL and TNF-α, suggesting less specificity to the TRAF6-RANK/CD40 binding site compared to the verified TRAF6 inhibitor 68770022 (A. Chatzigeorgiou *et al.*, 2014). Following this, the effects of the congener FSAS3 on the metastatic behaviour of PC3 cancer cells were studied. FSAS3 significantly reduced PC3 cell migration and invasion at

concentrations 10 times lower than the verified 6877002, which only showed a moderate decrease in the same metastatic capabilities.

To further investigate the selectivity of FSAS3 to TRAF6, the effect of FSAS3 on the viability of mock and TRAF6 knockdown PC3 cells was studied. This experiment provided a useful insight on the selective targeting of the novel FSAS3 inhibitor, showing that the PC3 cells with stable TRAF6 knockdown (70% reduction in TRAF6 expression, as reported in **Chapter 3**), were less sensitive but not resistant to treatment with the novel FSAS3 when compared to mock control. Whilst the results of this experiment indicate that FSAS3 exerts its anti-tumour – as well as anti-migratory and anti-osteoclastic – actions by a mechanism dependent at least in part on TRAF6, further work is required to elucidate the mechanism of binding and interaction of the novel FSAS3 with TRAF6 in the presence and absence of pro-inflammatory factors such as CD40L and RANKL and in both healthy and cancer cells.

Tumour-associated macrophages and their derived factors are major contributors to prostate carcinogenesis in the prostate and at metastatic sites such as bone (Soki *et al.*, 2015; Ylitalo *et al.*, 2017; Lo and Lynch, 2018). In this chapter, uncommitted Mø, anti-neoplastic M1 and pro-tumorigenic M2 macrophage subtypes, generated successfully from human monocyte-like THP-1 cells, showed that soluble factors produced by M1 cells significantly decreased migration and invasion. In contrast, derived factors from M2 macrophages significantly increased PC3 cell motility. These results are consistent with several previous reports (Lindholm *et al.*, 2010; Han *et al.*, 2019). Then, it was shown that tumour-promoting effects of M2 were significantly decreased in RM1-BM and PC3 cells treated with the novel FSAS3. The wound-healing migration assay *in vitro* would have been a useful input to further study the metastatic behaviour of the murine RM1-BM prostate cancer cell line; however, even though the wound-healing assay has been reported using RM1-BM (Moreira *et al.*, 2015), this study was limited by failure to generate a monolayer to perform the migration experiment (**Supplementary Figure 16**).

Next, it was observed that macrophages treated with the novel FSAS3 showed higher expression of the M1 marker CD80+, suggesting that FSAS3 influences early macrophage differentiation, thus skewing macrophage lineage commitment to an anti-tumorigenic subtype. FSAS3 also reduced the ability of PC3 prostate cancer cells to influence the viability of monocyte-like THP-1 and macrophage-like RAW 264.7 cells.

Osteoclast formation from macrophages relies on the TRAF6/RANK/RANKL pathway (Kobayashi *et al.*, 2001). The murine macrophage-like cell line RAW 264.7 was used as a model to study the effects of FSAS3 on RANKL-induced osteoclastogenesis in the absence of other cells such as osteoblasts, stromal or immune cells. As expected, pre-treatment of RAW264.7 cells with FSAS3 reduced the ability of RM1-BM cells and derived factors from RM1-BM and PC3 cells to support the formation of mature osteoclast formation in the presence of RANKL. Interestingly, after several attempts were made to generate osteoclasts in RAW264.2 cells in the presence of a panel of human prostate cancer cell lines, only murine RM1-BM cells were capable of supporting RANKL-induced osteoclast formation. This suggests that the human prostate cancer cell lines previously used produce the osteoclast inhibitor and RANKL decoy receptor OPG, as reported in previous studies (Holen *et al.*, 2002). Additionally, other findings have confirmed that anti-neoplastic M1 cells reduce osteoclastogenesis (Yamaguchi *et al.*, 2016); however, here it was shown that tumorigenic M2 macrophages increased osteoclastogenesis and these effects were decreased by treatment with the novel FSAS3. Thus, further experiments that test the effects of FSAS3 on the interactions between primary human Mø, M1 and M2 and prostate cancer cells *in vitro* are required.

Based on the aforementioned, the findings of this chapter identify the novel FSAS3 and future analogues as a class of anti-tumour, anti-migratory and antiresorptive agents which may be of value in the treatment of both skeletal and non-skeletal complications related to metastatic prostate cancer. However, further *in vivo* studies in mouse models of human and mouse prostate cancer are needed.

Chapter 7. General discussion

7.1.   Discussion

The pro-inflammatory TRAF6/NFκB signalling pathway is prominently implicated in prostate cancer (Gudey *et al.*, 2014; Sundar *et al.*, 2015; Aripaka *et al.*, 2019), and plays a critical role in osteoclastic bone loss (Lomaga *et al.*, 1999; Naito *et al.*, 1999). Previous studies have highlighted the contribution of constitutive canonical NFκB activation in prostate cancer progression (Garg *et al.*, 2012). Recent research conducted in our laboratory revealed that pharmacological inhibition of NFκB signalling decreased prostate cancer-related bone cell activity *in vitro* and osteolysis *ex vivo* (Marino *et al.*, 2019). TRAF proteins activate the NFκB signalling pathway and their expression is commonly altered in a variety of cancers (Zhu *et al.*, 2018). Among the seven TRAFs, TRAF6 is involved in prostate cancer progression (Sundar *et al.*, 2015; Hamidi *et al.*, 2017) and importantly supports the tumorigenic potential of prostate cancer cells (Yang *et al.*, 2009). In addition, TRAF6 has a unique binding interaction with receptors CD40 and RANK, two key regulators of bone and immune cell activity and differentiation (Gohda *et al.*, 2005). However, until now, TRAF6 manipulation during bone metastasis and osteolysis had not been investigated in murine models of prostate cancer. In this project, I present evidence from *in vitro* and *in vivo* studies showing that pharmacological inhibition and genetic knockdown of TRAF6 disrupts the ability of prostate cancer cells to grow, move and influence the differentiation of macrophages, osteoclasts and osteoblasts.

Several studies have shown that TRAF6 is highly expressed in prostate cancer tissues and is particularly elevated in bone metastatic prostate cancer patients (Liu *et al.*, 2015; S. Huang *et al.*, 2017; Aripaka *et al.*, 2019). Based on aforementioned reports, the expression of all TRAF proteins (TRAF1-7) was studied by comparing their expression in normal and cancerous prostate tissue. Bioinformatic analysis using publicly available databases confirmed that all seven TRAFs were genetically altered, either presenting deletions or amplifications. Furthermore, in patients with adenocarcinoma, most TRAFs were highly expressed, particularly TRAF2, and were linked to poor prognosis in prostate cancer. This confirmed

previous findings that correlated increased TRAF6 expression to poor prognosis in prostate cancer patients (Aripaka *et al.*, 2019).

Additionally, the association of the expression of TRAFs with contributors of prostate cancer progression was studied. AR, a key promoter of prostate cancer progression (Nabbi *et al.*, 2017), has been positively correlated with the NFκB transcriptional factor p65 in CPRC tissues (L. Zhang *et al.*, 2009). Interestingly, Huang and colleagues (2017) performed a study revealing that miR-141-3p inhibited NFκB activation via targeting TRAF5 and TRAF6 in prostate cancer cells (S. Huang *et al.*, 2017). This indicates that these proteins are strongly involved in AR and NFκB activation, and support prostate cancer progression. In the present study, it was confirmed that TRAF6 and TRAF3 were moderately correlated with AR expression at initial stages of prostate cancer. In the literature, there are several reports addressing the involvement of TRAF6 in prostate cancer (Yang *et al.*, 2009; Sundar *et al.*, 2015; Aripaka *et al.*, 2019); however, there is little evidence indicating TRAF3 as a contributor of prostate cancer progression (Zhu *et al.*, 2018). One plausible link between these TRAFs and AR is the modulatory action of TRAF6 in various signalling pathways (Bouraoui *et al.*, 2018), and evidence of TLR-induced recruitment of both TRAF3 and TRAF6 (Häcker *et al.*, 2006). Interestingly, in a cohort of metastatic androgen-insensitive prostate cancer patients, TRAF4 and TRAF7 were moderately correlated with AR; however, the correlation with TRAF6 was diminished, suggesting TRAF6 expression is not associated with AR at advanced and androgen-insensitive stages of prostate cancer. Moreover, TRAF6 participation in AR signalling has been reported by Lu and collaborators (2017), who showed that TRAF6 ubiquitination and degradation of a catalytic subunit that co-activates AR (EZH2) was promoted by the ubiquitin ligase of tumour suppressors S-phase kinase-associated protein 2 (SKP2) in prostate cancer (Lu *et al.*, 2017). In addition, elevated SKP2 expression was observed in prostate cancer patients (Cai *et al.*, 2020) and is correlated with loss of PTEN (Lu *et al.*, 2017), characteristic of prostate cancer progression.

Moreover, due to the role of tumour-infiltrating immune cells in cancer progression, the association between different immune cell populations and TRAFs expression was investigated. The expression of TRAF3, TRAF5 and TRAF6 was highly associated with major infiltration of most of the immune cell populations studied, including myeloid-derived neutrophils, macrophages and dendritic cells and lymphocytes (T cells and B cells). TRAF3 showed a homogenous infiltration of all immune cell populations and TRAF5 and TRAF6 shared a similar profile, with infiltration of myeloid-derived cells, unlike the opposite association with CD4+ and CD8+ (cytotoxic) T cells. The moderate association of CD4+ T cells with TRAF6 is attributed to the E3 ligase activity of TRAF6 on transcription factor FOXP3, allowing proper CD4+ T cell function (Valdman *et al.*, 2010; Ni *et al.*, 2019). Interestingly, TRAF6 expression was associated with the highest infiltration of cytotoxic T cells, which are a major proportion of tumour-infiltrating cells in prostate cancer (Sfanos *et al.*, 2009), and their high density has been associated with a higher risk of clinical prostate cancer progression (Petitprez *et al.*, 2019) and increased immunogenicity (Baxevanis, Fortis and Perez, 2019). Due to its relevant role in immune cell activation, TRAF6 is highly correlated with tumour-infiltrating immune cells overall and, in accordance with previous studies, TRAF6 deficiency reduces CD8+ T cells and increases CD4+ T cell infiltration in lymphoid organs (King *et al.*, 2006). Additionally, pharmacological inhibition with the small molecule TRAF6 inhibitor 6877002 decreased recruitment of monocytes to endothelial cells (Seijkens *et al.*, 2018).

Given the role of TRAF6 in various mechanisms that support the development of prostate cancer progression, TRAF6 interactions and associations with other TRAF proteins were studied. This analysis showed a strong connection between TRAF6 and all other TRAFs, except TRAF7, demonstrating its robust function in influencing other TRAFs and, in consequence, several biological processes. This is consistent with the literature, where several studies have linked TRAF6 recruitment with other TRAFs (Yoshida *et al.*, 2005; Häcker *et al.*, 2006; Xiao *et al.*, 2012). Furthermore, modifications in TRAF protein expression at initial and metastatic stages of prostate cancer were addressed. Amplifications in all TRAFs were the

notably observed in metastatic prostate cancer, in accordance with Aripaka and colleagues (2019). Specifically, TRAF6 had an amplified expression in metastatic prostate cancer patients compared to the primary tumour stage (Ahmed *et al.*, 2013; Wei, Ruan, *et al.*, 2017). Taken together, these findings led us to confirm TRAF6 as a promising target for the treatment of prostate cancer bone metastasis. In addition, we observed that several upstream and downstream components of the TRAF6/NFκB were amplified in metastasis, particularly the ligands CD40L and TNF-α, the receptors of TGFβ and IGF-1 and notably the transcriptional factor Akt, consistent with previous findings (Yang *et al.*, 2009; Shi, Liu and Xu, 2019).

Next, Western Blot analysis was used to further examine the expression levels of TRAF6 in a panel of human and mouse prostate cancer cell lines with different metastatic abilities. TRAF6 had the highest expression in the highly metastatic PC3 human prostate cancer cell line, known to readily metastasise to bone in nude mice (Angelucci *et al.*, 2006). This confirmed the role of TRAF6 in the advanced stages of prostate cancer. Studying the expression of CD40 and RANK in prostate cancer cells further corroborated these findings and showed that TRAF6-activating receptors are highly expressed in PC3 cells and more notably in the human androgen-insensitive prostate cancer cell line C42-B4. Even though the C42-B4 cell line represented a promising model for our study, the aims of the project were more inclined on addressing an advanced stage of prostate cancer involving cancer cell lines with androgen-independent and osteolytic characteristics. Due to this, DU145 and PC3 were selected to generate TRAF6 knockdown cell lines, based on previous reports in the literature (Cunningham and You, 2015). Interestingly, TRAF6 expression was significantly decreased in the anti-tumorigenic M1 when compared to uncommitted MØ and the tumour-promoting M2 macrophages, further validating the role of TRAF6 in the prostate cancer microenvironment.

Recent *in vitro* studies showed that knockdown of TRAF2 and TRAF4 reduced the metastatic abilities of prostate cancer cells (Wei, Liang, *et al.*, 2017; Singh *et al.*, 2018) and TRAF6 knockdown reduced the tumorigenic potential of prostate cancer cells *in vivo* (Yang *et al.*, 2009). Thus, stable TRAF6 knockdown cell lines were generated using the moderately

metastatic DU145 and the highly metastatic PC3 prostate cancer cells. The successful knockdown of TRAF6 with three different constructs in both cell lines was confirmed by Western Blot and two colonies, with the lowest TRAF6 expression were selected for the following experiments. In addition, the effects of the TRAF6 knockdown cells on NFκB activation were studied, which confirmed that TRAF6 knockdown reduced the accumulation of IκB-α and expression of the transcriptional factor p65. This is in accordance with previous studies investigating TRAF6 silencing in multiple myeloma cells (H. Huang *et al.*, 2017).

Next, the metastatic behaviour of TRAF6 knockdown in DU145 and PC3 cancer cell lines was investigated by assessing cell viability and their ability to invade and migrate. Knockdown of TRAF6 significantly reduced the metastatic behaviour of these prostate cancer cells, in particular of the metastatic PC3 cell line, which expresses higher levels of TRAF6. TRAF6 knockdown in these cells reduced their ability to support RANKL-induced osteoclast formation. In cultures of osteoblasts, conditioned media from prostate cancer cells increased osteoblast differentiation and bone nodule formation, and these effects were significantly inhibited in osteoblasts exposed to conditioned media from prostate cancer cells deficient in TRAF6. Interestingly, TRAF6 knockdown failed to decrease osteoblastic lesions generated by DU145 prostate cancer cells. This can be attributed to previous reports mentioning that DU145 cells produce factors that upregulate osteoblast proliferation *in vitro* and have suggested that these cells generate osteoblastic lesions (Mori *et al.*, 2007; Alsulaiman, Bais and Trackman, 2016). To gain additional insights into the role of TRAF6 in prostate cancer and osteoblast–osteoclast interactions, future studies should investigate the prostate cancer-derived factors present in the conditioned medium used, for example the use of a cytokine array.

A previous study by Yang and colleagues (2009) showed that subcutaneous injection of PC3-TRAF6 knockdown cells reduced tumour growth in mice compared to PC3 transduced with mock (Yang *et al.*, 2009). Here, *in vivo* studies using the intratibial mouse model showed that TRAF6 knockdown in human PC3 had no effect on bone volume in mice. Together, these *in vivo* studies led us to conclude that cancer-specific inhibition reduces the growth of human

PC3 cells but has no effect on their ability to cause bone loss after intratibial local injection. To confirm this, further detailed histological analysis is required.

TRAF6 is a potent activator of NFκB (Scudiero *et al.*, 2012) and as such, requires strong inhibition to reduce inflammatory behaviour in tumour microenvironment. The small-molecule inhibitor 6877002 was initially synthesized with the purpose of targeting CD40-TRAF6 interactions to block inflammatory pathways. Furthermore, treatment with the verified TRAF6 inhibitor 6877002 improved survival in a systemic inflammatory *in vivo* model (Zarzycka *et al.*, 2015). Based on the aforementioned, the effects of pharmacological TRAF6 inhibition in various aspects of prostate cancer were tested using 6877002. *In vitro*, treatment with the verified 6877002 compound showed a significant reduction in human DU145 and, particularly, PC3 prostate cancer cell viability in a dose-response manner. Furthermore, this treatment decreased the metastatic abilities of human DU145 and, particularly, PC3 prostate cancer cells. As observed with TRAF6 knockdown cells, the anti-tumour and anti-metastatic capabilities of this compound correlates with higher expression of TRAF6 in PC3. Consistent with the crucial role of RANK-TRAF6 interaction in osteoclastogenesis (Gohda *et al.*, 2005), 6877002 significantly reduced the *in vitro* formation of mature osteoclasts in the presence and absence of DU145 and PC3 prostate cancer cells in RANKL-stimulated macrophage-like RAW 264.7 cultures*.*

Moreover, the effects of TRAF6 inhibition on osteoblast viability, differentiation and maturation were studied with the osteoblast-like cell line Saos-2. This cell line was selected due to expressing higher levels of TRAF6 as shown in online resources (**Supplementary Figure 18**), and due to its previously reported use to study the ability of prostate cancer cells to influence bone nodule formation (Yuen *et al.*, 2010). As expected, pharmacological inhibition of TRAF6 by 6877002 in osteoblasts in the presence of soluble factors from DU145 and PC3 prostate cancer cells had a similar outcome when exposed to conditioned media from TRAF6 knockdown prostate cancer cells. Exposure to DU145 conditioned media followed by treatment with 6877002 increased bone nodule formation and decreased osteoblast viability, in contrast

with Saos-2 treated with 6877002 and exposed to soluble factors derived from PC3. Hence, this showed the opposite effect. The moderate effects observed in osteoblast studies can be attributed to the osteolytic nature of these prostate cancer cell lines (Quiroz-Munoz *et al.*, 2019) and, as previous studies have determined, NFκB activation in prostate cancer cells contributes to osteoclastogenesis more notoriously compared to the effects observed in osteoblasts (R. Jin *et al.*, 2015).

Unexpectedly, animal studies examining the effects of 6877002 on bone volume in male immunocompromised mice injected intratibially with PC3 cancer cells showed no effect on bone volume when compared to treatment with vehicle. Even though the intratibial model is a convenient alternative to study tumour-bone cell interaction, there were various limitations encountered with this approach. Among the advantages of this model are the reproducibility, production of uniform bone metastatic tumours (Park *et al.*, 2010) and the validation of previous reports confirming the generation of osteolytic lesions by PC3 cells; however, this model is restricted to only investigate late stages of the disease, being unable to fully explore the dissemination process. In addition, intratibial injection may generate damage to the tibia and due to this, negative controls subjected to injection with PBS in the healthy tibia of the same animal should be compared with positive controls to avoid bias from potential injury caused by injection. Moreover, the age of mice was another key factor to consider. Even though reports have shown that tumours grow faster in young mice (Oh *et al.*, 2018), it has been determined that intratibial injection should be performed in 6-12 weeks old mice (Park *et al.*, 2010) and that the use of old mice (>12 weeks) is suggested for generating an equivalent model to prostate cancer in humans (Jackson *et al.*, 2017). Additionally, regarding the use of the compound, recently published data from our lab group exploring the use of 6877002 in breast cancer osteolysis *in vivo* showed that treatment with 6877002 alone had no effect on osteolysis in immunocompetent mice after intracardiac injection of mouse 4T1 breast cancer cells (Bishop *et al.*, 2020). 6877002 alone reduced overt metastasis in this model but it only protected against osteolysis when given in combination with the chemotherapeutic agent Docetaxel. In

addition, another limitation of this agent was its poor solubility in PBS and water that restricted us from using high doses in both human PC3 and mouse 4T1 *in vivo* experiments. Given the crucial role of the TRAF6/NFκB signalling pathway in bone and immune cell function, future studies should test the effects of 6877002 in mouse models of prostate cancer, such as the RM1-BM model.

These results led us to design the novel FSAS family of compounds in collaboration with Professor Sparatore laboratory group at the University of Milan (Italy). We synthesised a number of congeners of the verified TRAF6 inhibitor 6877002 (Zarzycka *et al.*, 2015), and analogues of the NFκB inhibitor ABD56 (Idris *et al.*, 2008). In **Chapter 6**, the effects of the novel FSAS3 were tested on the ability of prostate cancer cells to grow, move and influence macrophage lineage commitment and differentiation, particularly into TAMs and multinucleated osteoclasts. The novel FSAS3 showed high potency in reducing prostate cancer cell viability and, as a result, was chosen for following experiments. Mechanistic studies revealed that FSAS3 inhibited RANKL-induced phosphorylation of IκB-α in prostate cancer cells and macrophages and, interestingly, in prostate cancer cells stimulated by TNF-α. In contrast, the verified 6877002 had no effect on TNF-α-phosphorylation of IκB-α and only caused a significant reduction in phosphorylation of IκB-α in RANKL-stimulated prostate cancer cells. Previous studies have confirmed that 6877002 inhibits the CD40-TRAF6 interaction (Zarzycka *et al.*, 2015) and we have recently showed that it inhibited RANKL-induced TRAF6-RANK binding, phosphorylation of IκB-α and NFκB activation in macrophages (Bishop *et al.*, 2020). In **Chapter 6**, it was shown that 6877002 inhibited RANKL-induced NFκB activation; however, the novel FSAS3 inhibited NFκB activation in cultures stimulated with both RANKL and TNF-α. Taken together, it was concluded that FSAS3 – unlike 6877002 – disrupts the activation of TRAF6 and other TRAF proteins, specifically TRAF2 which acts downstream of TNF-α (**Figure 7.1**).
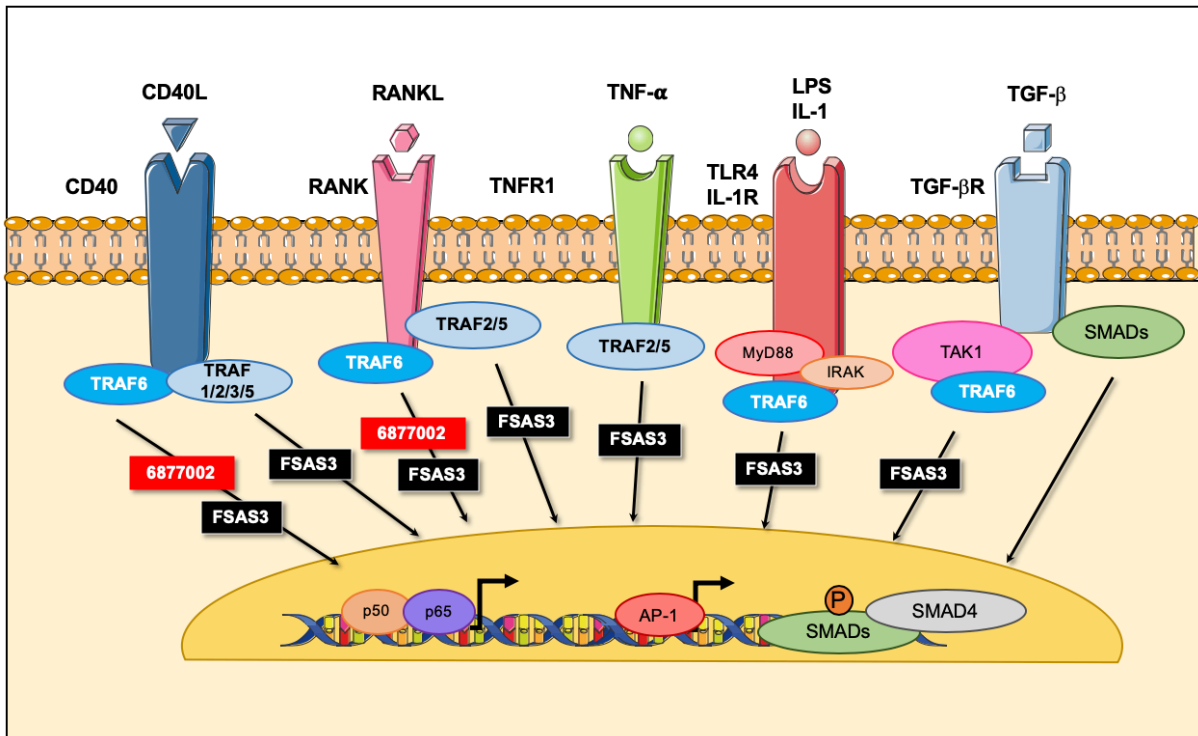
Figure 7.1. Hypothetical schematic model of mechanism(s) of action of the verified TRAF6 inhibitor 6877002 and the novel FSAS3 on TRAF-mediated NFκB activation. Refer to text for more details.

To gain a better insight into the involvement of TRAF6 action in the presence of the novel FSAS3, PC3-TRAF6 knockdown cells were treated with FSAS3 and cell viability was assessed. These experiments showed that TRAF6 knockdown PC3 cells were significantly less sensitive to growth inhibition by FSAS3 when compared to control cells. Whilst this experiment suggests that FSAS3 exerts its action via a TRAF6-mediated action, future studies should consider testing the effect of TRAF6 on cells over-expressing TRAF6. In addition, the fact that FSAS3 was significantly more active than 6877002 in reducing the growth of various prostate cancer cells indicates an involvement in multiple signalling pathways. Thus, additional mechanistic studies examining the effects of FSAS3 and its derivatives on multiple pathways activated by various stimuli of TRAF-mediated signalling (**Figure 7.1**) should be performed. In the future, an accurate approach to elucidate the mechanism of action and to confirm the binding interaction of FSAS3 with TRAF proteins is needed. One possibility is computer modelling approaches that examine the binding of FSAS3 to TRAF6 and TRAF2 (A. Chatzigeorgiou *et al.*, 2014; Zarzycka *et al.*, 2015). Alternatively, immunoprecipitation could be used to examine the effects of FSAS3 on the binding of TRAF6/RANK and TRAF2/TNFR in osteoclasts, TAMs and prostate cancer cells, as previously described (Bishop *et al.*, 2020).

Immune cells are major drivers of inflammation, which in consequence contributes to prostate cancer progression (Zhang *et al.*, 2019). Encouraged by the findings that FSAS3 inhibited NFκB activation and reduced prostate cancer growth acting – in part – on TRAF6, the effects of FSAS3 on the metastatic behaviour of prostate cancer cells influenced by different macrophage subtypes were assessed. It was shown that the novel FSAS3 significantly reduced prostate cancer cell viability, migration and invasion in the presence and absence of derived factors from pro-tumorigenic M2 macrophages with a 10-fold-lower concentration than the TRAF6 inhibitor 6877002. In addition, FSAS3 treatment reduced phosphorylation of IκB-α induced by M2 conditioned media in prostate cancer cells. To further approach the effects of TRAF6 inhibition on prostate cancer progression to metastasis, future studies should examine the effects of FSAS3 and 6877002 on EMT markers at mRNA and protein levels in whole-cell

lysates of prostate cancer cells, osteoclasts and macrophages as previously described (Fontana *et al.*, 2019).

Moreover, since macrophages produce a variety of pro-inflammatory factors, the reduction in M2-induced phosphorylation of IκB-α indicates that FSAS3 targets and inhibits multiple pathways that activate NFκB in cancer and immune cells. Prostate cancer cells on the other hand influence their environment by producing factors that alters the cytokine production of surrounding immune and bone cells to their benefit (Mazalova *et al.*, 2018). It was confirmed that soluble factors derived from PC3 prostate cancer cells increased cell viability of monocytic-like THP-1 and macrophage-like RAW 264.7 and these effects were significantly inhibited by treatment with FSAS3. Furthermore, osteoclast formation potentiated by RM1-BM cells or conditioned media from human PC3 or murine RM1-BM in RANKL-stimulated osteoclast precursors was significantly decreased by treatment with FSAS3. Interestingly, in studies developed by our lab group, we found a significant enhancement in the number of multinucleated osteoclasts in mouse osteoclast precursors stimulated with RANKL. However, this was only achieved with prostate cancer cells derived from the murine RM1-BM cell line and rat Mat-Ly-Lu cells (Marino *et al.*, 2019). These discrepancies can be attributed to cross-species effects when using human cells lines, such as PC3, with murine macrophage-like RAW 264.7 cells and/or due to the production of various osteoclast inhibitory factors such as the decoy OPG by prostate cancer cells.

The influence of different macrophage subtypes on RANKL-induced osteoclast formation was also studied. I showed that soluble factors produced by the pro-tumorigenic M2 phenotype caused a significant increase in osteoclast number and this effect was reduced by treatment with the novel FSAS3. To gain a better understanding of the effects of FSAS3 on macrophage polarisation, M1 and M2 markers were assessed in macrophages treated with FSAS3. These experiments were inspired by previous studies revealing that CD40-TRAF6 inhibition caused macrophages to produce anti-inflammatory cytokines, leading to the pro-tumorigenic M2 phenotype (Lutgens *et al.*, 2010). Additionally, it has been reported that TRAF2-deficient

macrophages produce high levels of pro-inflammatory cytokines, similar to the anti-tumorigenic M1 phenotype (J. Jin *et al.*, 2015). In the present study, macrophages exposed to FSAS3 were more inclined to become anti-tumorigenic, once again indicating that FSAS3 potentially targets other TRAFs.

7.2.   Alternative approaches and future perspectives

Regarding the potential improvement of the techniques used to study the metastatic behaviour of cells, even though Alamar Blue™ is an accurate and sensitive technique that allowed the study of cell viability, cell death studies are recommended. To determine the effects of TRAF6 inhibition on apoptosis, performing the TUNEL assay to detect DNA fragmentation by flow cytometry or studying the expression levels of caspase-3 is suggested to supplement the data obtained. In addition, time-lapse video is a reliable technique for the assessment of cell migration and it is recommended to increase the timepoint of exposure until wound closure is more evident to potentially observe a more marked effect in treated cells. Furthermore, to gain a better understanding of the effects of TRAF6 inhibition in the metastatic process, it is recommended to study the expression of EMT markers, a crucial step in cancer progression, and the production of soluble factors of TRAF6 knockdown cells or treated with 6877002/FSAS3 compared to mock/untreated prostate cancer cells.

About the studies involving monocytes-macrophages, the macrophage-like cells RAW 264.7 are commonly reported in the literature as osteoclast precursors and the monocytic THP-1 cells are regularly used for the study of macrophages; however, the use of human macrophages cultures obtained from peripheral blood monocytes from healthy patients would be more optimal for the study of osteoclastogenesis and macrophage polarisation, as reports indicate that human monocytes are more responsive to stimuli and have a more evident expression of markers related to macrophage polarisation compared to the mentioned cell lines.

Furthermore, in support of the signalling experiments, it would be useful to compare phosphorylation of IκB-α in cells treated with compounds 6877002/FSAS3 against verified

NFκB inhibitors such as parthenolide or bortezomib to determine the efficiency of NFκB inhibition. Importantly, it is highly recommended to define which TRAF proteins are targeted by FSAS3. To support the hypothetical interaction of FSAS3 with TRAF2 and/or TRAF6, co-immunoprecipitation of RANK-TRAF2/6 and CD40-TRAF2/6 should be performed to confirm the interaction with these receptors and these proteins of interest.

Moreover, alternative approaches were considered with the purpose of expanding the obtention of supporting data for the aims of the project. Given the restrictions encountered in the described intratibial model, future *in vivo* studies should address the metastatic dissemination process of prostate cancer cells by intracardiac injection of the luciferase-transfected and bone-seeking RM1-BM murine cell line in immunocompetent mice with the purpose of studying the effects of treatment with the TRAF inhibitor FSAS3 in tumour growth, immune cell populations involved at the tumour site and generation of osteolytic/osteoblastic lesions, both assessed by histology, and analysing modifications in the bone architecture by micro-CT. Based on recent findings (Bishop *et al.*, 2020), it is suggested to use a combinational approach with FSAS3 and a chemotherapeutic agent or immunomodulatory drug with the aim of reducing resistance, improve survival and decrease tumour growth and metastasis. Due to this, *in vitro* studies should be performed with a panel of standard agents used for prostate cancer treatment along with FSAS3, aiming to find the optimal combination for the *in vivo* experiment.

Collectively, the findings of the project suggest that targeting the TRAF/NFκB pathway shows promise for the treatment of advanced prostate cancer. However, further studies testing the effects of TRAF6/2 inhibitors, such as the novel FSAS3 or its novel derivatives, are needed. This is of particular importance if the compounds are used alone or in combination with an FDA chemotherapeutic agent to examine prostate cancer bone metastasis and local osteolysis in immunocompetent mouse models of prostate cancer.

References

Aarts, S. A. B. M. *et al.* (2017) 'Inhibition of CD40-TRAF6 interactions by the small molecule inhibitor 6877002 reduces neuroinflammation', *Journal of Neuroinflammation*. Journal of Neuroinflammation, 14(105), pp. 1–14. doi: 10.1186/s12974-017-0875-9.

Aggarwal, B. B. (2004) 'Nuclear factor-κB:The enemy within', *Cancer Cell*, 6.

Ahmed, F. *et al.* (2013) 'Tumor necrosis factor receptor associated factor-4: An adapter protein overexpressed in metastatic prostate cancer is regulated by microRNA-29a', *Oncology Reports*, 30(6), pp. 2963–2968. doi: 10.3892/or.2013.2789.

Aielli, F., Ponzetti, M. and Rucci, N. (2019) 'Molecular Sciences Bone Metastasis Pain, from the Bench to the Bedside', *International Journal of Molecular Sciences*, 20(280). doi: 10.3390/ijms20020280.

Allen, I. C. (2014) 'Non-inflammasome forming NLRs in inflammation and tumorigenesis', *Frontiers in Immunology*, 5(April), pp. 27–29. doi: 10.3389/fimmu.2014.00169.

Alsulaiman, M., Bais, M. V and Trackman, P. C. (2016) 'Lysyl oxidase propeptide stimulates osteoblast and osteoclast differentiation and enhances PC3 and DU145 prostate cancer cell effects on bone in vivo', pp. 17–31. doi: 10.1007/s12079-015-0311-9.

American Cancer Society (2018) 'Cancer Facts & Figures 2018', *Atlanta: American Cancer Society*.

Angelucci, A. *et al.* (2006) 'Suppression of EGF-R signaling reduces the incidence of prostate cancer metastasis in nude mice', *Endocrine-Related Cancer*, 13(1), pp. 197–210. doi: 10.1677/erc.1.01100.

Aripaka, K. *et al.* (2019) 'TRAF6 function as a novel co-regulator of Wnt3a target genes in prostate cancer', *EBioMedicine*, 45, pp. 192–207. doi: 10.1016/j.ebiom.2019.06.046.

Armstrong, A. P. *et al.* (2008) 'RANKL Acts Directly on RANK-Expressing Prostate tumor Cells and Mediates Migration and Expression of tumor Metastasis Genes', *The Prostate*, 68, pp. 92–104. doi: 10.1002/pros.

Arora, K. and Barbieri, C. E. (2018) 'Molecular Subtypes of Prostate Cancer', *Curr Oncol Rep*, 20(58). doi: 10.1007/s11912-018-0707-9.

Attard, G. *et al.* (2016) 'Prostate cancer', *The Lancet*, 387(10013), pp. 70–82. doi: 10.1016/S0140-6736(14)61947-4.

Barfeld, S. J. *et al.* (2012) 'Meta-analysis of prostate cancer gene expression data identifies a novel discriminatory signature enriched for glycosylating enzymes'. doi: 10.1186/s12920-014-0074-9.

Baskar, Rajamanickam *et al.* (2012) 'Cancer and Radiation Therapy: Current Advances and Future Directions', *Int. J. Med. Sci*, 9(3), pp. 193–199. doi: 10.7150/ijms.3635.

Baxevanis, C. N., Fortis, S. P. and Perez, S. A. (2019) 'Prostate cancer: any room left for immunotherapies?', *Immunotherapy*, 11(2), pp. 69–74. doi: 10.2217/imt-2018-0159.

Beer, T. M. *et al.* (2017) 'Randomized, double-blind, phase III trial of ipilimumab versus placebo in asymptomatic or minimally symptomatic patients with metastatic chemotherapy-naive castration-resistant prostate cancer', *Journal of Clinical Oncology*, 35(1), pp. 40–47. doi: 10.1200/JCO.2016.69.1584.

Van Den Berg, S. M. *et al.* (2015) 'Blocking CD40-TRAF6 interactions by small-molecule inhibitor 6860766 ameliorates the complications of diet-induced obesity in mice', *International Journal of Obesity*, 39, pp. 782–790. doi: 10.1038/ijo.2014.198.

Berish, R. B. *et al.* (2018) 'Translational models of prostate cancer bone metastasis', *NaTure reviewS | UROlOgy*, 15, p. 403. doi: 10.1038/s41585-018-0020-2.

Bishop, R. T. *et al.* (2020) 'Combined administration of a small-molecule inhibitor of TRAF6 and Docetaxel reduces breast cancer skeletal metastasis and osteolysis', *Cancer Letters*.

De Bono, J. S. *et al.* (2011) 'Abiraterone and Increased Survival in Metastatic Prostate Cancer', *Cancer Research*, pp. 215–224. doi: 10.1056/NEJMoa1603827.

De Bono, J. S. *et al.* (2019) 'Randomized phase II study evaluating AKT blockade with ipatasertib, in combination with abiraterone, in patients with metastatic prostate cancer with and without PTEN loss', *Clinical Cancer Research*, 25(3), pp. 928–936. doi: 10.1158/1078-0432.CCR-18-0981.

Bosch, L. *et al.* (2019) 'Small molecule-mediated inhibition of CD40-TRAF6 reduces adverse cardiac remodelling in pressure overload induced heart failure', *International Journal of Cardiology*. doi: 10.1016/j.ijcard.2018.12.076.

Bouraoui, Y. *et al.* (2018) 'Immune profiling of human prostate epithelial cells determined by expression of p38/TRAF-6/ERK MAP kinases pathways', *The Kaohsiung Journal of Medical Sciences*. Elsevier (Singapore) Pte Ltd, 34(3), pp. 125–133. doi: 10.1016/j.kjms.2017.10.002.

Bray, F. *et al.* (2018) 'Global Cancer Statistics 2018: GLOBOCAN Estimates of Incidence and Mortality Worldwide for 36 Cancers in 185 Countries', *Ca Cancer J Clin*, 68, pp. 394–424. doi: 10.3322/caac.21492.

Brown, J. M. *et al.* (2001) 'Osteoprotegerin and rank ligand expression in prostate cancer.', *Urology*, 57(4), pp. 611–6. Available at: http://www.ncbi.nlm.nih.gov/pubmed/11306358.

Buenrostro, D. *et al.* (2016) 'The Bone Microenvironment: a Fertile Soil for Tumor Growth', *Curr. Osteporos Rep.*, 14(4), pp. 151–158. doi: 10.1007/s11914-016-0315-2.The.

Cai, Z. *et al.* (2020) 'The Skp2 Pathway: A Critical Target for Cancer Therapy'. doi: 10.1016/j.semcancer.2020.01.013.

Campbell, G. M., Ominsky, M. S. and Boyd, S. K. (2011) 'Bone quality is partially recovered after the discontinuation of RANKL administration in rats by increased bone mass on existing trabeculae: An in vivo micro-CT study', *Osteoporosis International*, 22(3), pp. 931–942. doi: 10.1007/s00198-010-1283-5.

Campbell, G. M. and Sophocleous, A. (2014) 'Quantitative analysis of bone and soft tissue by micro-computed tomography: applications to ex vivo and in vivo studies', *BoneKEy Reports*. Nature Publishing Group, 3(AUGUST), pp. 1–12. doi: 10.1038/bonekey.2014.59.

Carrasco Gonzalez, D. G. C. (2017) *The role of TRAF6/NF-Kappa B in Prostate Cancer Metastasis*. University of Sheffield.

Center, M. M. *et al.* (2012) 'International variation in prostate cancer incidence and mortality rates', *European Urology*, 61(6), pp. 1079–1092. doi: 10.1016/j.eururo.2012.02.054.

Cerami, E. *et al.* (2012) 'The cBio Cancer Genomics Portal: An Open Platform for Exploring Multidimensional Cancer Genomics Data', *Cancer Discov.*, 2(5), pp. 401–404. doi: 10.1158/2159-8290.CD-12-0095.

Chandrashekar, D. S. *et al.* (2017) 'UALCAN: A Portal for Facilitating Tumor Subgroup Gene Expression and Survival Analyses 1', *Neoplasia*, 19, pp. 649–658. doi: 10.1016/j.neo.2017.05.002.

Chang, A. J. *et al.* (2014) '"High-Risk" Prostate Cancer: Classification and Therapy', *Nat. Rev. Clin. Oncol.*, 11, pp. 308–323. doi: 10.1038/nrclinonc.2014.68.

Chang, J. *et al.* (2009) 'Inhibition of Osteoblast Functions by IKK/NF-kB in Osteoporosis', *Nature medicine*, 15(6), p. 682. doi: 10.1038/nm.1954.Inhibition.

Chatzigeorgiou, Antonios *et al.* (2014) 'Blocking CD40-TRAF6 signaling is a therapeutic target in obesity-associated insulin resistance', *Proceedings of the National Academy of Sciences*. National Academy of Sciences, 111(7), pp. 2686–2691. doi: 10.1073/PNAS.1400419111.

Chatzigeorgiou, A. *et al.* (2014) 'Blocking CD40-TRAF6 signaling is a therapeutic target in obesity-associated insulin resistance', *Proceedings of the National Academy of Sciences*, 111(7), pp. 2686–2691. doi: 10.1073/pnas.1402460111.

Cheever, M. A. and Higano, C. S. (2011) 'PROVENGE (sipuleucel-T) in prostate cancer: The first FDA-approved therapeutic cancer vaccine', *Clinical Cancer Research*, 17(11), pp. 3520–3526. doi: 10.1158/1078-0432.CCR-10-3126.

Chen, D. *et al.* (2005) 'Recent advances in bone biology research', in *Current Topics in Bone Biology*. World Scientific, pp. 497–510.

Chen, G. *et al.* (2006) 'Expression of RANKL / RANK / OPG in Primary and Metastatic Human Prostate Cancer as Markers of Disease Stage and Functional Regulation', *Cancer*, 107(2), pp. 289–298. doi: 10.1002/cncr.21978.

Chen, X. *et al.* (2018) 'Osteoblast-Osteoclast Interactions', *Connect Tissue Res.*, 59(2), pp. 99–107. doi: 10.1080/03008207.2017.1290085.

Chen, Z. J. (2013) 'Ubiquitination in Signaling to and Activation of IKK', *Immunol Rev.*, 246(1), pp. 95–106. doi: 10.1111/j.1600-065X.2012.01108.x.Ubiquitination.

Chong, J. T., Oh, W. K. and Liaw, B. C. (2018) 'Profile of apalutamide in the treatment of metastatic castration-resistant prostate cancer: evidence to date', *OncoTargets and Therapy*, 11, pp. 2141–2147. doi: 10.2147/OTT.S147168.

Colotta, F. *et al.* (2009) 'Cancer-related inflammation , the seventh hallmark of cancer : links to genetic instability', 30(7), pp. 1073–1081. doi: 10.1093/carcin/bgp127.

Comiskey, M. C., Dallos, M. C. and Drake, C. G. (2018) 'Immunotherapy in Prostate Cancer: Teaching an Old Dog New Tricks', *Current Oncology Reports*. Current Oncology Reports, 20(9), pp. 1–10. doi: 10.1007/s11912-018-0712-z.

Cotter, K., Konety, B. and Ordonez, M. A. (2016) 'Contemporary Management of Prostate Cancer', *F1000Research*, 5, pp. 1–8. doi: 10.12688/f1000research.7183.1.

Culig, Z. and Santer, F. R. (2014) 'Androgen receptor signaling in prostate cancer', *Cancer Metastasis Rev*, 33, pp. 413–427. doi: 10.1007/s10555-013-9474-0.

Cunningham, D. and You, Z. (2015) 'In vitro and in vivo model systems used in prostate cancer research', *J. Biol. Methods*, 2(1), pp. 1–28. doi: 10.14440/jbm.2015.63.In.

D'amico, L. and Roato, I. (2015) 'The Impact of Immune System in Regulating Bone Metastasis Formation by Osteotropic Tumors', *Journal of Immunology Research*, 2015. doi: 10.1155/2015/143526.

Dai, C., Heemers, H. and Sharifi, N. (2017) 'Androgen signaling in prostate cancer', *Cold Spring Harbor Perspectives in Medicine*, 7(9). doi: 10.1101/cshperspect.a030452.

Dai, J. *et al.* (2016) 'Mouse models for studying prostate cancer bone metastasis', *BoneKEy Reports*. Nature Publishing Group, 5(FEBRUARY), pp. 1–10. doi: 10.1038/bonekey.2016.4.

Dainichi, T. *et al.* (2019) 'Immune control by TRAF6-mediated pathways of epithelial cells in the EIME (epithelial immune microenvironment)', *Frontiers in Immunology*, 10(MAY), pp. 1–19. doi: 10.3389/fimmu.2019.01107.

Darnay, B. G. *et al.* (2013) 'TRAFs in RANK Signaling', in *TNF Receptor Associated Factors (TRAFs)*. New York: Advances in Experimental Medicine and Biology, Springer, pp. 152–159.

David Roodman, G. and Silbermann, R. (2015) 'Mechanisms of osteolytic and osteoblastic skeletal lesions', *BoneKEy Reports*. Nature Publishing Group, 4(September), pp. 1–7. doi: 10.1038/bonekey.2015.122.

Davies, C. C. *et al.* (2005) 'TRAF6 Is Required for TRAF2-Dependent CD40 Signal Transduction in Nonhemopoietic Cells', *Molecular and Cellular Biology*, 25(22), pp. 9806–9819. doi: 10.1128/mcb.25.22.9806-9819.2005.

Dehne, N. *et al.* (2017) 'Cancer cell and macrophage cross-talk in the tumor microenvironment', *Current Opinion in Pharmacology*, 35, pp. 12–19. doi: 10.1016/j.coph.2017.04.007.

Drake, C. G. (2010) 'Prostate cancer as a model for tumour immunotherapy', 8(24), pp. 4017–4018. doi: 10.1002/bmb.20244.DNA.

Eeles, R. *et al.* (2014) 'The genetic epidemiology of prostate cancer and its clinical implications', *Nature Reviews Urology*. Nature Publishing Group, 11(1), pp. 18–31. doi: 10.1038/nrurol.2013.266.

Erlandsson, A. *et al.* (2019) 'M2 macrophages and regulatory T cells in lethal prostate cancer', *Prostate*, 79(4), pp. 363–369. doi: 10.1002/pros.23742.

Escamilla, J. *et al.* (2015) 'CSF1 receptor targeting in prostate cancer reverses macrophage-mediated resistance to androgen blockade therapy', *Cancer Research*, 75(6), pp. 950–962. doi: 10.1158/0008-5472.CAN-14-0992.

Fang, L.-Y. *et al.* (2013) 'Infiltrating macrophages promote prostate tumorigenesis via modulating androgen receptor-mediated CCL4-STAT3 signaling', *Cancer Res.*, 73(18). doi: 10.1158/0008-5472.CAN-12-3228.

Feng, X. and Mcdonald, J. M. (2011) 'Disorders of Bone Remodeling'. doi: 10.1146/annurev-pathol-011110-130203.

Fizazi, K. *et al.* (2011a) 'Denosumab versus zoledronic acid for treatment of bone metastases in men with castration-resistant prostate cancer: A randomised, double-blind study', *The Lancet*. doi: 10.1016/S0140-6736(10)62344-6.

Fizazi, K. *et al.* (2011b) 'Denosumab versus zoledronic acid for treatment of bone metastases in men with castration-resistant prostate cancer: A randomised, double-blind study', *The Lancet*, 377(9768), pp. 813–822. doi: 10.1016/S0140-6736(10)62344-6.

Fizazi, K. *et al.* (2019) 'Darolutamide in Nonmetastatic, Castration-Resistant Prostate Cancer', *The New Englad Journal of Medicine*, 380(13). doi: 10.1056/NEJMoa1815671.

Fontana, F. *et al.* (2019) 'Epithelial-To-Mesenchymal Transition Markers and CD44 Isoforms

Are Differently Expressed in 2D and 3D Cell Cultures of Prostate Cancer Cells'. doi: 10.3390/cells8020143.

Forrester, M. A. *et al.* (2018) 'Similarities and differences in surface receptor expression by THP-1 monocytes and differentiated macrophages polarized using seven different conditioning regimens', *Cellular Immunology*. Academic Press, 332, pp. 58–76. doi: 10.1016/J.CELLIMM.2018.07.008.

Futakuchi, M., Fukamachi, K. and Suzui, M. (2016) 'Heterogeneity of tumor cells in the bone microenvironment: Mechanisms and therapeutic targets for bone metastasis of prostate or breast cancer', *Advanced Drug Delivery Reviews*. Elsevier B.V., 99, pp. 206–211. doi: 10.1016/j.addr.2015.11.017.

Galli, S., Borregaard, N. and Wynn, T. (2011) 'Phenotypic and functional plasticity of cells of innate immunity: macrophages, mast cells and neutrophils', *Nature immunology*, 12(11), pp. 1035–1044. doi: 10.1038/ni.2109.Phenotypic.

Gao, J. *et al.* (2014) 'Integrative Analysis of Complex Cancer Genomics and Clinical Profiles Using the cBioPortal', *Sci Signal*, 6(269). doi: 10.1126/scisignal.2004088.

Garg, R. *et al.* (2012) 'Activation of Nuclear Factor K B (NF-KB) in Prostate Cancer Is Mediated by Protein Kinase C E(PKCE)', *The Journal of Biological Chemistry*, 287(44), pp. 37570–37582. doi: 10.1074/jbc.M112.398925.

Garraway, I. P. (2013) 'Targeting the RANKL Pathway: Putting the Brakes on Prostate Cancer Progression in Bone', *Journal of Clinical Oncology*, 31(30).

Gasparian, A. V *et al.* (2002) 'The role of IKK in constitutive activation of NF- κ B transcription factor in prostate carcinoma cells', *Journal of Cell Science*, 115, pp. 141–151.

Genin, M. *et al.* (2015) 'M1 and M2 macrophages derived from THP-1 cells differentially modulate the response of cancer cells to etoposide', *BMC Cancer*. BMC Cancer, 15(1), pp. 1–14. doi: 10.1186/s12885-015-1546-9.

Gohda, J. *et al.* (2005) 'RANK-mediated amplification of TRAF6 signaling leads to NFATc1 induction during osteoclastogenesis', *The EMBO Journal*, 24, pp. 790–799. doi: 10.1038/sj.emboj.7600564.

Goldman, M. *et al.* (2018) 'The UCSC Xena platform for public and private cancer genomics data visualization and interpretation', *bioRxiv*, 326470. doi: 10.1101/326470.

Gollapudi, K. *et al.* (2013) 'Association between tumor-associated macrophage infiltration , high grade prostate cancer , and biochemical recurrence after radical prostatectomy', *Am J Cancer Res*, 3(5), pp. 523–529.

Gudey, S. K. *et al.* (2014) 'TRAF6 Stimulates the Tumor-Promoting Effects of TGF b Type I Receptor Through Polyubiquitination and Activation of Presenilin 1', *Cancer*, 7(307), pp. 1–14.

Gurova, K. V. *et al.* (2005) 'Small molecules that reactivate p53 in renal cell carcinoma reveal a NF- B-dependent mechanism of p53 suppression in tumors', *Proceedings of the National Academy of Sciences*, 102(48), pp. 17448–17453. doi: 10.1073/pnas.0508888102.

Häcker, H. *et al.* (2006) 'Specificity in Toll-like receptor signalling through distinct effector functions of TRAF3 and TRAF6'. doi: 10.1038/nature04369.

Hamid, A. A. *et al.* (2019) 'Compound Genomic Alterations of TP53, PTEN, and RB1 Tumor Suppressors in Localized and Metastatic Prostate Cancer', *European Urology*. doi: 10.1016/j.eururo.2018.11.045.

Hamidi, A. *et al.* (2017) 'TGF-β promotes PI3K-AKT signaling and prostate cancer cell migration through the TRAF6-mediated ubiquitylation of p85α', *Science Signaling*, 10(486), pp. 1–16. doi: 10.1126/scisignal.aal4186.

Han, Y. *et al.* (2019) 'Tumor-associated macrophages promote lung metastasis and induce epithelial-mesenchymal transition in osteosarcoma by activating the COX-2/STAT3 axis', *Cancer Letters*. Elsevier, 440–441(11), pp. 116–125. doi: 10.1016/j.canlet.2018.10.011.

Hanahan, D. and Weinberg, R. A. (2011) 'Hallmarks of Cancer: The Next Generation', *Cell*, 144, pp. 646–674.

Heerboth, S. *et al.* (2015) 'EMT and tumor metastasis'. doi: 10.1186/s40169-015-0048-3.

Hieronymus, H. *et al.* (2014) 'Copy number alteration burden predicts prostate cancer relapse.', *Proceedings of the National Academy of Sciences of the United States of America*. National Academy of Sciences, 111(30), pp. 11139–44. doi: 10.1073/pnas.1411446111.

Higano, C. S. *et al.* (2009) 'Integrated data from 2 randomized, double-blind, placebo-controlled, phase 3 trials of active cellular immunotherapy with sipuleucel-T in advanced prostate cancer', *Cancer*, 115(16), pp. 3670–3679. doi: 10.1002/cncr.24429.

Hirata, T. *et al.* (2016) 'Specific bone region localization of osteolytic versus osteoblastic lesions in a patient-derived xenograft model of bone metastatic prostate cancer', *Asian Journal of Urology*. doi: 10.1016/j.ajur.2016.09.001.

Hoesel, B. and Schmid, J. A. (2013) *The complexity of NF-κB signaling in inflammation and cancer*, *Molecular Cancer*. doi: 10.1186/1476-4598-12-86.

Holen, I. *et al.* (2002) *Osteoprotegerin (OPG) Is a Survival Factor for Human Prostate Cancer Cells1*.

Hotte, S. J. and Saad Md, F. (2010) 'Current management of castrate-resistant prostate cancer', *Urologic Oncology*, 17(2).

Huang, H. *et al.* (2017) 'The effect of marrow stromal cells on TRAF6 expression levels in myeloma cells', *Oncology Letters*, 14(2), pp. 1464–1470. doi: 10.3892/ol.2017.6322.

Huang, S. *et al.* (2017) 'Downregulation of miR-141-3p promotes bone metastasis via activating NF-κB signaling in prostate cancer', *Journal of Experimental & Clinical Cancer Research*. Journal of Experimental & Clinical Cancer Research, 36, pp. 1–13. doi: 10.1186/s13046-017-0645-7.

Hyeon, J. *et al.* (2018) 'Targeted deep sequencing of gastric marginal zone lymphoma identified alterations of TRAF3 and TNFAIP3 that were mutually exclusive for MALT1 rearrangement', *Modern Pathology*, 31, pp. 1418–1428. doi: 10.1038/s41379-018-0064-0.

Idris, A. *et al.* (2008) 'ABD56 causes osteoclast apoptosis by inhibiting the NFjB and ERK pathways', *Biochemical and Biophysical Research Communications*, 371, pp. 94–98.

Idris, A. I. *et al.* (2009) 'Identification of Novel Biphenyl Carboxylic Acid Derivatives as Novel Antiresorptive Agents that Do Not Impair Parathyroid Hormone-Induced Bone Formation', *Endocrinology*, 150(1), pp. 5–13. doi: 10.1210/en.2008-0998.

Idris, A. I. (2012) 'Analysis of Signalling Pathways by Western Blotting and Immunoprecipitation', in. Humana Press, Totowa, NJ, pp. 223–232. doi: 10.1007/978-1-61779-415-5_15.

Jabara, H. H. *et al.* (2002) 'The Binding Site for TRAF2 and TRAF3 but Not for TRAF6 Is

Essential for CD40-Mediated Immunoglobulin Class Switching', *Immunity*, 17(3), pp. 265–276. doi: 10.1016/S1074-7613(02)00394-1.

Jackson-Bernitsas, D. G. *et al.* (2007) 'Evidence that TNF-TNFR1-TRADD-TRAF2-RIP-TAK1-IKK pathway mediates constitutive NF-jB activation and proliferation in human head and neck squamous cell carcinoma', *Oncogene*, 26, pp. 1385–1397. doi: 10.1038/sj.onc.1209945.

Jackson, S. J. *et al.* (2017) 'Does age matter? The impact of rodent age on study outcomes', *Laboratory Animals*, 51(2), pp. 160–169. doi: 10.1177/0023677216653984.

James, N. D. *et al.* (2016) 'Addition of docetaxel, zoledronic acid, or both to first-line long-term hormone therapy in prostate cancer (STAMPEDE): Survival results from an adaptive, multiarm, multistage, platform randomised controlled trial', *The Lancet.* doi: 10.1016/S0140-6736(15)01037-5.

Jang, T. L., Bianco, F. and Scardino, P. T. (2007) 'Low Risk Prostate Cancer in Men under Age 65: The Case for Definitive Treatment', *Urologic Oncology*, 25, pp. 510–514. doi: 10.1016/j.urolonc.2007.05.025.

Jansen, M. F. *et al.* (2016) 'CD40 in coronary artery disease: a matter of macrophages?', *Basic Research in Cardiology*. Springer Berlin Heidelberg, 111(4). doi: 10.1007/s00395-016-0554-5.

Jäntti, M. H. *et al.* (2018) 'Anticancer activity of the protein kinase C modulator HMI-1a3 in 2D and 3D cell culture models of androgen-responsive and androgen-unresponsive prostate cancer', *FEBS Open Bio*, 8(5), pp. 817–828. doi: 10.1002/2211-5463.12419.

Jeong, H. M., Cho, S. W. and Park, S. I. (2016) 'Osteoblasts are the centerpiece of the metastatic bone microenvironment', *Endocrinology and Metabolism*, 31(4), pp. 485–492. doi: 10.3803/EnM.2016.31.4.485.

Jin, J. *et al.* (2015) 'Proinflammatory TLR signaling is regulated by a TRAF2-dependent proteolysis mechanism in macrophages HHS Public Access'. doi: 10.1038/ncomms6930.

Jin, Renjie *et al.* (2013) 'Activation of NF-kappa B Signaling Promotes Growth of Prostate Cancer Cells in Bone', *PLoS ONE*, 8(4). doi: 10.1371/journal.pone.0060983.

Jin, R. *et al.* (2013) 'Activation of NF-kappa B Signaling Promotes Growth of Prostate Cancer Cells in Bone', *PLOS ONE*, 8(4). Available at: https://journals.plos.org/plosone/article/file?id=10.1371/journal.pone.0060983&type=printable (Accessed: 11 October 2019).

Jin, R. *et al.* (2015) 'Inhibition of NF-kappa B signaling restores responsiveness of castrate-resistant prostate cancer cells to anti-androgen treatment by decreasing androgen receptor-variant expression', *Oncogene*, 34(28), pp. 3700–3710. doi: 10.1038/onc.2014.302.

Jin, R. J. *et al.* (2008) 'The NF-κB Pathway Controls Progression of Prostate Cancer to Androgen Independent Growth', *Cancer Res*, 68(16), pp. 6762–6769. doi: 10.1158/0008-5472.CAN-08-0107.

Jin, Renjie *et al.* (2014) 'NF-κB gene signature predicts prostate cancer progression', *Cancer Res*, 74(10), pp. 2763–2772. doi: 10.1158/0008-5472.CAN-13-2543.

Jin, X. and Mu, P. (2015) 'Targeting Breast Cancer Metastasis', *Libertas Academica*, 9, pp. 23–34. doi: 10.4137/BCBCR.S25460.TYPE.

Jones, D. H. *et al.* (2006) 'Regulation of cancer cell migration and bone metastasis by RANKL', 440, pp. 8–12. doi: 10.1038/nature04524.

Kang, M. *et al.* (2017) 'Concurrent treatment with simvastatin and NF-κB inhibitor in human castration-resistant prostate cancer cells exerts synergistic anticancer effects via control of the NF-κB/LIN28/ let-7 miRNA signaling pathway', *PLoS ONE*, 12(9), pp. 1–13. doi: 10.1371/journal.pone.0184644.

Kantoff, P. W. *et al.* (2010) 'Sipuleucel-T Immunotherapy for Castration-Resistant Prostate Cancer', *The New England Journal of Medicine*, 363(5), pp. 411–422.

King, C. G. *et al.* (2006) 'TRAF6 is a T cell-intrinsic negative regulator required for the maintenance of immune homeostasis'. doi: 10.1038/nm1449.

Kirby, R. S. and Patel, M. I. (2009) *Fast Facts: Prostate Cancer*.

Kittai, A., Meshikhes, M. and Aragon-Ching, J. B. (2014) 'A potential immunologic agent in the treatment of metastatic castration-resistant prostate cancer', *Cancer Biology and Therapy*, 15(10), pp. 1299–1300. doi: 10.4161/cbt.29928.

Kobayashi, N. *et al.* (2001) 'Segregation of TRAF6-mediated signaling pathways clarifies its role in osteoclastogenesis', *EMBO Journal*, 20(6), pp. 1271–1280. doi: 10.1093/emboj/20.6.1271.

Kobayashi, T. *et al.* (2003) 'TRAF6 is a critical factor for dendritic cell maturation and development', *Immunity*. doi: 10.1016/S1074-7613(03)00230-9.

Kobayashi, T., Walsh, M. C. and Choi, Y. (2004) 'The role of TRAF6 in signal transduction and the immune response', *Microbes and Infection*. doi: 10.1016/j.micinf.2004.09.001.

Konno, H. *et al.* (2009) 'TRAF6 establishes innate immune responses by activating NF-κB and IRF7 upon sensing cytosolic viral RNA and DNA', *PLoS ONE*. doi: 10.1371/journal.pone.0005674.

Kraft, A. S. *et al.* (2011) 'Combination therapy of recurrent prostate cancer with the proteasome inhibitor bortezomib plus hormone blockade', *Cancer Biology and Therapy*, 12(2), pp. 119–124. doi: 10.4161/cbt.12.2.15723.

Kroon, J. *et al.* (2016) 'Improving Taxane-Based Chemotherapy in Castration-Resistant Prostate Cancer', *Trends in Pharmacological Sciences*. doi: 10.1016/j.tips.2016.03.003.

Kunisch, E. *et al.* (2004) 'Macrophage specificity of three anti-CD68 monoclonal antibodies (KP1, EBM11, and PGM1) widely used for immunohistochemistry and flow cytometry', *Ann Rheum Dis*, 63, pp. 774–784. doi: 10.1136/ard.2003.013029.

Lalani, A. I. *et al.* (2018) 'TRAF Molecules in Inflammation and Inflammatory Diseases', *Current Pharmacology Reports*. Current Pharmacology Reports, 4(1), pp. 64–90. doi: 10.1007/s40495-017-0117-y.

Lamothe, B. *et al.* (2007) 'TRAF6 Ubiquitin Ligase is Essential for RANKL Signaling and Osteoclast Differentiation', *Biochem Biophys Res Commun.*, 359(4), pp. 1044–1049. doi: 10.1111/j.1743-6109.2008.01122.x.Endothelial.

Lawrence, T. (2009) 'The Nuclear Factor NF-kappaB Pathway in Inflammation', *Cold Spring Harb Perspect Biol*, 1, pp. 1–10.

Leslei, S. W., Soon-Sutton, T. L. and Siref, L. E. (2018) *Cancer, Prostate*.

Li, T. *et al.* (2017) 'TIMER: A web server for comprehensive analysis of tumor-infiltrating immune cells', *Cancer Research*, 77(21), pp. e108–e110. doi: 10.1158/0008-5472.CAN-17-0307.

Lindholm, P. F. *et al.* (2010) 'Role of monocyte-lineage cells in prostate cancer cell invasion and tissue factor expression', *Prostate*, 70, pp. 1672–1682. doi: 10.1002/pros.21202.

Lindsten, T. *et al.* (2017) 'Effect of macrophages on breast cancer cell proliferation, and on expression of hormone receptors, uPAR and HER-2', *International Journal of Oncology*, 51(1), pp. 104–114. doi: 10.3892/ijo.2017.3996.

Liu, Q. *et al.* (2013) 'Interleukin-1β promotes skeletal colonization and progression of metastatic prostate cancer cells with neuroendocrine features', *Cancer Research*, 73(11), pp. 3297–3305. doi: 10.1158/0008-5472.CAN-12-3970.

Liu, Runhua *et al.* (2015) 'FOXP3-microRNA-146-NF-κB axis and therapy for precancerous lesions in prostate HHS Public Access miR-146-NF-κB axis may provide a new therapeutic approach for prostate cancers with FOXP3 defects', *Cancer Res*, 75(8), pp. 1714–1724. doi: 10.1158/0008-5472.CAN-14-2109.

Lo, C. H. and Lynch, C. C. (2018) 'Multifaceted roles for macrophages in prostate cancer skeletal metastasis', *Frontiers in Endocrinology*, 9(MAY), pp. 1–12. doi: 10.3389/fendo.2018.00247.

Lomaga, M. A. *et al.* (1999) 'TRAF6 deficiency results in osteopetrosis and defective interleukin-1, CD40, and LPS signaling', *Genes and Development*, 13(8), pp. 1015–1024. doi: 10.1101/gad.13.8.1015.

Lu, W. *et al.* (2015) 'SKP2 inactivation suppresses prostate tumorigenesis by mediating JARID1B ubiquitination', *Oncotarget*, 6(2), pp. 771–788. doi: 10.18632/oncotarget.2718.

Lu, W. *et al.* (2017) 'SKP2 loss destabilizes EZH2 by promoting TRAF6-mediated ubiquitination to suppress prostate cancer', *Oncogene*, 36(10), pp. 1364–1373. doi: 10.1038/onc.2016.300.

Lu, Y. *et al.* (2014) 'TRAF6 upregulation in spinal astrocytes maintains neuropathic pain by integrating TNF-α and IL-1β signaling', *Pain*. International Association for the Study of Pain, 155(12), pp. 2618–2629. doi: 10.1016/j.pain.2014.09.027.

Lutgens, E. *et al.* (2010) 'Deficient CD40-TRAF6 signaling in leukocytes prevents atherosclerosis by skewing the immune response toward an antiinflammatory profile', *Journal of Experimental Medicine*, 207(2), pp. 391–404. doi: 10.1084/jem.20091293.

Madan, R. A. *et al.* (2009) 'Prostvac-VF: A vector-based vaccine targeting PSA in prostate cancer', *Expert Opinion on Investigational Drugs*, 18(7), pp. 1001–1011. doi: 10.1517/13543780902997928.

Maolake, A. *et al.* (2017) 'Tumor-associated macrophages promote prostate cancer migration through activation of the CCL22-CCR4 axis', *Oncotarget*, 8(6), pp. 9739–9751. doi: 10.18632/oncotarget.14185.

Maolake, A. *et al.* (2018) 'Tumor necrosis factor-a induces prostate cancer cell migration in lymphatic metastasis through CCR7 upregulation'. doi: 10.1111/cas.13586.

Marino, S. *et al.* (2019) 'Pharmacological Inhibition of NFκB Reduces Prostate Cancer Related Osteoclastogenesis In Vitro and Osteolysis Ex Vivo', *Calcified Tissue International*. Springer US, 105(2), pp. 193–204. doi: 10.1007/s00223-019-00538-9.

Martinez-Marin, D. *et al.* (2017) 'PEDF increases the tumoricidal activity of macrophages towards prostate cancer cells in vitro', *PLoS ONE*, 12(4), pp. 1–22. doi: 10.1371/journal.pone.0174968.

Mateo, J. *et al.* (2015) 'DNA-Repair Defects and Olaparib in Metastatic Prostate Cancer', *The New England Journal of Medicine*, 373(18), pp. 1697–1708. doi: 10.1016/j.juro.2016.01.052.

Mazalova, L. *et al.* (2018) 'Effect of prostate cancer cell line supernatant on functional polarization in macrophages', *Bratisl Med J*, 119(8), pp. 516–521. doi: 10.4149/BLL.

Mitra, A. *et al.* (2008) 'Prostate cancer in male BRCA1 and BRCA2 mutation carriers has a more aggressive phenotype', pp. 502–507. doi: 10.1038/sj.bjc.6604132.

Mizutani, K. *et al.* (2009) 'The Chemokine CCL2 Increases Prostate Tumor Growth and Bone Metastasis through Macrophage and Osteoclast Recruitment', *Neoplasia*. Neoplasia Press, Inc., 11(11), pp. 1235–1242. doi: 10.1593/neo.09988.

Moh, S. H. *et al.* (2011) 'Effects of Lotus Root Extract on Osteoblast and Osteoclast', in *Grid and Distributed Computing: International Conferences, GDC 2011*, pp. 603–612.

Moilanen, A.-M. *et al.* (2015) 'Discovery of ODM-201, a new-generation androgen receptor inhibitor targeting resistance mechanisms to androgen signaling-directed prostate cancer therapies', *Nature Publishing Group*. doi: 10.1038/srep12007.

Montanari, M. *et al.* (2017) 'Epithelial-mesenchymal transition in prostate cancer: an overview', *Oncotarget*, 8(21), pp. 35376–35389. doi: 10.18632/oncotarget.15686.

Moreira, Â. *et al.* (2015) 'Adipocyte secreted factors enhance aggressiveness of prostate carcinoma cells', *PLoS ONE*, 10(4), pp. 1–16. doi: 10.1371/journal.pone.0123217.

Mori, K. *et al.* (2007) 'DU145 human prostate cancer cells express functional receptor activator of NFκB: New insights in the prostate cancer bone metastasis process', *Bone*. Elsevier Inc., 40(4), pp. 981–990. doi: 10.1016/j.bone.2006.11.006.

Moriya, J. *et al.* (2015) 'Structure-Based Development of a Protein-Protein Interaction Inhibitor Targeting Tumor Necrosis Factor Receptor-Associated Factor 6', *Journal of Medicinal Chemistry*, 58(14), pp. 5674–5683. doi: 10.1021/acs.jmedchem.5b00778.

Morris, M. J. *et al.* (2007) 'A Phase II Trial of Bortezomib and Prednisone for Castration Resistant Metastatic Prostate Cancer', *Journal of Urology*, 178(6), pp. 2378–2384. doi: 10.1016/j.juro.2007.08.015.

Morrissey, C. and Vessella, R. L. (2007) 'The Role of Tumor Microenvironment in Prostate Cancer Bone Metastasis', *Journal of Cellular Biochemistry*, 101, pp. 873–886. doi: 10.1002/jcb.21214.

Mounier, C., Bouraoui, L. and Rassart, E. (2014) 'Lipogenesis in cancer progression (Review)', *International Journal of Oncology*, 45, pp. 485–492. doi: 10.3892/ijo.2014.2441.

Moutasim, K., Nystrom, M. L. and Thomas, G. J. (2011) 'Cell Migration and Invasion Assays Karwan', in *Methods in molecular biology (Clifton,*. doi: 10.1007/978-1-61779-080-5.

Mukaka, M. M. (2012) 'Statistics corner: A guide to appropriate use of correlation coefficient in medical research', *Malawi Medical Journal*, 24(3), pp. 69–71.

Mukherjee, R. *et al.* (2011) 'Upregulation of MAPK pathway is associated with survival in castrate-resistant prostate cancer', *British Journal of Cancer*, 104, pp. 1920–1928. doi: 10.1038/bjc.2011.163.

Nabbi, A. *et al.* (2017) 'ING3 promotes prostate cancer growth by activating the androgen receptor', *BMC Medicine*, 15(103). doi: 10.1186/s12916-017-0854-0.

Nadiminty, N. *et al.* (2013) 'NF-κB2/p52 Induces Resistance to Enzalutamide in Prostate Cancer: Role of Androgen Receptor and Its Variants', *Mol Cancer Ther*, 12(8), pp. 1629–1637. doi: 10.1158/1535-7163.MCT-13-0027.

Naito, A. *et al.* (1999) 'Severe osteopetrosis , defective interleukin-1 signalling and lymph node organogenesis in TRAF6-deficient mice', *Genes to Cells*, 4, pp. 353–362.

Narayan Biswal, B. *et al.* (2017) 'Alteration of cellular metabolism in cancer cells and its therapeutic prospects', *J Oral Maxillofac Pathol.*, 21(2), pp. 244–251.

Naugler, W. E. and Karin, M. (2008) 'NF-κB and cancer - identifying targets and mechanisms', *Current Opinion in Genetics and Development*. doi: 10.1016/j.gde.2008.01.020.

Nazim, S. M. and Abbas, F. (2015) 'Role of surgery in locally advanced prostate cancer', *Pakistan Journal of Medical Sciences.* Professional Medical Publications, pp. 710–716. doi: 10.12669/pjms.313.7103.

Nevedomskaya, E., Baumgart, S. J. and Haendler, B. (2018) 'Recent Advances in Prostate Cancer Treatment and Drug Discovery', *International Journal of Molecular Sciences*, 19.

Ni, X. *et al.* (2019) 'TRAF6 directs FOXP3 localization and facilitates regulatory T-cell function through K63-linked ubiquitination', *The EMBO Journal*, 38. doi: 10.15252/embj.201899766.

Nielsen, S. R. and Schmid, M. C. (2017) 'Macrophages as Key Drivers of Cancer Progression and Metastasis', *Mediators Inflammation*, 2017, pp. 1–11. doi: 10.1155/2017/9624760.

Nonomura, N. *et al.* (2011) 'Infiltration of tumour-associated macrophages in prostate biopsy specimens is predictive of disease progression after hormonal therapy for prostate cancer', *BJU International*, 107(12), pp. 1918–1922. doi: 10.1111/j.1464-410X.2010.09804.x.

Nyberg, T. *et al.* (2020) 'Prostate Cancer Risks for Male BRCA1 and BRCA2 Mutation Carriers: A Prospective Cohort Study', *European Urology*. Elsevier B.V., 77(1), pp. 24–35. doi: 10.1016/j.eururo.2019.08.025.

Odero-Marah, V. A. *et al.* (2008) 'Receptor activator of NF-κB Ligand (RANKL) expression is associated with epithelial to mesenchymal transition in human prostate cancer cells', *Cell Research*, 18, pp. 858–870. doi: 10.1038/cr.2008.84.

Oeckinghaus, A., Hayden, M. S. and Ghosh, S. (2011) 'Crosstalk in NF-kappaB signaling pathways', *Nature Immunology*, 12(8). doi: 10.1038/ni.2065.

Oh, J. *et al.* (2018) 'Age-related tumor growth in mice is related to integrin α 4 in CD8+ T cells', *JCI insight*, 3(21). Available at: https://www.ncbi.nlm.nih.gov/pmc/articles/PMC6238736/pdf/jciinsight-3-122961.pdf (Accessed: 14 September 2020).

Oien, D. B. *et al.* (2019) 'Repurposing quinacrine for treatment-refractory cancer', *Seminars in Cancer Biology*. doi: 10.1016/j.semcancer.2019.09.021.

Paik, J. H. *et al.* (2011) 'MicroRNA-146a downregulates NFκB activity via targeting TRAF6 and functions as a tumor suppressor having strong prognostic implications in NK/T cell lymphoma', *Clinical Cancer Research*, 17(14), pp. 4761–4771. doi: 10.1158/1078-0432.CCR-11-0494.

Paller, C. J., Carducci, M. A. and Philips, G. K. (2012) 'Management of bone metastases in refractory prostate cancer-role of denosumab', *Clinical Interventions in Aging*, 7, pp. 363–372. doi: 10.2147/CIA.S27930.

Park, E. K. *et al.* (2007) 'Optimized THP-1 differentiation is required for the detection of

responses to weak stimuli', *Inflammation Research*, 56(1), pp. 45–50. doi: 10.1007/s00011-007-6115-5.

Park, H. H. (2018) 'Structure of TRAF Family: Current Understanding of Receptor Recognition', *Frontiers in immunology*, 9(August), p. 1999. doi: 10.3389/fimmu.2018.01999.

Park, S. I. *et al.* (2010) 'Pre-Clinical Mouse Models of Human Prostate Cancer and their Utility in Drug Discovery NIH Public Access', *Curr Protoc Pharmacol*, 51. doi: 10.1002/0471141755.ph1415s51.

Parker, C. *et al.* (2013) 'Alpha emitter radium-223 and survival in metastatic prostate cancer', *The New England Journal of Medicine*, 369(3), pp. 213–223. doi: 10.1016/j.juro.2013.11.087.

Pearson, L. L., Castle, B. E. and Kehry, M. R. (2001) *CD40-mediated signaling in monocytic cells: up-regulation of tumor necrosis factor receptor-associated factor mRNAs and activation of mitogen-activated protein kinase signaling pathways*, *International Immunology*.

Pecorino, L. (2016) 'Infectious agents and inflammation', in *Molecular Biology of Cancer*, pp. 302–325.

Peisch, S. F. *et al.* (2017) 'Prostate cancer progression and mortality: a review of diet and lifestyle factors', *World Journal of Urology*, 35, pp. 867–874. doi: 10.1007/s00345-016-1914-3.

Peramuhendige, P. *et al.* (2018) 'TRAF2 in osteotropic breast cancer cells enhances skeletal tumour growth and promotes osteolysis', *Scientific Reports*. Nature Publishing Group, 8(1). doi: 10.1038/s41598-017-18327-5.

Petitprez, F. *et al.* (2019) 'PD-L1 Expression and CD8+ T-cell Infiltrate are Associated with Clinical Progression in Patients with Node-positive Prostate Cancer', *European Association of Urology*, 5(2), pp. 192–196.

Petrucelli, N., Daly, M. B. and Feldman, G. L. (2010) 'Hereditary breast and ovarian cancer due to mutations in BRCA1 and BRCA2', *Genetics in Medicine*, 12(5), pp. 245–259. doi: 10.1097/GIM.0b013e3181d38f2f.

Pitt, J. M. *et al.* (2016) 'Targeting the tumor microenvironment: removing obstruction to anticancer immune responses and immunotherapy', *Annals of Oncology*, 27, pp. 1482–1492. doi: 10.1093/annonc/mdw168.

Polascik, T. J. and Mouraviev, V. (2008) *Zoledronic acid in the management of metastatic bone disease*, *Therapeutics and Clinical Risk Management*.

Power, C. A. *et al.* (2009) 'A novel model of bone-metastatic prostate cancer in immunocompetent Mice', *The Prostate*, 69(15), pp. 1613–1623. doi: 10.1002/pros.21010.

Quiroz-Munoz, M. *et al.* (2019) 'Mechanisms of Osteoblastic Bone Metastasis in Prostate Cancer: Role of Prostatic Acid Phosphatase', 3(3). doi: 10.1210/js.2018-00425.

Rafiei, S. and Komarova, S. V. (2013) 'Molecular Signaling Pathways Mediating Osteoclastogenesis Induced by Prostate Cancer Cells', *BMC Cancer*, 13(November 2014). doi: 10.1186/1471-2407-13-605.

Rafiei, S. and Komarova, S. V (2013) *Molecular Signaling Pathways Mediating Osteoclastogenesis Induced by Prostate Cancer Cells*. Available at: http://www.biomedcentral.com/1471-2407/13/605 (Accessed: 12 July 2019).

Rampersad, S. N. (2012) 'Multiple Applications of Alamar Blue as an Indicator of Metabolic

Function and Cellular Health in Cell Viability Bioassays', pp. 12347–12360. doi: 10.3390/s120912347.

Ramprasad, M. P. *et al.* (1996) *Cell surface expression of mouse macrosialin and human CD68 and their role as macrophage receptors for oxidized low density lipoprotein*, *Medical Sciences*. Available at: https://www.ncbi.nlm.nih.gov/pmc/articles/PMC26222/pdf/pq014833.pdf (Accessed: 22 May 2019).

Reinstein, Z. Z. *et al.* (2017) 'Overcoming immunosuppression in bone metastases', *Critical Reviews in Oncology/Hematology*, 117, pp. 114–127. doi: 10.1016/j.critrevonc.2017.05.004.

Ren, D. *et al.* (2017) 'Oncogenic miR-210-3p promotes prostate cancer cell EMT and bone metastasis via NF-κB signaling pathway', *Molecular Cancer*, 16(117). doi: 10.1186/s12943-017-0688-6.

Roato, I. *et al.* (2008) 'Osteoclasts Are Active in Bone Forming Metastases of Prostate Cancer Patients', *PLoS ONE*, 3(11). doi: 10.1371/journal.pone.0003627.

Robinson, D. R. *et al.* (2017) 'Integrative Clinical Genomics of Metastatic Cancer', *Nature*, 548(7667), pp. 297–30. doi: 10.1038/nature23306.

Roca, H. *et al.* (2009) 'CCL2 and interleukin-6 promote survival of human CD11b+ peripheral blood mononuclear cells and induce M2-type macrophage polarization', *Journal of Biological Chemistry*, 284(49), pp. 34342–34354. doi: 10.1074/jbc.M109.042671.

Rubin, M. A. and Demichelis, F. (2018) 'The Genomics of Prostate Cancer: emerging understanding with technologic advances', *Modern pathology : an official journal of the United States and Canadian Academy of Pathology, Inc*. Nature Publishing Group, 31(S1), pp. S1–S11. doi: 10.1038/modpathol.2017.166.

Rucci, N. (2008) 'Molecular biology of bone remodelling', *Clinical Cases in Mineral and Bone Metabolism* , 5(2), pp. 49–56.

Rucci, N. and Angelucci, A. (2014) 'Prostate Cancer and Bone: The Elective Affinities', *BioMed Research International*. doi: 10.1155/2014/167035.

Rutkovskiy, A. E. *et al.* (2016) 'Osteoblast Differentiation at a Glance', *Med Sci Monit Basic Res*, 22, pp. 95–106. doi: 10.12659/MSMBR.901142.

Sabokbar, A. *et al.* (1994) 'A rapid, quantitative assay for measuring alkaline phosphatase activity in osteoblastic cells in vitro', *Bone and Mineral*, 27(1), pp. 57–67. doi: 10.1016/S0169-6009(08)80187-0.

Santoni, M. *et al.* (2017) 'Activity and Functions of Tumor-associated Macrophages in Prostate Carcinogenesis', *European Urology, Supplements*. doi: 10.1016/j.eursup.2017.09.002.

Scudiero, I. *et al.* (2012) 'Tumor Necrosis Factor (TNF) Receptor-associated Factor 7 Is Required for TNF-induced Jun NH 2-terminal Kinase Activation and Promotes Cell Death by Regulating Polyubiquitination and Lysosomal Degradation of c-FLIP Protein *'. doi: 10.1074/jbc.M111.300137.

Sebastian de Bono, J. *et al.* (2010) 'Prednisone plus cabazitaxel or mitoxantrone for metastatic castration-resistant prostate cancer progressing after docetaxel treatment: a randomised open-label trial', in *The Lancet*, pp. 1147–1154. doi: 10.1016/S0140-6736(10)61389-X.

Seijkens, T. T. P. *et al.* (2018) 'Targeting CD40-Induced TRAF6 Signaling in Macrophages Reduces Atherosclerosis', *Journal of the American College of Cardiology*. doi: 10.1016/j.jacc.2017.11.055.

Sfanos, K. and Marzo, A. (2014) 'Prostate Cancer and Inflammation', *Histopathology,* 60(11), pp. 199–215. doi: 10.1111/j.1365-2559.2011.04033.x.Prostate.

Sfanos, K. S. *et al.* (2009) 'Human Prostate-Infiltrating CD8 + T Lymphocytes are Oligoclonal and PD-1 +', *Prostate*, 69(15), pp. 1694–1703. doi: 10.1002/pros.21020.

Shi, J., Liu, Z. and Xu, Q. (2019) ' Tumor necrosis factor receptor-associated factor 6 contributes to malignant behavior of human cancers through promoting AKT ubiquitination and phosphorylation', *Cancer Science*, 110, pp. 1909–1920. doi: 10.1111/cas.14012.

Shi, J. and Sun, S. (2018) 'Tumor Necrosis Factor Receptor-Associated Factor Regulation of Nuclear Factor κB and Mitogen-Activated Protein Kinase Pathways.', *Frontiers in Immunology*, 9(August), pp. 1–13. doi: 10.3389/fimmu.2018.01849.

Shupp, A. B. *et al.* (2018) 'Cancer metastases to bone: Concepts, mechanisms, and interactions with bone osteoblasts', *Cancers*, 10(6), pp. 1–37. doi: 10.3390/cancers10060182.

Singh, R. *et al.* (2018) 'TRAF4-mediated ubiquitination of NGF receptor TrkA regulates prostate cancer metastasis', *Journal of Clinical Investigation*. American Society for Clinical Investigation, 128(7), pp. 3129–3143. doi: 10.1172/JCI96060.

Slatkoff, S. *et al.* (2011) 'PSA testing: when it's useful, when it's not.', *The Journal of family practice*, 60(6), pp. 357–60. Available at: http://www.pubmedcentral.nih.gov/articlerender.fcgi?artid=3183963&tool=pmcentrez&rendert ype=abstract.

Small, E. J. *et al.* (2006) 'Placebo-controlled phase III trial of immunologic therapy with Sipuleucel-T (APC8015) in patients with metastatic, asymptomatic hormone refractory prostate cancer', *Journal of Clinical Oncology*, 24(19), pp. 3089–3094. doi: 10.1200/JCO.2005.04.5252.

Smith, M. R. *et al.* (2012) 'Denosumab and Bone Metastasis-Free Survival in Men With Castration-Resistant Prostate Cancer: Results of a Global Phase 3, Randomised, Placebo-Controlled Trial', *Lancet*, 379(9810), pp. 39–46. doi: 10.1016/S0140-6736(11)61226-9.

Soki, F. N. *et al.* (2015) 'Bone marrow macrophages support prostate cancer growth in bone', *Oncotarget*, 6(34), pp. 35782–35796. doi: 10.18632/oncotarget.6042.

Staal, J. and Beyaert, R. (2018) 'Inflammation and NF-κB Signaling in Prostate Cancer: Mechanisms and Clinical Implications', *Cells*, 7(9), p. 122. doi: 10.3390/cells7090122.

Starczynowski, D. T. *et al.* (2011) 'TRAF6 is an amplified oncogene bridging the RAS and NF-κB pathways in human lung cancer', *Journal of Clinical Investigation*, 121(10), pp. 4095–4105. doi: 10.1172/JCI58818.

Stephan, C. *et al.* (2014) 'Prostate-specific antigen (PSA) screening and new biomarkers for prostate cancer (PCa)', *The Journal of the International Federation of Clinical Chemistry and Laboratory Medicine*, 25(1), pp. 55–78.

Sun, J. *et al.* (2019) 'Identification of critical pathways and hub genes in TP53 mutation prostate cancer by bioinformatics analysis', *Biomark. Med.*, 13(10). doi: 10.2217/bmm-2019-0141.

Sun, Q. *et al.* (2014) 'MiR-146a functions as a tumor suppressor in prostate cancer by targeting Rac1', *Prostate*, 74(16), pp. 1613–1621. doi: 10.1002/pros.22878.

Sundar, R. *et al.* (2015) 'TRAF6 promotes TGF b -induced invasion and cell-cycle regulation via Lys63-linked polyubiquitination of Lys178 in TGF b type I receptor', *Cell Cycle*, 14(4), pp. 554–565.

Sundararajan, S. and Vogelzang, N. (2014) 'Chemotherapy in the Treatment of Prostate Cancer-The Past, the Present, and the Future', *The American Journal of Hematology/Oncology*, 10(6), pp. 14–21. Available at: www.ajho.com (Accessed: 31 March 2020).

Szklarczyk, D. *et al.* (2018) 'STRING v11: protein-protein association networks with increased coverage, supporting functional discovery in genome-wide experimental datasets', *Nucleic Acids Research*, 47, pp. 607–613. doi: 10.1093/nar/gky1131.

Tang, Z. *et al.* (2017) 'GEPIA: a web server for cancer and normal gene expression profiling and interactive analyses', *Web Server issue Published online*, 45. doi: 10.1093/nar/gkx247.

Taylor, B. S. *et al.* (2010) 'Integrative Genomic Profiling of Human Prostate Cancer', *Cancer Cell*. doi: 10.1016/j.ccr.2010.05.026.

Tedesco, S. *et al.* (2018) 'Convenience versus Biological Significance: Are PMA-Differentiated THP-1 Cells a Reliable Substitute for Blood-Derived Macrophages When Studying in Vitro Polarization?', *Frontiers in pharmacology*. Frontiers Media SA, 9, p. 71. doi: 10.3389/fphar.2018.00071.

Torre, L. A. *et al.* (2015) 'Global Cancer Statistics, 2012', *CA: a cancer journal of clinicians.*, 65(2), pp. 87–108. doi: 10.3322/caac.21262.

Tu, J. *et al.* (2017) 'Simvastatin Inhibits IL-1β-Induced Apoptosis and Extracellular Matrix Degradation by Suppressing the NF-kB and MAPK Pathways in Nucleus Pulposus Cells', *Inflammation*, pp. 725–734. doi: 10.1007/s10753-017-0516-6.

Valdman, A. *et al.* (2010) 'Distribution of Foxp3- , CD4- and CD8-positive lymphocytic cells in benign and malignant prostate tissue', *APMIS*, 25, pp. 360–365. doi: 10.1111/j.1600-0463.2010.02604.x.

Vapiwala, N. and Glatstein, E. (2013) 'Fighting Prostate Cancer with Radium-223-Not Your Madame's Isotope'. doi: 10.1056/NEJMe1304041.

Vela, I. *et al.* (2007) 'Bone and prostate cancer cell interactions in metastatic prostate cancer', *BJU International*, 99(4), pp. 735–742. doi: 10.1111/j.1464-410X.2006.06670.x.

Vitkin, N. *et al.* (2019) 'The Tumor Immune Contexture of Prostate Cancer', *Frontiers in Immunology*, 1, p. 603. doi: 10.3389/fimmu.2019.00603.

Walsh, M. C. and Choi, Y. (2014) 'Biology of the RANKL-RANK-OPG system in immunity, bone, and beyond', *Frontiers in Immunology*, 5(OCT), pp. 1–11. doi: 10.3389/fimmu.2014.00511.

Walsh, M. C., Lee, J. and Choi, Y. (2015) 'Tumor necrosis factor receptor- associated factor 6 (TRAF6) regulation of development, function, and homeostasis of the immune system', *Immunological Reviews*. doi: 10.1111/imr.12302.

Wang, G. *et al.* (2018) 'Genetics and biology of prostate cancer', *Genes and Development*, 32(17–18), pp. 1105–1140. doi: 10.1101/gad.315739.118.

Weagel, E. *et al.* (2015) 'Macrophage Polarization and Its Role in Cancer', *Journal of Clinical & Cellular Immunology*, 6(4), pp. 4–11. doi: 10.4172/2155-9899.1000338.

Wei, B., Ruan, J., *et al.* (2017) 'Knockdown of TNF receptor-associated factor 2 (TRAF2) modulates in vitro growth of TRAIL-treated prostate cancer cells', *Biomedicine and Pharmacotherapy*. Elsevier Masson SAS, 93, pp. 462–469. doi: 10.1016/j.biopha.2017.05.145.

Wei, B., Liang, J., *et al.* (2017) 'TRAF2 is a valuable prognostic biomarker in patients with prostate cancer', *Medical Science Monitor*, 23, pp. 4192–4204. doi: 10.12659/MSM.903500.

Wu, H. and Arron, J. R. (2003) 'TRAF6 , a molecular bridge spanning adaptive immunity , innate immunity and osteoimmunology', (10), pp. 1096–1105. doi: 10.1002/bies.10352.

Xia, L., Shen, S., V. I. M. (2014) 'NF-kappaB, an active player in human cancers', *Cancer Immunol.*, 2(9), pp. 823–830. doi: 10.1158/2326-6066.CIR-14-0112.NF-.

Xiao, N. *et al.* (2012) 'Ubiquitin-specific protease 4 (USP4) targets TRAF2 and TRAF6 for deubiquitination and inhibits TNFα-induced cancer cell migration', *Biochemical Journal*, 441, pp. 979–987. doi: 10.1042/BJ20111358.

Xie, P. (2013) 'TRAF molecules in cell signaling and in human diseases', *Journal of Molecular Signaling*. Journal of Molecular Signaling, 8(7). doi: 10.1186/1750-2187-8-7.

Xu, K. *et al.* (2012) 'EZH2 Oncogenic Activity in Castration Resistant Prostate Cancer Cells is Polycomb-Independent', *Science*, 338(6113), pp. 1465–1469. doi: 10.1016/j.jsbmb.2011.07.002.Identification.

Yamaguchi, T. *et al.* (2016) 'Proinflammatory M1 macrophages inhibit RANKL-induced osteoclastogenesis', *Infection and Immunity*, 84(10), pp. 2802–2812. doi: 10.1128/IAI.00461-16.

Yamamoto, H. *et al.* (2017) 'TRAF1 Is Critical for DMBA/Solar UVR-Induced Skin Carcinogenesis', *J Invest Dermatol.*, 137(6), pp. 1322–1332. doi: 10.1016/j.jid.

Yang, M. *et al.* (2016) 'Macrophage phenotypic subtypes diametrically regulate epithelial-mesenchymal plasticity in breast cancer cells', *BMC Cancer*, 16(1), pp. 1–13. doi: 10.1186/s12885-016-2411-1.

Yang, W. L. *et al.* (2009) 'The E3 Ligase TRAF6 regulates akt ubiquitination and activation', *Science*, 325(5944), pp. 1134–1138. doi: 10.1126/science.1175065.

Yang, W. L. *et al.* (2010) 'Regulation of Akt signaling activation by ubiquitination', *Cell Cycle*, 9(3), pp. 486–497. doi: 10.4161/cc.9.3.10508.

Yap, T. A. *et al.* (2016) 'Drug discovery in advanced prostate cancer: Translating biology into therapy', *Nature Reviews Drug Discovery*. Nature Publishing Group, 15(10), pp. 699–718. doi: 10.1038/nrd.2016.120.

Yazlovitskaya, E. M. *et al.* (2015) 'Integrin α3β1 regulates kidney collecting duct development via TRAF6-dependent K63-linked polyubiquitination of Akt.', *Molecular biology of the cell*, 26(October), p. mbc.E14-07-1203. doi: 10.1091/mbc.E14-07-1203).

Ye, H. *et al.* (2018) 'Tumor-associated macrophages promote progression and the Warburg effect via CCL18/NF-kB/VCAM-1 pathway in pancreatic ductal adenocarcinoma', *Cell Death and Disease*. Springer US, 9(5). doi: 10.1038/s41419-018-0486-0.

Yip, K. *et al.* (2015) 'Using routinely collected data to stratify prostate cancer patients into phases of care in the United Kingdom: Implications for resource allocation and the cancer survivorship programme', *British Journal of Cancer*. Nature Publishing Group, 112, pp. 1594–1602. doi: 10.1038/bjc.2014.650.

Ylitalo, E. B. *et al.* (2017) 'Subgroups of Castration-resistant Prostate Cancer BoneMetastases Defined Through an Inverse Relationship BetweenAndrogen Receptor Activity and Immune Response', *European Urology*, 71, pp. 776–787.

Yoshida, H. *et al.* (2005) 'The Tumor Suppressor Cylindromatosis (CYLD) Acts as a Negative Regulator for Toll-like Receptor 2 Signaling via Negative Cross-talk with TRAF6 and TRAF7 * Downloaded from', *THE JOURNAL OF BIOLOGICAL CHEMISTRY*, 280(49), pp. 41111–41121. doi: 10.1074/jbc.M509526200.

Yuan, A. *et al.* (2015) 'Opposite Effects of M1 and M2 Macrophage Subtypes on Lung Cancer Progression', *Scientific Reports*. Nature Publishing Group, 5, pp. 1–12. doi: 10.1038/srep14273.

Yuen, H. F. *et al.* (2010) 'Prostate cancer cells modulate osteoblast mineralisation and osteoclast differentiation through Id-1', *British Journal of Cancer*. Nature Publishing Group, 102(2), pp. 332–341. doi: 10.1038/sj.bjc.6605480.

Zabaleta, J. *et al.* (2008) 'Interactions of cytokine gene polymorphisms in prostate cancer risk', *Carcinogenesis*, 29(3), pp. 573–578. doi: 10.1093/carcin/bgm277.

Zapata, J. M. *et al.* (2000) 'TNFR-Associated Factor Family Protein Expression in Normal Tissues and Lymphoid Malignancies', *J Immunol*, 165, pp. 5084–5096. doi: 10.4049/jimmunol.165.9.5084.

Zarzycka, B. *et al.* (2015) 'Discovery of small molecule CD40-TRAF6 inhibitors', *Journal of Chemical Information and Modeling*, 55(2), pp. 294–307. doi: 10.1021/ci500631e.

Zeigler-Johnson, C. M. *et al.* (2008) 'Evaluation of prostate cancer characteristics in four populations worldwide.', *The Canadian journal of urology*, 15(3), pp. 4056–4064.

Zhang, Jian, Patel, L. and Pienta, K. J. (2010) 'CC chemokine ligand 2 (CCL2) promotes prostate cancer tumorigenesis and metastasis', *Cytokine and Growth Factor Reviews*. Elsevier Ltd, 21(1), pp. 41–48. doi: 10.1016/j.cytogfr.2009.11.009.

Zhang, J., Patel, L. and Pienta, K. J. (2010) 'Targeting chemokine (C-C motif) ligand 2 (CCL2) as an example of translation of cancer molecular biology to the clinic', *Prog Mol Biol Transl Sci.*, 95, pp. 31–53. doi: 10.1016/B978-0-12-385071-3.00003-4.Targeting.

Zhang, L. *et al.* (2009) 'NF-κB regulates androgen receptor expression and prostate cancer growth', *American Journal of Pathology*, 175(2), pp. 489–499. doi: 10.2353/ajpath.2009.080727.

Zhang, Q. *et al.* (2009) 'Nuclear Factor- κ B-Mediated Transforming Growth Factor- β -Induced Expression of Vimentin Is an Independent Predictor of Biochemical Recurrence after Radical Prostatectomy', 15(10), pp. 3557–3567. doi: 10.1158/1078-0432.CCR-08-1656.

Zhang, Q. *et al.* (2019) 'Tumor infiltrating M2 macrophages could predict biochemical recurrence of localized prostate cancer after radical prostatectomy', *Experimental Cell Research*. Elsevier Inc., 384(1). doi: 10.1016/j.yexcr.2019.111588.

Zhang, W. *et al.* (2020) 'Role of the DNA damage response in prostate cancer formation, progression and treatment', *Prostate Cancer and Prostatic Diseases*. Springer US, 23(1), pp. 24–37. doi: 10.1038/s41391-019-0153-2.

Zhang, X. (2019) 'Interactions between cancer cells and bone microenvironment promote bone metastasis in prostate cancer', *Cancer Communications*. BioMed Central, 39(1), pp. 1–10. doi: 10.1186/s40880-019-0425-1.

Zhao, E. *et al.* (2012) 'Regulatory T cells in the bone marrow microenvironment in patients with prostate cancer'. doi: 10.4161/onci.1.2.18480.

Zheng, R. P., Wang, W. and Wei, C. D. (2015) 'Bortezomib inhibits cell proliferation in prostate

cancer', *Experimental and Therapeutic Medicine*, 10(3), pp. 1219–1223. doi: 10.3892/etm.2015.2617.

Zhu, S. *et al.* (2018) 'Genetic alterations of TRAF proteins in human cancers', *Frontiers in Immunology*. doi: 10.3389/fimmu.2018.02111.

Zhuang, C. *et al.* (2017) 'TRAF6 regulates the effects of polarized maturation of tolerability: Marrow-derived dendritic cells on collagen-induced arthritis in mice', *Biomedical Reports*, 6, pp. 206–210. doi: 10.3892/br.2017.836.

Ziaee, S. *et al.* (2015) 'Prostate cancer metastasis : roles of recruitment and reprogramming , cell signal network and three-dimensional growth characteristics', 4(1), pp. 438–454. doi: 10.3978/j.issn.2223-4683.2015.04.10.

Zotti, T., Scudiero, I. and Vito, P. (2016) 'The Emerging Role of TRAF7 in Tumor Development', (November), pp. 1233–1238. doi: 10.1002/jcp.25676.

Supplementary figures
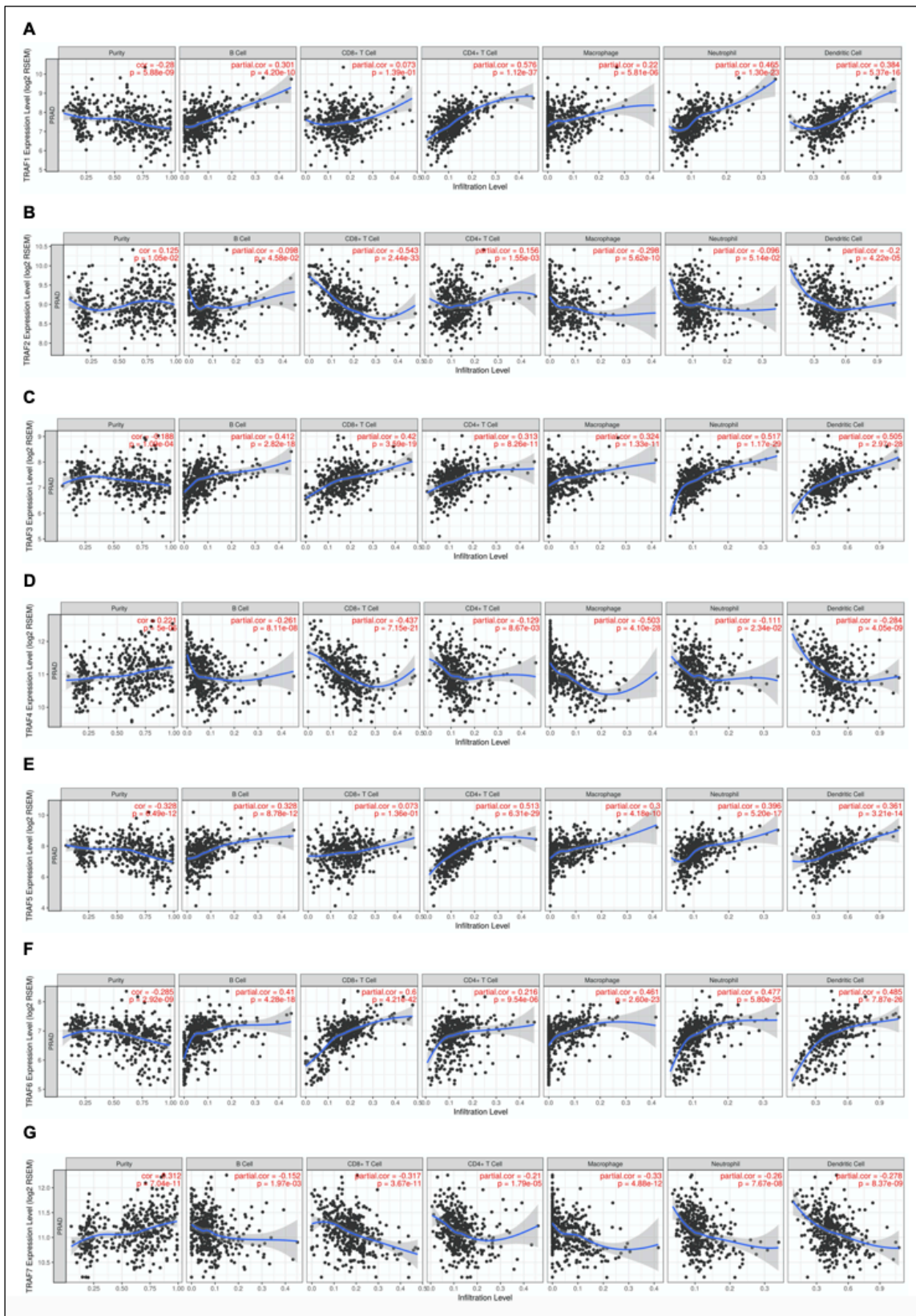
Supplementary Figure 1. Graphs of Spearman correlation values of TRAF proteins with infiltrating immune cells obtained from TIMER. Correlation of TRAF1-7 (A-G) with the specified immune cell populations. Negative association with tumour purity was used to determine highly expressed genes in the microenvironment. Data obtained from TCGA database of prostate cancer patients (n=497). p-values were determined by the TIMER software with Spearman's correlation.
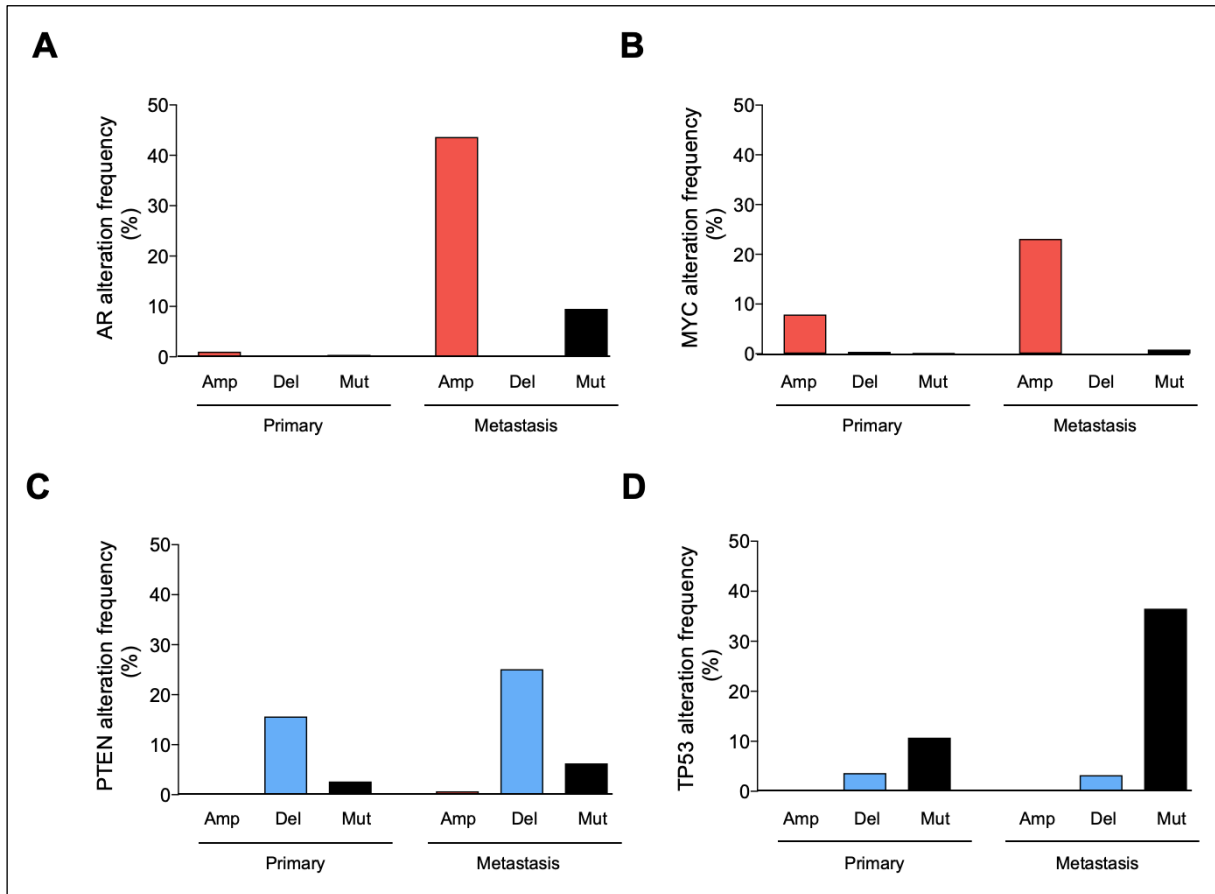
Supplementary Figure 2. Alterations commonly found in primary and metastatic prostate cancer. Amplification in (A) AR and (B) MYC, (C) loss of PTEN and (D) mutations in TP53 expression in advanced stages of prostate cancer compared to primary prostate tumour using cBioPortal. Data obtained from TCGA databases of primary (n=494) and metastatic (n=463) prostate cancer patients. Amp=Amplification, Del=Deletion, Mut=Mutation.
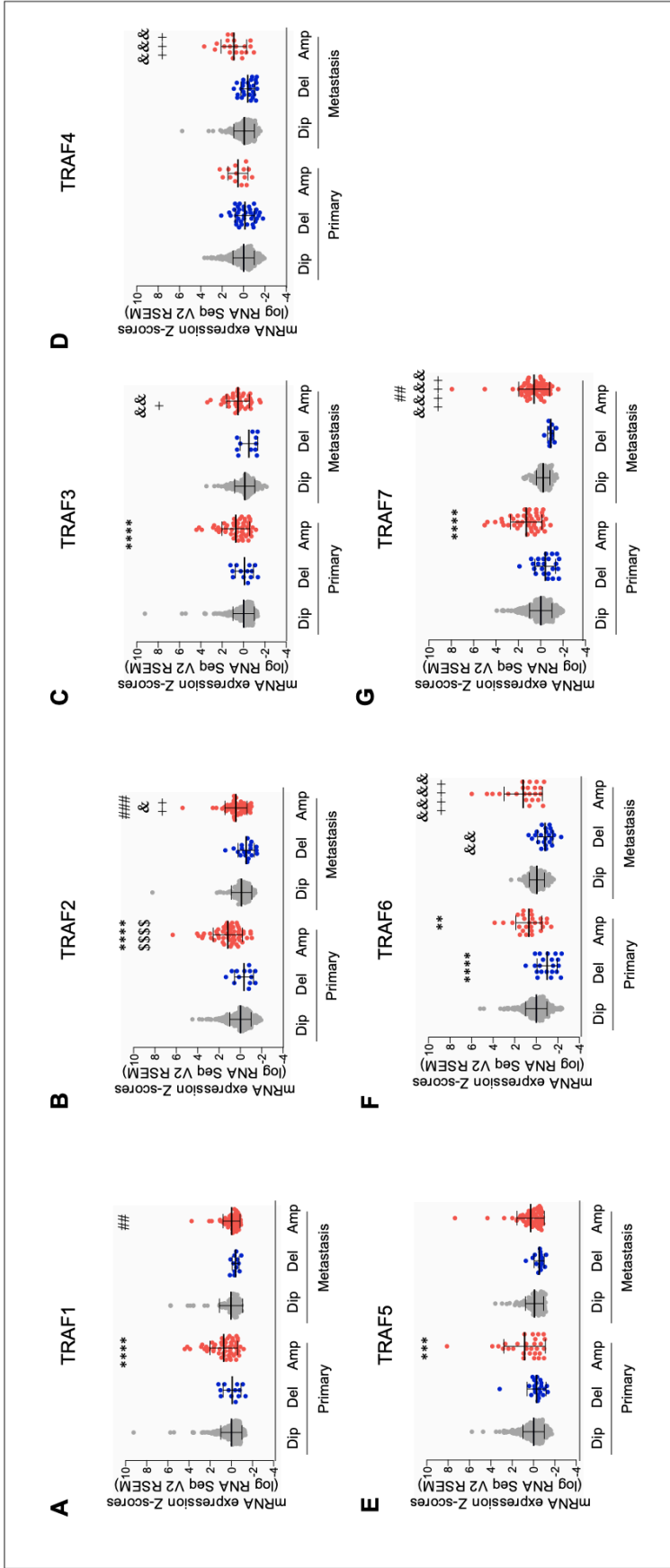
Supplementary Figure 3. mRNA expression of TRAF proteins in primary and metastatic prostate cancer patients using cBioPortal. TRAF1-7 (A-G) mRNA expression Z-scores in different stages of prostate cancer. Data obtained from TCGA databases of primary (n=494) and metastatic (n=463) prostate cancer patients. Dip=Diploid, Del=Deletion, Amp=Amplification. p-values were obtained from ordinary ANOVA test followed by Tukey *post hoc* test. ****p<0.0001, ***p<0.005 and **p<0.01 compared to control, ###p<0.005 and ## p<0.01 compared to amplification in primary tumour, $$$$p<0.001 compared to deletion in primary tumour, &&&&p<0.001, &&&p<0.005, &&p<0.01, &p<0.05 compared to diploid in metastasis, ++++p<0.001, +++p<0.005, ++p<0.01 and +p<0.05 compared to deletion in metastasis.

201
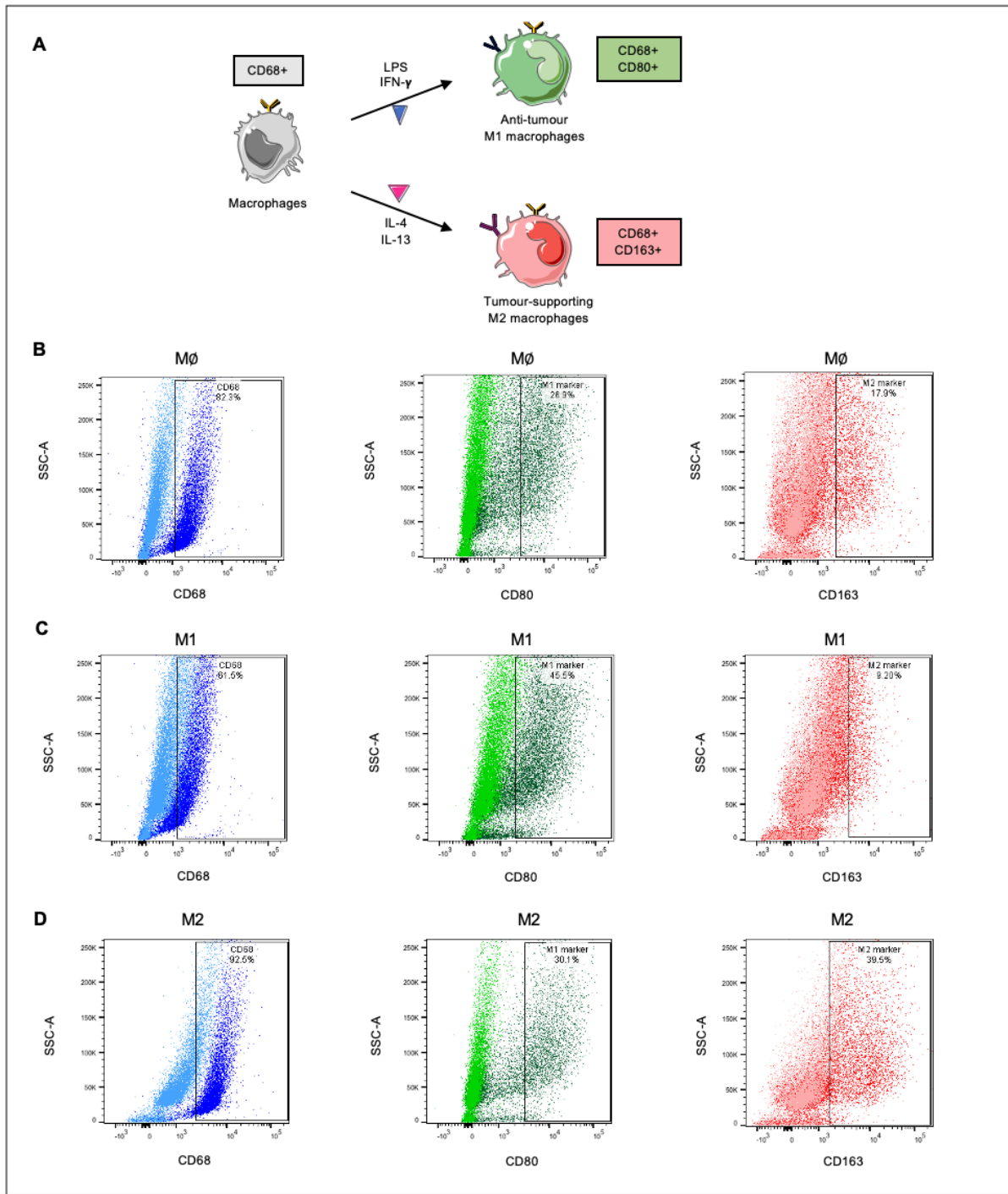
Supplementary Figure 4. Macrophage subtypes determined by multicolour flow cytometry. (A) Schematic representation of macrophage activation and polarisation. Representative dot plots obtained by flow cytometry of (B) uncommitted MØ macrophages, (C) anti-tumorigenic M1 macrophages activated by LPS and IFN-γ and (D) pro-tumorigenic M2 macrophages activated by IL-4 and IL-13. All macrophage subtypes express CD68+ and M1 and M2 are distinguished by the representative markers CD80+ and CD163+, respectively. Unstained cells are presented in light blue, green and red and percentage of cells stained with their respective marker are gated and presented with dark blue, green and red.
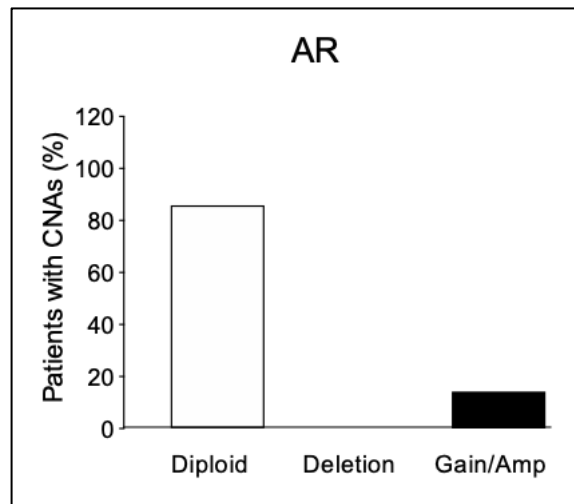
Supplementary Figure 5. Expression of androgen receptor (AR) in prostate cancer bone metastasis using cBioPortal. Percentage of patients with diploid or copy-number alterations including deletion and gain/amplification (Gain/Amp) in AR expression. Data obtained was accessed with cBioPortal from the publicly available TCGA database "The Metastatic Prostate Cancer Project" (n=30).
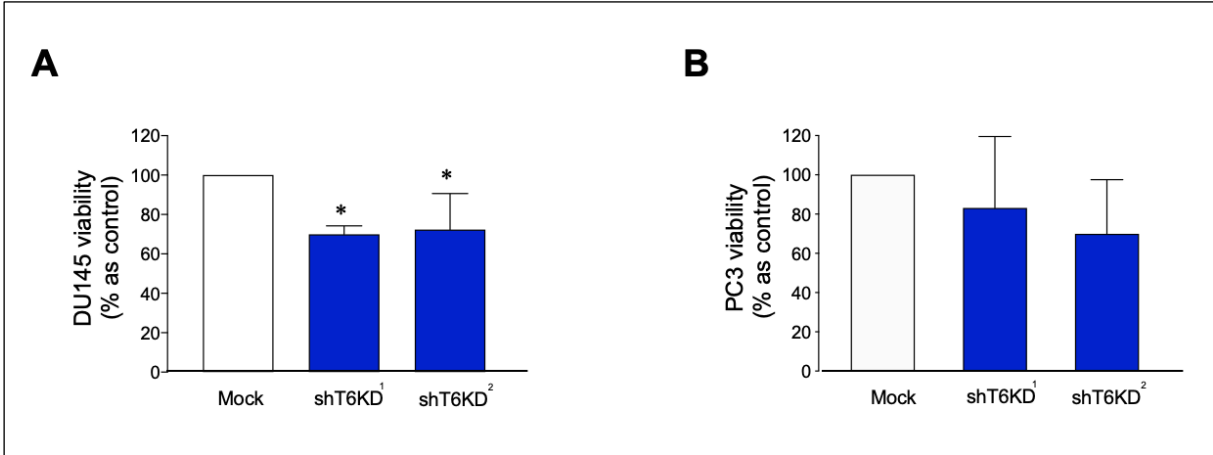
Supplementary Figure 6. Cell viability of TRAF6 knockdown prostate cancer cells after 14 hours post-wound-healing migration assay. Percentage of viability of DU145 (A) and PC3 (B) TRAF6 knockdown prostate cancer cells compared to cells silenced with control shRNA. p-values were obtained from one-way ANOVA test followed by Tukey *post hoc* test. *p<0.05 compared to mock transfected cells.
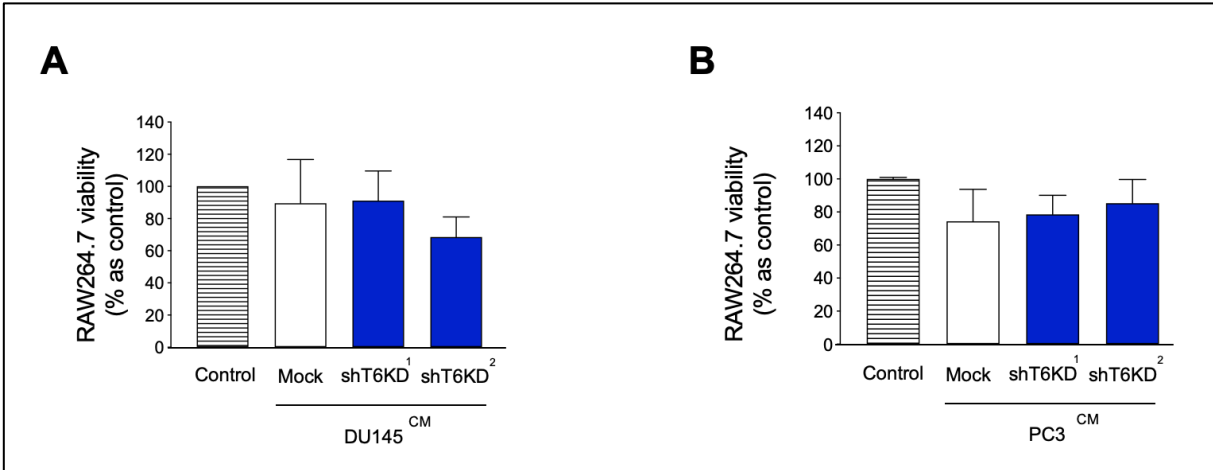
Supplementary Figure 7. Cell viability of RAW 264.7 cells in osteoclast formation induced by control and TRAF6 knockdown prostate cancer cells. Viability of RAW 264.7 cells stimulated with RANKL and treated with conditioned media from mock and TRAF6 knockdown DU145 (A) and PC3 (B) prostate cancer cells, measured by Alamar Blue ™.
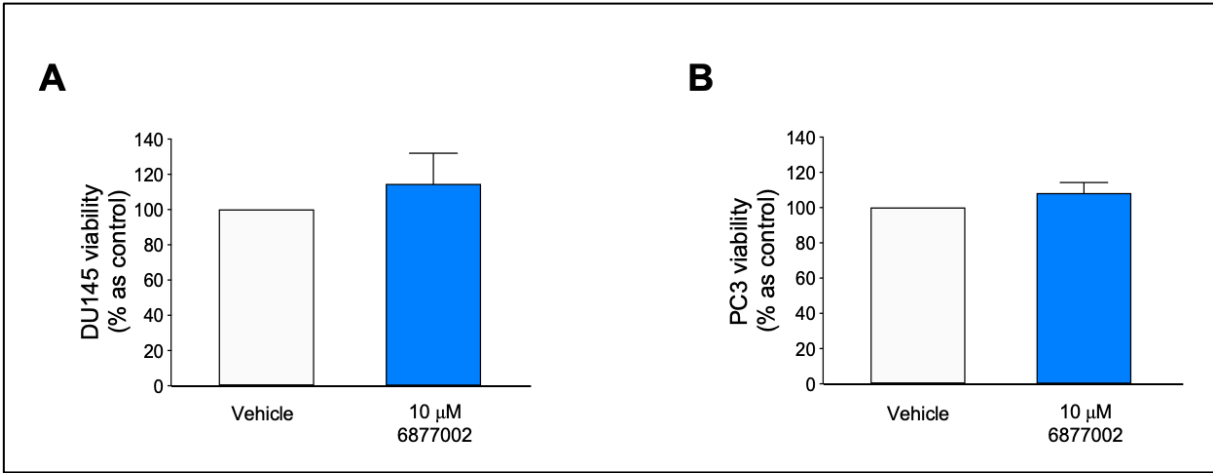
Supplementary Figure 8. Cell viability of DU145 and PC3 prostate cancer cells treated with the verified TRAF6 inhibitor after 14 hours post-wound-healing migration assay. Percentage of viability of DU145 (A) and PC3 (B) prostate cancer cells treated with vehicle or the TRAF6 inhibitor 6877002 (10 µM).
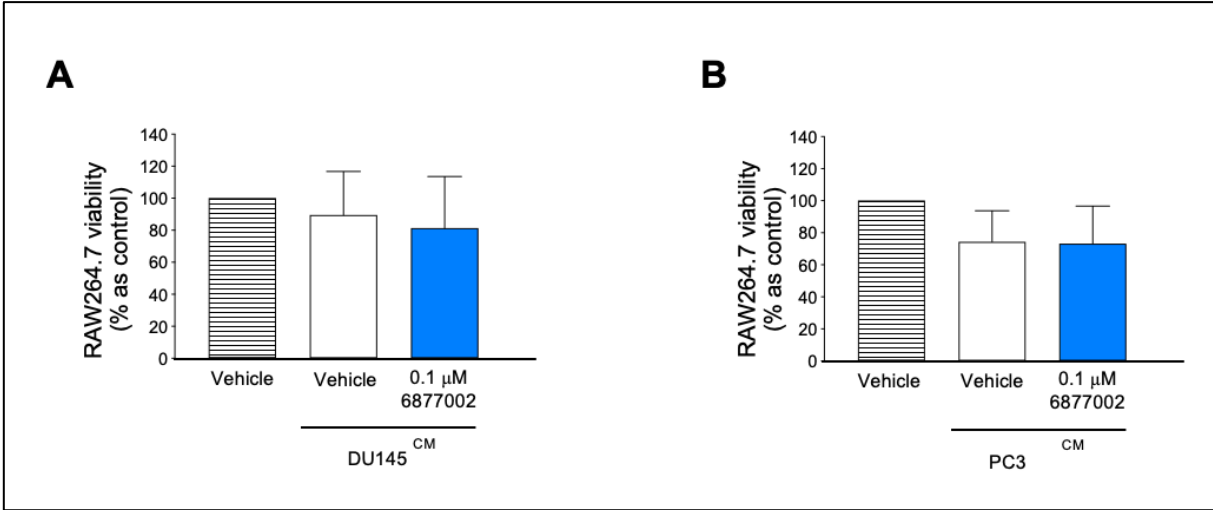

Supplementary Figure 9. Cell viability of RAW 264.7 cells in osteoclast formation treated with soluble factors from prostate cancer cells and the TRAF6 inhibitor 6877002. Viability of RAW 264.7 cells treated with the TRAF6 inhibitor 6877002 and stimulated with RANKL and conditioned media from DU145 (A) and PC3 (B) prostate cancer cells, measured by Alamar Blue ™.
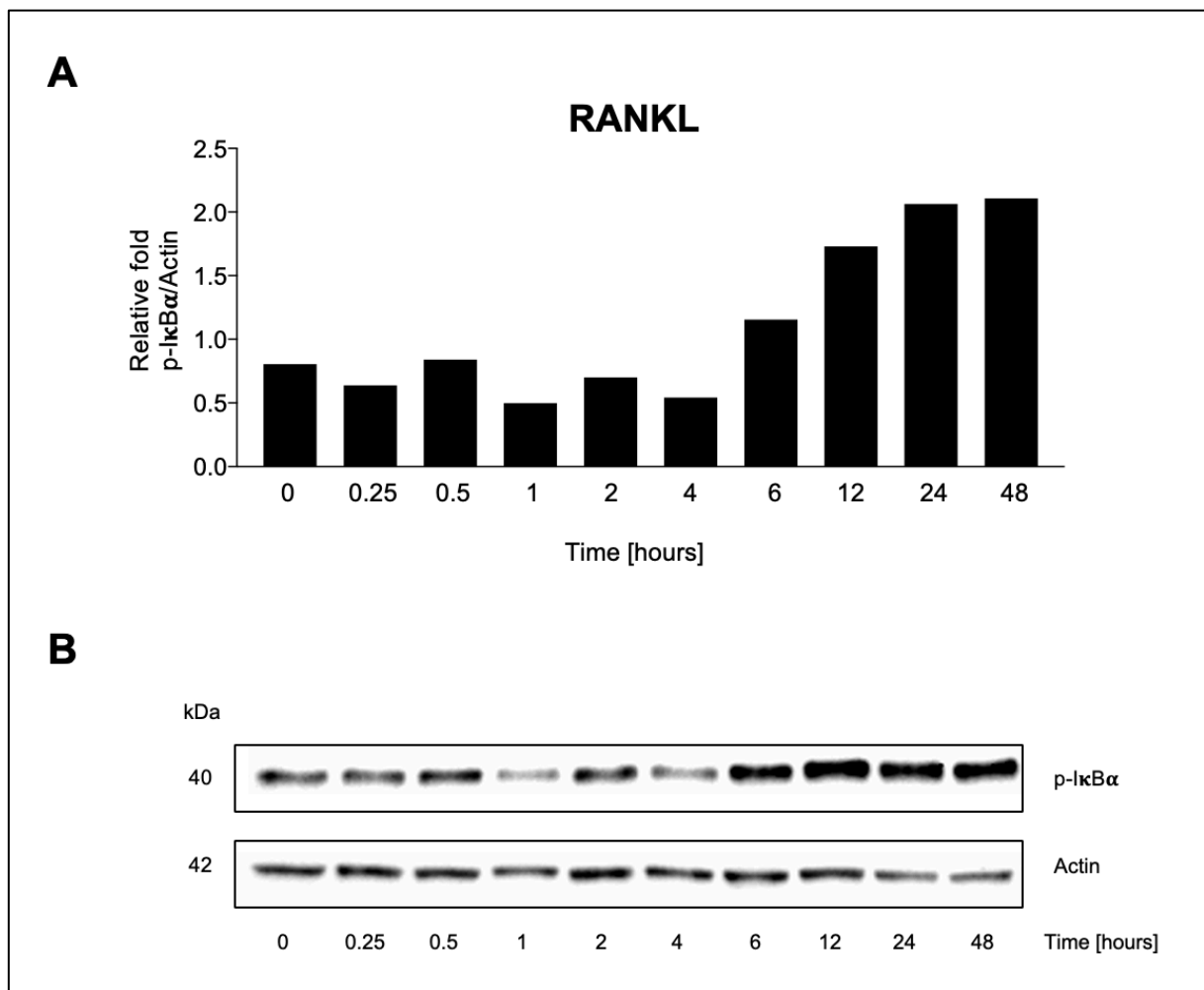
Supplementary Figure 10. Phosphorylation of IκB-α in RAW 264.7 induced by RANKL. (A)Relative fold of phosphorylated-IκB-α/Actin expression of murine macrophage-like RAW 264.7 cells exposed to RANKL (100 ng/ml) for the specified timepoints. (B)Representative Western Blot images of expression of p-IκB-α and actin of RAW 264.7 cells exposed to RANKL.
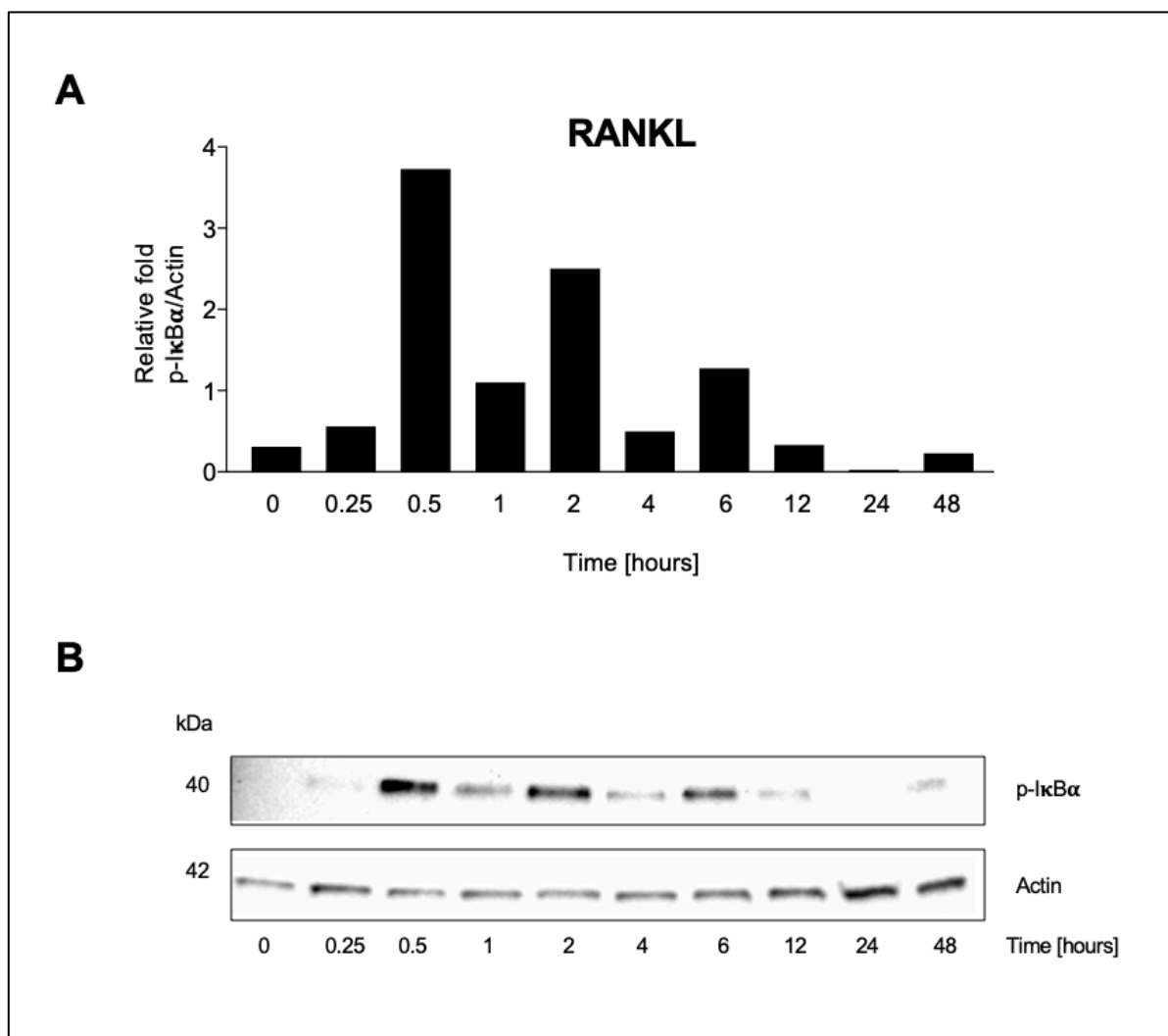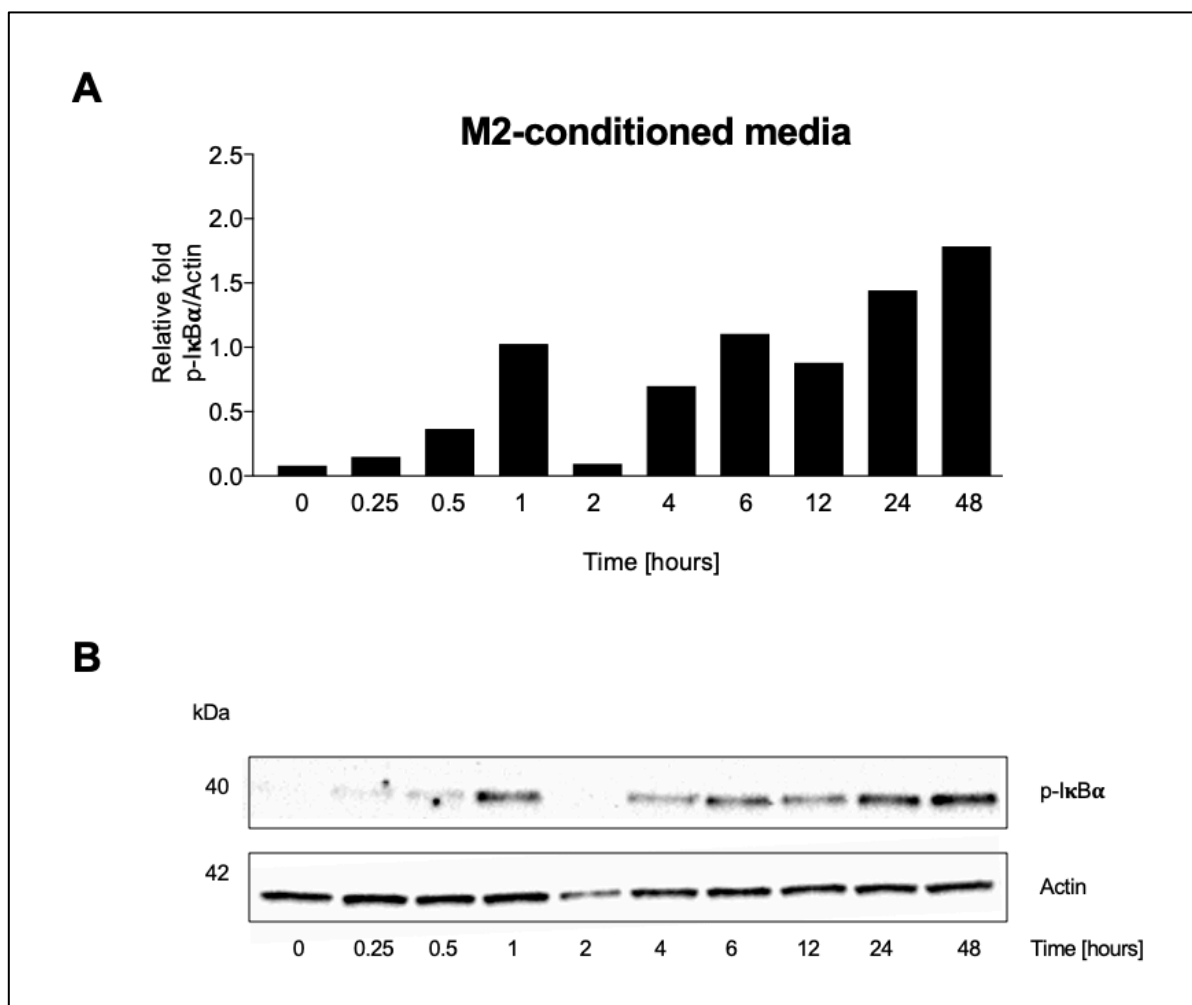
Supplementary Figure 11. Phosphorylation of IκB-α in PC3 induced by RANKL. (A)Relative fold of phosphorylated-IκB-α/Actin expression of human PC3 prostate cancer cells exposed to RANKL (100 ng/ml) for the specified timepoints. (B)Representative Western Blot images of expression of p-IκB-α and actin of PC3 cells exposed to RANKL.
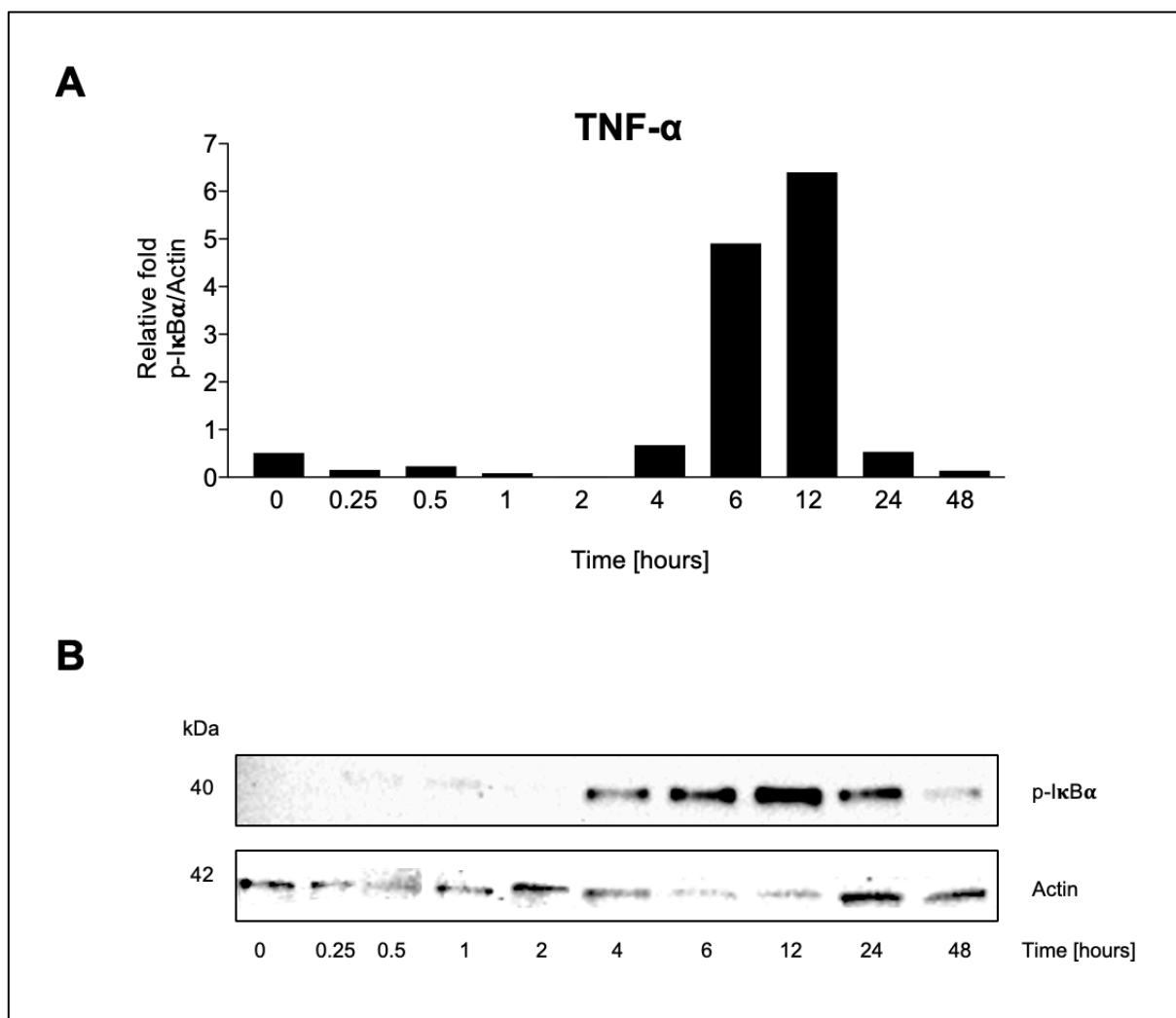
Supplementary Figure 12. Phosphorylation of IκB-α in PC3 induced by TNF-α. (A)Relative fold of phosphorylated-IκB-α/Actin expression of human PC3 prostate cancer cells exposed to TNFα (10 ng/ml) for the specified timepoints. (B)Representative Western Blot images of expression of p-IκB-α and actin of PC3 cells exposed to TNF-α.
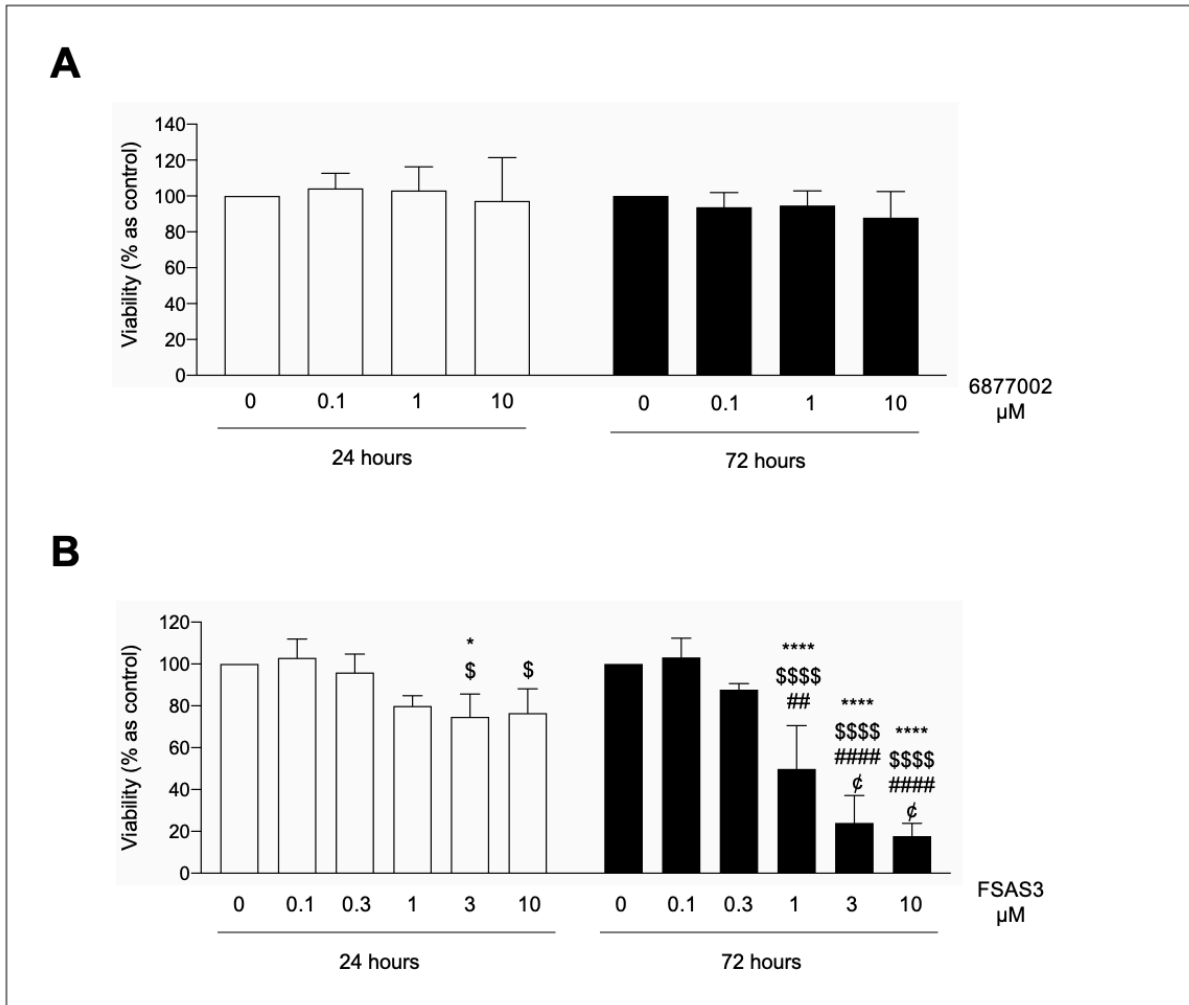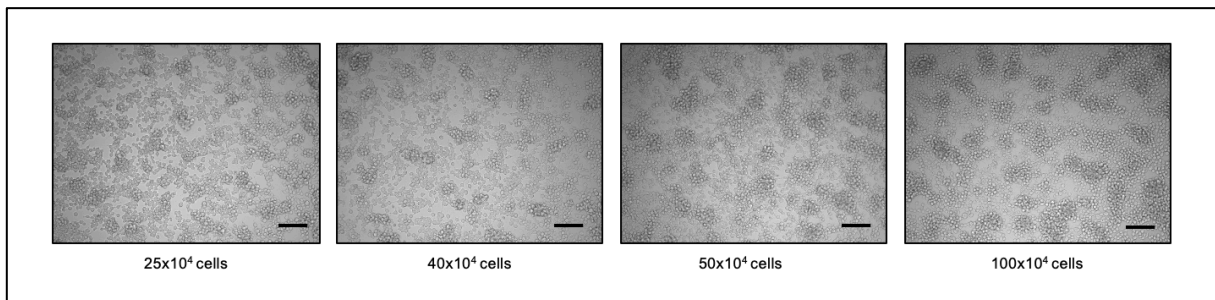
Supplementary Figure 13. Viability of human PC3 prostate cancer cells exposed to the verified 6877002 and the novel FSAS3 (0-10 μM) after 24 and 72 hours. PC3 cell viability after 24 and 72 hours of treatment with (A) 6877002 or (B) FSAS3. p-values were obtained from one-way ANOVA test followed by Tukey *post hoc* test. ****$p<0.001$ and *$p<0.05$ compared to vehicle, \$\$\$\$$p<0.001$ and \$$p<0.05$ compared to 0.1 μM, ####$p<0.001$ and ##$p<0.01$ compared to 0.3 μM, ¢$p<0.05$ compared to 1 μM.

Supplementary Figure 14. Phosphorylation of IκB-α in PC3 induced by pro-tumorigenic M2 conditioned media. (A)Relative fold of phosphorylated-IκB-α/Actin expression of human PC3 prostate cancer cells exposed to M2 conditioned media (20% v/v) for the described timepoints. (B)Representative Western Blot images of expression of p-IκB-α and actin of PC3 cells exposed to M2-conditioned media.
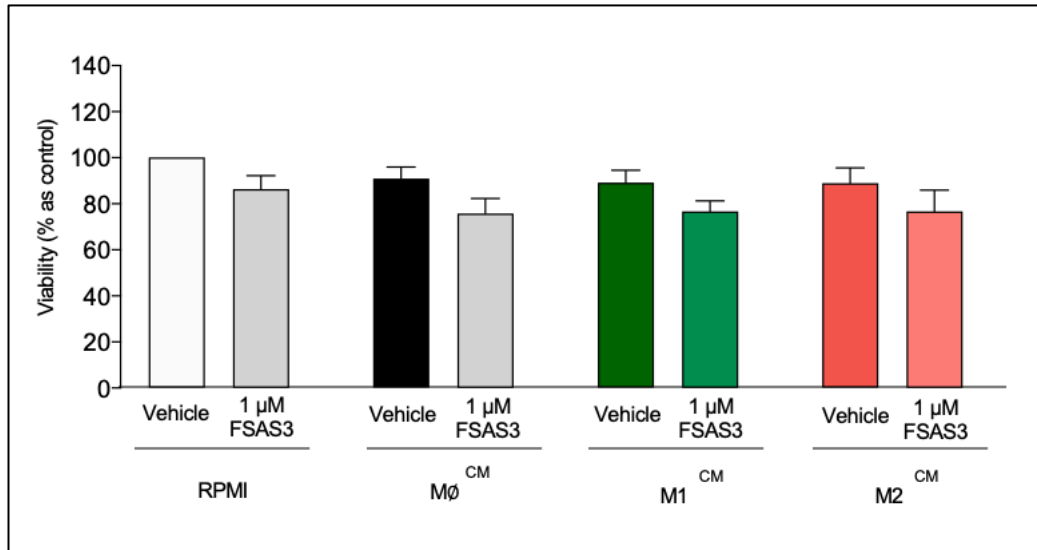
Supplementary Figure 15. Cell viability after 14-hours post-wound-healing assay of human PC3 prostate cancer cells exposed to macrophage conditioned media and treated with FSAS3. Percentage of viability of PC3 prostate cancer cells exposed to RMPI or conditioned media of uncommitted MØ, anti-tumorigenic M1 or pro-tumorigenic M2 macrophages and treated with vehicle or FSAS3 (1 µM).


Supplementary Figure 16. Seeding densities of RM1-BM aiming to generate a monolayer for the wound-healing migration assay. Scale bar=100 µM.
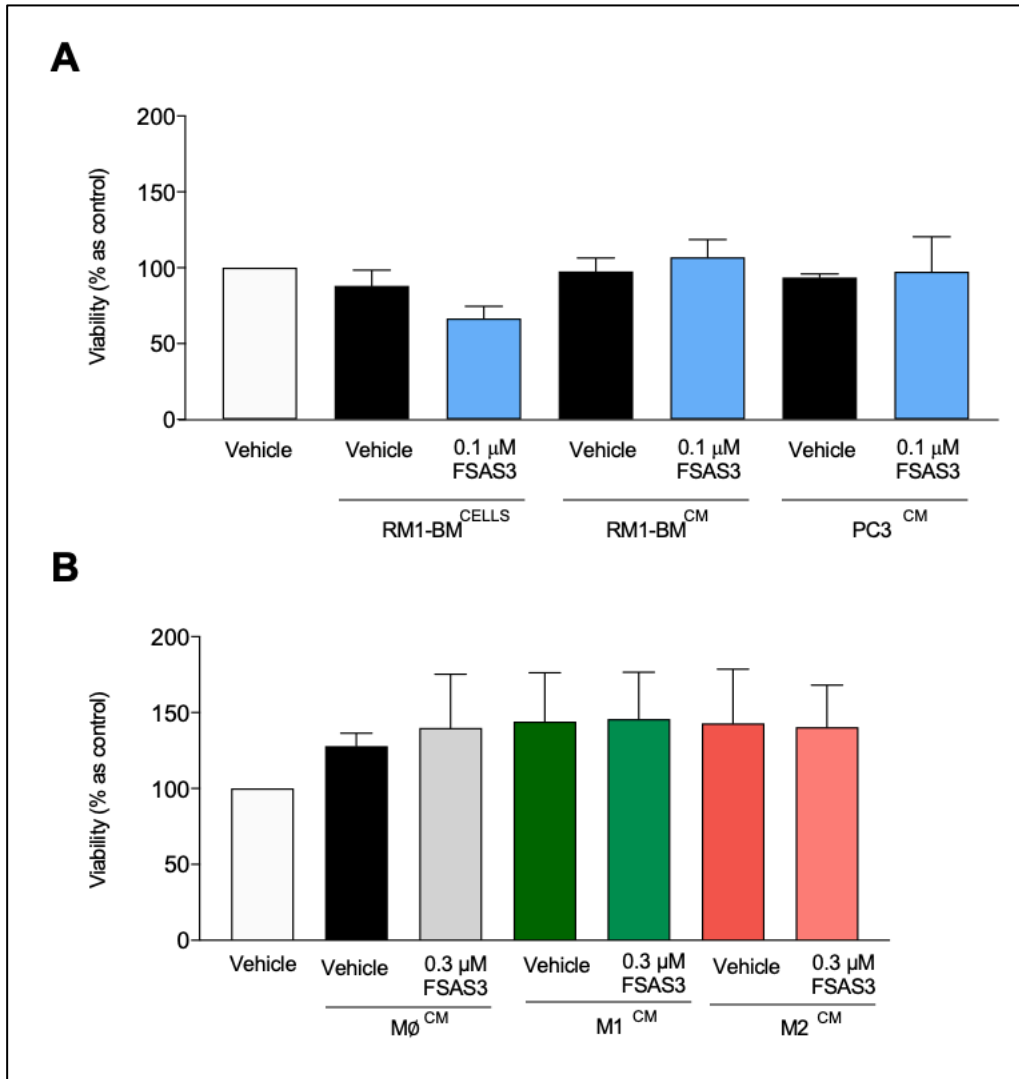
Supplementary Figure 17. Cell viability of RAW 264.7 cells was not affected in osteoclast formation assay exposed to soluble factors from prostate cancer cells and treated with the novel FSAS3. Viability of RAW 264.7 cells treated with the TRAF inhibitor FSAS3, stimulated with RANKL and exposed to (A) mouse RM1-BM cells or conditioned media and human PC3 conditioned media or various subtypes of macrophage conditioned media, measured by Alamar Blue ™.
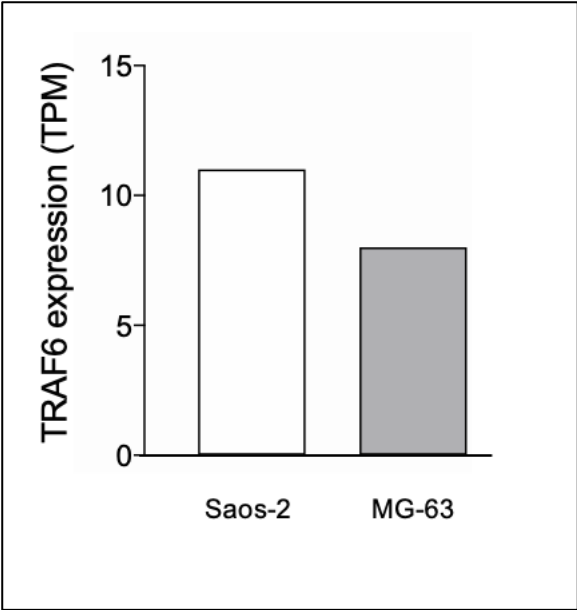
Supplementary Figure 18. Expression of TRAF6 in osteoblast-like cell lines Saos-2 and MG-63 obtained from RNA-seq of 934 human cancer cell lines from the Cancer Cell Line Encyclopedia, Expression Atlas website.

Scientific Appendix

Buffers	
ALP lysis buffer	1 M Diethanolamine (Sigma-Aldrich, No. D8885) and 1mM MgCl$_2$, leave overnight and check 9.8 pH. Add 0.05% Triton X-100.
ARS solution	Dissolve 0.547 g of ARS (Sigma-Aldrich, No. A5533) in 40 ml de-ionised water. Adjust pH between 4.1-4.3 with ammonium hydroxide (10% v/v).
Loading buffer	5.2 ml Trizma HCl (Sigma-Aldrich, No. T3253;1 M) pH 6.8 (use Trizma Base (Sigma-Aldrich, No. T6066) 1M to adjust pH) 1g DL-Dithiothreitol (DTT; Sigma-Aldrich, No. 43819) 1.3 g SDS (Melford, No. B2008) in 37ºC to dissolve. 6.5 ml glycerol (Sigma-Aldrich, No. G9012) 130 µl 10% Bromophenol Blue (Sigma-Aldrich, No. B6896) **Stir for 30 min.** **Store in -20 ºC.**
RIPA lysis buffer	1 ml 1% Triton X-100 0.5 g 0.5% (w/v) sodium deoxycholate (Sigma-Aldrich, No. D6750) 0.1 g 0.1% (w/v) SDS Trizma HCl (50 mM using 0.788 g in 100 ml) pH 7.4 0.877 g NaCl (Thermo Fisher Scientific, No. S/3100/65;150mM)
Staining solution	For 4 full plates: • Naphtol-AS-BI-phosphate solution: 15 mg Naphtol-AS-BI-phosphate (Sigma-Aldrich, No. N2250) in 1.5 ml Dimethylformamide (Sigma-Aldrich, No. D4551) • Solution A: -1.5 ml Naphtol-AS-BI-phosphate solution

	-7.5 ml Veronal buffer (1.17 g sodium acetate anhydrous (Sigma-Aldrich, No. S2889) and 2.94 g sodium 5,5-diethylbarbiturate (Sigma-Aldrich, No. B0500) in 100 ml distilled water)
	-9 ml Acetate buffer (0.82 g sodium acetate anhydrous in 100 ml distilled water and 0.6 ml acetic acid glacial in 10 ml distilled water)
	-9 ml Acetate buffer with 100 mM sodium tartrate (0.82 g sodium acetate anhydrous in 100 ml distilled water, 2.3 g sodium tartrate (Sigma-Aldrich, No. S4797) and 0.6 ml acetic acid glacial in 100 ml distilled water)
	• Solution B:
	-1.2 ml Pararosaniline solution (1 g Pararosaniline hydrochloride (Sigma-Aldrich, No. P1528) in 20 ml distilled water and 5 ml concentrated HCl (Honeywell, No. 30721))
	-1.2 ml Sodium nitrite (4%)
	Pour solution A into B and filter with Acrodisc® Syringe pore size of 0.45 µm.
Tris buffer saline solution (TBS)	For 1 L: 60.57 g Trizma Base (500 mM) 78.8 g Trizma HCl (500 mM) 175.32 g NaCl (3 M)

Copyright

The following figures were created with the resource Servier Medical Art ([SMART Creative commons license](#)):

- Figure 0.1. Schematic representation of the effects of knockdown and pharmacological inhibition of TRAF6 on prostate cancer cell – macrophage – osteoclast – osteoblast interactions.

- Figure 1.1. Schematic representation of the bone remodelling process.

- Figure 1.5. Vicious cycle of prostate cancer – bone cell interactions.

- Figure 2.2. Cell viability assessed by Alamar Blue™ assay.

- Figure 2.3. Cell migration assessed by wound-healing assay and cell invasion assessed by Transwell® invasion assay.

- Figure 2.4. Western Blot technique.

- Figure 7.1. Hypothetical schematic model of mechanism(s) of action of the verified TRAF6 inhibitor 6877002 and the novel FSAS3 on TRAF-mediated NFκB activation.

- Supplementary Figure 4A. Macrophage subtypes determined by multicolour flow cytometry.

The following images were created on Microsoft Power Point and partially based on the specified sources:

- Figure 1.1. Schematic representation of the bone remodelling process. Based on Figure 1 from (Aielli, Ponzetti and Rucci, 2019) under the Creative Commons [CC-BY 4.0 License](#).

- Figure 1.5. Vicious cycle of prostate cancer – bone cell interactions. Based on Figure 1 from (Aielli, Ponzetti and Rucci, 2019) under the Creative Commons [CC-BY 4.0 License](#).

- Figure 1.3. Gleason grading system. Based on "Gleasonscore.jpg" from Wikimedia Commons on the public domain.
- Figure 1.4. Prostate cancer progression and metastasis. Based on Figure 2 from (Jin and Mu, 2015) under the Creative Commons [CC-BY-NC 3.0 License].